

ABSTRACT

Title of Dissertation: SOIL-STRUCTURE INTERACTION OF FRP
PILES IN INTEGRAL ABUTMENT BRIDGES

Yaser Mahmoud Mustafa Jaradat, Doctor of Philosophy, 2005

Dissertation directed by: Professor Amde M. Amde
Department of Civil and Environmental Engineering

The rapid degradation of conventional material piling is one of the major problems in the bridge and civil infrastructure industry. Conventional construction materials have major disadvantages that increase their maintenance cost and reduce their service life especially in aggressive environments. The use of advanced composite materials such as Fiber Reinforced Polymers (FRPs) offers a better alternative to conventional building materials in terms of strength, weight, durability, and life cycle cost.

Integral abutment bridges are a special type of bridges that are built without bearings or expansion joints. These bridges are usually subjected to cycles of expansion and contraction that causes horizontal movements of the pile foundations. Accommodating such movements requires some flexibility in the piling system. Fiber

reinforced composites (FRPs) have the strength and flexibility and can be custom designed as needed. An extensive literature and market survey indicated that composite materials are increasingly being considered for use in civil infrastructure applications ranging from the retrofit and rehabilitation of buildings and bridges to the construction of new structural systems. Very little research has been conducted on FRPs as piling materials. The current research investigates the use of fiber reinforced composites as piling materials for jointless bridges.

Three-dimensional finite element models were developed and analyzed using the multi purpose FEM package ANSYS. The models were built to take into consideration multiple design parameters including the non-linear behavior of soil and concrete and the orthotropic behavior of unidirectional composites. Investigation results showed that FRP composites are good candidates for use in piling systems. Because of their flexibility in both geometrical shaping and layer lay-up, FRPs provide more options to designers to come up with suitable systems based on their needs. A new pile section is introduced to be used with or without concrete filling. The section consists of two flanges and a double web to allow flexibility in controlling the size of concrete filling between the webs. Analysis results showed that flexibility of the geometry of the new pile section and the flexibility of tailoring multi-layered unidirectional FRP composites make the pile customizable for best performance. FRP composites lend themselves to be optimized to achieve desired properties. The study showed that favorable stiffness and stress results can be obtained for composite piles in integral abutment bridges by optimizing the section's geometry while keeping a fixed cross-sectional area.

SOIL-STRUCTURE INTERACTION OF FRP PILES IN INTEGRAL ABUTMENT BRIDGES

by

Yaser Mahmoud Mustafa Jaradat

Dissertation submitted to the Faculty of the Graduate School of the
University of Maryland, College Park in partial fulfillment
of the requirements for the degree of
Doctor of Philosophy
2005

Advisory Committee:

Professor Amde M. Amde, Chairman/Advisor
Professor David Schelling
Professor M. Sherif Aggour
Associate Professor Chung C. Fu
Associate Professor Omar Ramahi

DEDICATION

To My Parents

To My Sisters

To My brothers

ACKNOWLEDGMENTS

First of all, I would like thank Allah (God) for giving me the patience, the knowledge and the strength to finish this work.

I would like to express my deep gratitude to Professor Amde M. Amde whom under his supervision this study was performed. His technical guidance and continuous support and encouragement proved to be invaluable.

I would like to thank Professors M. S. Aggour, D. Schelling, and Chung Fu, and Dr. Omar Ramahi, for kindly serving on my advisory committee.

I also would like to thank my beloved parents for the continuous support and encouragement over the years of my study.

TABLE OF CONTENTS

DEDICATION	II
ACKNOWLEDGMENTS.....	III
TABLE OF CONTENTS.....	IV
LIST OF TABLES.....	X
LIST OF FIGURES.....	XII
LIST OF ABBREVIATIONS.....	XXIII
NOMENCLATURE	XXIV
CHAPTER 1 - INTRODUCTION	1
1.1 STATEMENT OF THE PROBLEM	1
1.2 BACKGROUND	2
1.3 OBJECTIVES AND SCOPE	4
1.4 THESIS ORGANIZATION	6
CHAPTER 2 - COMPOSITE MATERIALS AND APPLICATIONS.....	7
2.1 INTRODUCTION	7
2.2 FRP IN AEROSPACE INDUSTRY	8
2.3 FRP COMPOSITES FOR BRIDGE APPLICATIONS	8
2.3.1 Structural Considerations	9
2.4 REPAIR AND REHABILITAION OF EXISTING STRUCTRES.....	12
2.5 COMPOSITE MATERIALS FOR PILING	14

2.5.1	The 69 th Street Composite Pier.....	16
2.5.2	Cape May – Lewes Ferry Dolphins.....	17
2.5.3	The CPAR Program.....	20
2.5.4	The NELP Program	27
2.6	HYBRIDIZATION TECHNIQUE	28
2.7	COMPOSITE PILES IN THE MARKET	29
2.8	DRIVABILITY OF FRP COMPOSITE PILES	36
CHAPTER 3 - MECHANICS OF COMPOSITE MATERIALS		43
3.1	INTRODUCTION	43
3.2	MATERIAL COMPOSITION	44
3.2.1	Reinforcing Fibers	46
3.2.2	Resins	48
3.3	RULES OF MIXTURE.....	49
3.3.1	Stress-Strain Relations.....	52
3.4	FAILURE CRITERIA	60
3.4.1	Maximum Stress Criterion	61
3.4.2	Maximum Strain Criterion	62
3.4.3	Tsai-Hill Failure Criterion.....	63
3.4.4	Tsai-Wu Failure Criterion	63
3.5	MECHANICAL PROPERTIES	64
CHAPTER 4 - SOIL-PILE INTERACTION		65
4.1	CLASSIFICATION OF PILES	65

4.2	CHOICE OF PILING METHOD AND ECONOMIC OF DESIGN.....	66
4.3	SELECTION OF FOUNDATION.....	67
4.4	DESIGN REQUIREMENTS FOR PILES	68
4.5	FORCES ACTING ON PILES	69
4.5.1	Axially Loaded Piles	70
4.5.2	Laterally Loaded Piles	72
4.6	PILE SECTIONS.....	73
4.7	PILING MATERIALS.....	73
4.7.1	Steel Piles	73
4.7.2	Concrete Piles	74
4.7.3	Timber Piles.....	74
4.8	SOIL-PILE BEHAVIOR	74
4.9	LOAD – DISPLACEMENT BEHAVIOR.....	75
4.9.1	Laterally Loaded Piles	76
4.9.2	Subgrade Reaction Method	77
4.9.3	Load-Displacement Curves	79
4.9.4	Axially Loaded Piles	90
4.9.5	The Modified Ramberg Osgood Model	93
4.10	PILES IN INTEGRAL BRIDGES	98
4.11	COMPOSITE PILES FOR INTEGRAL BRIDGES.....	100
CHAPTER 5 - FORMULATION OF THE NUMERICAL MODEL		103
5.1	ANALYSIS TOOLS	103
5.2	BUILDING THE COMPUTER MODEL	104

5.2.1	Selecting The Coordinates System.....	105
5.2.2	Generation of The Solid Model.....	105
5.3	ANALYSIS OF COMPOSITE MATERIALS	109
5.4	STRESS-STRAIN RELATIONSHIPS	109
5.5	SOIL-PILE MODEL	117
CHAPTER 6 - BEHAVIOR OF PILES AND PILING MATERIALS		123
6.1	SELECTION OF PILES	124
6.2	SELECTION OF PILE SECTIONS	127
6.3	FRP COMPOSITE PILES	128
6.4	SOIL BEHAVIORS	128
6.5	STRESS-STRAIN MODELS FOR FRP CONFINED CONCRETE	132
6.6	STRESSES IN FRP COMPOSITES.....	138
6.7	BEHAVIOR OF LATERALLY LOADED COMPOSITE PILES	141
6.7.1	Friction Piles.....	141
6.7.2	End-Bearing Piles	142
6.8	AXIAL STRESSES AND DEFORMATIONS.....	143
6.9	BENDING STRESSES	145
CHAPTER 7 - NUMERICAL INVESTIGATION OF THE FRP PILE-SOIL		
INTERACTION		151
7.1	OBJECTIVES OF THE NUMERICAL INVESTIGATION.....	151
7.2	THE SOIL-PILE MODEL	152
7.3	MAXIMUM LOAD CAPACITY	153

7.4	EFFECT OF THE DIFFERENT PARAMETERS ON THE BEHAVIOR OF LATERALLY LOADED PILES.....	164
7.4.1	Soil Type	164
7.4.2	Concrete Filling.....	179
7.4.3	Material Type	189
7.4.4	Layer Orientation.....	200
7.4.5	Cross-Section Area.....	219
7.4.6	Predrilled Hole.....	225
7.4.7	Section Geometry	239
CHAPTER 8 - OPTIMIZATION OF COMPOSITE PILES.....		253
8.1	COMPOSITE MATERIALS OPTIMIZATION	253
8.2	ELEMENTS OF OPTIMIZATION PROBLEM.....	255
8.2.1	Design Variables	256
8.2.2	Desing Constraints.....	257
8.2.3	Objective Function	257
8.3	DESIGN SETS	257
8.4	OPTIMAL LAMINATE CONFIGURATIONS	257
8.5	FAILURE CRITERIA	258
8.6	OPTIMIZATION OF LAYER ORIENTATIONS.....	260
8.6.1	Optimization of The Hollow Double-Web Pile.....	261
8.7	OPTIMIZATION OF THE SECTION GEOMETRY FOR MINIMUM STRESSES	275
8.8	OPTIMIZATION OF THE PILE SECTION FOR BEST AXIAL LOAD	280

CHAPTER 9-SUMMARY, CONCLUSIONS, AND RECOMMENDATIONS.	287
9.1 SUMMARY	287
9.2 CONCLUSIONS	288
9.2.1 Literature and Market Survey:.....	288
9.2.2 Present Study	289
9.3 RECOMMENDATIONS FOR FUTURE WORK	295
APPENDIX A.....	296
APPENDIX B.....	299
APPENDIX C.....	308
BIBLIOGRAPHY.....	320

LIST OF TABLES

Table 2-1: Mechanical properties of the composites used (Goldstick 1998).	17
Table 2-2: Mechanical properties of pile laminates (Bryan 1998).....	18
Table 2-3: Summary of laboratory test for piles in competition (Lampo 1998a).	21
Table 2-4: Summary of average results for cold radial compression tests on fender pile specimens (Lampo 1998a).....	22
Table 2-5: Bearing pile compressive test results (Lampo 1998a).	24
Table 2-6: Flexural Data: Fiberglass Tubular Piling (Hardcore).	27
Table 2-7: Composite piling specifications (Seaward)	31
Table 2-8: Standard Composite Tubular Piling (Hardcore)	32
Table 2-9: Fiberglass tubular piling flexural data (Hardcore).....	33
Table 2-10: Physical properties of Lancaster composite piling	34
Table 2-11: Piling material properties (Ashford et al 2001)	38
Table 3-1: Typical values of fiber properties.	47
Table 3-2: Chemical composition for glass by weight (Eric Green 2000).....	47
Table 4-1: Representative values of undrained shear strength and ϵ_{50}	83
Table 4-2: Representative values of k in sand	88
Table 4-3: Values of k_f as a function of angle of internal friction of sand (Mosher) ...	91
Table 4-4: Analytical forms of p - y curves.....	94
Table 4-5 - Analytical forms of f - z curves.....	96
Table 4-6 - Analytical forms of q - z curves.....	97

Table 4-7 - Parameters used in the modified Ramberg-Osgood models for clay and sand.....	98
Table 6-1: Cohesionless soil typical values (Amde et al 1982)	125
Table 6-2: Cohesive soil typical values (Amde et al 1982).....	125
Table 7-1: Effect of the section size on the moment of inertia	219
Table 7-2: Variation of stresses with cross-sectional geometry	240
Table A-1: Properties of typical unidirectional composite materials (Daneil 1994)..	296
Table A-1: Properties of typical unidirectional composite materials (Vectorply).....	297
Table A-3: Properties of experimentally tested unidirectional composite materials (Yoon1993).....	298

LIST OF FIGURES

Figure 2-1: Tic-tac-toe pile of Creative Pultrusions.....	25
Figure 2-2: Three-point bending test (HardCore).	26
Figure 2-3: Lancaster Composites piling installation.....	34
Figure 2-4: Hardcore piling.	36
Figure 2-5: Ultimate bearing capacity as a function of penetration resistance for (a) 31- kN.m Hammer; (b) 69-kN.m hammer; (c) 151-kN.m hammer (Ashford et al 2001).....	41
Figure 2-6: Different pile configurations available in the market.....	42
Figure 2-7: Drivability of polymeric piles using different hammers (Iskander et al 2001).....	42
Figure 3-1: Load transfer between fiber and resin.	45
Figure 3-2: Deformation of a composite element under axial tensile stress.	50
Figure 3-3: Composite lamina with fibers rotated an angle θ from the x-y plane.....	55
Figure 3-4: In-plane forces and moments on a flat laminate.....	58
Figure 3-5: A stack of different fiber oriented laminas.....	58
Figure 4-1: Schematic of laterally loaded pile (Mosher 200).....	77
Figure 4-2: Nonlinear p-y curves for laterally loaded piles at various depths x.	80
Figure 4-3: Characteristic shapes of the p - y curves for soft clay below water table (Mosher 200).	82
Figure 4-4: Characteristic shapes of p - y curves for static loading in stiff clay below water table.	84

Figure 4-5: Characteristic shapes of p - y curves for cyclic loading in stiff clay below water table.	84
Figure 4-6: Characteristic shape of p - y curve for static loading in stiff clay	85
Figure 4-7: Characteristic shape of p - y curves for cyclic loading in stiff clay above the water table.	85
Figure 4-8: Characteristic shape of p - y curves in sand.	87
Figure 4-9: Values of coefficients \overline{A}_c and \overline{A}_s	89
Figure 4-10: Non-dimensional coefficient B for soil resistance versus depth.	89
Figure 4-11: f - w curve (Mosher 2000).	91
Figure 4-12: Values of ultimate side friction as a function of relative depth (Mosher 2000).	92
Figure 4-13: f - w curves (Vijayvergiya 1977).	93
Figure 4-14: Sketch for an integral abutment.	99
Figure 5-1: Global coordinate system (Ansys).	105
Figure 5-2: Isometric view for an area defined by keypoints and lines.	106
Figure 5-3: Mapped meshed area.	108
Figure 5-4: Free and mapped meshed areas (Ansys).	108
Figure 5-5: Quadrilateral and triangular elements (Ansys).	108
Figure 5-6: Stress tensors (Ansys).	110
Figure 5-7: Characteristic shape of SOLID46 element (Ansys).	112
Figure 5-8: Stress output for Shell99 element (Ansys).	116
Figure 5-9: 3-D solid model.	118
Figure 5-10: Mapped meshing for lines.	119

Figure 5-11: Mapped meshing for areas.....	119
Figure 5-12: Force-displacement curves for spring elements (Ansys).....	120
Figure 5-13: Stiffness computation for spring elements (Ansys).....	121
Figure 6-1: p-y curves for dense sand.	128
Figure 6-2: Axial load – friction (f-z) curves for typical properties of dense sand....	129
Figure 6-3: Axial load-bearing (q-z) curves for typical properties of dense sand.....	129
Figure 6-4: Effect of soil density on the deflected shape under the same loading.	131
Figure 6-5: Effect of soil density on stress variation.....	132
Figure 6-6: Stress-strain model for concrete confined by FRP (Bogdanovic 2002)..	133
Figure 6-7: Lateral forces produced by confinement with rectangular and circular jackets (Marques 2004).	135
Figure 6-8: Parameters of bilinear confinement model.....	137
Figure 6-9: Stress-Strain curves for FRP confined concrete.....	138
Figure 6-10: Variation of failure stress with fiber orientation angle for glass and carbon epoxy.	139
Figure 6-11: End-bearing pile model.	142
Figure 6-12: Load-deformation curves for different pile lengths.....	143
Figure 6-13: Stress envelope for a pile under axial compression.....	144
Figure 6-14: Development of the stress (σ_1) due to lateral pile movement (bending only).....	147
Figure 6-15: Development of the stress (σ_2) due to lateral pile movement (bending only).....	148

Figure 6-16: Development of the shear stress (τ_{12}) due to lateral pile movement (bending only).	149
Figure 6-17: Bending stresses (σ_1) at different depths of the pile shaft due to lateral head movement (Compression side).	150
Figure 6-18: Bending stresses (σ_1) at different depths of the pile shaft due to lateral head movement (Tension side).....	150
Figure 7-1: Combined stresses in a pile under dead loads and lateral movements. ...	154
Figure 7-2: Stress envelopes for a pile under axial compression only (Load=900 kips).	158
Figure 7-3: Effect of lateral movement on axial capacity, stress σ_1	159
Figure 7-4: Effect of lateral movement on axial capacity, stress σ_2	160
Figure 7-5: Effect of lateral movement on axial capacity, stress τ_{12}	161
Figure 7-6: Stress (σ_1) development with time.....	163
Figure 7-7: Stress (σ_2) development with time.....	163
Figure 7-8: Lateral displacement curves for a pile in different soil profiles under lateral load.	167
Figure 7-9: Lateral displacement curves for a pile under horizontal force in different	168
Figure 7-10: Lateral displacement curves for a pile under constant displacement in different soil profiles.	168
Figure 7-11: Stress variation with time at a point located at 0-ft from the top.	172
Figure 7-12: Normalized stress variation with time at a point located at 0-ft from the top.....	172

Figure 7-13: Stress variation along the depth of the pile shaft in both tension and compression sides.....	173
Figure 7-14: Stress variation with time at a point located at 1-ft from the top.	173
Figure 7-15: Stress variation with time at a point located at 3.5-ft from the top.	174
Figure 7-16: Stress variation with time at a point located at 10-ft from the top.	174
Figure 7-17: Stress variation with time in concrete at a point located at 0-ft from the top.....	175
Figure 7-18: Stress variation in concrete along the depth of the pile shaft in both tension and compression sides.....	175
Figure 7-19: Stress envelopes along the pile length for all layers at load step 8.	176
Figure 7-19: Stress envelopes along the pile length for all layers at load step 8 (cont'd).	177
Figure 7-20: Concrete crack patterns for piles in different soils.	178
Figure 7-21: Load-deformation curves for a composite shell with different sizes of concrete fillings.	181
Figure 7-22: Lateral displacement curves for hollow and concrete-filled piles.	182
Figure 7-23: Variation of stress (σ_1) at point for hollow and filled piles.	183
Figure 7-24: Variation of stress (σ_2) at a point for hollow and filled piles.	184
Figure 7-25: Variation of shear stress (τ_{12}) at a point for hollow and filled piles.	184
Figure 7-26: Major stress envelopes for all layers at load step 8.	185
Figure 7-27: Load-deformation curves for an FRP pile filled with different grades of plain concrete under axial compression.	187
Figure 7-28: Stress variation in the FRP at a point 0-ft from the pile's top.	187

Figure 7-29: Stress variation in FRP at a point 0-ft from the pile’s top.....	188
Figure 7-30: Stresses in concrete at a point 0-ft from the pile’s top.	188
Figure 7-31: Compressive stresses in concrete at a line along the depth of the pile..	189
Figure 7-32: Comparison of elastic modulus for composites, concrete and steel.	190
Figure 7-33: Comparison of strong direction modulus of elasticity for different glass composites and plain concrete.....	191
Figure 7-34: Comparison of weak direction modulus of elasticity for different glass composites and plain concrete.....	191
Figure 7-35: Variation of the elastic modulus with fiber orientation angle for different composite materials.....	192
Figure 7-36: Vertical deformation curves for piles made of different composite materials.	195
Figure 7-37: Lateral displacement curves for piles made of different composite materials.	196
Figure 7-38: Stress variation at a point for a pile made of different composite materials.	196
Figure 7-39: Stress variation at a point for a pile made of different composite materials.	197
Figure 7-40: Stress variation along the whole depth for a pile made of different composite materials.....	197
Figure 7-41: Crack patterns for piles with different composite shells.	198
Figure 7-42: Stress envelopes for piles made of different composite materials.....	199

Figure 7-43: Normalized deformation curves for piles with different fibers structure.	204
Figure 7-44: First stress component (σ_1) envelopes along a pile made of 0-degree fibers.	205
Figure 7-45: Second stress component (σ_2) envelopes along a pile made of 0-degree fibers.	206
Figure 7-46: Shear stress (τ_{12}) envelopes along a pile made of 0-degree fibers.	207
Figure 7-47: First stress component variation in different layers within the same pile.	208
Figure 7-48: Second stress component variation in different layers within the same pile.	208
Figure 7-49: Third stress component variation in different layers within the same pile.	209
Figure 7-50: Stress (σ_1) envelopes for different layer orientations.	210
Figure 7-51: Stress (σ_2) envelopes for different layer orientations.	211
Figure 7-52: Stress (τ_{12}) envelopes for different layer orientations.	212
Figure 7-53: Stress variation with time in different FRP layers in a multi-layer pile subjected to axial compression only.	214
Figure 7-54: Stress variation with time in different FRP layers in a multi-layer pile subjected to axial compression and lateral movement.	215
Figure 7-55: Effect of variation of fiber orientations on the different stresses.	218
Figure 7-56: Comparison of lateral displacements for different pile sizes in very stiff clay.	222

Figure 7-57: Comparison of lateral displacements for different pile sizes in soft clay.	223
Figure 7-58: Comparison of lateral displacements for different pile sizes in very stiff clay and 6-ft predrilled holes.	223
Figure 7-59: Effect of cross sectional area on stresses (no predrilled holes).	224
Figure 7-60: Lateral displacement curves for piles with different radius.	225
Figure 7-61: Load-displacement curves for a pile with different predrilled holes.	228
Figure 7-62: Effect of predrilled hole depth on lateral stiffness.	228
Figure 7-63: Lateral displacements along the pile depth for different predrilled holes.	229
Figure 7-64: Effect of predrilled hole depth on pile stresses (0-ft depth).	231
Figure 7-65: Effect of predrilled hole depth on pile stresses (1-ft depth).	232
Figure 7-66: Effect of predrilled hole depth on pile stresses (2-ft depth).	232
Figure 7-67: Stress variation along the depth of the pile shaft in both tension and compression sides for different predrilled holes.	233
Figure 7-68: Variation of stress at point for a pile with different predrilled holes.....	234
Figure 7-69: Variation of stress at point for a pile with different predrilled holes.....	234
Figure 7-70: Variation of FRP Stress (σ_1) in a single layer with the depth of the predrilled hole.....	235
Figure 7-71: Variation of FRP Stress (σ_1) with the depth of the predrilled hole.	236
Figure 7-72: Variation of FRP Stress (σ_2) with the depth of the predrilled hole.	237
Figure 7-73: Crack patterns in piles with different predrilled holes.	238

Figure 7-74: Variation of moment of inertia of a rectangular section with variation of (b/h)	241
Figure 7-75: Normalized lateral head displacements for different section geometries with no predrilled hole.....	245
Figure 7-76: Normalized lateral head displacements for different section geometries with 4-ft predrilled hole.....	245
Figure 7-77: Stress envelopes for piles with different section geometries.....	246
Figure 7-78: Stress variation at a point located at 0-ft from the top (0° - layer).	248
Figure 7-79: Stress variation along the pile's depth at the compression side.	248
Figure 7-80: Stress variation at a point for located at 0-ft from the top (0° - layer)....	249
Figure 7-81: Stress variation along the pile's depth at the compression side.	249
Figure 7-82: Stress envelopes for piles with different cross-sectional shapes and 6-ft predrilled hole.....	250
Figure 7-82: Stress envelopes for piles with different cross-sectional shapes and 6-ft predrilled hole (cont'd).	251
Figure 7-82: Stress envelopes for piles with different cross-sectional shapes and 6-ft predrilled hole (cont'd).....	252
Figure 8-1: Variation of stress ratios with the fiber angles for a 2-layer laminate (1-variable).....	264
Figure 8-2: Variation of stress ratios with the fiber angles for a 4-layer laminate (1-variable).....	265
Figure 8-3: Variation of stress ratios with the fiber angle for a 4-layer laminate (2-variables).	265

Figure 8-4: Variation of stress ratios with the fiber angles for a 4-layer laminate (2-variables).	266
Figure 8-5: Variation of stress ratios with the fiber angles for a 6-layer laminate (1-variable).	267
Figure 8-6: Variation of stress ratios with the fiber angles for a 6-layer laminate (2-variables).	267
Figure 8-7: Variation of stress ratios with the fiber angles for a 6-layer laminate (3-variables).	268
Figure 8-8: Variation of stress ratios with the fiber angles for an 8-layer laminate (1-variable).	270
Figure 8-9: Variation of stress ratios with the fiber angles for an 8-layer laminate (2-variables).	270
Figure 8-10: Variation of stress ratios with the fiber angle for an 8-layer laminate (3-variables).	271
Figure 8-11: Variation of stress ratios with the fiber angles for an 8-layer laminate (4-variables).	271
Figure 8-12: Effect of layer-orientation's optimization on pile stresses.	272
Figure 8-13: Variation of element stresses during optimization.	273
Figure 8-14: Variation of stress ratios with the fiber angles for a 12-layer laminate (6-variables).	274
Figure 8-15: Effect of section geometry and concrete filling size on stresses developed after lateral displacements.	278

Figure 8-16: Effect of dead load value on stresses developed after lateral deformations.	283
Figure 8-17: Comparison of stress ratios in the pile shell for different dead load values.	284
Figure 8-18: Stress envelopes for axial load optimization.	285

LIST OF ABBREVIATIONS

DL	Dead load
FRP	Fiber reinforced polymers
ksi	Kilo pounds per square inches
LL	Live load
LM	Lateral movement
MC	Pile compression due to lateral movement's bending moment
Msi	Mega pounds per square inches
MT	Pile tension due to lateral movement's bending moment
UV	Ultraviolet

NOMENCLATURE

B	width of pile
b_f	Flange width of H pile (ft.)
C	shear strength at depth z
C_a	Adhesion between soil and pile $= \alpha c_u$ (psf)
C_u	Undrained cohesion indicated for an unconsolidated undrained laboratory test
d	Section depth of H pile or diameter of pipe pile (ft.)
$[D]$	Elasticity matrix
$E_1, E_2,$ and E_3	Young's moduli in the 1, 2, and 3 directions respectively.
E_{11}	Elastic modulus in the fibers direction
E_{22}	Elastic modulus in the perpendicular direction to fibers
E_c	Initial Elasticity modulus of concrete
E_{sec}	Concrete secant modulus corresponding to peak strength
E_x	Young's modulus in the x-direction
f'_c	Unconfined concrete compressive strength
f'_{cc}	Confined concrete peak strength
f_c	Axial stress of concrete
f_j	Stress acting on jacket
f_l	Lateral pressure

f_{max}	The ultimate side friction
G_{12} , G_{23} and G_{31}	Shear moduli in the 1-2, 2-3, and 3-1 planes respectively.
G_{xy}	Shear modulus
I	Moment of inertia
J	Constant taken as 0.5 for soft clay and 0.25 for medium clay
k_f	The initial slope of a load-displacement curve
k_h	Initial lateral stiffness
k_p	$= \frac{1 + \sin \phi}{1 - \sin \phi}$
l_g	Gross perimeter of the pile (ft.)
M_x	x- moment per unit length
N	Newton
N	Average standard penetration blow count
N	Shape parameter
N	Average standard penetration blow count
N_{corr}	Corrected standard penetration test (SPT) blow count at depth of pile tip
N_x	Transverse x-shear force per unit length
p	Generalized soil resistance
p_u	Ultimate lateral soil resistance
p_u	Ultimate lateral soil resistance per unit length of the pile
S	Shear strength
T	Current temperature

t_j	Thickness of layer j
T_{REF}	Reference temperature (strain –free)
T_x	In-plane force per unit length
V_f	Volume of fiber in the composite
V_m	Volume of matrix
x	Depth from soil surface
X_c	Compressive strength in the fiber direction
X_t	Tensile strength in the fiber direction
y	Generalized displacement
y	Lateral movement of the soil
y_{50}	Displacement at one-half ultimate soil reaction
y_{50}	Lateral movement of the soil corresponding to 50% of the ultimate lateral soil resistance.
Y_c	Compressive strength in the transverse direction
Y_t	Tensile strength in the transverse direction
z	Coordinate normal to shell, with $z=0$ being at shell midsurface
z	Depth from ground surface to the p - y curve
z_j^b	z - coordinate for bottom layer j
z_c	Relative displacement required to develop f_{max}
z_c	Relative displacement required to develop q_{max}
z_j^t	z - coordinate of top of layer j
α	Shear strength reduction factor, see Figure xx below
α_x	Thermal coefficient of expansion in the x - direction

γ	Effective unit soil weight
ΔT	$T - T_{REF}$
$\{\varepsilon\}$	Total strain vector = $\{\varepsilon_x \ \varepsilon_y \ \varepsilon_z \ \varepsilon_{xy} \ \varepsilon_{yz} \ \varepsilon_{xz}\}^T$
$\{\varepsilon^e\}$	Elastic strain vector = $\{\varepsilon\} - \{\varepsilon^t\}$
$\{\varepsilon^t\}$	Thermal strain vector.
ε_{50}	Strain at 50 percent of the ultimate strength from a laboratory stress-strain curve
ε_c	Axial strain of concrete
ε'_c	Axial strain corresponding to unconfined concrete strength f'_c
ε'_{cc}	Axial strain corresponding to confined concrete compressive strength f'_{cc}
ν_{ij}	Poisson's ratio, the ratio of the strain in the j -direction to the strain in the i direction when stresses applied in the i -direction.
ν_{xy}	Major Poisson's ratio
ν_{yx}	Minor Poisson's ratio
$\{\sigma\}$	Stress vector = $\{\sigma_x \ \sigma_y \ \sigma_z \ \sigma_{xy} \ \sigma_{yz} \ \sigma_{xz}\}^T$
σ_1	Layer stresses in the fibers direction
σ_2	Layer stresses in the in perpendicular direction to fibers
$\sigma^b_{x,j}$	Stress at bottom of layer j in element x direction
σ_D	Dead load stresses
σ_f	Stresses in fibers
σ_m	Stresses in matrix
σ_{MC}	Lateral movement stresses at the compression side
σ_{MT}	Lateral movement stresses at the tension side

$\sigma_{x,j}^t$	Stress at top of layer j in element x direction
$\sigma_{xz,j}$	Average transverse shear stress in layer j in element x-z plane
τ_{12}	Layer shear stress
ϕ	Angle of internal friction
γ'	Average effective unit weight from ground surface to p - y curve

INTRODUCTION

1.1 STATEMENT OF THE PROBLEM

The rapid degradation of conventional material piling is a problem in the bridge and infrastructure industry especially in aggressive environments. The corrosion of steel and deterioration of concrete and timber piling costs millions of dollars each year in repairs and reconstruction. Fiber reinforced composites (FRPs) are the newest construction materials that have been introduced to the construction market recently. The use of FRPs in rehabilitation and retrofitting of existing structures has achieved a remarkable success in the past decades. Post strengthening of a structure in service becomes essential when its safety and serviceability become suspicious and no longer guaranteed.

Integral abutment bridges are subjected to cycles of expansion and contraction that cause horizontal movements of the pile foundations. The amount of movement depends on bridge length and temperature extremes in the bridge location. Accommodating such movements requires some flexibility in the piling system. Fiber reinforced composites have the strength and flexibility and can be custom designed as needed

Studies on FRP composites as piling materials showed some signs of encouragement that pushed researchers to proceed in that field. Extensive research programs have been performed in several institutes and research centers in the United States (Lampo 1998a and Hardcore 1997). Experimental investigations of FRP composite piles under different types of loading showed that composites are highly competitive to conventional piling materials. Their unique properties such as light weight, specific strength (the yield strength divided by the density) and resistance to corrosion and chemicals make them well suited for certain applications.

Fiber reinforced composites offer a wide range of properties because of the variety in their constituents, the fibers and the matrix. Reinforcing fibers can be produced from different types of materials that have a wide range of strength and stiffness. Reinforcement fibers are available in various forms, such as woven fabrics, tows or roving. The reinforcement fibers are combined with the resin material in a variety of forms to create the laminate.

The lack of information on the history of composites as structural materials places many obstacles that block their wide use in the market. The long term performance of these materials has to be tested and demonstrated in order for the construction industry to accept them as alternate construction materials

1.2 BACKGROUND

Piles are structural members used in transferring loads from structures founded on soft soils to hard strata below the ground surface. They were used in prehistorical times to support buildings founded on weak soils. The demand on pile foundations has increased in the last century especially for bridges and other massive constructions. Conventional

piles are commonly made of concrete, steel, timber or a combination of them. Because of their outstanding mechanical properties and reasonable initial cost, reinforced concrete and H-steel piles are still the most popular in use. Also their long clean history and the support of the extensive studies that have been performed on concrete and steel as piling materials have kept them dominant in the construction market.

In spite of their superior properties, conventional piling materials are still encountering some serious problems especially in aggressive environments. Surface treated timber pilings are usually subjected to organic attack in marine environments that causes disposal problems upon replacement. On the other hand, chloride attack on reinforced concrete members and corrosion of steel elements are major sources of piling damage. Lampo et. Al. (1998) estimated an annual expenditure of \$1 billion because of pile deterioration in marine and waterfront structures.

Recently, the construction industry has introduced Fiber Reinforced Polymer (FRP) composites as an alternative construction material to current conventional piling materials. They have been successfully used in beam and column wrapping as well as in some bridge structures.

Fiber reinforced composites offer perfect characteristics especially on the basis of weight. They have a very low density when compared to metals and reinforced concrete. Because of their high strength to weight ratio characteristics, they used in the aerospace industry for spacecraft and airplane parts. The use of composite material in civil engineering was started a few years ago and is still very limited due to the shortage in knowledge of the long-term behavior of these materials.

1.3 OBJECTIVES AND SCOPE

The primary objective of this research is to investigate the feasibility of using fiber reinforced composites as piling materials and their application in integral abutment bridges. The use of conventional piling materials in aggressive environments is usually accompanied by the problem of deterioration and corrosion which reduces the life of the structure and increases the life-cycle cost. The new piling material will provide an alternative solution to resolve this problem and is expected to lower the life-cycle cost of the structure. Because of the nature of their chemical composition, FRP composites are expected to withstand severe environmental conditions. The study will take into account the current market experience in using such materials in bridge applications.

The lack of adequate research history on FRPs as a construction material has kept them from being a major competitive construction material. Also their high initial cost is another major factor. In spite of some disadvantages, fiber reinforced composites are still very strong candidates when considering the overall life-cycle cost of the structure in aggressive environments. Extensive studies are needed to investigate the feasibility of using FRP materials for piles in integral abutment bridges.

From an engineering point of view, a well designed structure is expected to satisfy safety and serviceability requirements. On the other hand, economy is the other major consideration in a satisfactorily engineered structural design. Safety can be achieved by designing the structure according to the required specifications. Serviceability can be achieved by designing the structure to meet serviceability specifications. Finally, economy also can be achieved by minimizing the cost of the structure and raising its efficiency over its expected life of service.

Fiber reinforced composites have the capability of being optimized by tailoring the fibers to the direction of best performance. The optimization process always increases the composite efficiency when fibers are arranged appropriately to the desired direction. Mechanical properties for a composite section will vary dramatically when the fibers orientation changes in any layer. The section is considered optimally designed when appropriate fiber orientations are selected

Similar studies to those done on concrete and steel piles are now necessary for FRP composite piles. Fiber composite materials have different properties and behavior compared to steel and concrete. Concrete and steel are isotropic materials, and they have similar properties in all directions. On the other hand, fiber reinforced composites are non-isotropic materials. Since composites consist of fibers embedded in a resin matrix, the mechanical properties are direction-dependent such that the properties in the fiber direction are different from those in the transverse direction.

This study will focus on selecting a pile configuration that fits the desired requirements and then optimizing that configuration for best performance and lowest cost.

Objectives summary

1. Study the ability of fiber reinforced composites as piling materials.
2. Design a new pile section that fits the bridge and soil conditions.
3. Optimize the pile section for best performance.
4. Study the behavior of the composite pile in terms of stresses and stiffness.
5. Apply the new pile in integral abutment bridges.

1.4 THESIS ORGANIZATION

Chapter 2 talks about the advantages of composite materials and explains why they are preferred over conventional materials in some construction applications. It also presents the different applications of fiber reinforced composites as piling and structural materials in the construction industry with some facts about those applications.

Chapter 3 presents the theory of fiber reinforced composite in terms of stress-strain relations, mechanical and material properties. It also discusses the basic composition of composites regarding their basic constituents such as fiber and resin types.

Chapter 4 talks about pile analysis and soil-pile interaction behaviors. Different approaches in the analysis of both axially and laterally loaded piles are presented.

Chapter 5 talks about the finite element modeling of the soil-pile mechanism. It also presents the basic theory used by the ANSYS computer code.

Chapter 6 talks about the behavior of piles and their constituent materials such as load-deflection and stress-strain behaviors.

Chapter 7 includes the parametric study and the results of the finite element analysis for all models and discusses the effect of different parameters on composite piles.

Chapter 8 talks about optimization and about its basic elements. It also presents some optimization results for composite piles.

Chapter 9 presents a short summary and conclusions of the market survey and the finite element analysis results.

COMPOSITE MATERIALS AND APPLICATIONS

2.1 INTRODUCTION

In recent years the construction industry has started using fiber-reinforced polymers (FRPs) which have some advantages over conventional materials. Fiber Reinforced Polymers have emerged as a potential solution to overcome some of the problems associated with structures built using conventional materials. Their specific strength and high resistance to corrosion and other electro-chemical reactions have made them attractive for some applications. During the last decade, there has been a surge of activities in the civil engineering research community to test and demonstrate the viability of these new materials for the construction of more durable structures and for the repair and strengthening of existing structures.

Advanced composite materials were originally developed to be used in the defense and aerospace systems. They have been used in military and aerospace applications since 1940 to take advantage of their high strength, light weight, chemical resistance, good fatigue strength, and non-magnetic properties (Alampalli 1999).

The use of FRPs in bridge construction has started recently to gain more popularity in the United States. Europe and Japan have been using FRPs in bridge

applications for many years. It has been used in a wide variety of new and old bridge projects (Alampalli 1999). Civil engineers are beginning to gain confidence and experience in applying this technology to civil structures (Tang 1999).

2.2 FRP IN AEROSPACE INDUSTRY

The aerospace industry has been utilizing fiber reinforced composite materials for its products for more than 50 years. Fiber reinforced composites also have very wide applications in spacecrafts. The weight reduction is the main reason for using such applications. Also their dimensional stability over a wide range of temperature range makes them favorable over other materials.

Military aircraft manufacturers were among the beginners who introduced FRP composite materials to be a replacement for traditional materials. The designers realized the tremendous potential of composite materials, especially their high specific strength, stiffness and light weight. This has lead to a rapid acceleration in the development of advanced composites in military aircraft applications. Several composite structural elements were used in such applications such as horizontal and vertical stabilizers, flaps, wing skins, and other control surfaces (Gibson 1994).

2.3 FRP COMPOSITES FOR BRIDGE APPLICATIONS

Every year a large number of bridge structures are reaching their design service lives and need to be repaired or replaced. The major construction materials for bridge structures are still concrete and steel. The rapid deterioration of concrete and corrosion of steel, especially in aggressive environments, such as marine areas, reduces the designed service life of the bridge structure. The use of the same materials to repair or rehabilitate

the structure will not resolve the problem. A need for a long term, practical and economical solution is essential.

New techniques in overcoming such problems have been utilized. The use of fiber reinforced polymer composites (FRPs) to replace the conventional materials in rehabilitating old and building new structures is becoming more common. FRP is the newest building material available in the market for large projects construction. The recent advancement in material technology and manufacturing techniques has made it easier to develop materials with the ability to satisfy conditions that could not be achieved by conventional materials. Confidence in the use of FRP composites in bridge engineering has increased in the last few years. This material has been widely used in retrofitting and rehabilitation of a wide variety of existing structures.

2.3.1 STRUCTURAL CONSIDERATIONS

High Strength

FRP composites are made of a wide range of fiber/polymer combinations that provides a very high strength that can range from the strength of mild steel to stronger than prestressed steel tendons. The tensile strength of FRP composites comes from the fibers immersed in the plastic matrix. Fiber volume fraction and fiber orientation are two main factors in determining the strength of composite laminates. Fibers can be proportioned and oriented to give the strength in the desired direction.

Corrosion Resistance

Corrosion of steel is a major problem especially in salty soils and marine environments. FRP composites have the advantage over steel in corrosion resistance. The plastic matrix (resins) has the ability to withstand many chemical reactions as well as the

effect of acidic, salt and fresh water which are corrosive for ferrous metals (Engineering 1997).

Light Weight

Fiber reinforced composites have very low densities compared to other construction materials like steel and concrete. Because of their high strength and low density, they provide very high specific strengths which are up to 60 times that of high strength steels (Engineering 1997). The specific strength of a material is the ratio of yield strength to its density.

Fatigue Resistance

Fiber composite materials offer fatigue resistance much better than conventional materials. The initial imperfections in composite materials such as broken fibers, delamination, matrix cracking, fiber debonding, voids, etc., can be much larger than corresponding imperfections in conventional metals such as cracks. However, the growth of damage in a metal is typically much more abrupt and hence potentially more dangerous than in a composite material (Jones 1999).

Life-cycle costs

While the initial cost of composite materials is usually higher than alternative construction materials, there are a number of economic considerations which make their use feasible and economic. Corrosion protection was mentioned as an area where composites are beneficial to the cost of maintenance. Many life-cycle costs could be eliminated or drastically reduced with the use of FRP composites. The costs associated with periodically repainting steel to protect it against corrosion are maintenance costs that would be eliminated if materials that did not require such coatings were used. The costs

of rehabilitating structures damaged by corrosion, such as blast cleaning of steel to remove corrosion products, would be eliminated with non-corrosive composite materials. In general, periodic maintenance of structures would be reduced and replacement costs would be delayed through greater use of FRP composites. Some FRPs could require coating protection for aesthetic reasons or for exceptionally harsh environments.

Reduced environmental toxicity.

Many of the building materials that we presently use are harmful to our environment in some way or another. Examples of such materials are lead-based paints, creosote and other petroleum products used in piling to kill or ward off marine borers and shipworms. The components of FRP materials are, for the most part, inert and will not leach into the environment. The use of conventional maintenance coatings on structures can be toxic to the environment. The use of FRP's eliminates some of these hazardous chemicals. Pilings made from FRP materials do not rot nor are they attacked by marine organisms so there is no need to treat pilings with harmful chemicals such as creosote.

Recycling. Many of the plastic materials that we use as food containers and composite components of automobiles can be recycled when no longer needed. These recycled plastics and glass fibers can be reused to make FRP composite components, thereby reducing the volume of waste we put in our landfills. Marine piles are currently being produced from recycled materials (Taylor 1994). High density polyethylene plastics that are recycled from milk jugs, juice containers, and detergent bottles are being combined with fiberglass pultruded reinforcing elements to produce these piles. As many as 15,000 containers can be recycled into one 18-m (59-ft) pile. FRP composites themselves can be

recycled when their useful life is through. These components can be reprocessed to recover most of their original materials and the materials reused.

2.4 REPAIR AND REHABILITATION OF EXISTING STRUCTURES

Aging and deterioration of bridges and civil engineering structures has become a critical problem in the bridge industry. This problem is more severe in marine and industrial areas where the corrosion effects of salts on steel structural members are quite devastating. Also concrete in marine and industrial environments is highly susceptible to chloride attack. The repair and rehabilitation of these structures have become a major challenge to civil engineers.

Strengthening of reinforced concrete members with externally bonded steel plates is one of the repair techniques used since the 1960s. In spite of the extensive research that has been done regarding this technique, it still has some difficulties and disadvantages. The heavy weight of the steel plate and its high potential to corrosion makes it impractical for doing repair. Corrosion of steel at the adhesive interface will lead to a high cost in both installation and maintenance. Steel plates can be replaced by high-strength fiber reinforced composite sheets. The main advantage of composite plates over steel plates is high strength-to-weight ratio, their excellent resistance to corrosion, and their nonmagnetic and nonconductive properties (M'Bazza 1996)

Sonti (1996) investigated the use of fiber reinforced plastic wraps to strengthen the glue laminated timber beams of a timber bridge. The study included three types of fiber systems (1) unidirectional carbon fiber sheets, (2) non-woven glass cloth, and (3) a woven glass cloth. A total of eight beams were tested, five wrapped and three unwrapped. An epoxy based adhesive was used in the wrapping process. The test results showed that

fiber orientation has a big effect on the strength and stiffness of the wrapped beams. Beams wrapped with fiber orientation perpendicular to the longitudinal axis of the beam gained higher strength and stiffness than other beams. It has been noticed that the failure of beams occurred outside the wrapped area or very close to the end portion of the wrapped area and never in the middle of the wrap.

The strengthening of reinforced concrete beams with externally bonded composite laminates relies substantially upon the force transfer between concrete and composite material at the interface (Juvandes 1998). The performance of concrete beams strengthened with carbon fiber reinforced plastic (CFRP) laminates has been studied based on an experimental test performed in two series of reinforced concrete beams with externally bonded carbon-fiber-reinforced plastic laminates. Results showed that the strengthening techniques using CFRP sheets improves the ultimate load capacity and to a lesser extent in flexural stiffness.

Confinement of concrete cylinders with carbon fibers sheets to improve ductility and strength was also investigated by Picher et al (1996). Deteriorated reinforced concrete columns can be strengthened either by adding longitudinal steel bars or by placing a steel jacket around the columns. Both methods are not effective in the long run because the corrosion problem will remain unresolved. Wrapping the deteriorated column with fiber reinforced composite sheets has more advantages than the steel jacket. Such advantages are high strength, low thickness and weight, and ease of construction. Results proved that fiber reinforced composite sheets improve the compressive strength and ductility of confined concrete cylinders. The fiber orientation within the composite sheets has a big effect on the axial stiffness of the confined cylinder.

Mirmiran et al (1996) discussed the use of multi-layer FRPs in confining concrete columns based on the fact that high performance concrete can be achieved by confining normal strength concrete and the fact that lateral confining pressure increases strength and ductility of concrete in the axial direction. As a part of that study, a composite column was proposed to be used as a form, protective jacket, confining member, and bi-directional external reinforcement. The filament-wound tubular composite shell was a multi-layer angle-ply or normal axial wound pipe. Experimental test results showed that the strength of the standard concrete cylinder was tripled after being confined by the FRP composite shell.

2.5 COMPOSITE MATERIALS FOR PILING

Marine piling has been a common problem for structural engineers in that the wetting and drying due to storm activity and tidal fluctuations result in accelerated decay of steel, concrete and wood pilings. The use of composite materials in piling has started recently. Because of the lack of history, specifications and experience on composite materials, they are still somewhat controversial when they are considered as a construction material. Their short history as construction materials is one of the factors that limit their use.

Concrete, steel, and timber, the traditional materials for piling exhibit many problems when used in corrosive soils and harsh environments. Millions of dollars are spent each year for maintenance and rehabilitation of concrete and steel piles. Fiber reinforced polymers have performance advantages over concrete and steel or timber. Also they can be custom designed to fit certain requirements and specifications.

In spite of their advantages over other materials, steel and concrete have disadvantages especially in harsh environments. As stated earlier, steel corrosion and concrete deterioration are the main problems. The reduction in the section area with time is a major problem that risks the safety of the structure. The use of composite materials (FRPs) can be an alternative solution for such problem.

The use of FRP composite piles as a load bearing structure is still under extensive study. The lack of experience and history about such materials is a major concern. Also the high initial cost of composite materials is another important issue.

The use of composite materials in piling structures started a few years ago. Most of its usage was by the navy as marine fenders. They showed better performance over other piles due to their high strength and durability. Composite piles have been installed in multiple locations of demonstration projects in the New York Metropolitan area. The Tiffany Street Pier was constructed entirely from recycled plastics (Iskandar 1998).

Composite piles are also being used for bearing as well as fendering. A group of composite piles were driven in San Diego between September and November of 1996 (Goldstik 1998). The piles were 14 in. in diameter and up to 80 ft in length with wall thickness of $\frac{1}{2}$ in. They were driven using a regular diesel hammers. Their ultimate capacities exceeded 240 kips. It was found that these piles were capable of absorbing high energy when they are driven hollow. They have tensile strengths around 60 ksi and a compressive strength of 55 ksi with an axial wall stiffness of 3,000,000 psi. Their flexural stiffness can be increased by concrete filling before or after driving.

2.5.1 THE 69TH STREET COMPOSITE PIER

The 587 ft long pier was located in the Bay Ridge, Brooklyn, New York with a total of fifty bents mainly of timber piles and reinforced concrete deck. Underwater surveys found that the timber piles were severely damaged because of a marine borer attack. The New York City then decided to replace the deteriorated pier and construct new pier. The construction company chose to reconstruct the pier with fiber reinforced composite piles. The selection of composites was due to their specific advantages over other traditional materials. The chosen material offers several advantages (Goldstick 1998): durability, lower maintenance cost and lower life cycle cost. Also it has the flexibility to be manufactured in different shapes and it has the ability to be joined which led to lower construction cost and time.

The construction engineering company selected the E-glass reinforcement in vinyl ester resin to maximize performance and reduce cost. The reinforcement fabrics were selected with the fibers tailored to the direction of maximum performance. Mechanical properties of the material used are shown in Table 2-1 .

Table 2-1: Mechanical properties of the composites used (Goldstick 1998).

Property	Material				
	E-glass Unidirectional	E-glass Triaxial TVM 3408	E-glass Quadraxial QM 5608	Balsa 15.5 pcf	Balsa 9.5 pcf
E ₁₁ (Msi)	7.00	3.45	3.00	1.12	0.59
E ₂₂ (Msi)	1.67	2.23	3.00	1.12	0.59
E ₃₃ (Msi)	1.65	1.9	1.50	1.12	0.59
X _t (ksi)	80.00	82.00	60.00	3.45	1.90
X _c (ksi)	60.00	82.00	55.00	3.85	1.90

Full scale field testing and laboratory tests proved new construction materials to be very competitive with conventional materials in terms of structural properties, durability, joinability, fabrication, and life cycle cost. The materials also are environmentally safer, UV stable and non-hazardous.

2.5.2 CAPE MAY – LEWES FERRY DOLPHINS

The Cape May – Lewes Ferry terminals are located in an area between New Jersey and Delaware. The breasting dolphins at the terminal require periodical maintenance and replacement for their timber piles. In a forward step towards reducing the cost, the owner and the river authority supported the use of high performance composite materials to replace the timber piles. The high performance composites offer high strength, corrosion and fatigue resistance, and flexibility to absorb energy when compared to timber, steel and concrete piles (Bryan 1998).

The new piles manufactured by Hardcore-DuPont Composites of New Castle, Delaware were fiber glass tubes 18” in diameter filled with concrete. The pile shell was

made of woven E-glass fibers with vinyl ester resin. The SCRIMP (Seemann Composite Resin Transfer Molding) method, in which the resin is sucked into the reinforcing composite fabric, which is already laid up dry in the molds, through distribution channels and lamina, was used in manufacturing. Mechanical properties of piles used in the project are shown in the following table.

Table 2-2: Mechanical properties of pile laminates (Bryan 1998)

Property	Kip/in.sq.
Tensile Modulus	5,210
Compressive Modulus	4,970
Tensile Strength	75
Compressive Strength	60
In Plane Shear Strength	16
Interlaminar Shear Strength	4

A test pile was driven in a local area near the project area. The pile then was loaded laterally to test the design data provided by the manufacturer. The pile sustained the test load without failure but with large deflection at the head. No apparent damage has been noticed after the pile was pulled out. The pile was then reused for other purposes in a different location.

A second verification test was for the 10 - dolphin under impact loading. The newly constructed dolphin was subjected to 2100 metric tons impact load applied by one of the Ferry vessels. The dolphin was impacted four times and the test was recorded using high speed cameras mounted on marked targets at the dolphin. The test concluded that fiberglass piles have great potential to absorb impact energy due to their superior strength and corrosion resistance. Despite their high strength, fiberglass piles are flexible and light weight and do not drive well with impact hammers. It is recommended to drive them

open with a vibratory hammer. Steel shoes can be used for unfilled piles in the areas of hard driving.

Frank March and Marie Colturi (1998) discussed the market advancement for composite marine piling in the United States. They reported an estimate of \$4.7 billion to be spent by the U.S. Department of Transportation on the shore side facilities' construction and modernization before 1999. The estimated cost for system deteriorations of the marine waterfront structures is about \$2 billion a year. The authors' recommendations were to take advantage of fiber reinforced composites to replace traditional materials for marine constructions. The new materials have the strength and capability to withstand anticipated impacts without over stressing and deflections to absorb energy of impacts. The life cycle cost of these materials is competitive for several reasons and reported by them as follows:

- Initial cost
- Driving/installation costs
- Administrative cost of purchasing/engineering
- Inspection costs
- Maintenance costs
- Removal costs
- Disposal costs
- Environmental overhead costs
- Lifetime/ frequency or replacement.

2.5.3 THE CPAR PROGRAM

In a cooperative effort between the U.S. Army Corps of Engineers' Construction Productivity Advancement Research (CPAR) Program' and other agencies and academic institutions, a research program has been initiated by the Center for Plastics Recycling Research at Rutgers University to develop, test, and demonstrate high-performance polymer composite fender, load bearing, and sheet piles for marine civil engineering applications. The program was a form of competition between manufacturers to develop innovative designs for high-performance polymer composite piles for waterfront applications. The selected products for development during that competition were analyzed and tested. Products with best potential to meet the performance criteria have been installed at selected demonstration sites.

Several manufacturers participated in the competition with different types of composite pilings. The products developed and tested under this competition involved both reinforced thermoplastic and thermoset resins with different forms of glass fibers reinforcements (i.e. continuous fibers or roving, chopped fibers, and cloths or mats) (Lampo 1998).

Composite piles in the program were mostly of circular cross-sectional composite shells, hollow or filled with concrete. Some other configurations such as a tic-tac-toe FRP pile encased with high density polyethylene (HDPE) plastic shell are also included. Fully recycled plastic matrix reinforced with FRP reinforcing bars was also available.

The candidate piling products in the program underwent a series of laboratory tests to see if they meet the performance target goals. Five different fender piling

products; five different load bearing pilings; and three different sheet pile products were selected for testing. A summary of the laboratory tests is shown in the table below.

Table 2-3: Summary of laboratory test for piles in competition (Lampo 1998a).

Pile type	Tests
Fender	Flexural test to determine EI. Cold bending (flexural) test to evaluate fracture potential in cold conditions. Cold radial compression test to evaluate behavior in a crushing mode.
Bearing	Flexural test to determine EI (for buckling). Compression to determine compressive strength and load capacity. Creep measurement.
Sheet	Flexural test to determine EI and bending strength. Determine potential for built-up structures (to increase moment of inertia).

Three types of laboratory tests were conducted on piles. The tests were selected upon the recommendations of the research team based on the types of loading situations and weather conditions that these piles may be subjected to.

1. Radial Compression test “Screening”, at -40 deg. F (-40 deg. C), 100 percent/minute Strain Rate. This test was to evaluate the pile capacity of energy absorption without causing any permanent damage to the pile. Fender piles are usually used in the ports to protect structures from ship impacts. This experiment is meant to evaluate usefulness in an installation where a boat impinges on a pile backed by a concrete slab.

Samples were tested on a full cross section at a radial compression strain rate of 100 percent per minute. The piles were loaded to failure, or past 20 percent strain, whichever came first. A summary of the test results is shown in the following table.

Table 2-4: Summary of average results for cold radial compression tests on fender pile specimens (Lampo 1998a).

Company Name	NO. of piles tested	Initial Slope of F/D* curve (lb/in)	Force at Failure	Displacement at failure (in)	Energy Absorbed (lb-ft)	Indication of Failure
Lancaster Composite	1	120,718	9,435	0.29	23	Yes
Creative Pultrusions Type 1	1	6,513	20,750	1.34	595	Yes
Creative Pultrusions Type 1 Skewed	2	8,222	975	0.32	15.5	Yes
Creative Pultrusions Type 2	2	7,850	50,000+	1.10	590+	No
Creative Pultrusions Type 2 Skewed	2	4,806	7,875	1.40	311	Yes
Trimax	3	346,710	22,728	0.28	44	Yes
Seaward	4	317,151	18,237	0.18	26	Yes
Hardcore Type 1	3	584	492	----	12	No
Hardcore Type 2	4	1,727	1,150	----	29	1-yes 3-no
Hardcore Type 3	4	4,871	2,875	2.23	71	Yes
Wood, new chemically treated	3	1,503,125	80,438	0.39	42	Yes
* F/D : Force/ Displacement						

2. Flexural Test to Determine EI. The resistance of piles to bending forces is an important engineering issue. Stiffness in fender piles is a very important property relative to energy absorption. The bending stiffness of a pile or column is dependent on the elastic modulus and the moment of inertia of the cross section. This test was performed on two different categories of fender piles: a long span with a minimum length of 22 ft and a short span of 10 ft length with a pile diameter of 12 to 16-in.. Testing was performed on long and short

spans to estimate the error associated with using the less expensive (shorter span) and testing to correlate properties. The test also included recycled plastic reinforced pile and the fiber reinforced concrete filled pile. Results showed that all the composite piles tested at long spans exceeded the target EI of 600×10^6 lb-sq in.. Short span results of recycled plastic reinforced pile showed a reduction in EI when compared to long span results. A 36 percent decrease in EI for a short span has been noticed. On the other hand, the fiber reinforced concrete filled piles showed better results.

In load bearing piles, stiffness is also an important issue regarding resistance to buckling during pile driving or when the pile is in service. Flexural testing was also performed on load bearing piles similar to that done on fender piles. No results have been reported on this test.

3. Compression testing of load bearing piles. This test is also performed on both the reinforced recycled matrix pile and the FRP concrete filled piles. Five feet long test specimens were used to minimize the possibility of buckling. Compression was conducted until specimen failure or until reaching the machine load limit. Test results showed that some piles satisfied the performance goals and reached the design limit and others failed to reach that goal.

Table 2-5: Bearing pile compressive test results (Lampo 1998a).

Manufacturer	Compressive failure load, kips	Cross-sectional area, sq-in	Compressive failure stress, ksi	Modulus, E psi x 10 ⁶
Creative Pultrusions	248.5	14	17.8	5.1
Hardcore Composites	765.6	148.5	5.15	0.85
Lancaster Composite	>856	130	>6.58	1.15
Seaward International	>856	201	>4.26	0.55

4. Cold Flexural Test. This experiment is meant to evaluate whether a piling in a system designed for bending will be subject to fracture at small strains at low temperatures. A piling that is excessively brittle at low temperatures is undesirable and would not be able to absorb significant berthing energy. Because of size restrictions in the controlled low-temperature (-20 °F) testing room, the ASTM recommended 16:1 length: diameter (L:D) ratio could not be met, and shorter (10-ft) spans must be tested.

Practically, for all of the mechanical property testing of fender pilings, excellent correlation (within 10 percent) was found when multiple samples were tested in any given experiment.

The test results showed different variations in the mechanical properties under the different tests for the different types of piles. The tic-tac-toe pile which is mainly flat composite plates joined at 90 degrees as shown in Figure 2-1 did not satisfy the required

load limits in the compression test. The pile failed at a lower load but did take higher stress before failure than other piles in the program. This low capacity is because of the smaller cross sectional area compared to other piles. The overall performance of this pile was much better than others. A pile from Seaward international which is a recycled plastic matrix reinforced with FRP bars did satisfy the load carrying capacity and did not fail even at the limit of the testing machine but with lower stress capacity compared to Creative Pultrusions pile.

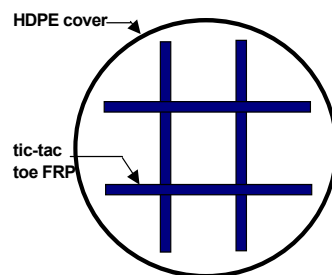


Figure 2-1: Tic-tac-toe pile of Creative Pultrusions.

Composite materials (FRP) have the advantage of high strength and durability. Its ability to corrosion resistance and other chemical attacks gives it the advantage of lasting longer than steel and concrete. Low stiffness is one of the major problems that accompanied the use of FRPs in pile structures.

Piles in bridges are subjected to different kinds of forces: axial forces due the weight of the superstructure and the vehicles, lateral forces due to temperature changes and impact and braking forces of the vehicles and soil and earth pressure in the substructure. To overcome the problem of lack of stiffness of composite materials, the hybridization technique can be used by combining the FRP with another stiff material like steel or concrete.

Flexural testing of the standard Hardcore Composites tubular piling was performed at the ATLSS Multidirectional Laboratory at Lehigh University. Specimens were tested filled with concrete. The nominal concrete strength was 4000 psi. Each specimen was tested in three-point bending with a 16:1 span to diameter ratio. Load was applied at mid-span.

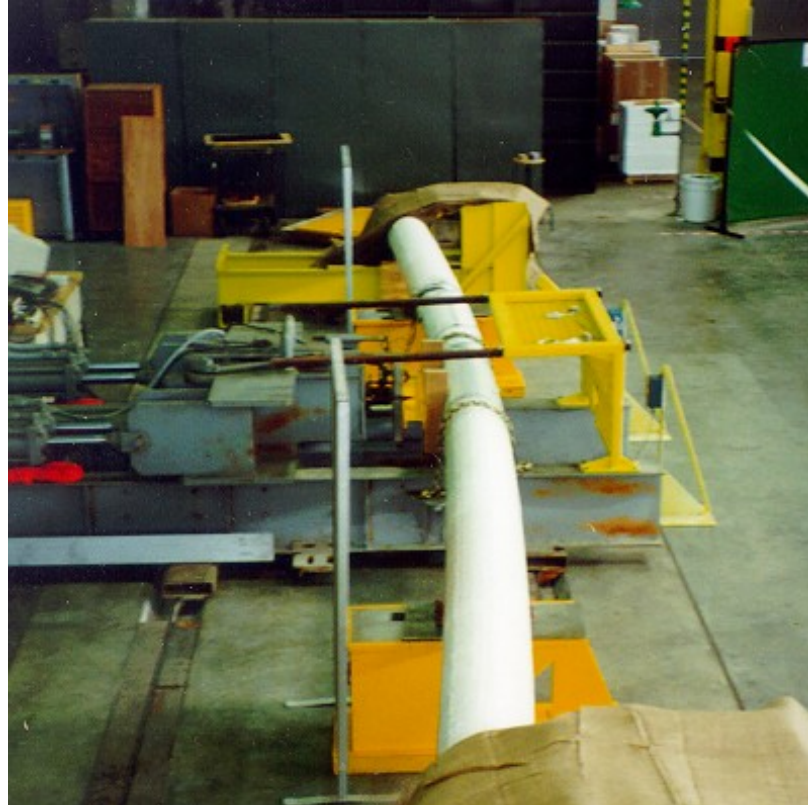


Figure 2-2: Three-point bending test (HardCore).

Testing protocol consisted of loading to 25% of predicted maximum deflection at a rate of two inches per minute; return to zero; load to 50% of predicted maximum deflection; return to zero; then finally test to failure. Table 2-6 lists the ultimate flexural properties of the standard tubular piling.

Table 2-6: Flexural Data: Fiberglass Tubular Piling (Hardcore).

Specimen No.	Bending Stiffness, EI (lb-in²)	Ultimate Bending Moment (in-lb)
1	4.49 x 10 ⁸	1.15 x 10 ⁶
2	9.78 x 10 ⁸	2.04 x 10 ⁶
3	1.38 x 10 ⁹	2.80 x 10 ⁶
4	1.76 x 10 ⁹	3.43 x 10 ⁶
5	4.59 x 10 ⁹	5.66 x 10 ⁶
6	5.78 x 10 ⁹	7.60 x 10 ⁶

2.5.4 THE NELP PROGRAM

This program was initiated in support of the Navy Environmental Leadership Program (NELP) and Tetra Tech EM inc. to evaluate the using of fiberglass and steel reinforced pilings installed in several naval station locations. Two types of piling were in the study: fiberglass –reinforced and steel-reinforced. The fiberglass pilings consist of a foamed plastic in the core reinforced with fiberglass bars incased in a dense plastic shell from the outside. The plastic inner core is made of 100 percent recycled plastic obtained from recycled plastic materials, such as plastic milk jugs. The fiberglass reinforcing bars are arranged in a concentric pattern within the inner core of the plastic piling and extend the entire length of the piling (Tetra 1999). The plastic piling evaluation focused on assessing the plastic piling durability, strength, cost, and environmental integrity.

The main objectives of this program were to provide plastic piling users with the necessary technical information that enables them to assess and evaluate the piling applicability for different sites. Plastic pilings have many performance characteristics

over traditional pilings, such as their high capacity of energy absorption and capability of reserving capacity even after yielding.

The study included two types of plastic pilings: fiberglass reinforced and steel reinforced piles. The fiberglass reinforced plastic piles which are manufactured by Seaward International consists of an outer skin of high density plastic and inner core of 100% recycled plastic matrix.

2.6 HYBRIDIZATION TECHNIQUE

A hybrid pile system consists of a concrete section that is reinforced with an FRP shape. The FRP shape can be in the form of a filament-wound shell or tube, plate, panel, or pultruded section. The most common characteristics of hybrid systems are as follows: (a) the FRP shape acts as permanent form for concrete, (b) reinforcement for concrete is provided externally and solely by the FRP shape, (c) capacity and performance of the system both depend on the composite action between concrete and FRP, and (d) the system lends itself to optimization based on material properties of each component.

Studies done in the past mostly dealt with steel, concrete and timber piles or their combinations. Due to the difference in material properties and structural behavior between FRPs and traditional materials, the results and findings of these studies may not be valid for the new materials. New studies and extensive research should be performed concerning the FRP materials and their applicability in bridge structures. The studies should include all factors that affect the safety and life of the structure.

2.7 COMPOSITE PILES IN THE MARKET

As stated earlier, FRP composite piles have gained some acceptance in the construction market in the last few years. Their use has been limited to waterfront barriers, fender piles, and bearing piles for lightweight structures.

Many manufacturers are currently producing FRP composite piles. Most of the products are made of glass fibers in a resin matrix. The most common glass fiber used in piling products is E-glass (lime aluminum borosilicate) because it has acceptable strength properties and reasonable price.

Seaward International, Inc.

Seaward International, Inc. produces high performance energy absorption and structural protection products for marine applications (Seaward). Their products include foam-filled marine fenders and buoy, plastic piling and timber. The marine fenders are manufactured using heat-laminated flexible resilient foam inside the fender and a high quality filament-reinforced polyurethane elastomer skin. The fenders are available in a wide variety of diameters and lengths, from the 2 ft x 4 ft (0.6 m x 1.2 m) to the tanker-scaled 14 ft x 28 ft (4.3 m x 8.5 m). The company claims that all Seaward fenders meet the operational performance expectations the industry has grown to depend on.

SEA GUARD Fenders are fabricated from closed-cell resilient foam that absorbs significant quantities of energy when compressed. The foam is protected by a thick, filament reinforced elastomer skin. The claim is that this construction offers a number of important features and advantages:

- High energy absorption with low reaction force
- Tough outer skin that won't snag hull protrusions or dock fittings

- Totally buoyant - won't sink if punctured
- Burst resistance
- Low maintenance
- Reliable performance
- Simple installation.

SEAPILE and SEATIMBER composite marine products are plastic piling and timbers made from 100% recycled plastic, which provide alternatives to traditional chemically treated wooden piling and timbers.

Reinforced with fiberglass rebar for added strength, SEAPILE and SEATIMBER Composite Marine Piling and Timbers are also abrasion resistant, and the plastic matrix incorporates ultraviolet inhibitors to ensure a long life. They are environmentally safe and are impervious to marine borers.

Seaward's SEAPILE[®] composite marine piling is a high-performance, environmentally-friendly replacement for traditional wood piling. The piling has a round cross-section with diameters of 10 inch (250mm), 13 inch (330mm), and 16 inches (400mm). SEAPILE composite marine piling is made of plastic, which has been structurally reinforced with fiberglass reinforcing bars, making the product non-corrosive as well as impervious to marine borers.

Table 2-7: Composite piling specifications (Seaward)

Piling Size (Diameter)		Number and Size of Reinforcements			Stiffness, EI		Weight per foot (meter)	
in	mm	#	in	mm	lb-in ²	kN•m ²	lb/ft	kg/m
10	250	6	1	25	2.25E+08	647	24 - 29	36 - 43
10	250	6	1.25	32	3.06E+08	878	25 - 31	37 - 46
10	250	6	1.375	35	3.54E+08	1017	26 - 32	38 - 47
10	250	8	1	25	2.84E+08	817	25 - 30	37 - 45
10	250	8	1.25	32	3.92E+08	1 125	26 - 32	39 - 48
10	250	8	1.375	35	4.57E+08	1 311	27 - 33	40 - 49
10	250	8	1.5	38	5.26E+08	1 509	28 - 35	42 - 51
13	330	8	1	25	6.57E+08	1 886	39 - 48	59 - 72
13	330	8	1.25	32	8.90E+08	2 556	41 - 50	61 - 75
13	330	8	1.375	35	1.03E+09	2 959	42 - 51	62 - 76
13	330	12	1	25	9.17E+08	2 633	41 - 50	61 - 74
13	330	12	1.25	32	1.27E+09	3 639	43 - 53	64 - 79
13	330	12	1.375	35	1.48E+09	4 243	45 - 55	66 - 81
13	330	12	1.5	38	1.70E+09	4 883	46 - 57	69 - 84
16	400	16	1	25	2.00E+09	5 746	61 - 74	90 - 111
16	400	16	1.25	32	2.76E+09	7 911	64 - 78	95 - 117
16	400	16	1.375	35	3.21E+09	9 210	66 - 81	98 - 120
16	400	16	1.5	38	3.69E+09	10 584	68 - 83	101 - 124

Hardcore Composites

The Hardcore Composites tubular pile was described earlier in this chapter. The pile mainly consists of a high strength fiber reinforced cylindrical shell that can be driven either with a driving shoe or be driven open-ended. Hardcore uses the Vacuum Assisted Resin Infusion Method (VARTM) in manufacturing their products. Piles produced in this method have less than 0.5% voids in the composite. Tubular piling products are available in standard size diameters from 10 to 18 inches. In addition to the standard sizes, custom size production is up to 60 inches in diameter with any shippable lengths. Table 2-8 lists the standard piling products of Hardcore composites.

Table 2-8: Standard Composite Tubular Piling (Hardcore)

Product Identification	Nominal O.D. (in)	Fiberglass Shell Thickness (in)	Optional Acrylic Skin Thickness (in)
10-2	10.00	0.182	0.030
12-2	12.75	0.182	0.030
12-3	12.75	0.273	0.030
14-3	14.00	0.273	0.030
18-3	18.13	0.273	0.040
18-4	18.13	0.364	0.040

The tubular piling of Hardcore composites is capable of carrying compressive, tensile, shear, and torsion loads. Axial load and bending moment capacity of the pile can be improved by using concrete filler in the pile. The inner surface of the tube can be roughened to develop mechanical interlock between the concrete and the piling

composite material. Results of flexural testing of the standard Hardcore Composites tubular piling filled with concrete of a 4000 psi nominal strength are listed in Table 2-9.

Table 2-9: Fiberglass tubular piling flexural data (Hardcore)

Product Identification	Bending Stiffness, EI (<i>lb-in²</i>)	Ultimate Bending Moment (<i>in-lb</i>)
10-2	4.49×10^8	1.15×10^6
12-2	9.78×10^8	2.04×10^6
12-3	1.38×10^9	2.80×10^6
14-3	1.76×10^9	3.43×10^6
18-3	4.59×10^9	5.66×10^6
18-4	5.78×10^9	7.60×10^6

Lancaster Composites

Lancaster Composites produces a composite pile similar to that of hardcore with a commercial name CP40. It consists of fiber reinforced polymer shell filled with high strength concrete core which acts compositely with the polymer shell. The FRP shell provides the necessary strength to resist tension and bending forces while the concrete core increases the compression capacity as well as flexural rigidity and protection for the pile from damage. Table 2-10 shows the mechanical properties of some of their products. Figure 2-3 shows a picture of piles installation in the field.



Figure 2-3: Lancaster Composites piling installation.

Table 2-10: Physical properties of Lancaster composite piling

Property	Value
Bending Stress	25,000 psi
Bending Modulus	2.8×10^6 psi
Compressive Stress	25,000 psi
Compressive Modulus	2.8×10^6 psi
Shear Stress	8,000 psi
Water Absorption	0.07%
Strain	0.09%
Density	145 lbs/ft ³

According to Lancaster Composites, the composite pile CP40 has several benefits some of them are list below:

- Cannot rust, rot, or corrode. Withstands harsh environments (salt, harsh chemicals, low temperatures, freeze/thaw, etc.)
- Not subject to marine borer damage.
- Low/No maintenance.
- 75 year plus service life.
- Reliable design loads.
- Piles available in any length, any quantity.
- Standard Sizes: 6", 8", 10", 12", 14", 16" OD's. Continuous lengths up to 115 feet. (Monopiles & columns up to 8' OD available.)
- Cost: Competitive with traditional materials of similar strength, corrosion resistance, and service life
- Skin Friction / Capacity: Overwrap of glass roving wrapped into the lower section of the FRP tube during manufacture creates surface ridges, resulting in exceptional skin friction.

2.8 DRIVABILITY OF FRP COMPOSITE PILES

Drivability is a major requirement for a pile to be accepted as a load carrying structure. A pile should have the ability to be driven to the designated depths without any damage or change in physical and mechanical properties. Material stiffness and strength are the major properties that usually determine the pile drivability.

Hardcore composites conducted a test program on installation and loading of fiberglass tubular piling in New Castle, Delaware. A composite tubular piling is a cylindrical shell fabricated of high-strength fiber reinforced composite materials as shown in Figure 2-4. The outer surface of the shell can be coated with a rubber toughened, acrylic skin. The acrylic skin provides additional protection against abrasion, ultraviolet (UV) light, and chemicals.

The inner surface is textured to create a mechanical lock with a filler material, usually concrete. The piling is molded, shipped and driven as a hollow shell and then is filled with concrete or other appropriate core material. If required, the piling can be filled with concrete at the factory and shipped as a complete unit.

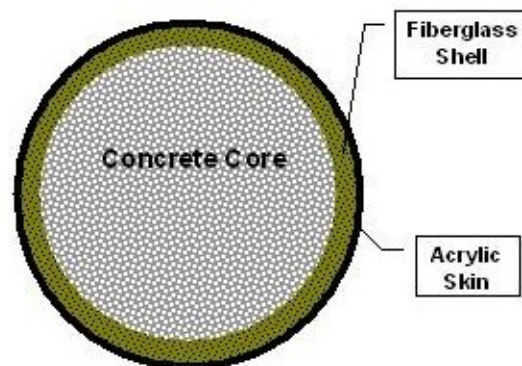


Figure 2-4: Hardcore piling.

The resulting structure is a piling system with approximately the same stiffness as timber piling, but is 4 times stronger and 15 times more energy absorbent.

The project included installation, dynamic testing, and static load testing of Hardcore fiberglass tubular piles at a site on the premises of the Hardcore pile production plant (Hardcore 1997). A group of fifteen Hardcore piles in addition to steel and timber piles were driven to refusal in the test site. The steel and timber piles were included in the test program for comparison purposes only. The composite piles were made of an acrylic-coated fiberglass shell with length from 15 ft to 60 ft and diameter of 10 in to 12 in.. The wall thickness was from 0.182 in. to 0.364 in. Pile installation was by using a pile driving crane with a 46ft-kips per blow hammer.

The test piles were driven to depths from 6.5 to 32 feet before encountering refusal (12 blows or more per one inch) or exhibiting head damage. Half of the hollow piles were driven open-ended and the other half using a steel boot plate. The timber pile was driven to the full length of 42 feet. The steel pile was driven to a depth of 15 feet before the top of the pile was damaged by hard driving. Static load tests, in accordance with ASTM D-1143, were performed on 6 of the test piles. Load was applied incrementally from 3- to 10-tons with loading period of 2.5- to 15-minutes. Tests continued till reaching ultimate pile failure. The ultimate failure load was taken as the load at which the pile settlement continues to increase substantially without any load increment, the plunging failure load.

Hardcore composite piles showed good performance in the test program. The test proved that these piles can be driven using the conventional driving equipment. In hard driving conditions “brooming” of the pile top may occur especially at refusal blow count.

Most piles in the test failed at the pile top because of brooming. Using thicker wall piles at the top or a pile cap with enclosure is recommended in hard driving conditions.

Bending of long piles (40 to 70 feet) during installation at the midspan point was also observed. Using a restraining system is recommended during pile installation in hard soils so that it will support the pile against lateral movement.

In a technical paper published in 2001, Ashford and Jakrapiyanun presented a review of several composite pile designs that are currently available in the market. Their study included driving analysis of six piles with different size and material properties. Two piles were conventional material pilings: square precast, prestressed concrete pile and steel pipe pile. The other four were FRP composite piles with different manufacturing techniques selected for comparison purposes. Pile types and material properties are listed in Table 2-11 as presented by the authors.

Table 2-11: Piling material properties (Ashford et al 2001)

Pile (1)	Outside diameter (cm) (2)	Inside diameter (cm) (3)	Area A (cm ²) (4)	Moment of inertia I (cm ⁴) (5)	Stiffness EI (kN · m ²) (6)	Impedance ρcA (Mg/s) (7)	Impedance ratio (8)
CON	— ^a	— ^a	929	71,900	22.32	790	9.9
CON/GFRP ^b	32.5	30.5	830	54,800	17.01	690	8.6
STL	34.0	32.1	99	13,440	26.88	390	4.9
STL/PE	25.4	22.4	113	8,120	22.64	450	5.6
GFRP/RTM	35.6	33.0	137	20,100	4.58	90	1.1
GFRP/FW	38.1	35.6	147	24,900	4.30	80	1

^aSquare concrete pile 30.5 by 30.5 cm.

^bInside of pipe filled with concrete.

Pile type (1)	Abbreviation (2)	γ (kN/m ³) (3)	ρ (Mg/m ³) (4)	E (MN/m ²) (5)	c (m/s) (6)	Compressive strength ^a (MPa) (7)	Tensile strength ^a (MPa) (8)
Standard concrete	CON	22.8	2.32	31	3,660	24.5	6.3
Concrete filled GFRP pipe	CON/GFRP	22.8	2.24	31	3,720	29.3	1.4
Standard steel pipe	STL	77.0	7.85	200	5,050	223	223
Plastic encased steel pipe	STL/PE	77.0	7.85	200	5,050	329	329
RTM GFRP pipe	GFRP/RTM	18.9	1.92	23	3,440	345	517
Filament wound GFRP pipe	GFRP/FW	17.6	1.79	17	3,100	345	517

^aAllowable strength for steel and concrete from ASCE (1997).

The driving analysis was performed on the test piles and concentrated on the axial stresses induced in each pile during driving and the ultimate bearing capacity of the pile based on penetration resistance. The study considered two soil profiles; the first profile is dense sand overlaid by soft clay layer where 90% of the total capacity was contributed by end bearing. The second profile was mainly a thick layer of stiff clay where only 10% of the total pile capacity was contributed by end bearing.

Three different single acting diesel hammers were used:

- Small hammer with 32 kN.m rated energy.
- Medium hammer with 69 kN.m rated energy.
- Large hammer with up to 153 kN.m rated energy.

The study results were presented for all piles on an ultimate bearing capacity basis and penetration resistance as shown in Figure 2-5 below. The allowable driving stresses were not exceeded.

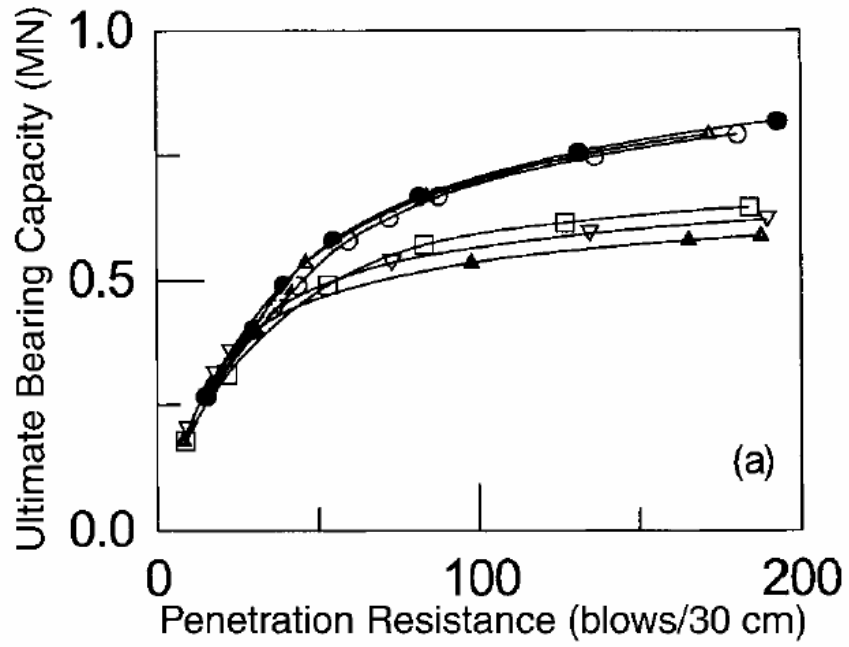


Figure 2-5 (a)

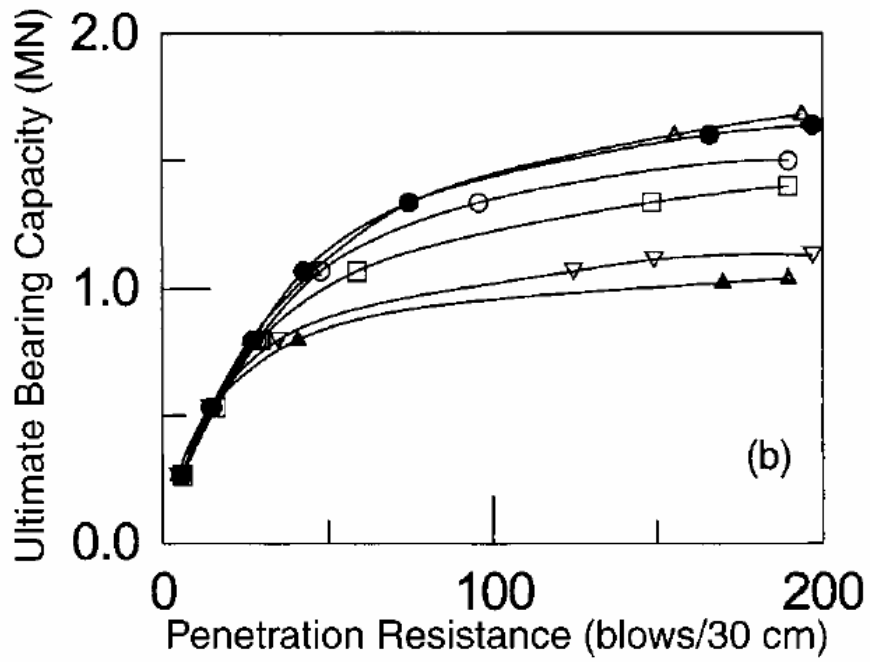


Figure 2-5 (b)

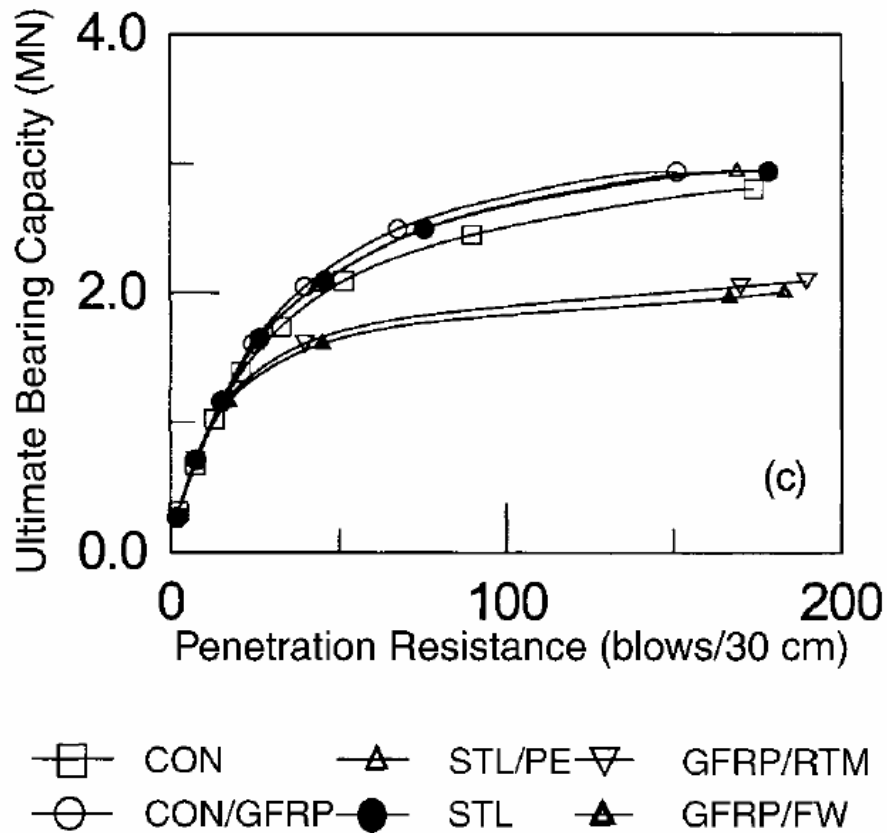


Figure 2-5 (c)

Figure 2-5: Ultimate bearing capacity as a function of penetration resistance for (a) 31-kN.m Hammer; (b) 69-kN.m hammer; (c) 151-kN.m hammer (Ashford et al 2001).

Iskander et al (2001) presented a review for the current market products of piles and piling materials, Figure 2-6. They performed a theoretical parametric study on the effect of various pile properties and soil conditions on the drivability of FRP composite piling in a typical waterfront site. The parametric study utilized the wave equation analysis of piles (WEAP) to investigate the influence of the different parameters on the drivability of composite piles. The findings and conclusions were summarized by the authors as follows:

- The modulus of elasticity and specific weight are the main factors that affect the drivability of polymeric materials, while drivability of stiffer materials is governed by the soil properties.
- On theoretical basis, driving of polymeric piles is more efficient when using a single-acting steam hammer
- Single –acting steam hammers appear to be more efficient than diesel hammers in driving polymeric piles as shown in Figure 2-7.

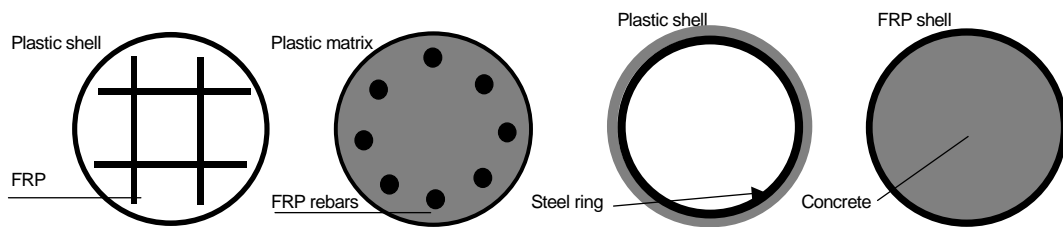


Figure 2-6: Different pile configurations available in the market.

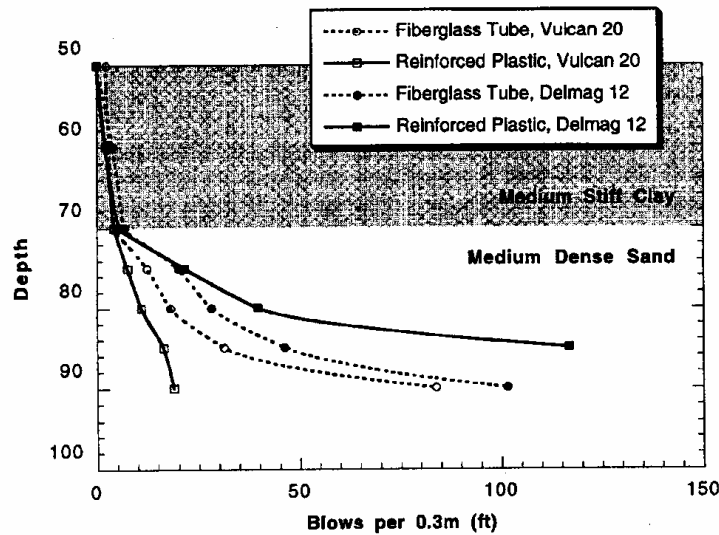


Figure 2-7: Drivability of polymeric piles using different hammers (Iskander et al 2001).

MECHANICS OF COMPOSITE MATERIALS

3.1 INTRODUCTION

A composite material is a combination of two or more materials different in form or composition on a macro scale and act as unit to perform a particular function. In civil engineering, an FRP composite can be defined as "A matrix of polymeric material that is reinforced by fibers or other reinforcing materials".

Classical composites generally consist of a polymer matrix reinforced with fibers. A polymer matrix may have the form of polyester, vinylester, epoxy, phenolic, thermoplastic, etc. The reinforcement fibers can be made of glass, carbon, aramid, etc. Other terminology for composites include fiber-reinforced plastic, glass fiber reinforced plastic (GFRP), carbon fiber-reinforced plastics (CFRP), reinforced plastics (RP), and others.

The use of composite materials was started about 50 years ago. Along the years composite materials proved to be extremely effective in high-performance applications where traditional materials have failed, especially in aggressive environments.

3.2 MATERIAL COMPOSITION

From its definition, a composite material is a mix of more than one material combined together to form a new material with different properties and behavior. Generally, a composite material consists of reinforcement, resin, and core material.

Fiber reinforced composite materials consist of fibers embedded in a resin matrix to act as a single unit. The constituent materials usually retain their physical and chemical identities in their new form. The new product will have improved properties with higher performance than if the constituents act separately. Fibers are principal components of the composite work as reinforcement that provide strength and stiffness to the composite. They have higher strength and stiffness than conventional materials or the bulk material that the fibers made were from. Resins which are used as a matrix to contain the fibrous reinforcement in a composite material are an organic polymer or prepolymer. The organic matrix may be a thermoset or a thermoplastic and may contain a wide variety of components or additives to influence handleability, processing behavior, and ultimate properties (Military 1997).

Glass fibers are the most common materials used in reinforced plastics because of their relative strength and reasonable cost. Almost 90% of the reinforced plastics used are made of glass fibers. E-glass (lime aluminum borosilicate) is the most commonly used glass fibers. Typical E- glass fibers have a tensile strength of 500 ksi and an ultimate elongation of 4.8% (Eric 2000). Core materials are any materials that can physically separate strong, laminated skins and transmit shearing forces across the sandwich (Eric 2000).

Fibers and resin are combined together to form a composite unit (lamina). A lamina is a single ply arrangement of unidirectional fibers in a matrix. The laminae are stacked together in different fiber orientations to form a laminate. The fibers work as reinforcement for the lamina. The resin serves to transmit loads between the plies.

The basic mechanism in the fiber-resin system is that the resin which surrounds and bonds every fiber in the unit transmits the load to the fiber through shear stress τ as shown in Figure 3-1. Because of the tension force F , a shear stress acts on the outer surface of the fiber. This stress will cause a tensile stress σ within the fiber. The shear stress on the surface of the fiber is high near the ends of the fiber, and the tensile stress within the fiber is low. As the distance from the end increases, the shear stress decreases and the tensile stress increases. After a certain distance from the end, the shear stress becomes very small and the tensile stress reaches its maximum value.

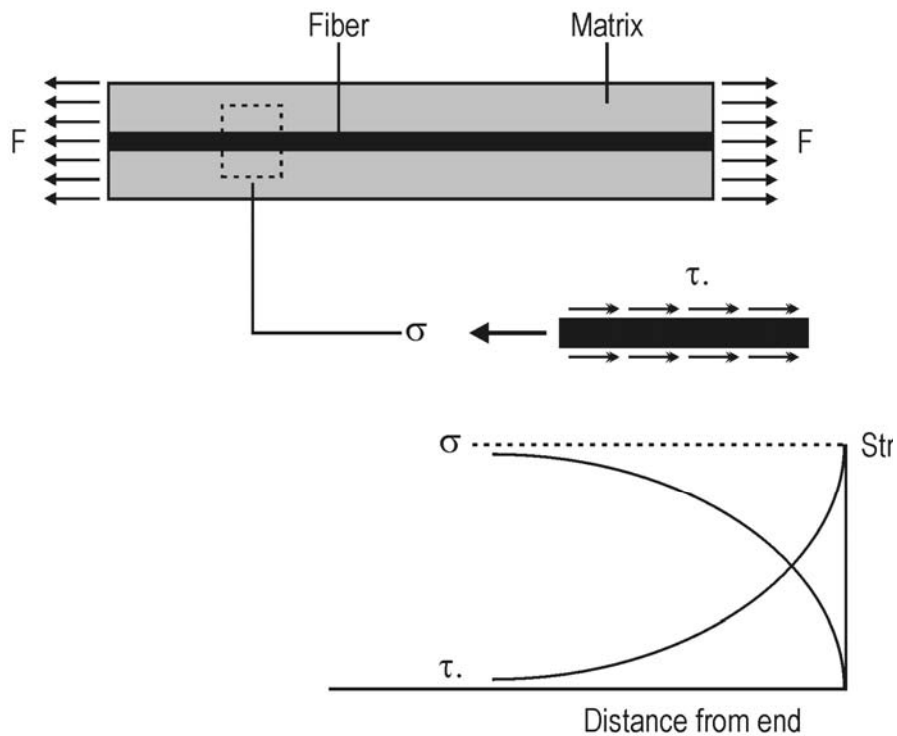


Figure 3-1: Load transfer between fiber and resin.

3.2.1 REINFORCING FIBERS

Fibers are the major part of the fiber-reinforced composite material. They usually contribute more than 50% of the volume fraction of the composite structure and carry the major portion of the applied load. Reinforcement fibers have some superiority over other materials because of their high stiffness, strength and light weight. Fibers do not necessarily need to be used in a continuous form. They can be used in a continuous or discontinuous form in the composite as desired. When used as continuous reinforcement, they have to be aligned in the matrix with required percentage and direction.

Different types are available for commercial use. The most common types are carbon, glass, Kevlar, and boron fibers. Table 3-1 lists some of these fibers with their physical and mechanical properties.

3.2.1.1 GLASS FIBERS

Glass fibers are the most commonly used fibers in composites reinforcement. They have relatively good strength and stiffness; besides, they are inexpensive compared to other types of fibers. Because of these characteristics, they account for almost 90% of the fibers used in the low-cost composite industry. Glass fibers are silica based materials in which silicone dioxide (SiO_2) occupies more than 50-60% of the chemical composition of the fibers. They also contain other oxides like calcium, boron, sodium, aluminum, and iron. Table 3-2 shows the composition of some commonly used glass fibers.

Table 3-1: Typical values of fiber properties.

Fiber	Axial Tensile Modulus, GPa (10 ⁶ psi)	Axial Tensile Strength, MPa (10 ³ psi)	Axial Elongation at Break, percent	Density, g/cm ³ (lb/ft ³)
Carbon—low modulus	170 (24.6)	1380 (200)	0.9	1.90 (119)
Carbon—high modulus	380 (55.1)	1720 (249)	0.4	2.00 (124)
Carbon—very high modulus	760 (110)	2210 (320)	0.3	2.15 (135)
E—glass	81 (11.7)	3450 (500)	4.88	2.60 (162)
S—glass	89 (12.9)	4590 (666)	5.7	2.48 (155)
Aramid—high toughness	83 (12.0)	3620 (525)	4.00	1.44 (90)
Aramid—high modulus	131 (19.0)	3620-4140 (525-600)	2.80	1.44 (90)
Aramid—very high modulus	186 (27.0)	3450 (500)	2.00	1.47 (92)

¹ From *Engineered Materials Handbook (1987)* and *Engineers' Guide to Composite Materials (1987)*.

Table 3-2: Chemical composition for glass by weight (Eric Green 2000)

	E-Glass	S-Glass
Silicone Dioxide	52 - 56%	64 - 66%
Calcium Oxide	16 - 25%	0 - .3%
Aluminum Oxide	12 - 16%	24 - 26%
Boron Oxide	5 - 10%	—
Sodium & Potassium Oxide	0 - 2%	0 - .3%
Magnesium Oxide	0 - 5%	9 - 11%
Iron Oxide	.05 - .4%	0 - .3%
Titanium Oxide	0 - .8%	—
Fluorides	0 - 1.0%	—

Three types of glass fibers are available for commercial use. E-glass (Electrical) fibers is the most popular reinforcement used where high strength and chemical resistance's needed. It is usually used in marine constructions because of its good resistance to corrosion and water degradation. S-glass (where S stands for strength) has better tensile strength and better fatigue resistance compared to E-glass. It has a limited use because its cost is about three to four times that of E-glass. C-glass (C for corrosion) has better corrosion resistance than other glasses and is limited to corrosion resistance applications.

3.2.1.2 CARBON FIBERS

Carbon or “graphite” fibers are strong light fibers containing at least 90% carbon usually produced by subjecting organic precursor fibers such as polyacrylonitrile (PAN) or rayon to a sequence of high temperature until the precursor converted to carbon by pyrolysis. Those kinds of fibers are the most dominant in the aerospace industry because of their high strength and stiffness of all commonly used fibers. Carbon fibers are very brittle materials; they usually fail at a very low strain when subjected to bending.

The major factor that limits the widespread use of carbon fiber is the high cost. Carbon fiber costs approximately five to seven times the cost of glass fibers.

3.2.2 RESINS

Epoxy Resins

Epoxy resins have the best performance in the resins family because they contain a reactive functional group in their molecular structure. They are used in advanced composite materials for structural and aerospace applications more than all other resins. That's because of their several advantages over other resins such as their mechanical

properties, resistance to chemicals, and excellent adhesion with most fiber types. The only obstacles that limit their wide use are the high cost and long curing times.

Polyester resins

Polyester resins are the most economical and widely used resins in composites manufacturing. They can be produced in mass quantities with lower cost and a wide range of properties. Their rigidity can be controlled by the ratio of saturated to unsaturated acids.

Vinyl ester resins

Vinyl ester resins have moderate adhesive strengths compared to epoxy resins. They are prepared by the reaction of monofunctional unsaturated acid with a bisphenol diepoxide, then mixed with unsaturated monomer. They have the performance advantages of epoxies and handling properties of polyesters.

3.3 RULES OF MIXTURE

The properties of a composite laminate depend on the properties of its constituents: the resin and the fibers. The fibers' material generally determines the mechanical properties of a composite laminate. Three types of fibers are being used in the composite industry. The most common used fibers are glass fibers. The following table shows different types of fibers and their mechanical properties.

The mechanical properties of a composite are strongly influenced by the proportions and properties of the matrix and the fibers. The commonly used method in expressing constituents' proportions is by volume fraction.

The fiber volume fraction is defined as the ratio of the volume of fiber to the total volume,

$$V_f = \frac{\text{volume of fiber}}{\text{total volume}} \quad (3-1)$$

and the matrix volume fraction is also given in a similar manner

and as a result

$$V_f + V_m = 1 \quad (3-2)$$

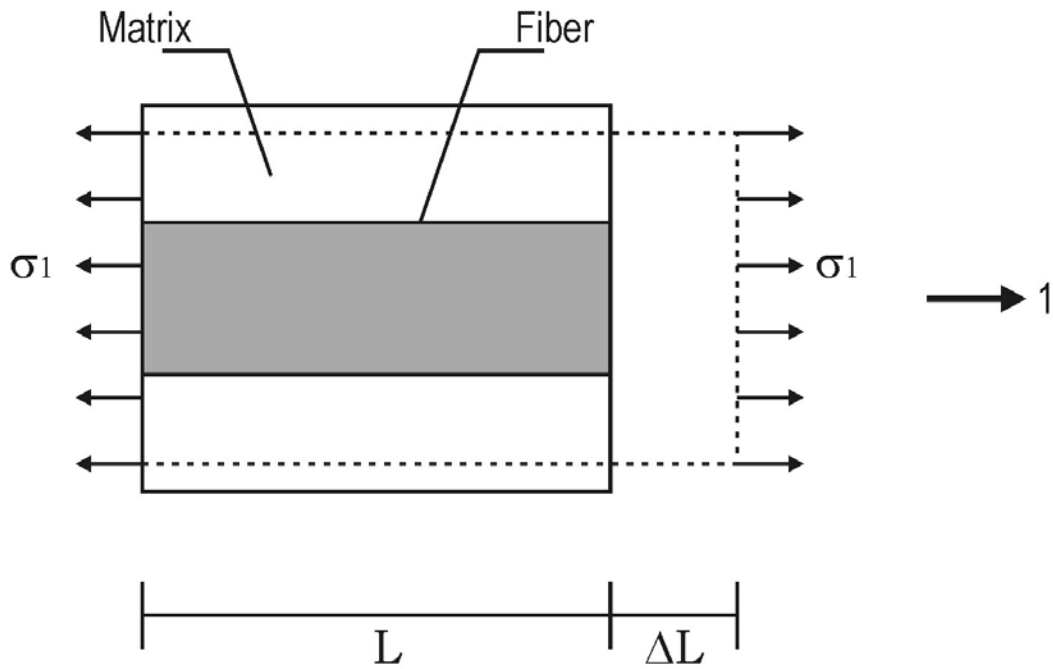


Figure 3-2: Deformation of a composite element under axial tensile stress.

For a composite element of initial length L loaded in 1- direction as show in Figure 3-2, an elongation of ΔL in the direction of loading has occurred. The strain in the composite can be given as

$$\varepsilon_1 = \frac{\Delta L}{L} \quad (3-3)$$

where ε_1 applies to both the fiber and the matrix. Since both materials are isotropic and elastic then the stress-strain relation in the direction of fiber can be given as

$$\sigma_f = E_f \cdot \varepsilon_1$$

$$\sigma_m = E_m \cdot \varepsilon_1$$

The total area on which stress is applied is the summation of the fibers area and matrix area

$$A = A_f + A_m$$

Then the total force on the composite element can be given as

$$P = \sigma_1 A = \sigma_f A_f + \sigma_m A_m$$

Then

$$\sigma_1 = \varepsilon_1 (E_f V_f + E_m V_m)$$

where

$$V_f = \frac{A_f}{A} \quad \text{and} \quad V_m = \frac{A_m}{A}$$

and

$$\sigma_1 = E_1 \varepsilon_1$$

From that it can be found that

$$E_1 = E_f V_f + E_m V_m \tag{3-4}$$

This equation is known as the rule of mixtures for the apparent Young's modulus of the composite material in the fibers direction (Jones 1999).

The apparent modulus in the transverse direction can be calculated in a similar manner

$$E_2 = \frac{E_f E_m}{V_m E_f + V_f E_m} \tag{3-5}$$

3.3.1 STRESS-STRAIN RELATIONS

The stress strain relations for a composite material can be expressed using Hooke's law

$$\sigma_i = C_{ij} \varepsilon_j \quad i, j = 1, \dots, 6 \quad (3-6)$$

where σ_i , and ε_i , are the stress and strain vectors respectively and C_{ij} is the material elastic stiffness matrix.

In orthotropic materials where there are two orthogonal planes of material symmetry, the stress-strain relations can be expressed with nine independent constants in the stiffness matrix in the form

$$\begin{bmatrix} \sigma_1 \\ \sigma_2 \\ \sigma_3 \\ \tau_{23} \\ \tau_{31} \\ \tau_{12} \end{bmatrix} = \begin{bmatrix} C_{11} & C_{12} & C_{13} & 0 & 0 & 0 \\ C_{12} & C_{22} & C_{23} & 0 & 0 & 0 \\ C_{13} & C_{23} & C_{33} & 0 & 0 & 0 \\ 0 & 0 & 0 & C_{44} & 0 & 0 \\ 0 & 0 & 0 & 0 & C_{55} & 0 \\ 0 & 0 & 0 & 0 & 0 & C_{66} \end{bmatrix} \begin{bmatrix} \varepsilon_1 \\ \varepsilon_2 \\ \varepsilon_3 \\ \gamma_{23} \\ \gamma_{31} \\ \gamma_{12} \end{bmatrix} \quad (3-7)$$

This equation applies for an orthotropic material in a state of three-dimensional stresses. Composites are generally used in a form of plates or shells or members with a very small thickness compared to the two other dimensions, so a two dimensional analysis is recommended. A composite lamina can not withstand high stresses in the direction other than that of the fibers, so it is not practical to subject it to unnatural stresses such as σ_3 (Jones 1999).

The strain-stress relation can also be expressed in a similar manner according to Hooke's law

$$\varepsilon_i = S_{ij} \sigma_j \quad i, j = 1, \dots, 6 \quad (3-8)$$

where S is the compliance matrix which is the inverse of the stiffness matrix C .

In expanded form, equation (3-8) can be written in the following form

$$\begin{bmatrix} \varepsilon_1 \\ \varepsilon_2 \\ \varepsilon_3 \\ \gamma_4 \\ \gamma_5 \\ \gamma_6 \end{bmatrix} = \begin{bmatrix} S_{11} & S_{12} & S_{13} & 0 & 0 & 0 \\ S_{12} & S_{22} & S_{23} & 0 & 0 & 0 \\ S_{13} & S_{23} & S_{33} & 0 & 0 & 0 \\ 0 & 0 & 0 & S_{44} & 0 & 0 \\ 0 & 0 & 0 & 0 & S_{55} & 0 \\ 0 & 0 & 0 & 0 & 0 & S_{66} \end{bmatrix} \begin{bmatrix} \sigma_1 \\ \sigma_2 \\ \sigma_3 \\ \tau_{23} \\ \tau_{31} \\ \tau_{12} \end{bmatrix} \quad (3-9)$$

The compliance matrix for an orthotropic material in terms of engineering constants can be given as

$$[S_{ij}] = \begin{bmatrix} \frac{1}{E_1} & -\frac{\nu_{21}}{E_2} & -\frac{\nu_{31}}{E_3} & 0 & 0 & 0 \\ -\frac{\nu_{12}}{E_1} & \frac{1}{E_2} & -\frac{\nu_{32}}{E_3} & 0 & 0 & 0 \\ -\frac{\nu_{13}}{E_1} & -\frac{\nu_{23}}{E_2} & \frac{1}{E_3} & 0 & 0 & 0 \\ 0 & 0 & 0 & \frac{1}{G_{23}} & 0 & 0 \\ 0 & 0 & 0 & 0 & \frac{1}{G_{31}} & 0 \\ 0 & 0 & 0 & 0 & 0 & \frac{1}{G_{12}} \end{bmatrix} \quad (3-10)$$

Where

$E_1, E_2,$ and $E_3 =$ Young's moduli in the 1, 2, and 3 directions respectively.

$\nu_{ij} =$ Poisson's ratio, the ratio of the strain in the j-direction to the strain in the i direction when stresses applied in the i-direction.

$G_{12}, G_{23},$ and $G_{31} =$ Shear moduli in the 1-2, 2-3, and 3-1 planes respectively.

The stress strain relation for an orthotropic material in the principal material coordinates under plane stresses will have the form

$$\begin{bmatrix} \sigma_1 \\ \sigma_2 \\ \tau_{12} \end{bmatrix} = \begin{bmatrix} Q_{11} & Q_{12} & 0 \\ Q_{12} & Q_{22} & 0 \\ 0 & 0 & Q_{66} \end{bmatrix} \begin{bmatrix} \varepsilon_1 \\ \varepsilon_2 \\ \gamma_{12} \end{bmatrix} \quad (3-11)$$

with

$$\sigma_3 = \tau_{23} = \tau_{31} = 0$$

where

$$Q_{11} = \frac{S_{22}}{S_{11}S_{22} - S_{12}^2} = \frac{E_1}{1 - \nu_{12}\nu_{21}}$$

$$Q_{12} = -\frac{S_{12}}{S_{11}S_{22} - S_{12}^2} = \frac{\nu_{12}E_2}{1 - \nu_{12}\nu_{21}} = Q_{21}$$

$$Q_{22} = \frac{S_{11}}{S_{11}S_{22} - S_{12}^2} = \frac{E_2}{1 - \nu_{12}\nu_{21}}$$

$$Q_{66} = \frac{1}{S_{66}} = G_{12}$$

or in other form

$$\begin{bmatrix} \varepsilon_1 \\ \varepsilon_2 \\ \gamma_{12} \end{bmatrix} = \begin{bmatrix} \frac{1}{E_1} & -\frac{\nu_{12}}{E_1} & 0 \\ -\frac{\nu_{12}}{E_2} & \frac{1}{E_2} & 0 \\ 0 & 0 & \frac{1}{G_{12}} \end{bmatrix} \begin{bmatrix} \sigma_1 \\ \sigma_2 \\ \tau_{12} \end{bmatrix} \quad (3-12)$$

The previous equations can be applied for composites where the direction of fibers is in the direction of the applied forces. Composites in practical situations are used with multi-layer laminates. Any composite member will have multiple layers of fiber reinforced materials and each layer has its own fiber orientation.

Figure 3-3 shows a composite lamina with the fibers rotated an angle θ from the

x-y axis. The stresses in the x-y direction can be related to the stresses in the fiber 1-2 direction with a transformation matrix T,

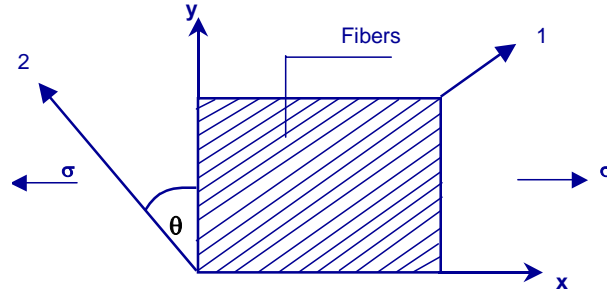


Figure 3-3: Composite lamina with fibers rotated an angle θ from the x-y plane.

$$T = \begin{bmatrix} \cos^2 \theta & \sin^2 \theta & 2 \sin \theta \cos \theta \\ \sin^2 \theta & \cos^2 \theta & -2 \sin \theta \cos \theta \\ -\sin \theta \cos \theta & \sin \theta \cos \theta & (\cos^2 \theta - \sin^2 \theta) \end{bmatrix} \quad (3-13)$$

The stress transformation equation will have the form,

$$\begin{bmatrix} \sigma_x \\ \sigma_y \\ \tau_{xy} \end{bmatrix} = [T]^{-1} \begin{bmatrix} \sigma_1 \\ \sigma_2 \\ \tau_{12} \end{bmatrix}$$

and the transformed strain

$$\begin{bmatrix} \varepsilon_x \\ \varepsilon_y \\ \frac{\gamma_{xy}}{2} \end{bmatrix} = [T]^{-1} \begin{bmatrix} \varepsilon_1 \\ \varepsilon_2 \\ \frac{\gamma_{12}}{2} \end{bmatrix}$$

If a new matrix R is defined as follows

$$[R] = \begin{bmatrix} 1 & 0 & 0 \\ 0 & 1 & 0 \\ 0 & 0 & 2 \end{bmatrix}$$

Then we can get

$$\begin{bmatrix} \varepsilon_x \\ \varepsilon_y \\ \gamma_{xy} \end{bmatrix} = [\mathbf{R}] \begin{bmatrix} \varepsilon_x \\ \varepsilon_y \\ \frac{\gamma_{xy}}{2} \end{bmatrix}$$

$$\begin{bmatrix} \varepsilon_1 \\ \varepsilon_2 \\ \gamma_{12} \end{bmatrix} = [\mathbf{R}] \begin{bmatrix} \varepsilon_1 \\ \varepsilon_2 \\ \frac{\gamma_{12}}{2} \end{bmatrix}$$

From equation (3-11) we have

$$\begin{bmatrix} \sigma_1 \\ \sigma_2 \\ \tau_{12} \end{bmatrix} = [\mathbf{Q}] \begin{bmatrix} \varepsilon_1 \\ \varepsilon_2 \\ \gamma_{12} \end{bmatrix}$$

Then we obtain

$$\begin{bmatrix} \sigma_x \\ \sigma_y \\ \tau_{xy} \end{bmatrix} = [\mathbf{T}]^{-1} [\mathbf{Q}] [\mathbf{R}] [\mathbf{T}] [\mathbf{R}]^{-1} \begin{bmatrix} \varepsilon_x \\ \varepsilon_y \\ \gamma_{xy} \end{bmatrix}$$

By setting

$$[\bar{\mathbf{Q}}] = [\mathbf{T}]^{-1} [\mathbf{Q}] [\mathbf{R}] [\mathbf{T}] [\mathbf{R}]^{-1}$$

and noting that

$$[\mathbf{R}] [\mathbf{T}] [\mathbf{R}]^{-1} = [\mathbf{T}]^{-T}$$

then

$$[\bar{\mathbf{Q}}] = [\mathbf{T}]^{-1} [\mathbf{Q}] [\mathbf{T}]^{-T}$$

Finally the stress-strain relation in the x-y plane can be written as

$$\begin{bmatrix} \sigma_x \\ \sigma_y \\ \tau_{xy} \end{bmatrix} = [\bar{Q}] \begin{bmatrix} \varepsilon_x \\ \varepsilon_y \\ \gamma_{xy} \end{bmatrix}$$

where

$$[\bar{Q}] = \begin{bmatrix} \bar{Q}_{11} & \bar{Q}_{12} & \bar{Q}_{16} \\ \bar{Q}_{12} & \bar{Q}_{22} & \bar{Q}_{26} \\ \bar{Q}_{16} & \bar{Q}_{26} & \bar{Q}_{66} \end{bmatrix}$$

where

$$\bar{Q}_{11} = Q_{11} \cos^4 \theta + 2(Q_{12} + 2Q_{66}) \sin^2 \theta \cos^2 \theta + Q_{22} \sin^4 \theta$$

$$\bar{Q}_{12} = (Q_{11} + Q_{22} - 4Q_{66}) \sin^2 \theta \cos^2 \theta + Q_{12} (\sin^4 \theta + \cos^4 \theta)$$

$$\bar{Q}_{22} = Q_{11} \sin^4 \theta + 2(Q_{12} + 2Q_{66}) \sin^2 \theta \cos^2 \theta + Q_{22} \cos^4 \theta$$

$$\bar{Q}_{16} = (Q_{11} - Q_{12} - 2Q_{66}) \sin^3 \theta \cos^3 \theta + (Q_{12} - Q_{22} + 2Q_{66}) \sin^3 \theta \cos \theta$$

$$\bar{Q}_{26} = (Q_{11} - Q_{12} - 2Q_{66}) \sin^3 \theta \cos \theta + (Q_{12} - Q_{22} + 2Q_{66}) \sin \theta \cos^3 \theta$$

$$\bar{Q}_{66} = (Q_{11} + Q_{22} - 2Q_{12} - 2Q_{66}) \sin^2 \theta \cos^2 \theta + Q_{66} (\sin^4 \theta + \cos^4 \theta)$$

LAMINATE ANALYSIS

Fiber composite materials are generally used as a stack of multiple layers in a form of a laminate. Each layer is assumed to have different fiber orientation than the adjacent one.

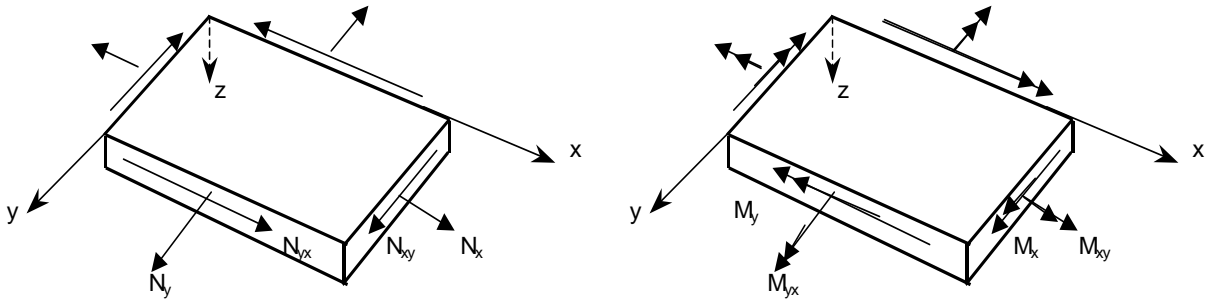


Figure 3-4: In-plane forces and moments on a flat laminate.

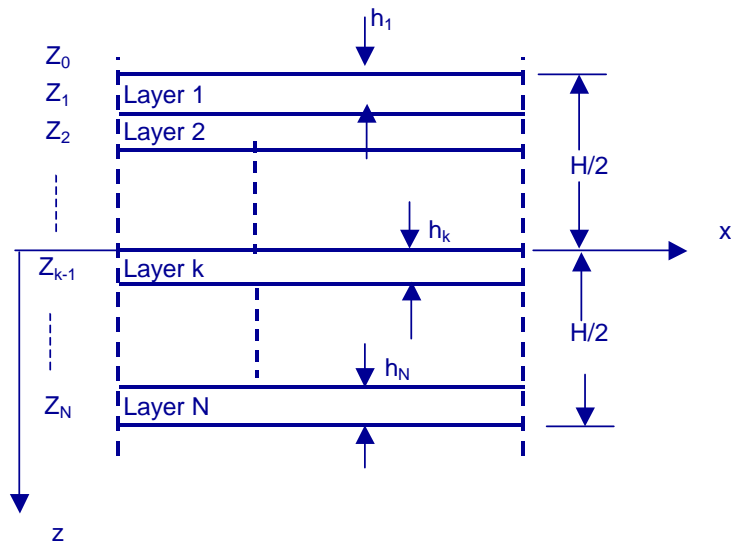


Figure 3-5: A stack of different fiber oriented laminas.

When a laminate is subjected to a bending moment, M , the stack of laminas will not have the same level of bending. Figure 3-4 shows a composite laminate subjected to in-plane forces and moments and Figure 3-5 shows its layout geometry. The laminate has a total thickness of H and N number of layers. The x -axis is passing through the mid surface of the section.

The total force and moment on the laminate in any direction can be obtained by integrating the stresses in each layer over the whole thickness H,

$$N_x = \int_{-H/2}^{H/2} \sigma_x dz \quad M_x = \int_{-H/2}^{H/2} \sigma_x z dz$$

Forces and moments in other directions can be obtained in a similar way.

The total load and moment vectors are given as

$$\begin{bmatrix} N_x \\ N_y \\ N_{xy} \end{bmatrix} = \int_{-H/2}^{H/2} \begin{bmatrix} \sigma_x \\ \sigma_y \\ \tau_{xy} \end{bmatrix} dz = \sum_{k=1}^N \int_{z_{k-1}}^{z_k} \begin{bmatrix} \sigma_x \\ \sigma_y \\ \tau_{xy} \end{bmatrix} dz$$

and

$$\begin{bmatrix} M_x \\ M_y \\ M_{xy} \end{bmatrix} = \int_{-H/2}^{H/2} \begin{bmatrix} \sigma_x \\ \sigma_y \\ \tau_{xy} \end{bmatrix} z dz = \sum_{k=1}^N \int_{z_{k-1}}^{z_k} \begin{bmatrix} \sigma_x \\ \sigma_y \\ \tau_{xy} \end{bmatrix} z dz$$

and the general equation that relates between forces, moments, middle-surface strains, and middle-surface curvature in a fiber reinforced composite laminate can be given as

$$\begin{bmatrix} N_x \\ N_y \\ N_{xy} \\ M_x \\ M_y \\ M_{xy} \end{bmatrix} = \begin{bmatrix} A_{11} & A_{12} & A_{16} & B_{11} & B_{12} & B_{16} \\ A_{12} & A_{22} & A_{26} & B_{12} & B_{22} & B_{26} \\ A_{16} & A_{26} & A_{66} & B_{16} & B_{26} & B_{66} \\ B_{11} & B_{12} & B_{16} & D_{11} & D_{12} & D_{16} \\ B_{12} & B_{22} & B_{26} & D_{12} & D_{22} & D_{26} \\ B_{16} & B_{26} & B_{66} & D_{16} & D_{26} & D_{66} \end{bmatrix} \begin{bmatrix} \epsilon_x \\ \epsilon_y \\ \epsilon_{xy} \\ \kappa_x \\ \kappa_y \\ \kappa_{xy} \end{bmatrix} \quad (3-14)$$

where

A_{ij}, B_{ij}, D_{ij} are function of Q_{ij} and z_k

$$A_{ij} = \sum_{k=1}^N (\bar{Q}_{ij})_k (z_{-k} - z_{k-1})$$

$$B_{ij} = \frac{1}{2} \sum_{k=1}^N (\bar{Q}_{ij})_k (z_{-k}^2 - z_{k-1}^2)$$

$$D_{ij} = \frac{1}{3} \sum_{k=1}^N (\bar{Q}_{ij})_k (z_{-k}^3 - z_{k-1}^3)$$

3.4 FAILURE CRITERIA

Structural design is usually performed on the basis of comparing the stresses or strains due to the applied loads with allowable stress or strain capacity of the structural material. Structural failure will occur when the applied stresses exceed the allowable; at that point, the structural element cannot continue to perform its function. A failure criteria envelope that includes the allowable ranges of stress or strains is an important step in the design.

The analysis of FRP composite structures is similar but more difficult than that of isotropic material structures. For most isotropic materials, like metals, where initial failure can be indicated by material yielding, the maximum stress criterion theory or von Mises yield criterion where commonly used. Fiber reinforced composites are neither isotropic, nor do they follow the yielding theory. Therefore, the current criteria of isotropic materials will not be valid for composite materials. Other failure criteria have to be employed instead.

The difficulty in analysis of composite structures appears in stress variation through the laminate thickness. The composite laminate consists of multiple layers with

different fiber orientation in each layer. Therefore, the stress distribution in the layers will not be uniform through the laminate thickness even though it is subjected to uniform in-plane loads. The material properties in orthotropic materials are directional dependent so that it is higher in the fiber direction than the other directions. The increase in laminate loading may cause some layers to reach their stress limit before other layers depending on the stacking sequence of the layers. Damage in those layers with stresses higher than allowable stress will appear in the form of, most probably, brittle failure.

The other difficulty that may rise in the analysis of composite laminates is in the nature of the failure. Ductile materials such as steel which usually experience a failure that initiates in a form of local yielding at the points that have reached the stress limits. In composite materials which are composed of multiple unidirectional layers, the failure usually starts as a local failure in layers stressed beyond the allowable stress limits. The failure in most high performance unidirectional composite materials has been recognized as brittle failure (Gurdal 1999).

A failure criterion is a set of mathematical equations usually derived from field or laboratory tests to predict possible failures. The criterion is then modified or adjusted to fit cases where experimental data are not available. Many failure theories have been proposed in the field of composites to predict failures of unidirectional lamina.

3.4.1 MAXIMUM STRESS CRITERION

In this criterion, failure will occur if one of the principal stress components exceeds the allowable strength of the material. Thus, for a failure not to occur, all the following conditions have to be satisfied.

$$\sigma_1 \leq X_t \quad \sigma_2 \leq Y_t$$

$$\sigma_1 \geq X_c \quad \sigma_2 \geq Y_c$$

$$|\tau_{12}| \leq S$$

Where

σ_1 = Stress in the fiber direction

σ_2 = Stress perpendicular to the fiber direction

τ_{12} = Shear stress

X_t = Tensile strength in the fiber direction

X_c = Compressive strength in the fiber direction

Y_t = Tensile strength in the transverse direction

Y_c = Compressive strength in the transverse direction

S = Shear strength

3.4.2 MAXIMUM STRAIN CRITERION

The maximum strain failure criterion is similar to maximum stress criterion. This theory predicts failure when any of the principal material strains exceed the corresponding maximum allowable strain. The material will fail if at least one of the following conditions fails to satisfy.

$$\varepsilon_1 \leq \varepsilon_{1t} \quad \varepsilon_2 \leq \varepsilon_{2t}$$

$$\varepsilon_1 \geq \varepsilon_{1c} \quad \varepsilon_2 \geq \varepsilon_{2c}$$

$$|\gamma_{12}| \leq \gamma$$

Where:

- ϵ_1 = Strain in the fiber direction
- ϵ_2 = Strain perpendicular to the fiber direction
- γ_{12} = Shear strain
- ϵ_{1t} = Maximum tensile strain in the fiber direction
- ϵ_{1c} = Maximum compressive strain in the fiber direction
- ϵ_{2t} = Maximum tensile strain in the transverse direction
- ϵ_{2c} = Maximum compressive strain in the transverse direction
- γ = Maximum shear strain

3.4.3 TSAI-HILL FAILURE CRITERION

In the maximum stress and maximum strain failure theories, the stress and strain are assumed to act independently such that a failure will occur when any of the individual stresses or strains is not within the criterion limits. The Tsai-Hill approach is assuming an interaction between the three different stresses so that a failure criterion envelope is obtained by combinations of all element stresses. The Tsai-Hill criterion can be expressed as

$$\frac{\sigma_1^2}{X^2} - \frac{\sigma_1\sigma_2}{X^2} + \frac{\sigma_2^2}{Y^2} + \frac{\tau_{12}^2}{S^2} = 1 \quad (3-15)$$

3.4.4 TSAI-WU FAILURE CRITERION

The Tsai-Wu or the tensor failure criterion predicts failure of orthotropic materials through stress interaction equality which has the form

$$F_1\sigma_1 + F_2\sigma_2 + F_6\sigma_6 + F_{11}\sigma_1^2 + F_{22}\sigma_2^2 + F_{66}\sigma_6^2 + 2F_{12}\sigma_1\sigma_2 = 1 \quad (3-16)$$

Where F_i, F_{ij} are stress coefficients and are defined as

$$\begin{aligned}
F_1 &= \frac{1}{X_t} + \frac{1}{X_c} & F_2 &= \frac{1}{Y_t} + \frac{1}{Y_c} \\
F_{11} &= -\frac{1}{X_t X_c} & F_{22} &= -\frac{1}{Y_t Y_c} \\
F_6 &= 0 & F_{66} &= \frac{1}{S^2} \\
F_{12} &= \frac{1}{2\sigma^2} \left[1 - \left(\frac{1}{X_t} + \frac{1}{X_c} + \frac{1}{Y_t} + \frac{1}{Y_c} \right) \sigma + \left(\frac{1}{X_t X_c} + \frac{1}{Y_t Y_c} \right) \sigma^2 \right]
\end{aligned}$$

where F_{12} is calculated from data available from biaxial strength tests. In the absence of such data, the value of F_{12} can be taken as (Mallick 1993)

$$-\frac{1}{2}(F_{11}F_{22})^{1/2} \leq F_{12} \leq 0$$

3.5 MECHANICAL PROPERTIES

Laminated composite materials are unique in that their mechanical properties are highly directional dependent. The mechanical properties of the reinforcing fibers usually dictate the lamina properties. In a unidirectional lamina, the stiffness and strength in the fiber direction are much higher than that in the perpendicular direction. In multi layer laminates, the mechanical properties in the weaker directions can be improved by using multi directional layers through the laminate thickness.

Fiber reinforced composites can be made of a wide range of material properties. The basic constituents are the fibers and the resin with some other filler materials. As shown earlier in this chapter, fibers come from different sources with various stiffness and strength. Some selected mechanical properties for unidirectional composite materials are listed in appendix A, Table A-1 through Table A-3.

SOIL-PILE INTERACTION

Piles are driven in weak soils to support heavy structures and transfer their loads to the surrounding soils. They are usually subjected to lateral forces and moments as well as axial forces. Unlike axial forces, which normally produce deformations in the direction of the pile axis, lateral forces may produce deformations in any direction of the pile. The design of pile foundations under lateral loads normally is governed by the maximum deflection of the pile.

4.1 CLASSIFICATION OF PILES

Piles can be classified in many ways, for example, by the material it's made of, by method of load transfer, by amount of ground disturbance, by fabrication method, and by method of installation.

- Pile material: piles can be made of different materials such as, concrete, steel, timber and composite. Traditional composite piles are made of steel and concrete or timber and concrete.
- Method of load transfer: Piles can be classified according to the method of load transfer into; end-bearing piles, friction piles, combined end-bearing and friction piles, and laterally loaded piles.

- Amount of ground disturbance during installation: Large-displacement piles, small-displacement piles, and non-displacement piles.
- Pile fabrication method: prefabricated or cast in place.
- Method of installation, driven piles, bored piles and a combination of driven and bored piles (Prakash 1990).

The main conventional materials for piling systems are steel, concrete, timber or a combination between them.

4.2 CHOICE OF PILING METHOD AND ECONOMIC OF DESIGN

Like any other structure, piles should be designed to satisfy certain requirements. From engineering point of view, the design of piles should be effective, such that, the chosen piles have to be practical, economical and have an adequate margin of safety.

Pile foundations are different from other structures above the ground. Their design is always considered to be more conservative than other structures. Many factors are leading to this conservative design like the uncertainties in loads and in soil properties. The variability of soil in combination with unanticipated loads or subsequent soil movements can result in settlement problems over which the designer may have little control (Bowles 1996).

Environmental effects are another important factor in the selection and design of pile foundations. Chemical attacks on piles in severe environments are a major factor in reducing expected life of service. The corrosion of steel surface, the deterioration of timber and the spoiling of concrete are major problems that affect piles. The loss of pile section due to such problems will result in reduction of load capacity. The continuous decrease in cross section with time will lead to a major failure of the structure.

4.3 SELECTION OF FOUNDATION

The main factors that determine the selection of the type of piles are the bridge type and soil condition. The bridge type, including dimensions, type of bridge, and construction materials, dictates the design magnitude of loads and the allowable displacements and other performance criteria for the foundations. For example, a suspension bridge requires large lateral capacity for its end anchorage which can be a huge deadman, a high capacity soil or rock anchor system, a group of driven piles, or a group of large-diameter drilled shafts. Tower foundations of an over-water bridge require large compressive, uplift, lateral, and overturning moment capacities. The likely foundations are deep, large size footings using cofferdam construction, caissons, groups of large-diameter drilled shafts, or groups of a large number of steel piles.

Surface and subsurface geologic and geotechnical conditions are other main factors in determining the type of bridge foundations (Chellis 1961). Subsurface conditions, especially the depths to the load bearing soil layer or bedrock, are the most crucial factors. Seismicity over the region usually dictates the design level of seismic loads, which is often the critical and dominant loading condition. A water bridge has limited options to choose from in terms of the type of foundations.

Deformation compatibility of the foundations and bridge structure is an important consideration. Different types of foundations may behave differently; therefore, the same type of foundation should be used for one section of bridge structure. Diameters of the piles and inclined piles are two important factors to consider in terms of deformation compatibility.

4.4 DESIGN REQUIREMENTS FOR PILES

Piles in bridge structures are designed according to the applied forces and loads transferred from the super structure and the surrounding soil. The selection of a suitable pile type for bridge foundations is normally based on several considerations of soil and water conditions; (1) availability of materials, (2) construction schedule, (3) substructure element to be supported, (4) loads to be transferred, (5) and overall economy. In addition, relevant characteristics of the various pile types should be taken into account since in many cases they may dictate the choice (Xanthakos 1995). The type of the bridge determines the design requirements of the pile.

Piles should be designed for both axial and lateral loading conditions. The two principal design considerations for piles under axial loads are ultimate load capacity and settlement. The ultimate load capacity of a pile may be governed either by the structural capacity of the pile or the bearing capacity of the soil. Piles that are subjected to lateral loads must also be safe against ultimate failure of the soil or the pile, and excessive lateral deflections.

Axially loaded piles may fail in compression or by buckling. Buckling may occur in long and slender piles that extend for the portion of their lengths through water or air. A scour of the soil around the piles could expose portion of their lengths and increase the likelihood of buckling.

Laterally loaded piles will fail in flexure if the induced bending moment exceeds the moment capacity of the pile. The structural capacity of the pile is dependent on both the moment and axial load.

4.5 FORCES ACTING ON PILES

Pile foundations are structural members that give support and transfer loads from one structure to another. A pile can be considered as a special type of column that carries axial and flexural loads but with different cases of boundary conditions. Generally, the column is a cast-in-place structure whereas the pile is a pre-cast or prefabricated element which requires handling, transporting, and driving. Due to the different circumstances that involve the whole process of pile construction, the design should include all factors affecting its durability and performance.

Piles may be subjected to different kinds of forces during handling and while they are in service. Piles must be designed to handle loads without damage.

- (a) Crushing under the permanent design load
- (b) Crushing caused by impact force during driving
- (c) Bending stresses occurring during handling
- (d) Tension from uplift forces or from rebound during driving
- (e) Bending stresses due to horizontal forces
- (f) Bending stresses due to curvature in the pile
- (g) Column action for portions not receiving lateral support from the ground, but free standing in air, water, or very liquid mud.

Also piles must have adequate surface area, in the case of friction piles, so that they will provide the highest contact area to transfer the loads from the pile to the surrounding soil (Chellis 1961).

4.5.1 AXIALLY LOADED PILES

Piles are usually designed for full capacity which is the maximum load the pile can support without failure. The maximum allowable stress on a pile section should not exceed the allowable limits. A pile under axial compression may reach one of the following four limit states (Xanthakos 1995).

1. Structural failure of the pile body such as crushing or yielding.
2. Stability failure due to buckling.
3. Bearing capacity failure of the soil under the pile
4. Excessive pile settlement

4.5.1.1 ECCENTRICITY AND BENDING IN PILES

No pile is likely to be entirely straight. Any curvature causes bending stresses. It is important to give consideration to lateral as well as eccentric forces on piles, since stresses may increase rapidly from these causes when combined with stresses from direct axial loads (Chellis 1961).

4.5.1.2 BUCKLING OF PILES

An axially loaded pile may be subjected to buckling. The pile will buckle during service when the loading reaches or exceeds its critical buckling load. This case is rare but it may occur for end-bearing piles in soft soils or partially embedded piles. Also a pile may buckle during driving which may cause some deviation from the desired position.

For piles subjected to buckling, the general differential equation that governs is based on the subgrade modulus of the soil and is given as

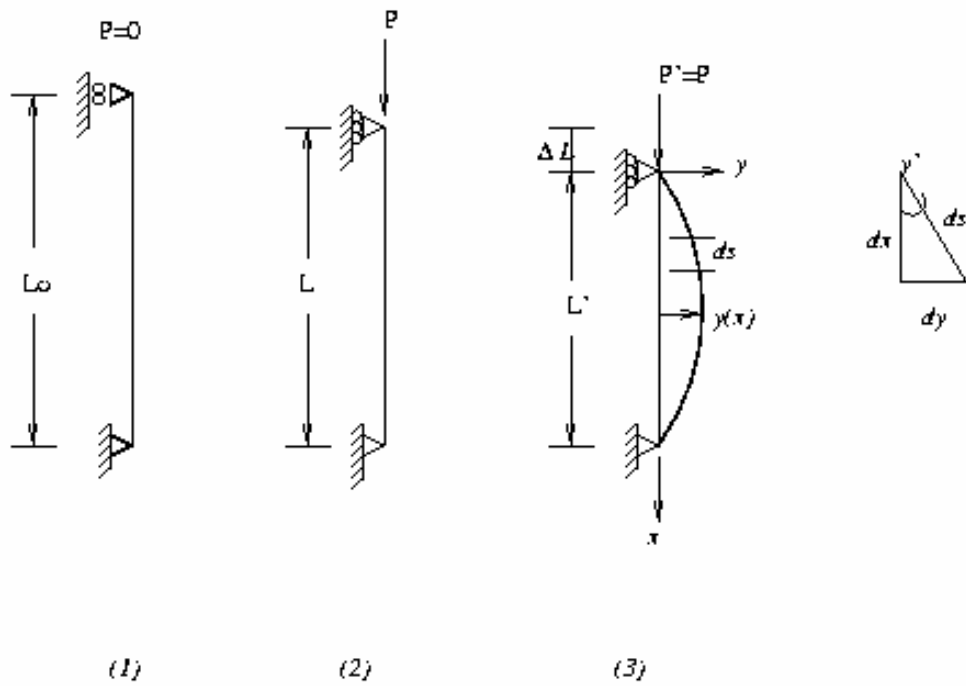
$$EI \frac{d^4 y}{dx^4} + P \frac{d^2 y}{dx^2} + ky = 0$$

where

EI = flexural stiffness of the pile;

P = axial load; and

K = soil subgrade modulus.



The critical buckling load for an ideal pin ended column is given by the Euler equation:

$$P_{cr} = \frac{\pi^2 EI}{L^2}$$

4.5.2 LATERALLY LOADED PILES

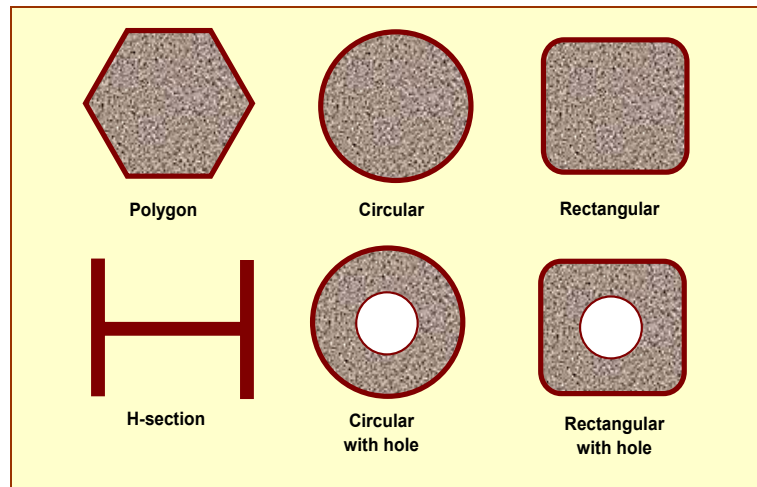
Lateral loads on piles usually come from different sources like wind pressure, horizontal live loads, earth and water pressure, and earthquake effects. Piles under lateral loads must be designed to withstand these loads or any combinations of loads without failing (Xanthakos 1995). Piles in groups are normally subjected to a combination of both axial and lateral loads. In the past, designers used to consider piles as axially loaded members only, and the lateral loads were assumed to be carried by batter piles. Current pile designers consider the full range of vertical (or battered) laterally loaded structural members, fully or partially embedded in the ground, as laterally loaded piles (Bowles 1996).

It has been found that the lateral support provided by any soil except the softest or most fluid is generally sufficient to prevent pile failure from buckling for the embedded portions. For portions in water or above the ground, unsupported, the pile should be designed as a column under direct loads unless lateral forces are present, in which case the design should include the lateral forces.

The design of laterally loaded vertical piles is normally governed by the maximum allowed deflection or the structural capacity of the pile. It has been found that reaching the ultimate capacity of the soil is something unattainable or unacceptable because it requires considerable displacement. Thus, in designing a single pile or a group of vertical piles, the lateral deflection and the structural capacity of the pile not the soil should be the determining factors (Xanthakos 1995).

4.6 PILE SECTIONS

Piles can be found in different types of cross sections as shown below. The most common shapes are the H-section for steel piles, circular sections for concrete piles and polygonal sections for prestressed piles.



4.7 PILING MATERIALS

The common used materials for piling are steel, concrete and timber. Because of their high performance as construction materials, they have been recommended over other materials.

4.7.1 STEEL PILES

Steel piles are normally used in the form of H or pipe piles. Steel has very high compressive and tensile strengths in addition to its high modulus of elasticity. It has a high capability of carrying heavy loads down to deep bearing strata. Steel piles have the advantages of high load capacity and ease of splicing so that they can be shipped in any required length. They also have the ability of being driven through different soil layers even soft rocks and hard material layers.

4.7.2 CONCRETE PILES

Concrete is the most common traditional construction material used today. It has the ability to carry large axial forces and bending forces when reinforced with steel bars. Concrete members can be designed for the desired shape and strength. They are easy to drive and have the ability to withstand hard driving. Concrete piles are available in the main categories:

1. Precast concrete piles.
2. Cast-in place concrete piles
3. Composite concrete piles.

4.7.3 TIMBER PILES

Timber piles are usually made of straight tree trunks after removing their branches. They are easy to cut, easy to handle and can last for long periods of time under normal environmental conditions. Timber piles can be found as round untrimmed logs or sawed square sections. They are usually used as friction piles in granular soils, sands, silts and clays

4.8 SOIL-PILE BEHAVIOR

Analysis and design of piles under the different types of loading usually start with the understanding of the soil-pile interaction process. Soils, in general, are non-homogenous materials that are found in layers along the pile length and each layer may have different properties from the next layer. The soil-pile interaction will not have the same behavior along the pile shaft; therefore, variation in soil properties has to be taken into consideration.

Piles embedded in soil can be represented by beam-column elements with geometric and material nonlinear behavior. Soil-pile behavior can be classified into two categories; the first category is axial load-friction behavior, in which a unique relationship is assumed between the skin friction, shear stress, and the relative deflection between soil and the pile at each depth. The second category is lateral load-displacement behavior, in which the pile will be subjected to a lateral soil pressure if it is battered or has a lateral loading in form of shear or moment applied at the top. (Yang 1982).

4.9 LOAD – DISPLACEMENT BEHAVIOR

Soil behavior can be represented by a set of load-displacement curves to describe its response under different types of loadings. Three major categories of curves are usually used in this regard; each of them describes a single characteristic of the soil: lateral load-displacement ($p-y$) curves, load-slip ($f-z$) curves, and load-settlement ($q-z$) curves. The soil response in all three categories is assumed to be nonlinear.

The modulus of subgrade reaction, which was originated by Winkler in 1867, is one of the most commonly used methods in pile analysis. In this method the surrounding soil to the embedded pile can be replaced by a series of vertical and lateral springs to represent both the longitudinal and lateral soil resistance. The spring properties are usually obtained from the load–displacements curves that represent the resistance force as a function of the displacement in the force direction.

The derivation of load displacement curves has been performed through means of continuum mechanics and from correlations with results from real field experiments on instrumented loaded piles (Mosher et al 2000). The accuracy of such curves to represent a

particular pile behavior depends on the similarity between the pile in the study and the pile test model in terms of soil properties and loading conditions.

4.9.1 LATERALLY LOADED PILES

Piles are primarily designed to carry axial loading, but in several situations they are subjected to lateral displacements as well as shear and moment applied at the pile head. Therefore, the pile foundation has to be designed to sustain static and cyclic lateral loads. The problem of piles under lateral loading is much more complex than that of axially loaded piles. Axially loaded piles may be designed using simple static methods, while laterally loaded piles require, sometimes, the solution of the fourth-order differential equation because of their non-linear behavior. The problem also can be solved as a beam on elastic foundation with nonlinear soil-pile interaction behavior (p-y curves). Numerous studies have been conducted trying to investigate the behavior of laterally loaded piles.

Figure 4-1 shows a schematic of a laterally loaded pile subjected to head shear and moment. Each point on the pile shaft will undergo a translation u in the x-direction and a rotation θ about the y-axis. The soil around the pile will also develop pressure p that resists the lateral displacement of the pile.

The most common approaches generally used in calculating lateral load deflections are the following: (1) Subgrade reaction approach and (2) The elastic continuum approach.

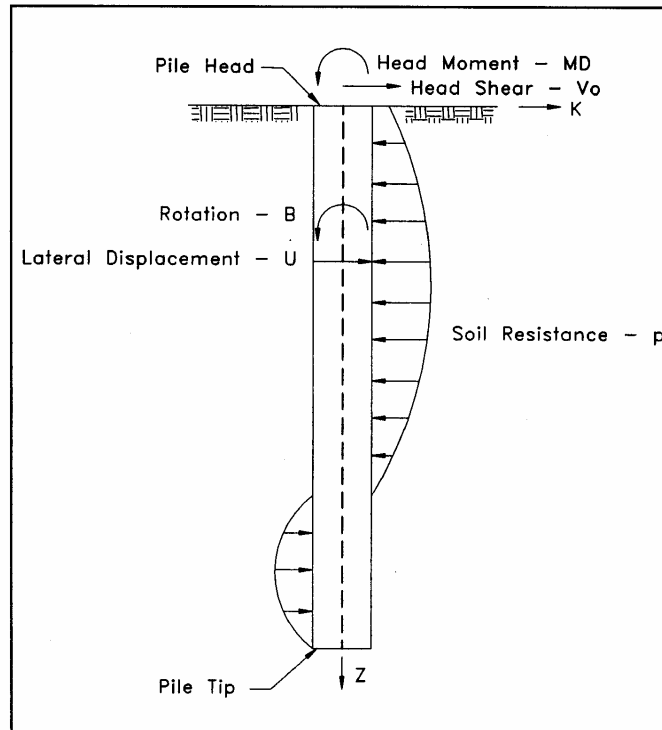


Figure 4-1: Schematic of laterally loaded pile (Mosher 200).

4.9.2 SUBGRADE REACTION METHOD

The subgrade reaction approach is based on the Winkler soil model in which the continuous nature of the soil medium is ignored and replaced by a series of infinitely spaced unconnected springs. The soil medium around the pile can be replaced with an equivalent series of independent springs with spring modulus calculated from the p - y curve at each desired location. The spring constant k_h which can be referred to as the modulus of subgrade reaction, can be written as

$$k_h = \frac{p}{y} \quad (4-1)$$

where

p = the soil reaction per unit length of the pile

y = pile deformation due to force p

This linear equation has a constant value of the soil modulus k_h at any point of the pile deformation curve. Because of the non-linearity of the load-deflection behavior of soil-pile system, this formula has to be modified to accommodate the actual behavior. The equation of a beam on elastic foundation then can be used to represent the soil-pile relation in its nonlinear form (Prakash 1990).

$$\frac{d^4 y}{dx^4} + \frac{k_h y}{EI} = 0 \quad (4-2)$$

where E and I are the modulus of elasticity and the moment of inertia of the pile respectively.

Another form of the subgrade reaction equation shown in the following equation was suggested by Palmer and Thompson (1948)

$$k_x = k_h \left(\frac{x}{L} \right)^n \quad (4-3)$$

where

k_h = value of kx at pile tip ($x=L$)

x = any point along the pile

n = a coefficient equal to or greater than zero and equals to 1 for sands and normally consolidated clays.

Many other approaches have tried to account for the nonlinearity of the load-displacement relationship in soil-pile problems. Kubo (1965) used a different form

relationship to represent the nonlinear behavior. The equation relates the deflection y with the load p and any depth x as follows:

$$p = kx^m y^n \quad (4-4)$$

where k , m and n are experimentally determined coefficients (Poulos 1980).

4.9.3 LOAD-DISPLACEMENT CURVES

The common approach in solving laterally loaded piles is through using p - y curves that represent the soil behavior under various loading. The p - y curves for laterally loaded piles can be established based on calculations from test results of instrumented full-scale piles. The p - y curves have to be fully nonlinear with respect to the distance variation along the pile axis, z and the pile deflection axis, y . Several factors may influence the accuracy of the p - y curves such as soil properties, number of tests, pile geometry, layers of soil, and nature of loading. Figure 4-2 shows a representation of a nonlinear p - y curves and their variation along the pile depth.

Several approaches for constructing the p - y curves were presented in different publications. Cox et al (1971) performed a series of lateral load tests on instrumented full-scale piles to measure the bending moment along the pile shaft.

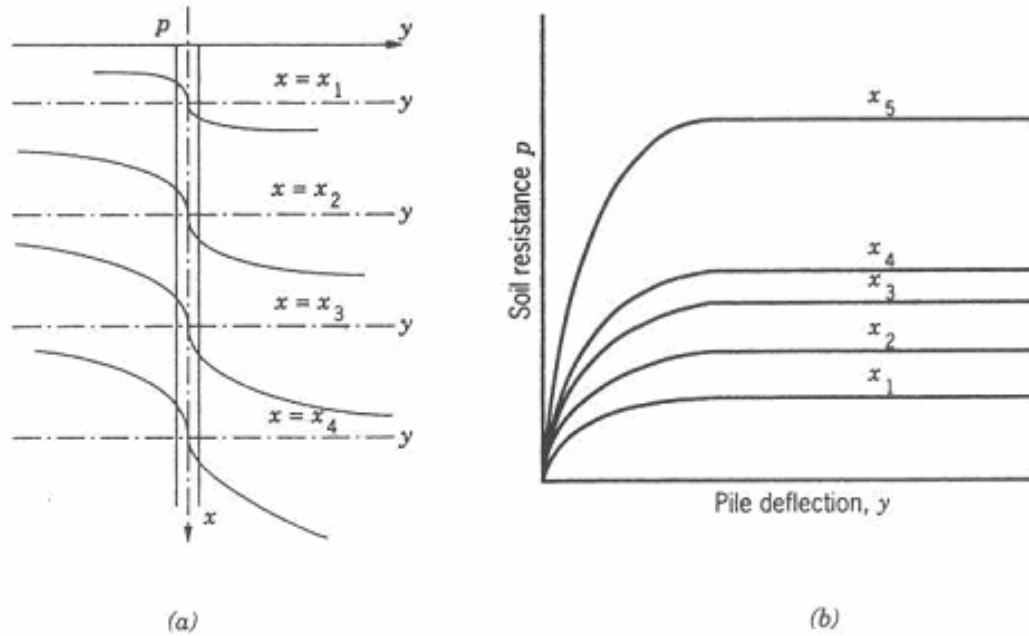


Figure 4-2: Nonlinear p-y curves for laterally loaded piles at various depths x.

P-Y CURVES FOR PILES IN SOFT CLAY

Matlock (1970) performed a series of lateral load tests on some instrumented 12.75 inches diameter and 42 feet long steel pipe piles driven in clays and subjected to static loads.

The lateral soil resistance was expressed in the following form

$$\frac{p}{p_u} = 0.5 \left(\frac{y}{y_{50}} \right)^{\frac{1}{3}} \quad (4-5)$$

where

p_u = ultimate lateral soil resistance per unit length of the pile

y_{50} = lateral movement of the soil corresponding to 50% of the ultimate lateral soil resistance.

y = lateral movement of the soil

The ultimate lateral resistance p_u can be calculated as the smaller of

$$p_u = \left(3 + \frac{\gamma'}{c} z + \frac{J}{b} z \right) c \cdot b \quad (4-6)$$

$$p_u = 9cb \quad (4-7)$$

where

γ' = average effective unit weight from ground surface to p - y curve

z = depth from ground surface to the p - y curve

C = shear strength at depth z

B = width of pile

J = constant taken as 0.5 for soft clay and 0.25 for medium clay

The lateral displacement at 50% of the ultimate soil resistance can be calculated from the following equation

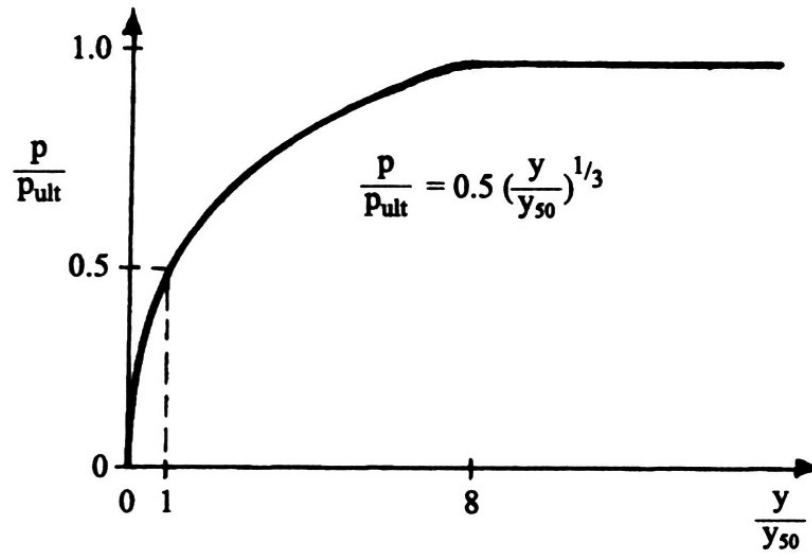
$$y_{50} = 2.5 \varepsilon_{50} b \quad (4-8)$$

where

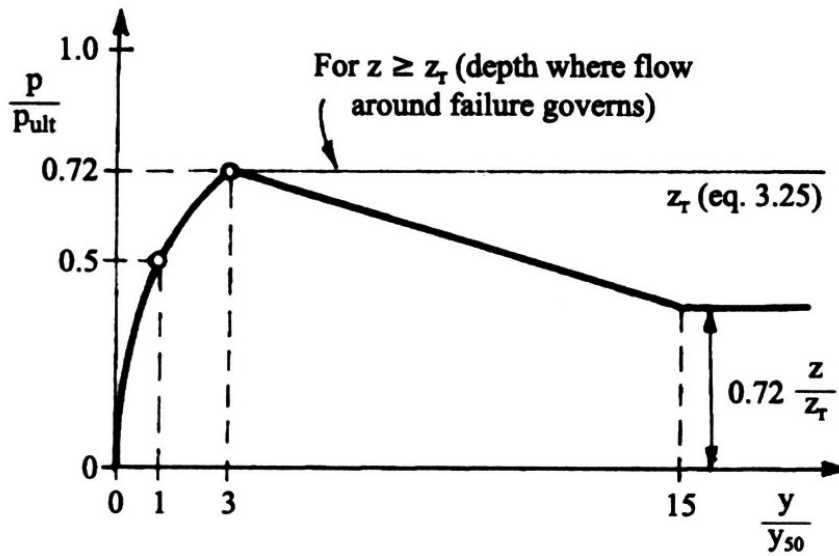
ε_{50} = Strain at 50 percent of the ultimate strength from a laboratory stress-strain curve

Typical values of ε_{50} are given in Table 4-1.

Figure 4-3 shows the shapes of the p - y curves for static and cyclic loading recommended by Matlock (1970) for soft clays above the water table.



(a) Static loading



(b) Cyclic loading

Figure 4-3: Characteristic shapes of the p - y curves for soft clay below water table (Mosher 200).

Table 4-1: Representative values of undrained shear strength and ϵ_{50}

Consistency of clay (psf)	Undrained shear strength psf	ϵ_{50}
Soft	250-500	0.020
Medium stiff	500-1000	0.010
Stiff	1000-2000	0.007
Very stiff	2000-4000	0.005
Hard	4000-8000	0.004

P-Y CURVES FOR PILES IN STIFF CLAYS BELOW WATER TABLE

Results from field tests performed by Reese, Cox and Koop (1975) on 24 in. 50 ft steel pipe piles driven in stiff clay in Texas were employed to derive the p-y curves. The measured undrained shear strength of the clay ranged from about 1 ton per square foot at the ground surface to 3 tons per square foot at 12 feet depth. The *p-y* curves for short-term static and cyclic loading can be calculated from a series of steps that end in the curve as shown in Figure 4-4 and Figure 4-5 respectively.

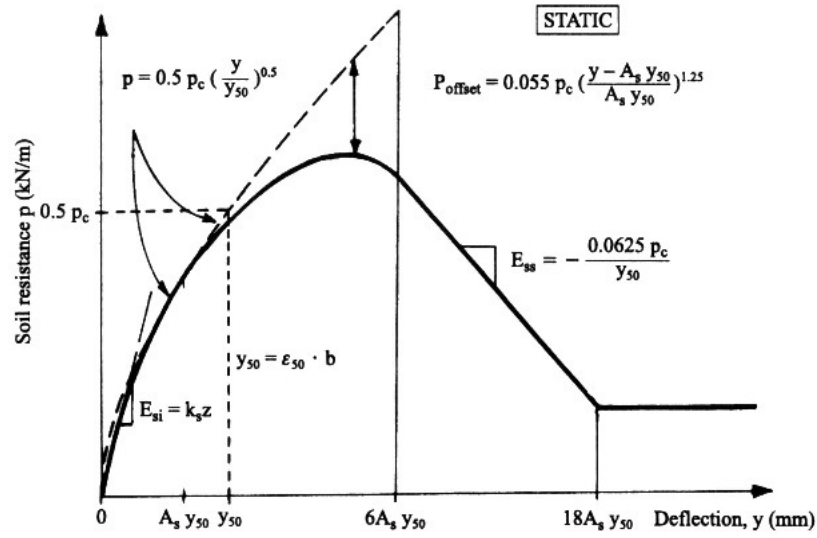


Figure 4-4: Characteristic shapes of p - y curves for static loading in stiff clay below water table.

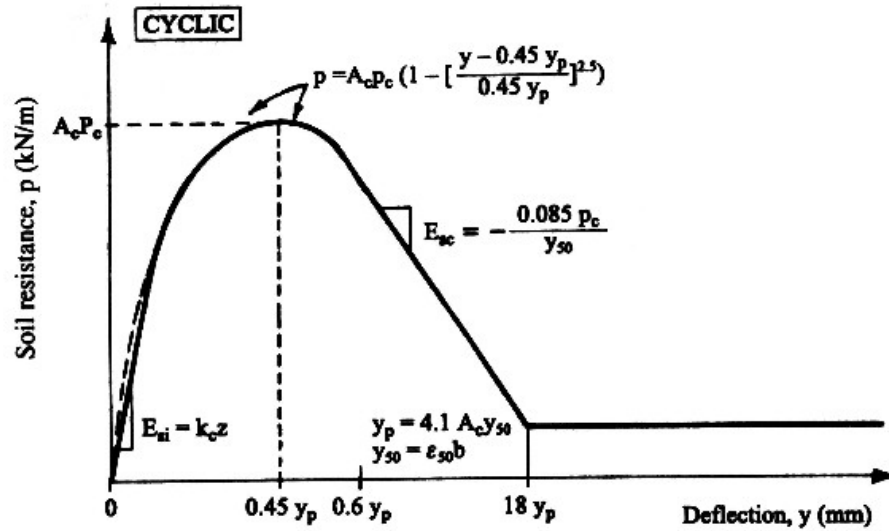


Figure 4-5: Characteristic shapes of p - y curves for cyclic loading in stiff clay below water table.

P-Y CURVES FOR PILES IN STIFF CLAYS ABOVE WATER TABLE

Test results of instrumented drill shafts, 30 inch in diameter and 42 feet in length performed by Reese and Welch (1975). The p - y curve for the experimental results of static and cyclic load tests are shown in Figure 4-6 and Figure 4-7 respectively.

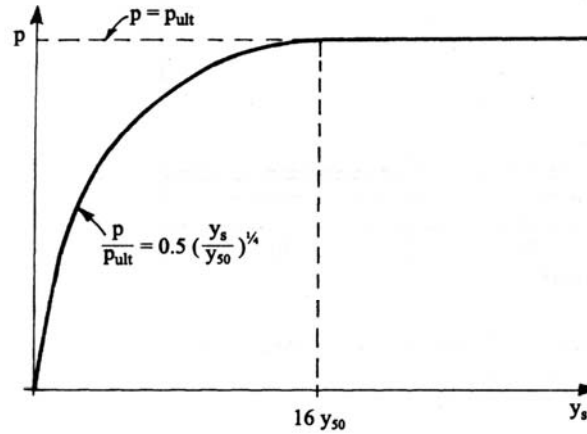


Figure 4-6: Characteristic shape of p - y curve for static loading in stiff clay above the water table.

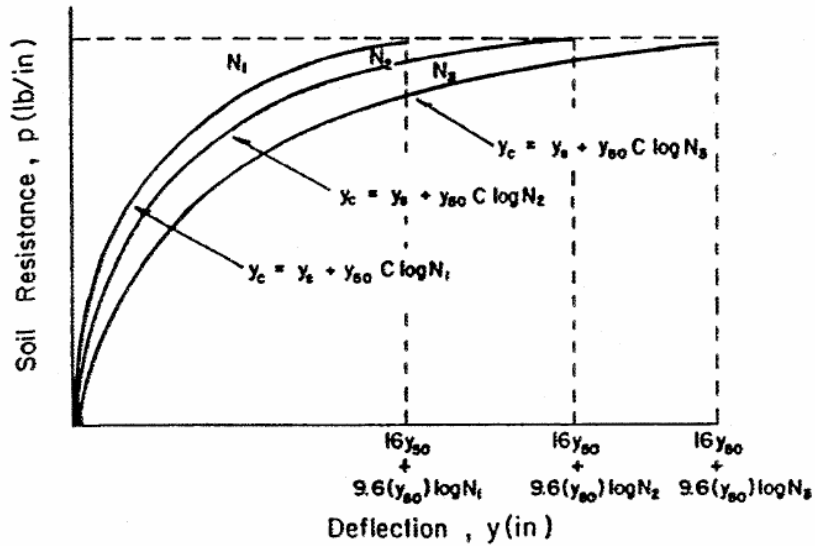


Figure 4-7: Characteristic shape of p - y curves for cyclic loading in stiff clay above the water table.

P-Y CURVES FOR PILES IN SAND

Experimental data for p - y curves of piles in sand were collected through a series of extensive tests performed on pipe piles driven in submerged sands (Reese 1983). The results were then adjusted to cover both sands below and above water table. The test piles were two steel pipes 24 inches in diameter driven into sand. The following steps show the procedure for computing the p - y curves as described by Reese, Cox, and Koop (1974).

Figure 4-8 shows typical p - y curve in sands which usually consists of the following segments:

SEGMENT	Curve type	Range of y	Range of p	p - y curve
1	Linear	0 to y_k	0 to p_k	$p = (kx)y$
2	Parabolic	y_k to y_m	p_k to p_m	$p = p_m \left(\frac{y}{y_m} \right)^n$
3	Linear	y_m to y_u	p_m to p_u	$p = p_m + \frac{p_u - p_m}{y_u - y_m} (y - y_m)$
4	Linear	$\geq y_u$	p_u	$p = p_u$

Where y_m and y_u , p_m and p_u can be determined directly from soil parameters.

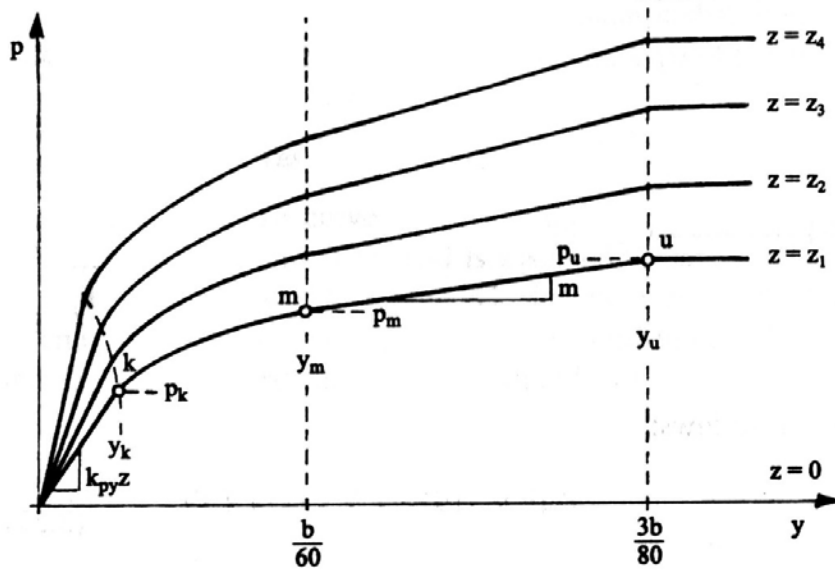


Figure 4-8: Characteristic shape of p-y curves in sand.

Get the following parameters:

$$\alpha = \frac{\phi}{2}; \quad \beta = 45 + \frac{\phi}{2}; \quad K_o = 0.4$$

$$K_a = \tan^2\left(45 - \frac{\phi}{2}\right)$$

Calculate the ultimate soil resistance P_u per unit length of the pile,

$$p_{st} = \gamma x \left[\frac{k_o \tan \phi \sin \beta}{\tan(\beta - \phi) \cos \alpha} + \frac{\tan \beta}{\tan(\beta - \phi)} (B + x \tan \beta \tan \alpha) \right.$$

$$\left. + K_o x \tan \beta (\tan \phi \sin \beta - \tan \alpha) - K_a B \right]$$

$$p_{sd} = K_a B \lambda x (\tan^8 \beta - 1) + K_o B \gamma x \tan \phi \tan^4 \beta$$

where

$$P_u = \text{Minimum of } (p_{st}, p_{sd})$$

$$y_u = \frac{3b}{80}$$

$$p_u = \overline{A}_s p_s \quad \text{or} \quad p_u = \overline{A}_c p_s$$

The values of \bar{A}_s and \bar{A}_c are in Figure 4-9.

$$y_m = \frac{b}{60}$$

$$p_m = B_s p_s \text{ or } p_m = B_c p_s$$

where B_s and B_c can be taken from Figure 4-10.

Construct the initial straight-line portion of the p - y curves

$$p = (kx)y$$

where k can be found in Table 4-2.

Table 4-2: Representative values of k in sand

Relative density	Loose	Medium	Dense
Recommended k for sand below water table (lb/in ³)	20	60	125
Recommended k for sand above water table (lb/in ³)	25	90	225

The parabolic section of the p - y curves is given as

$$p = \bar{C}y^{1/n}$$

and the slope of the line between points m and u is

$$m = \frac{p_u - p_m}{y_u - y_m}$$

The power of the parabolic section is given by

$$n = \frac{p_m}{my_m}$$

The coefficient \bar{C} is as follows

$$\bar{C} = \frac{p_m}{y_m^{1/n}}$$

and finally the values of y_k is

$$y_k = \left(\frac{\bar{C}}{kx} \right)^{n/n-1}$$

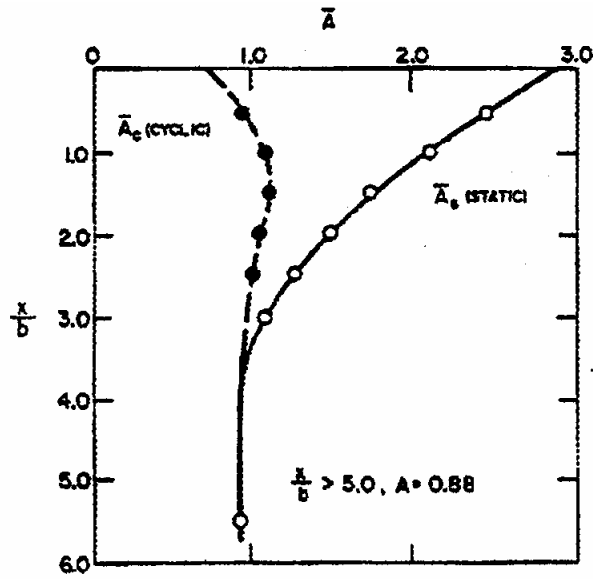


Figure 4-9: Values of coefficients \bar{A}_c and \bar{A}_s .

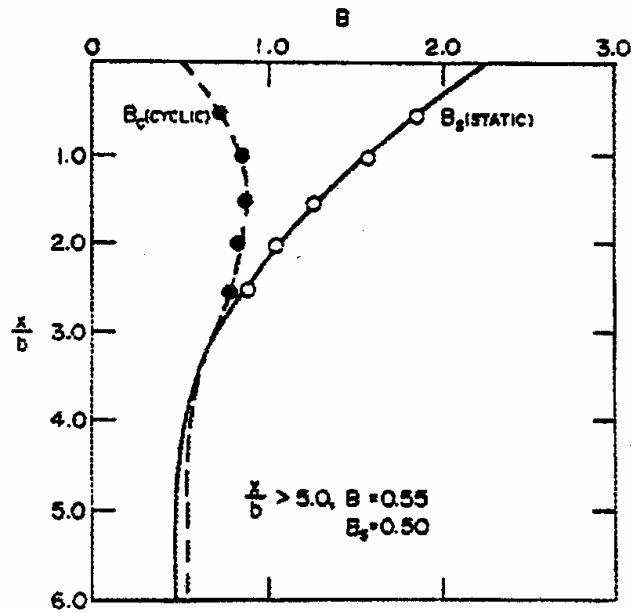


Figure 4-10: Non-dimensional coefficient B for soil resistance versus depth.

4.9.4 AXIALLY LOADED PILES

Piles normally used in groups such that the design capacity can be calculated based on single pile capacity. Axially loaded piles usually develop their carrying capacity by either bearing or skin friction along the soil-pile interface. In some situations, the pile capacity can be a combination of skin friction and end bearing at the pile tip.

The ultimate compressive capacity, Q_T of a single pile under axial load parallel to its axis is the sum of the surface friction capacity of the shaft Q_s , and the tip bearing capacity Q_b .

$$Q_T = Q_s + Q_b \quad (4-9)$$

or in a conservative form, the ultimate axial capacity can be written as

$$Q_T = Q_s + Q_b - W \quad (4-10)$$

Where W is the weight of the pile.

4.9.4.1 LOAD DISPLACEMENT CURVES

Several approaches have been developed in the past to predict the pile load-displacements curves behavior under axial compression. Mosher and Dawkins (2000) summarized some of the commonly used criteria of these curves. Based on a previous work done by Coyle and Castello (1981) and the results of load tests of prismatic pipe piles driven in sand, Mosher (1984) represented the load-slip relation as a hyperbolic curve as shown in Figure 4-11. The load is related to the displacement in terms of the initial slope of the curve k_f and the ultimate side friction f_{max} ,

$$f = \frac{w}{\frac{1}{k_f} + \frac{w}{f_{max}}} \quad (4-11)$$

Where k_f is a function of the angle internal friction and f_{max} is a function of relative depth and given in Table 4-3 and f_{max} is given in Figure 4-12.

Table 4-3: Values of k_f as a function of angle of internal friction of sand (Mosher)

Angle of internal friction (degrees)	k_f (psf/in)
28 – 31	6,000 – 10,000
32 – 34	10,000 – 14,000
35 – 38	14,000 – 18,000

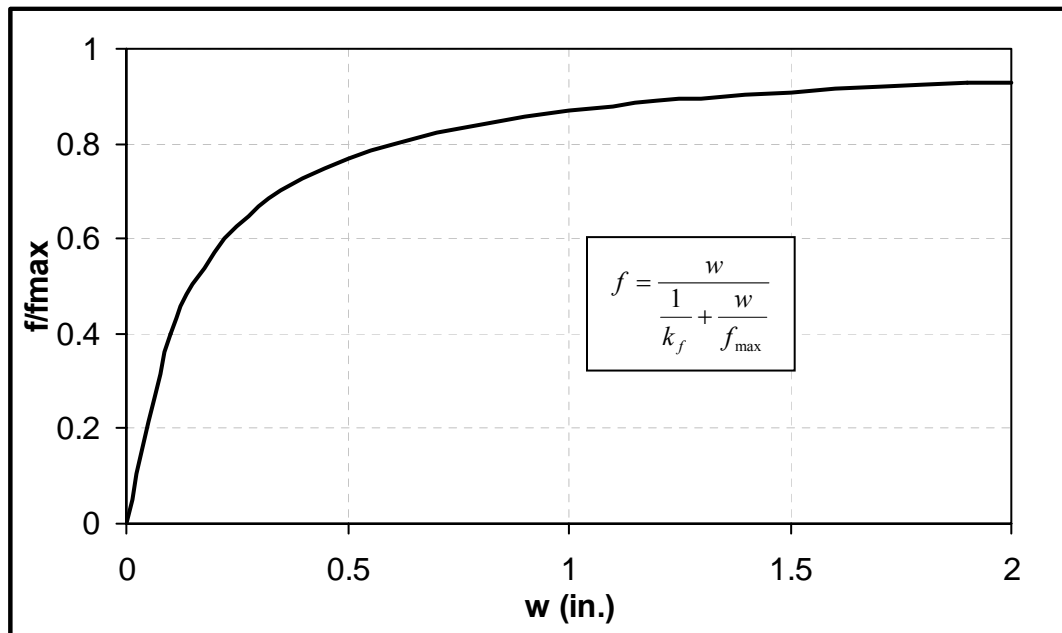


Figure 4-11: f-w curve (Mosher 2000).

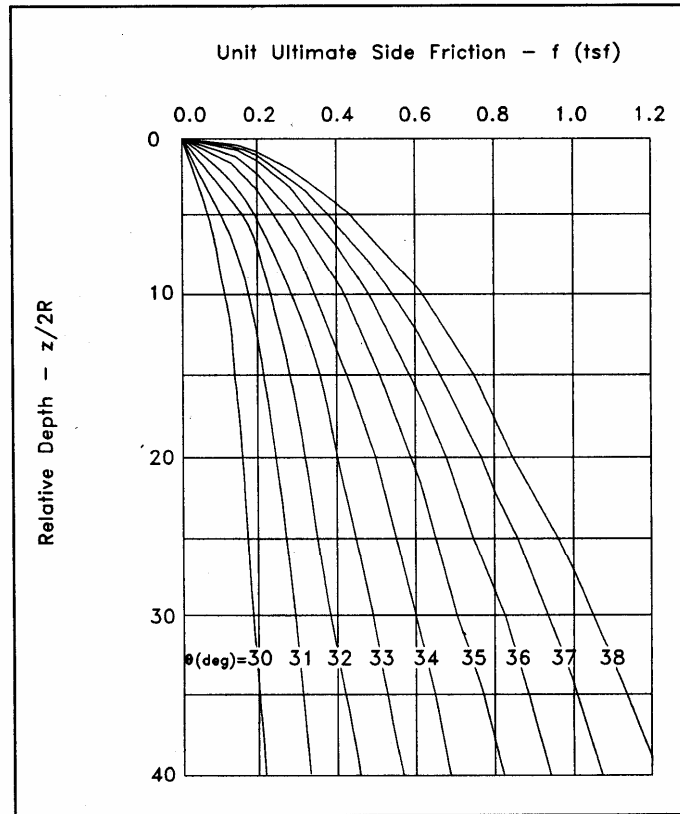


Figure 4-12: Values of ultimate side friction as a function of relative depth (Mosher 2000).

An other form of f - w curves has been proposed as a function of the ultimate side friction, f_{\max} and the displacement required to develop that force, w_c Vijayvergiya (1977). The relation has assumed to have some limitations on the values of f_{\max} and w_c or different types of soils. A typical f - w curve by this method is shown in Figure 4-13

$$\frac{f}{f_{\max}} = 2 \sqrt{\frac{w}{w_c}} - \frac{w}{w_c} \quad (4-12)$$

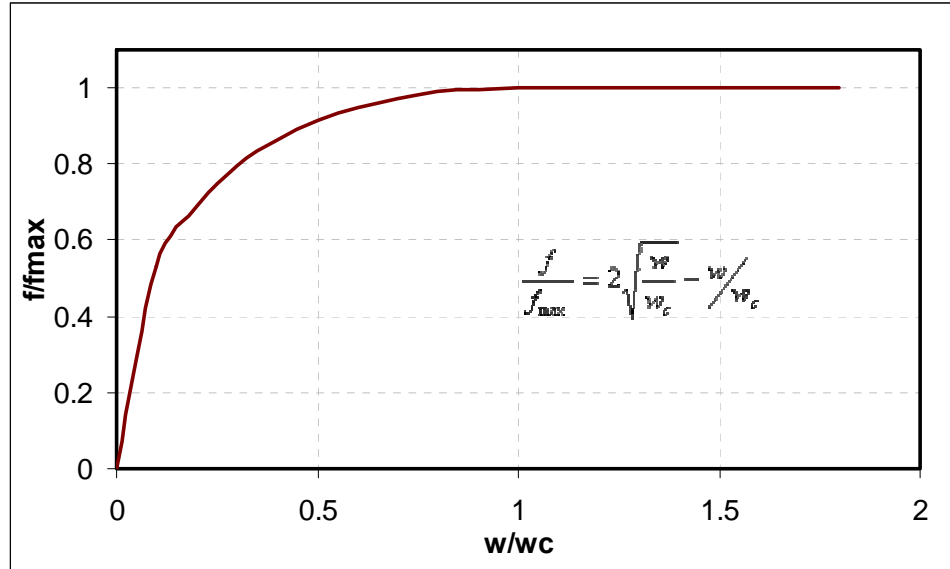


Figure 4-13: f - w curves (Vijayvergiya 1977).

4.9.5 THE MODIFIED RAMBERG OSGOOD MODEL

Amde et al (1982), Greimann et al (1984), and Greimann et al (1987) utilized an idealized model based on the modified Ramberg-Osgood formula to approximate the load-displacement curves for axially and laterally loaded piles. The required parameters for the model can be calculated from the soil and pile properties. This model can be used for the three types of curves with the appropriate soil parameters for each curve. The modified Ramberg-Osgood model has the following form,

$$p = \frac{k_h y}{\left[1 + \left[\frac{y}{y_u} \right]^n \right]^{1/n}} \quad (4-13)$$

with $y_u = \frac{p_u}{k_h}$

where

k_h = initial lateral stiffness

p = generalized soil resistance

p_u = ultimate lateral soil resistance

N = shape parameter

y = generalized displacement

This model has some advantages over other models and in addition it includes the hyperbola which is commonly used as a special case of the curve.

The following tables present the different types of load-displacement curves for different types of soils.

Table 4-4: Analytical forms of p - y curves

Case	n	P_u (Use Lesser Value)	k_h
Soft Clay, Static Load	1.0	$P_u = 9C_u B$ $P_u = (3 + \frac{\gamma}{C_u} x + \frac{0.5}{B} x) C_u B$	$\frac{P_u}{y_{50}}$
Stiff Clay, Static Load	1.0	$P_u = 9C_u B$ $P_u = (3 + \frac{\gamma}{C_u} x + \frac{0.5}{B} x) C_u B$	$\frac{P_u}{y_{50}}$
Very Stiff Clay, Static Load	2.0	$P_u = 9C_u B$ $P_u = (3 + \frac{\gamma}{C_u} x + \frac{2.0}{B} x) C_u B$	$\frac{P_u}{2y_{50}}$
Sand, Static Load	3.0	$P_u = \gamma x [B(k_p - k_a) + \eta + \mu]$ $P_u = \gamma x (k_p^3 + 2k_p^2 k_o \tan \phi - k_a) B$ $\eta = x k_p \tan \alpha \cdot \tan \beta$ $\mu = x k_o \tan \beta (\tan \phi - \tan \alpha)$	$\frac{J\gamma x}{1.35}$

Where:

C_u = Undrained cohesion indicated for an unconsolidated undrained laboratory test

B = Pile width

γ = Effective unit soil weight

x = Depth from soil surface

ϕ = Angle of internal friction

$$k_p = \frac{1 + \sin \phi}{1 - \sin \phi}$$

$$k_a = \frac{1 - \sin \phi}{1 + \sin \phi}$$

$$\alpha = \frac{\phi}{2} \text{ for dense or medium sand}$$

$$= \frac{\phi}{3} \text{ for loose sand}$$

$$\beta = 45^\circ + \frac{\phi}{2}$$

J = 200 for loose sand

= 600 for medium sand

= 1500 for dense sand

y_{50} Displacement at one-half ultimate soil reaction

= $2.5B\varepsilon_{50}$ for soft and stiff clay

= $2.0B\varepsilon_{50}$ for very stiff clay

ε_{50} From laboratory triaxial test, or use

= 0.02 for soft clay

= 0.01 for stiff clay

= 0.005 for very stiff clay

(Axial strain at 0.5 times peak stress difference)

Table 4-5 - Analytical forms of f - z curves

Case	Basic f - z Curves Equations	f_{\max} , (klf)	
		H Piles	Others
Clay, Static Load	$\frac{f}{f_{\max}} = 2\sqrt{\frac{z}{z_c}} - \frac{z}{z_c}$	The least of: $2(d + b_f)c_u$ $2(d + 2b_f)c_a$ $2(dc_u + b_fc_a)$	The lesser of: $l_g c_a$ $l c_u$
Sand, Static Load	$\frac{f}{f_{\max}} = 2\sqrt{\frac{z}{z_c}} - \frac{z}{z_c}$	$0.04N(d + 2b_f)$	$0.04Nl_g$

Where:

- C_u Undrained cohesion of the clay soil
= $97.0N + 114.0$ (psf)
- C_a Adhesion between soil and pile
= αc_u (psf)
- α Shear strength reduction factor.
- N Average standard penetration blow count
- z_c Relative displacement required to develop f_{\max}
= 0.4 in. for sand
= 0.25 in. for clay
- l_g Gross perimeter of the pile (ft.)
- d Section depth of H pile or diameter of pipe pile (ft.)
- b_f Flange width of H pile (ft.)

For pile tip-settlement (q - z) curves, the equations listed in Table 4-4 and Table 4-5 can be used to calculate the parameters k_q , q_{max} and n .

Table 4-6 - Analytical forms of q - z curves

Case	Basic q - z Curves Equations	f_{max} , ksf
Clay, Static Load	$\frac{q}{q_{max}} = \left(\frac{z}{z_c} \right)^{1/3}$	$9c_u$
Sand, Static Load	$\frac{q}{q_{max}} = \left(\frac{z}{z_c} \right)^{1/3}$	$8N_{corr}$

Where:

N_{corr} Corrected standard penetration test (SPT) blow count at depth of pile tip

= N (uncorrected) if $N \leq 15$

= $15 + 0.5(N - 15)$ if $N > 15$

C_u Undrained cohesion of the clay soil

= $97.0N + 114.0$ (psf)

N Average standard penetration blow count

z_c Relative displacement required to develop q_{max}

= 0.4 in. for sand

= 0.25 in. for clay

Table 4-7 - Parameters used in the modified Ramberg-Osgood models for clay and sand

Curve Type	Soil Type	Calculated		Used	
		k_h	n	k_h	N
p-y	Soft Clay	$0.669 \frac{P_u}{y_{50}}$	1.5	$\frac{P_u}{y_{50}}$	1.0
	Stiff Clay	$0.915 \frac{P_u}{y_{50}}$	1.07	$\frac{P_u}{y_{50}}$	1.0
	Very Stiff Clay	$0.539 \frac{P_u}{y_{50}}$	2.56	$\frac{P_u}{2y_{50}}$	2.0
	Sand			$\frac{J\gamma x}{1.35}$	3.0
f-z	All Soils	$7.32 \frac{f_{\max}}{z_c}$	1.33	$10 \frac{f_{\max}}{z_c}$	1.0
q-z	All Soils	$7.32 \frac{q_{\max}}{z_c}$	1.33	$10 \frac{q_{\max}}{z_c}$	1.0

4.10 PILES IN INTEGRAL BRIDGES

Interest in using integral bridges has increased in the last two decades. Economy, reliability and strength are the main reasons of that interest. Integral (or jointless) bridges are bridges with no joints between the superstructure and the supporting abutments. The bridge girders are integrally built with the abutment to form a rigid connection. The structural elements of a typical abutment in an integral bridge usually consist of an abutment wall, two wing walls, and several supporting piles. The abutment walls and wing walls are usually reinforced concrete elements. The piles are made with either structural steel or pre-cast concrete.

Abutments in integral bridges are subjected to forces similar to those in bridges with expansion joints plus the horizontal forces resulting from thermal movements. The abutment is monolithically connected to the deck to eliminate constructing any expansion joint. Joints are provided to accommodate longitudinal movements in bridges. Longitudinal movements are caused by thermal forces due to temperature changes, horizontal earth pressure, soil movements, and vehicles braking forces. The abutment movements that are usually absorbed by the expansion joints in regular bridges will be transferred to the supporting piles as lateral forces in integral abutment bridges. Piles in such bridges manner should be designed to have some amount of flexibility to accommodate these movements. Integral abutment piles are recommended to be driven vertically in a single row to achieve the highest flexibility performance. Piles are preferred to be oriented so that the weak axis of bending will be perpendicular to the bridge axis. However, because of flange buckling potential, the total lateral movement that can be absorbed will be more limited than that of strong axis orientation bending.

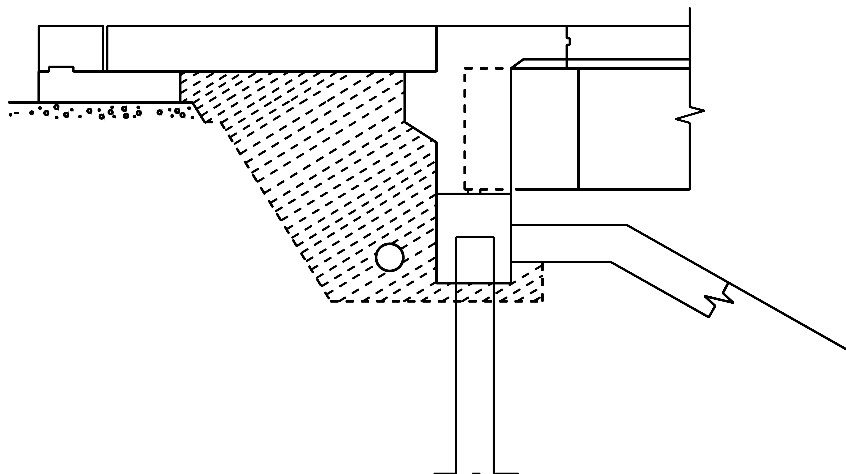


Figure 4-14: Sketch for an integral abutment.

Advantages of Jointless bridges

Jointless bridges have many advantages when compared to bridges with joints and expansion bearings. In addition to their good performance in the field, they are also less expensive in terms of initial cost and long term maintenance. Bridge bearings and joints are continuously subjected wear and damage as a result of heavy impact traffic loads and temperature effects. Corrosion is also a major problem especially when waterproof joints start to leak and stop providing any protection for bearings and joints.

4.11 COMPOSITE PILES FOR INTEGRAL BRIDGES

Depending on the type of superstructure, span length, and boundary conditions of the bridge, different types of expansion joints and bearings are used in the field. It is found that expansion joints and bearings do not serve their intended purpose for several reasons:

- Corrosion caused by deicing chemicals leaking through the joints.
- Accumulation of debris and other foreign restricting the free joint movement.
- Differential elevation at the joints causing additional impact forces.
- High initial maintenance costs of joints and bearings.

Integral abutments are structures connected to superstructure decks without joints, irrespective of the bridge length and the number of spans. The resulting restraining effect implies, therefore, that the abutment must be designed and constructed to resist and absorb any creep, shrinkage, and thermal movements of the superstructure. (Xanthakos 1995). Engineering experience has proved that integral bridges are performing better than

jointed bridges with reduced initial and life cycle costs and also with minimal maintenance problems.

Construction of integral bridges is simpler and faster than the construction of jointed bridges because they require fewer parts and less material and are less labor intensive. Also conversion of simply supported bridges into integral bridges has been successful and has been shown to improve the performance of the bridge.

In spite of the many advantages of jointless bridges over jointed bridges, large numbers of new jointless bridges are not being built and large numbers of jointed bridges are not being converted to jointless bridges (Thippeswamy et al 1994). The reasons may be attributed to the following:

- An inadequate understanding of integral bridge behavior under soil settlement, temperature, and earth pressure.
- Limited performance data
- Inadequate experimental and analytical evaluations
- A lack of design and construction specifications.
- A higher cost to convert jointed bridges to jointless bridges.

Piles in bridges are the main factors in the stability of the bridge structure. The piles of integral abutment bridge are subjected to lateral movements caused by thermal expansion and contraction. Such piles can be treated as piles subjected to lateral loads. Dealing with such problems is not as easy as dealing with columns subjected to lateral loads. The problem of laterally loaded piles is complex because it involves the interaction between a semi-rigid structural element and the embedding soil. The complication is

because of the non-homogeneity of the soil. Most natural soils are non-homogeneous and can be disturbed as piles are installed.

In spite of their strength, reliability and cost economy, steel and concrete, the traditional piling materials are associated with several problems when used as piling materials in corrosive soils and marine environments. The loss of section due to corrosion of steel and deterioration of concrete could cause a major problem because of the reduction in carrying capacity of the pile system. The gradual decrease in the carrying capacity of the pile system could lead to catastrophic failure of the bridge.

Composites can be designed to perform according to the required specifications for piling in adverse environments. Composite materials such as fiber-reinforced polymers (FRPs) can offer performance advantages when compared to steel, concrete or timber. Their inherent performance advantages include corrosion resistance, high oriented-strength structural shapes, durability, and low maintenance.

FORMULATION OF THE NUMERICAL MODEL

The finite element analysis was initially developed on a physical basis for the analysis of problems in structural mechanics, but it was realized later that this method can be applied to solutions for many other kinds of problems. The method is based on the principle of solving the problem by going from a small part to the whole. The whole medium of the problem is assumed to consist of a combination of small parts joined together to form the whole structure. The small parts (elements) then are assembled to reach the final solution. Solutions resulting from finite element analysis are not exact solutions. In many engineering problems a close form solution is hard to reach some times.

5.1 ANALYSIS TOOLS

Numerous finite element codes are available with high capabilities in handling very complicated structures. ANSYS is a multi-purpose software which has multiple finite element capabilities that range from simple linear static analysis to complex nonlinear, transient dynamic analysis. The ANSYS element library contains a wide range of element types that fit different types of structures.

Analysis using ANSYS can be performed in three major steps:

1. Build the model (Preprocessing).
2. Apply loads and obtain solutions (Solution).
3. Review the results (Post Processing).

5.2 BUILDING THE COMPUTER MODEL

The main objective of finite element modeling is to create a mathematical representation of any engineering system that reflects the actual geometry and behavior of that system. The model should have similar boundary conditions and the same loading schemes so that it can serve as a physical prototype of the real system. Building finite element models in ANSYS requires familiarity with the ANSYS operating manual and the ANSYS element library. Each element in ANSYS has specific properties and behaviors to be defined according to the structure in the problem.

Model generation by ANSYS can be approached through two different methods: solid modeling and the direct generation method. In solid modeling the model is defined geometrically by describing the general shape, boundaries, element shape and size. However, in direct generation the user has to predefine all node locations and the shape, size and connectivity of each element. The first method is more powerful with more flexibility in meshing and the element generation. It is more appropriate for large 3-D models because it allows later modifications for the model geometry and facilitates the model management.

The following sections describe the major steps in building a finite element model using ANSYS.

5.2.1 SELECTING THE COORDINATES SYSTEM

ANSYS offers multiple coordinate systems that fit different shapes and geometries:

- Global and local coordinate systems
- A nodal coordinate system that defines the nodes, their directions and degrees of freedom.
- An element coordinate system which describes the element results output and its material properties orientation.

ANSYS has three built-in global coordinate systems that share the same origin: Cartesian, cylindrical, and spherical as shown in Figure 5-1. The appropriate coordinate system has to be chosen according to the geometry of the problem.

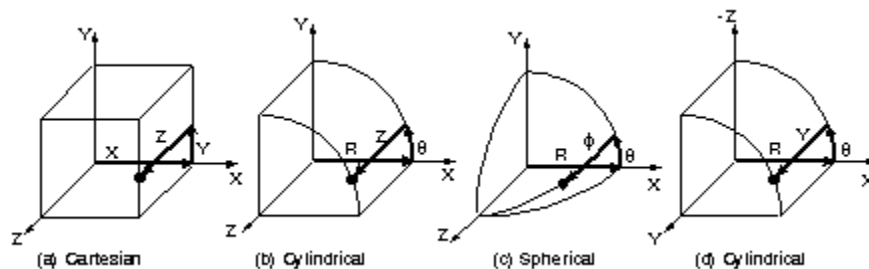


Figure 5-1: Global coordinate system (Ansys).

5.2.2 GENERATION OF THE SOLID MODEL

As presented earlier, the element generation can be done in different ways; each of them has its own advantages. The solid modeling method is more convenient in such models because of its flexibility over other methods. Several major steps are recommended to follow in this approach starting with keypoints and ending with the final meshed model.

The following steps summarize the basic steps in the solid modeling approach:

Step 1: Defining key points and lines

Keypoints are the lowest order of the solid model entities which normally define the vertices of the model. The keypoints work as a foundation for the solid model that locates the position of the model in the global coordinate system. A key point in the global system can be defined by three major coordinates; X,Y, and Z.

Step 2: Creating areas and volumes

The next step is to create an area or a volume from the previously defined keypoints and lines. Lines will serve as the boundaries for the created areas and volumes. Volume and area elements can be created directly through keypoints and line generation can be skipped. Lines should be created when mapped meshing is desired. Figure 5-2 shows an isometric view of an area created through keypoints and lines.

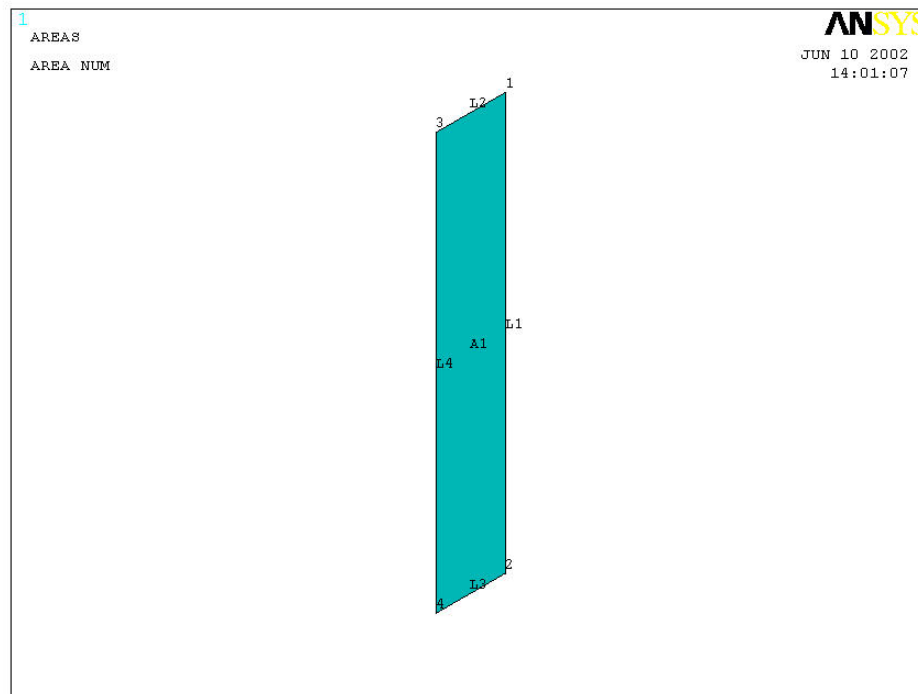


Figure 5-2: Isometric view for an area defined by keypoints and lines.

Step 3: Defining element attributes

Setting element attributes is necessary before generating elements and nodes from the solid model. Each element in the ANSYS library has specific properties and requires a set of attributes to be defined. The following attributes should be defined:

- Element type: in which the required elements have to be specified and defined before the meshing process.
- Real constants: The real constants usually describe the element geometrical properties such as thickness, area, inertia or fiber orientation angle and number of layers in the case of layered orthotropic materials.
- Material properties: Provide the necessary material properties, like elastic modulus, shear modulus, and Poisson's ratio.
- Element coordinate system: To locate the element axis system that's necessary for the output.

Step 4: Mesh generation

After setting all element types and attributes and before start meshing, it is required to set the mesh control. Two types of meshing are available: free and mapped meshing. Free meshing usually generated randomly without any restriction on the size and shape of the element. Mapped meshing is more restricted and done in a systematic way in terms of shape, size and elements pattern. ANSYS provides two mapped meshing options, quadrilateral and triangular elements. Figure 5-3 and Figure 5-4 show an illustration for a free and mapped meshed area. Figure 5-5 shows a sketch for the quadrilateral and triangular elements.

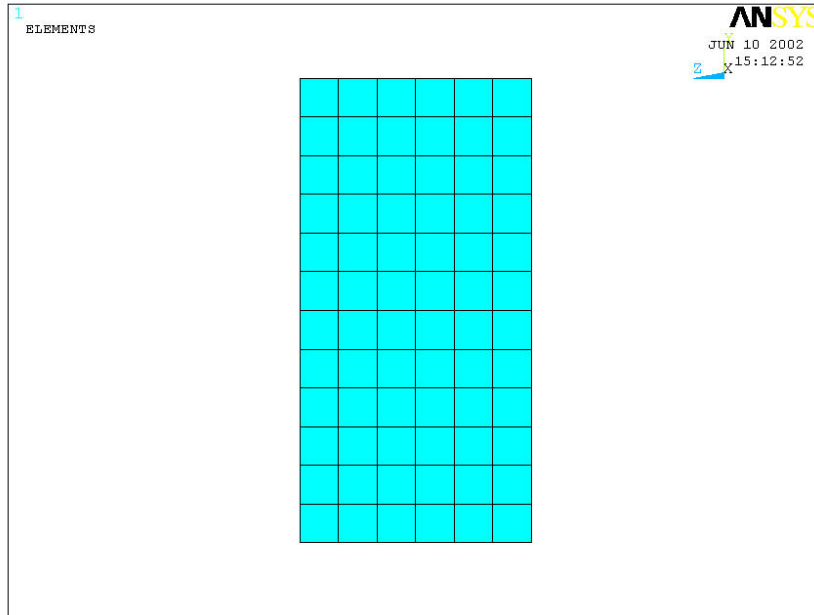
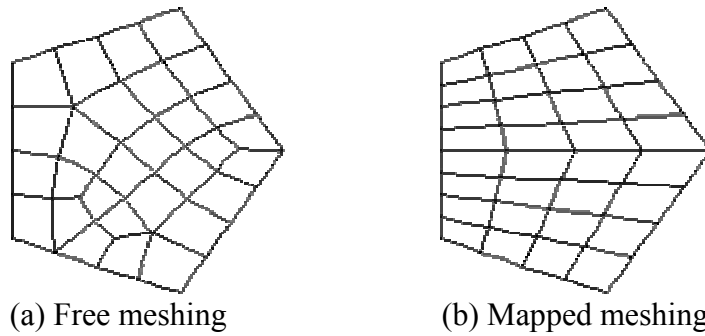


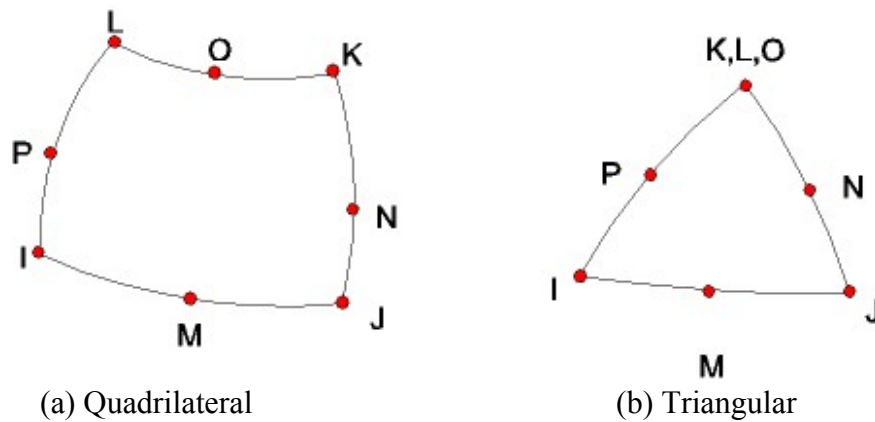
Figure 5-3: Mapped meshed area.



(a) Free meshing

(b) Mapped meshing

Figure 5-4: Free and mapped meshed areas (Ansys).



(a) Quadrilateral

(b) Triangular

Figure 5-5: Quadrilateral and triangular elements (Ansys).

Step 5: Applying loads and boundary conditions

Applying loads and boundary conditions is part of the solution phase in ANSYS. All loading and boundary conditions have to be specified before running the solution process.

5.3 ANALYSIS OF COMPOSITE MATERIALS

The finite element code ANSYS allows modeling FRP composite by using special layered elements that have the capability to represent the actual structure with its different layers and fiber orientations. Modeling orthotropic composites is different from regular isotropic materials in terms of directional material properties and failure criteria for the different layers. Special care has to be taken when specifying the element configuration and its local axis system.

Thin walled structures can be modeled using either a shell or solid element. The ANSYS library has two types of elements that can be used for layered structures. The first element is a 3-D structural, solid volume element with eight nodes, one at each corner. The second is a 3-D, 8-node structural shell element. The shell elements in the ANSYS library have 6 degrees of freedom at each node, three translational and 3 rotational. The solid elements only have 3 translational degrees at each node.

5.4 STRESS-STRAIN RELATIONSHIPS

The stress-strain relation is defined as

$$\{\sigma\} = [D]\{\epsilon^e\} \quad (5-1)$$

where :

$$\{\sigma\} = \text{Stress vector} = \{\sigma_x \ \sigma_y \ \sigma_z \ \sigma_{xy} \ \sigma_{yz} \ \sigma_{xz}\}^T$$

$$[D] = \text{Elasticity matrix}$$

$$\{\varepsilon^e\} = \text{Elastic strain vector} = \{\varepsilon\} - \{\varepsilon^t\}$$

$$\{\varepsilon\} = \text{Total strain vector} = \{\varepsilon_x \ \varepsilon_y \ \varepsilon_z \ \varepsilon_{xy} \ \varepsilon_{yz} \ \varepsilon_{xz}\}^T$$

$$\{\varepsilon^t\} = \text{Thermal strain vector.}$$

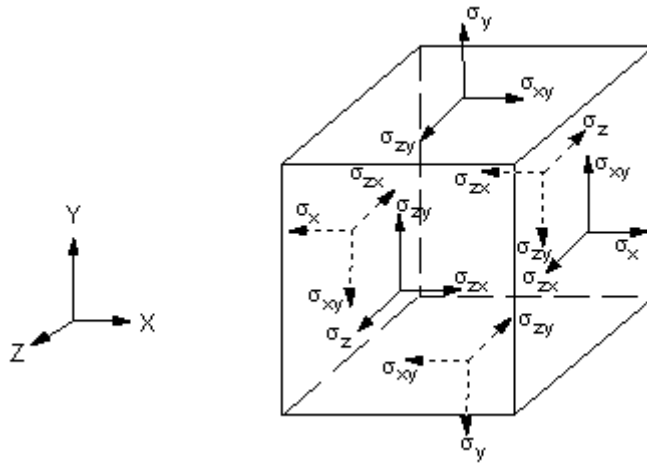


Figure 5-6: Stress tensors (Ansys).

Equation (5-1) can be inverted and written in the following form:

$$\{\varepsilon\} = \{\varepsilon^t\} + [D]^{-1} \{\sigma\} \quad (5-2)$$

where

$$\{\varepsilon^t\} = \Delta T \{\alpha_x \ \alpha_y \ \alpha_z \ 0 \ 0 \ 0\} \quad (5-3)$$

α_x = Thermal coefficient of expansion in the x- direction

$$\Delta T = T - T_{REF}$$

T = Current temperature

T_{REF} = Reference temperature (strain –free)

$$[D]^{-1} = \begin{bmatrix} \frac{1}{E_x} & -\frac{\nu_{xy}}{E_x} & -\frac{\nu_{xz}}{E_x} & 0 & 0 & 0 \\ -\frac{\nu_{yx}}{E_y} & \frac{1}{E_y} & -\frac{\nu_{yz}}{E_y} & 0 & 0 & 0 \\ -\frac{\nu_{zx}}{E_z} & -\frac{\nu_{yz}}{E_z} & \frac{1}{E_z} & 0 & 0 & 0 \\ 0 & 0 & 0 & \frac{1}{G_{xy}} & 0 & 0 \\ 0 & 0 & 0 & 0 & \frac{1}{G_{yz}} & 0 \\ 0 & 0 & 0 & 0 & 0 & \frac{1}{G_{xz}} \end{bmatrix} \quad (5-4)$$

where:

E_x = Young's modulus in the x-direction

ν_{xy} = Major Poisson's ratio

ν_{yx} = Minor Poisson's ratio

G_{xy} = Shear modulus

$$\frac{\nu_{yx}}{E_y} = \frac{\nu_{xy}}{E_x}$$

$$\frac{\nu_{zx}}{E_z} = \frac{\nu_{xz}}{E_x}$$

$$\frac{\nu_{zy}}{E_z} = \frac{\nu_{yz}}{E_y}$$

In an explicit form, equation (5-3) can be written as,

$$\varepsilon_x = \alpha_x \Delta T + \frac{\sigma_x}{E_x} - \frac{\nu_{xy} \sigma_y}{E_x} - \frac{\nu_{xz} \sigma_z}{E_x} \quad (5-5)$$

$$\varepsilon_y = \alpha_y \Delta T - \frac{\nu_{xy} \sigma_x}{E_x} + \frac{\sigma_y}{E_y} - \frac{\nu_{yz} \sigma_z}{E_y} \quad (5-6)$$

$$\varepsilon_z = \alpha_z \Delta T - \frac{\nu_{xz} \sigma_x}{E_x} - \frac{\nu_{yz} \sigma_z}{E_y} + \frac{\sigma_z}{E_z} \quad (5-7)$$

$$\varepsilon_{xy} = \frac{\sigma_{xy}}{G_{xy}} \quad (5-8)$$

$$\varepsilon_{yz} = \frac{\sigma_{yz}}{G_{yz}} \quad (5-9)$$

$$\varepsilon_{xz} = \frac{\sigma_{xz}}{G_{xz}} \quad (5-10)$$

Layered structural solid (SOLID46)

This element is designed to model layered thick shells or solids. It allows up to 250 layers of different materials. The element has 8 nodes with three translational degrees of freedom for each node.

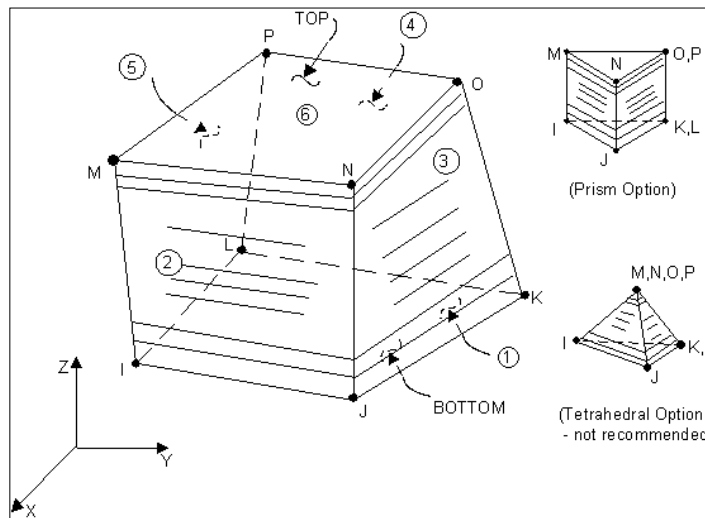
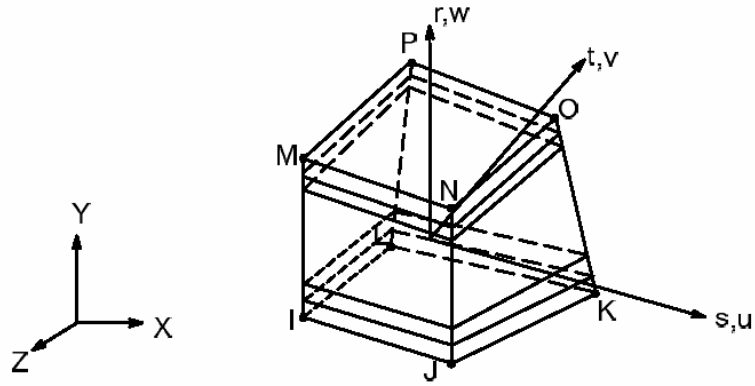


Figure 5-7: Characteristic shape of SOLID46 element (Ansys).

The element can be defined either by predefined nodal points or by meshing existing volumes. The element local x- axis is along the I-J side with the origin at node I. The y-axis is in the J-K direction and the z-axis is in the element thickness direction J-N. The element shape functions are given as follows:



$$u = \frac{1}{8} \begin{pmatrix} u_I(1-s)(1-t)(1-r) + u_J(1+s)(1-t)(1-r) \\ + u_K(1+s)(1+t)(1-r) + u_L(1-s)(1+t)(1-r) \\ + u_M(1-s)(1-t)(1+r) + u_N(1+s)(1-t)(1+r) \\ + u_O(1+s)(1+t)(1+r) + u_P(1-s)(1+t)(1+r) \end{pmatrix} \quad (5-11)$$

$$v = \frac{1}{8} \begin{pmatrix} v_I(1-s)(1-t)(1-r) + v_J(1+s)(1-t)(1-r) \\ + v_K(1+s)(1+t)(1-r) + v_L(1-s)(1+t)(1-r) \\ + v_M(1-s)(1-t)(1+r) + v_N(1+s)(1-t)(1+r) \\ + v_O(1+s)(1+t)(1+r) + v_P(1-s)(1+t)(1+r) \end{pmatrix} \quad (5-12)$$

$$w = \frac{1}{8} \begin{pmatrix} w_I(1-s)(1-t)(1-r) + w_J(1+s)(1-t)(1-r) \\ + w_K(1+s)(1+t)(1-r) + w_L(1-s)(1+t)(1-r) \\ + w_M(1-s)(1-t)(1+r) + w_N(1+s)(1-t)(1+r) \\ + w_O(1+s)(1+t)(1+r) + w_P(1-s)(1+t)(1+r) \end{pmatrix} \quad (5-13)$$

and the stress-strain relationship is give as follows:

$$\begin{Bmatrix} \varepsilon_x \\ \varepsilon_y \\ \varepsilon_z \\ \varepsilon_{xy} \\ \varepsilon_{yz} \\ \varepsilon_{xz} \end{Bmatrix} = \begin{Bmatrix} \alpha_{xj}\Delta T \\ \alpha_{yj}\Delta T \\ \alpha_{zj}\Delta T \\ 0 \\ 0 \\ 0 \end{Bmatrix} \begin{bmatrix} \frac{1}{E_{x,j}} & -\frac{\nu_{xy,j}}{E_{y,j}} & -\frac{\nu_{xz,j}}{E_{z,j}} & 0 & 0 & 0 \\ -\frac{\nu_{yx,j}}{E_{y,j}} & \frac{1}{E_{y,j}} & -\frac{\nu_{yz,j}}{E_{z,j}} & 0 & 0 & 0 \\ -\frac{\nu_{xz,j}}{E_{z,j}} & -\frac{\nu_{yz,j}}{E_{z,j}} & \frac{1}{E_{z,j}} & 0 & 0 & 0 \\ 0 & 0 & 0 & \frac{1}{G_{xy,j}} & 0 & 0 \\ 0 & 0 & 0 & 0 & \frac{1}{G_{yz,j}} & 0 \\ 0 & 0 & 0 & 0 & 0 & \frac{1}{G_{xz,j}} \end{bmatrix} \begin{Bmatrix} \sigma_x \\ \sigma_y \\ \sigma_z \\ \sigma_{xy} \\ \sigma_{yz} \\ \sigma_{xz} \end{Bmatrix} \quad (5-14)$$

where:

$\alpha_{x,j}$ = Coefficient of thermal expansion of layer j in the x –direction.

$E_{x,j}$ = Young’s modulus of layer j in the x-direction

$G_{xy,j}$ = Shear modulus of layer j in the x-direction

$\nu_{xy,j}$ = Poisson’s ratio of layer j in x-y plane

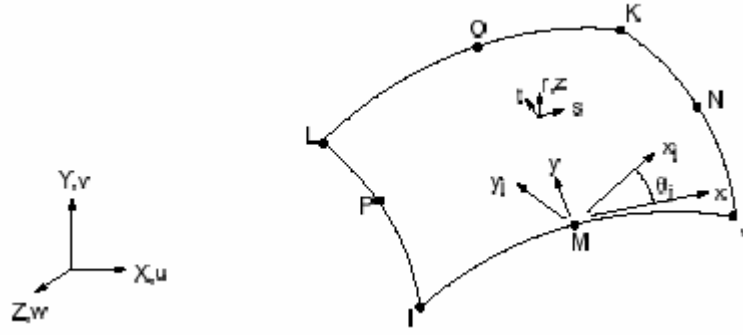
$\Delta T = T - T_{ref}$

$T =$ Temperature at point being studied

T_{ref} Reference temperature

Layered structural shell (Shell99)

This is an 8 node element with 6 degrees of freedom at each node. The shape functions for this element are given as follows:



$$\begin{Bmatrix} u \\ v \\ w \end{Bmatrix} = \sum_{i=1}^8 N_i \begin{Bmatrix} u_i \\ v_i \\ w_i \end{Bmatrix} + \sum_{i=1}^8 N_i \frac{rt_i}{2} \begin{bmatrix} a_{1,i} & b_{1,i} \\ a_{2,i} & b_{2,i} \\ a_{3,i} & b_{3,i} \end{bmatrix} \begin{Bmatrix} \theta_{x,i} \\ \theta_{y,i} \end{Bmatrix} \quad (5-15)$$

and the element strains and stresses are calculated as

$$\{\varepsilon\}_j = [T_m]_j [B] \{u_e\} \quad (5-16)$$

$$\{\sigma\}_j = [D]_j (\{\varepsilon\}_j - \{\varepsilon^t\}_j) \quad (5-17)$$

$$\{\sigma_e\}_j = [T_m]_j^T \{\sigma\}_j \quad (5-18)$$

where:

$\{u_e\}$ = Element displacement vector

$\{\varepsilon^t\}_j$ = Thermal strain at layer j

$\{\sigma_e\}_j$ = Stresses in element orientation

The in-plane forces and out of plane moments are calculated as follows:

$$T_x = \sum_{j=1}^{N_l} t_j \left(\frac{\sigma^t_{x,j} + \sigma^b_{x,j}}{2} \right) \quad (5-19)$$

$$T_y = \sum_{j=1}^{N_l} t_j \left(\frac{\sigma^t_{y,j} + \sigma^b_{y,j}}{2} \right) \quad (5-20)$$

$$T_{xy} = \sum_{j=1}^{N_l} t_j \left(\frac{\sigma_{xy,j}^t + \sigma_{xy,j}^b}{2} \right) \quad (5-21)$$

$$M_x = \frac{1}{6} \sum_{j=1}^{N_l} t_j (\sigma_{x,j}^b (2z_j^b + z_j^t) + \sigma_{x,j}^t (2z_j^t + z_j^b)) \quad (5-22)$$

$$M_y = \frac{1}{6} \sum_{j=1}^{N_l} t_j (\sigma_{y,j}^b (2z_j^b + z_j^t) + \sigma_{y,j}^t (2z_j^t + z_j^b)) \quad (5-23)$$

$$M_{xy} = \frac{1}{6} \sum_{j=1}^{N_l} t_j (\sigma_{xy,j}^b (2z_j^b + z_j^t) + \sigma_{xy,j}^t (2z_j^t + z_j^b)) \quad (5-24)$$

and the transverse shear forces are given as:

$$N_x = \sum_{j=1}^{N_l} t_j \sigma_{xz,j} \quad (5-25)$$

$$N_y = \sum_{j=1}^{N_l} t_j \sigma_{yz,j} \quad (5-26)$$

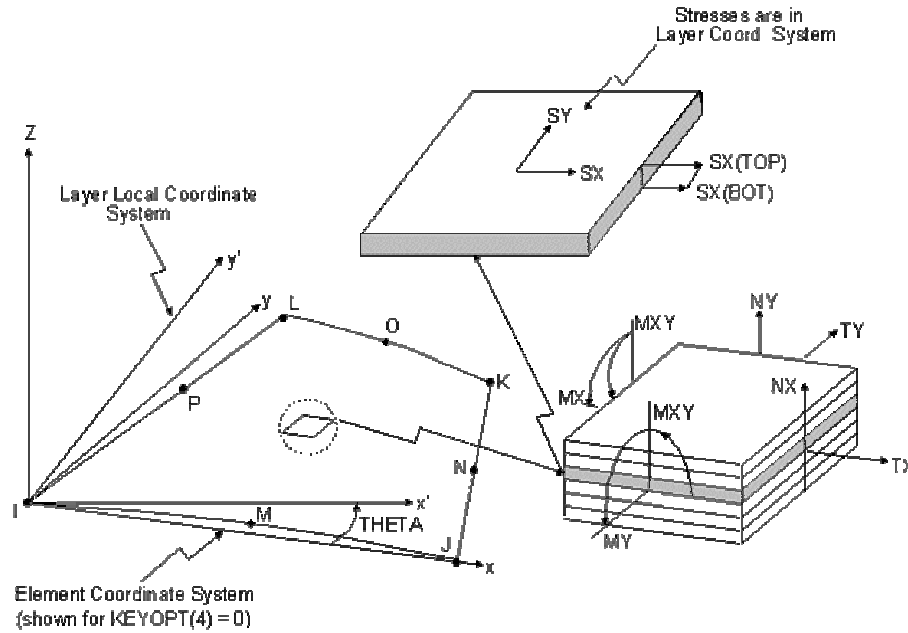


Figure 5-8: Stress output for Shell99 element (Ansys).

where:

$T_x =$ In-plane force per unit length

$\sigma_{x,j}^t$ = Stress at top of layer j in element x direction

$\sigma_{x,j}^b$ = Stress at bottom of layer j in element x direction

t_j = Thickness of layer j

M_x = x- moment per unit length

z_j^b = z- coordinate for bottom layer j

z_j^t = z- coordinate of top of layer j

z = Coordinate normal to shell, with $z=0$ being at shell midsurface

N_x = Transverse x-shear force per unit length

$\sigma_{xz,j}$ = Average transverse shear stress in layer j in element x-z plane

5.5 SOIL-PILE MODEL

As discussed in chapter 4 the soil pile interaction will be modeled using the subgrade reaction method that is based on the Winkler approach. The pile will be represented by a 3-D shell or solid elements connected to the nonlinear spring elements that represent the soil behavior.

The ANSYS finite element model will be generated using the solid modeling method. It will start from bottom to top ending with the final meshed model.

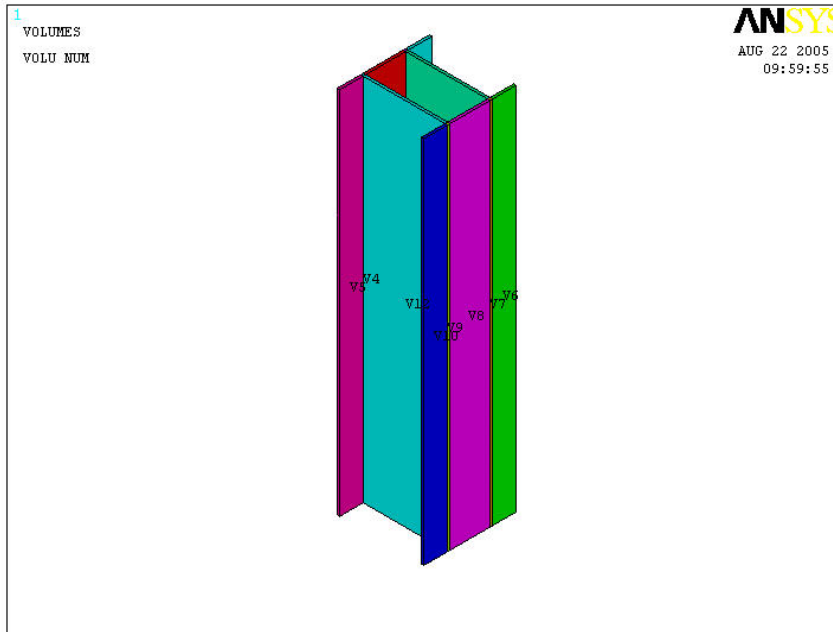


Figure 5-9: 3-D solid model.

The first model is a II section built up from solid sections connected to each other to work as one unit. Intersected volumes should share the keypoints and lines to work as a single unit. Unconnected areas or volumes will lead to a discontinuity in the model. To allow flexibility in section size and geometry, the section is built up of several volumes connected to each other through keypoints and lines. The second model has a circular cross-section generated using the cylindrical coordinates system.

Meshing:

The next step is the meshing process in which the created keypoints and areas are converted to nodes and elements. The mapped meshing is recommended in the present situation in which the areas will be divided into a uniform pattern of elements and nodes. This type of meshing gives more flexibility in node and element management. Mapped meshing on areas can be performed in several ways in ANSYS. One method is through the edge lines at each area as shown in the Figure 5-10. The line can be divided to the

required number of divisions such that parallel lines will have the exact number of divisions.

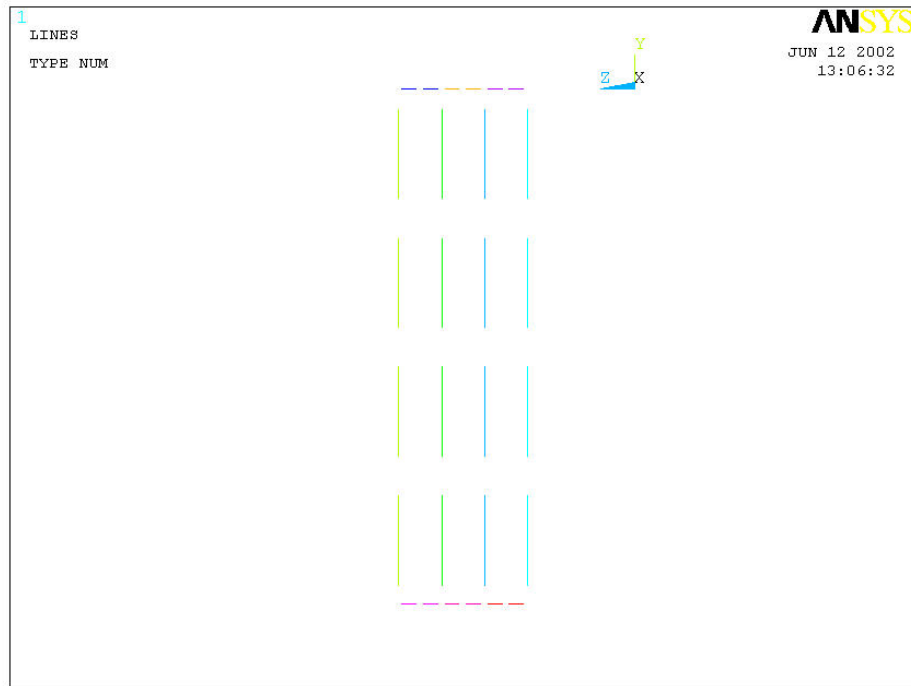


Figure 5-10: Mapped meshing for lines.

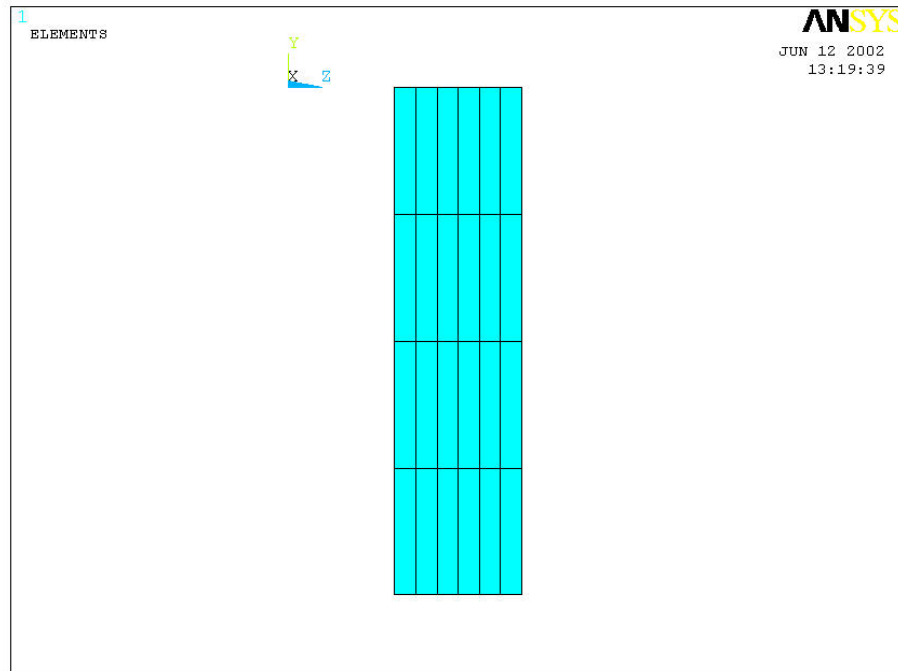


Figure 5-11: Mapped meshing for areas.

Soil springs:

The nonlinear behavior of the soil around the pile will be represented by spring elements distributed all over the pile. The springs may have different properties at various depths depending on the type of soil. ANSYS has several multi purpose spring elements with different capabilities. COMBIN39 is a unidirectional element with nonlinear force-deflection capability that fits different types of analysis. It can be define by the input of the force-deflection data points for both tension and compression sides. The force-deflection curve can take up to 20 data point in ascending order.

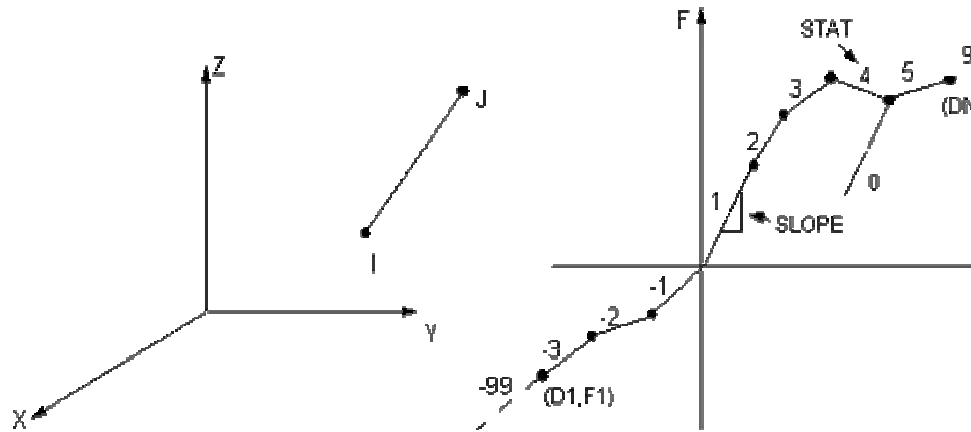


Figure 5-12: Force-displacement curves for spring elements (Ansys).

The element stiffness matrix and load [vectors] are given as

$$[K_e] = K^{tg} \begin{bmatrix} 1 & -1 \\ -1 & 1 \end{bmatrix} \quad (5-27)$$

$$\{F_e^{nr}\} = F_1 \begin{Bmatrix} 1 \\ -1 \end{Bmatrix} \quad (5-28)$$

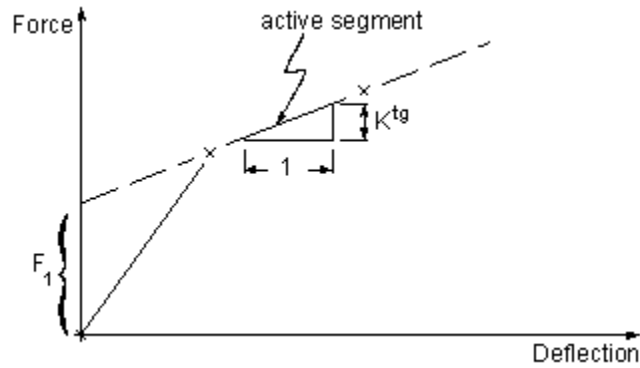


Figure 5-13: Stiffness computation for spring elements (Ansys).

where:

K^{tg} = Slope of the active segment from pervious iteration

F_1 = Force in element from previous iteration

A separate FORTRAN code was created to handle the creation of the spring load-displacement curves. The ANSYS batch file that generates the solid model creates several output files that contain the numbers and locations of the nodes to be connected to the spring elements. These files then serve as an input for the FORTRAN code from which it generates the nonlinear spring curves for all specified locations. All generated spring data and their connectivity nodes will be saved in new output files to be used by the ANSYS batch file. The newly created files will be used by the ANSYS file to complete the model.

Boundary conditions:

The boundary conditions depend on the nature of the pile installation in the field. The embedded length of the pile will be continuously connected to horizontal springs representing the lateral soil resistance. The vertical movement of the pile will be restricted by equivalent frictional springs along the pile shaft. The pile tips have more

than situation depending on driving conditions and soil properties at that level. If the driving reached rocks or solid strata, the pile tip should be restrained against vertical settlement; otherwise, end bearing soil springs should be used.

Applied loads:

Vertical piles are designed to carry axial loading while [the] lateral load [is] carried by battered piles. In jointless bridges where the deck and girders are integrally built with the abutment, the vertical pile has to accommodate lateral loads in addition to the axial loads. The lateral loads can be applied as a horizontal force or in a form of lateral displacement at the pile head.

A pile in an integral abutment bridge will carry three types of loads, namely: dead loads, lateral displacements, and live loads. The dead load is a permanent loading that has to be applied initially before any other load. The lateral displacements and live loads are unpredictable in terms of which load should come first.

BEHAVIOR OF PILES AND PILING MATERIALS

Piles in jointless bridges are subjected to combined bending and axial forces while in service. The axial forces result from the bridge dead and live loads as well as traffic loads. The bending moments are due to the lateral deformations (movements) of the integral abutment as a result of thermal expansion and contraction. Such deformations induce additional stresses on the upper part of the pile which cause a reduction in the pile vertical carrying capacity as bending stresses increase. Piles in conventional jointed bridges are designed to carry axial loads only without any considerations for pile lateral head displacements. Additional design considerations have to be taken into account for piles in jointless bridges.

The reduction in axial load carrying capacity of a bridge piling system is a very important factor when designing integral abutment bridges. The amount of stress resulting from lateral movements depends on several factors that include material and geometrical properties of the pile and the surrounding soil. Such properties are: bridge length, annual temperature range and thermal coefficients of the bridge materials and soil type. Another factor that has a major role in the amount of stresses is the pile section orientation. Axisymmetric sections, such as circular, have an infinite number of axes of

symmetry so that their geometrical properties are equal in all directions. Other types of sections have limited axis of symmetry such as polygonal, triangular and irregular sections. Those sections have their geometrical properties vary with the variation of the reference axis location within the section.

Axial stresses in structural members depend only on the cross sectional area of the member. On the other hand, bending stresses depend on the section flexural rigidity of the member cross section. For example, rectangular sections subjected to bending about their weak axis will produce different stresses than if they bent about their strong axis.

6.1 SELECTION OF PILES

The two major factors that dictate the type and size of the pile to be used in a bridge are soil conditions and bridge type. Exploring the geotechnical conditions of the construction site provides essential information to the design engineer in terms of pile section and length selection. Soil type and conditions, especially the variation in its properties with depth, are the most crucial factors. Soil is a non-homogeneous material and has variable properties even within the same spot.

Soil exists in different types and grades with different properties for each type. It has two major categories, cohesive and cohesionless soils. Each category is also divided in different grades depending on the unit weight, strength, and angle of internal friction. Sand is a cohesionless soil that is available in different grades and can be classified in three levels: loose, medium, and dense sand. Soil properties vary in density such that they increase as the density increases. Typical cohesionless soil properties are shown in Table 6-1 below. Cohesive soils are also available in different types and grades that range from very soft to very stiff clay as shown in Table 6-2.

Table 6-1: Cohesionless soil typical values (Amde et al 1982)

Sand	Natural unit weight lb/ft³	Submerged unit weight lb/ft³	Angle of friction	Blow count, N
Loose	90 –125	55 – 65	30	4 - 10
Medium	110 – 130	60 – 70	35	10 – 30
Dense	110 - 140	65 - 80	40	30 - 50

Table 6-2: Cohesive soil typical values (Amde et al 1982)

Clay	Cohesion, Cu lb/ft²	Natural unit weight lb/ft³	Submerged unit weight lb/ft³
Very stiff	Over 3000	120 – 140	60 –80
Stiff	1500 – 3000	115 – 135	55 – 75
Firm	750 – 1500	105 – 125	45 – 65
Soft	375 – 750	90 – 110	30 –50
Very soft	Under 375	90 – 100	30 40

Pile size and dimensions usually are determined according to the allowable soil properties in terms of bearing capacity and surface friction. Load bearing piles are designed for maximum section capacity either for material or geometrical failure. An end bearing pile will fail when its maximum stress exceeds the allowable limit or when the applied load exceeds the allowable buckling load for unbraced slender piles. On the other hand, a friction pile fails when the applied load exceeds the pile shaft frictional capacity.

The other factor that has a major role in determining the pile type and size is the bridge itself. The bridge type, length, dimensions, and construction materials strongly affect the decision in pile selection. In conventional bridges with expansion joints the

piles are designed to carry pure axial compression. In jointless bridges where thermal movements induce lateral deformations on the piling system, the pile should be designed for both axial and lateral loading.

When designing piles for jointless bridges, special considerations have to be taken for the thermal movements of the bridge abutment. The abutment has to be designed with a degree of flexibility to allow less resistance for the superstructure movements. The flexibility can be provided through the piling system such that the piles are installed in a single row with bending about their weak axis. This kind of pile orientation has an advantage in terms of flexibility in the direction of the movements.

The most commonly used piles in integral abutment bridges are steel H-piles. Steel has a very high strength and durability with a reasonable cost when compared to other materials. Also the H-shape has the advantage in providing two axes of bending with a reasonable margin of bending flexibility between the two axes. When weak axis bending is desired, the H-pile is preferred over the reinforced concrete piles, which normally have round cross sections. The round or cylindrical pile does not provide weak and strong axis bending properties. The section has its properties equal in all directions.

Pile size and cross-sectional dimensions should be selected by considering all factors that may affect the pile performance while in service. The first step after soil exploration is to determine the number of piles and the amount of load to be carried by each pile. Pile capacity is governed by the type of failure at the maximum load. The type of failure depends on the pile material, soil properties, and pile boundary conditions. Friction piles capacity is usually governed by the failure of the soil when the applied load exceeds the soil friction and bearing capacity. In end-bearing piles where the pile is

supported on hard strata, strength or geometrical failures of the pile material are always likely to happen.

6.2 SELECTION OF PILE SECTIONS

As discussed in the previous section, the pile cross-sectional properties have a major effect on the flexibility of the piles under lateral loads. The cross-section can be configured to provide the maximum flexibility while keeping the area unchanged.

Rigidity, which is the inverse of flexibility, is measured as the combination of the section and material properties. The rigidity is defined in terms of section moment of inertia, I and the modulus of elasticity of the section material, E . Its value is equal to the product of both properties (EI). An increase in any of the value of either E or I will increase the rigidity and vice versa.

Isotropic materials such as metals which have identical material properties in all directions have a constant value of E that can not be affected by material orientation. In such situations, the only way to control the section rigidity is through the section geometrical properties. Orthotropic materials, such as fiber reinforced composites have directional dependent material properties. The modulus of elasticity does not have a fixed value but varies within a range that is determined by the lowest and highest values of the material properties. This variation in properties within the same materials gives more flexibility to the designer to control the section rigidity. Unlike isotropic materials, where rigidity can be controlled only by the section properties, orthotropic materials allow rigidity control through both material and sectional properties.

6.3 FRP COMPOSITE PILES

Fiber reinforced composites are not very stiff materials when compared to steel and other metals. Their stiffness depends on the stiffness of the individual constituents; fibers and matrix. Stiffness for fiber reinforced composites usually is calculated according to the rule of mixtures. As a result, the final stiffness for a composite mainly depends on the percentage or the volume fraction of each constituent.

6.4 SOIL BEHAVIORS

The non-linear soil behavior is represented according to the Ramberg-Osgood model which consists of a set of load-deflection curves describing the pile deflection behavior under applied loads. Figure 6-1 through Figure 6-3 illustrate the different load-displacement curves for three grades of sands. The soil properties were listed in Table 6-1.

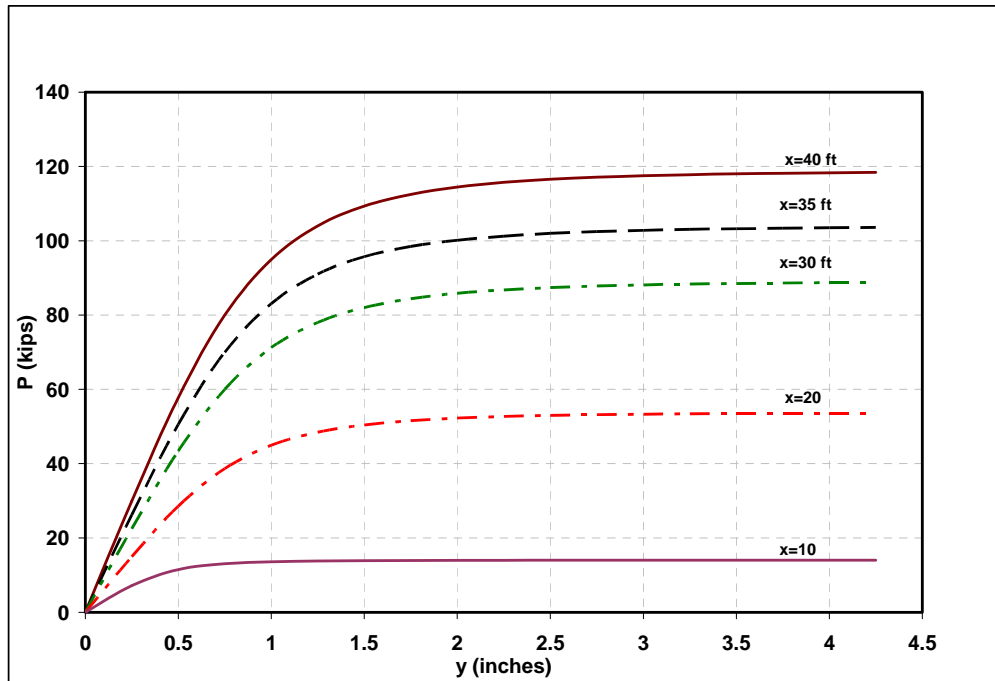


Figure 6-1: p-y curves for dense sand.

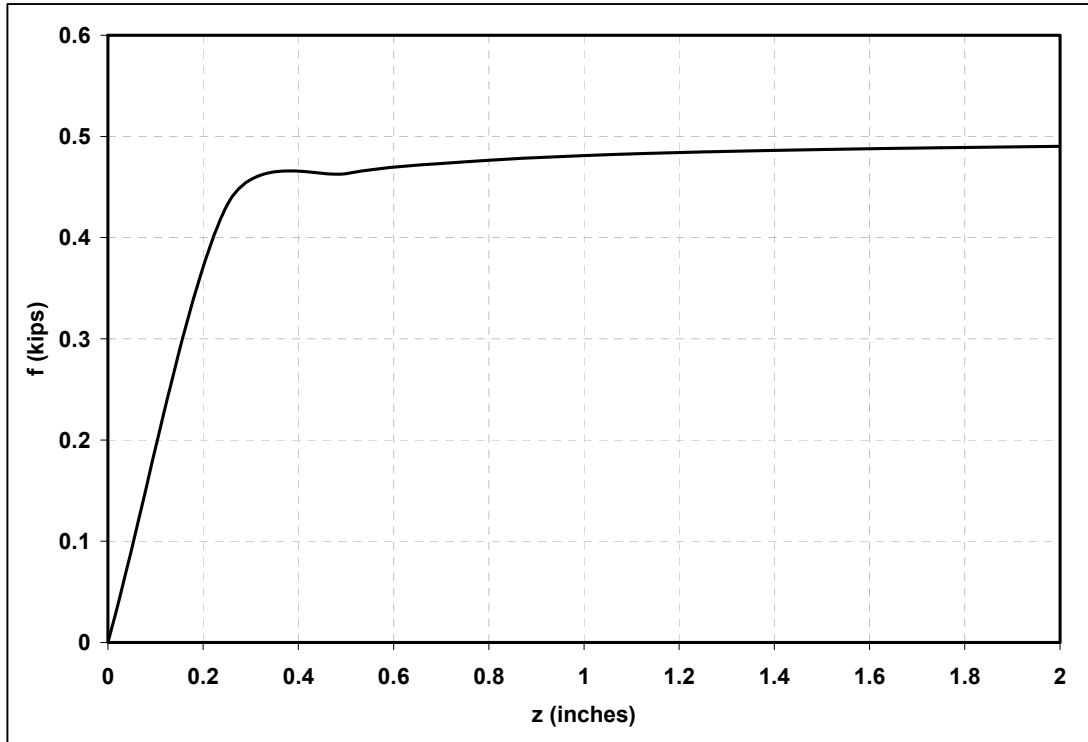


Figure 6-2: Axial load – friction (f - z) curves for typical properties of dense sand.

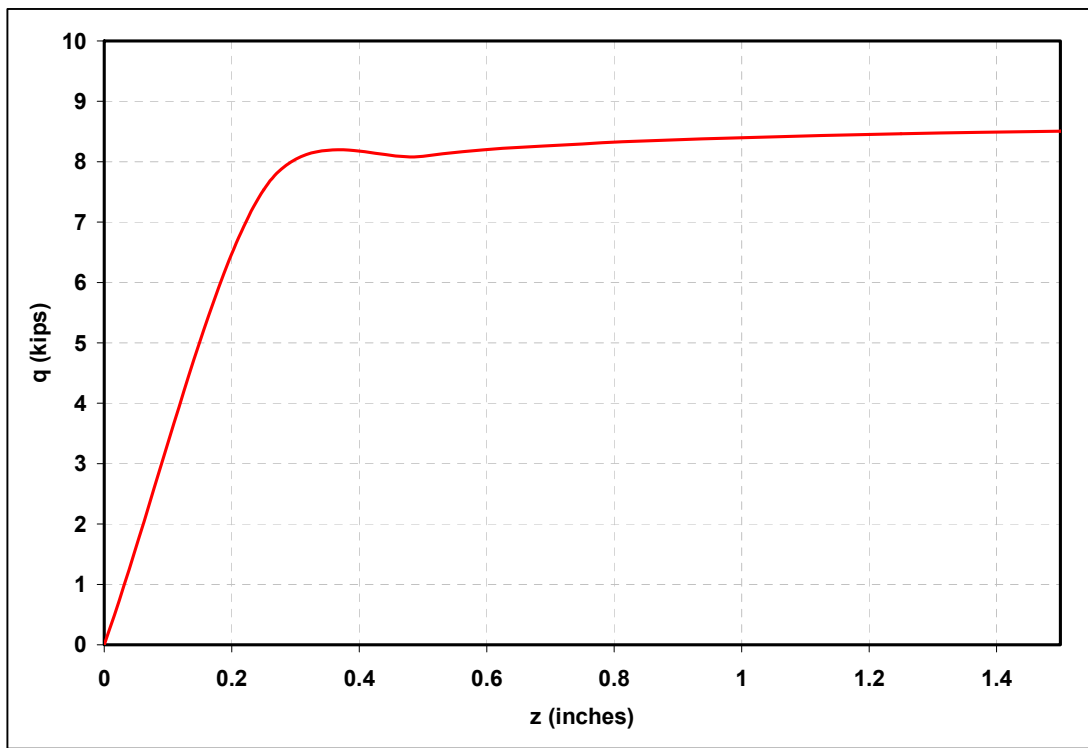
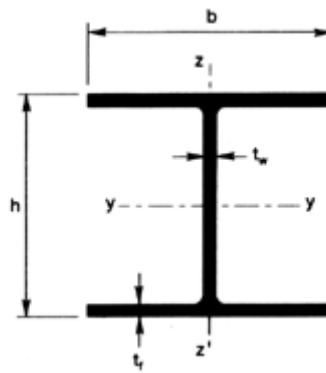


Figure 6-3: Axial load-bearing (q - z) curves for typical properties of dense sand.

It can be concluded that friction piles for integral abutment bridges are recommended to have cross sections that provide sufficient friction and bearing surfaces and allow the adequate flexibility to accommodate lateral thermal movements.

The most commonly used piling for integral abutment bridges is HP piles. Steel is a stiff and strong material that is capable of carrying heavy structural loads with small section areas. The steel H piles got their name from their shape. The pile has the shape of the letter H that provides a major axis of symmetry which allows bending to be on a strong or weak axis. Integral abutment piles usually are oriented to bend about their weak axis to allow adequate flexibility for lateral movements.



Analysis of HP 10x42 friction pile in cohesionless soils under combined axial loading and lateral movement shows that the pile is highly prone to failure from plastic hinge rather than soil failure. The formation of plastic hinge depends on the amount of stress resulting from the lateral movement and the vertical loads of the superstructure. The surrounding soil also has a major effect on the pile head stresses. The stiffer the soil, the more resistance there will be on the pile lateral movement and higher stresses will be generated.

Figure 6-4 shows a comparison between the deflected shapes of an HP10x42 pile under the same lateral loading for different soil densities. As can be seen, the denser the

soil, the smaller the deflection. On the other hand, Figure 6-5 shows the stress variation in the same pile for different soil densities and under the same lateral displacement. It's clear from the figure that the stresses increase as the soil gets denser.

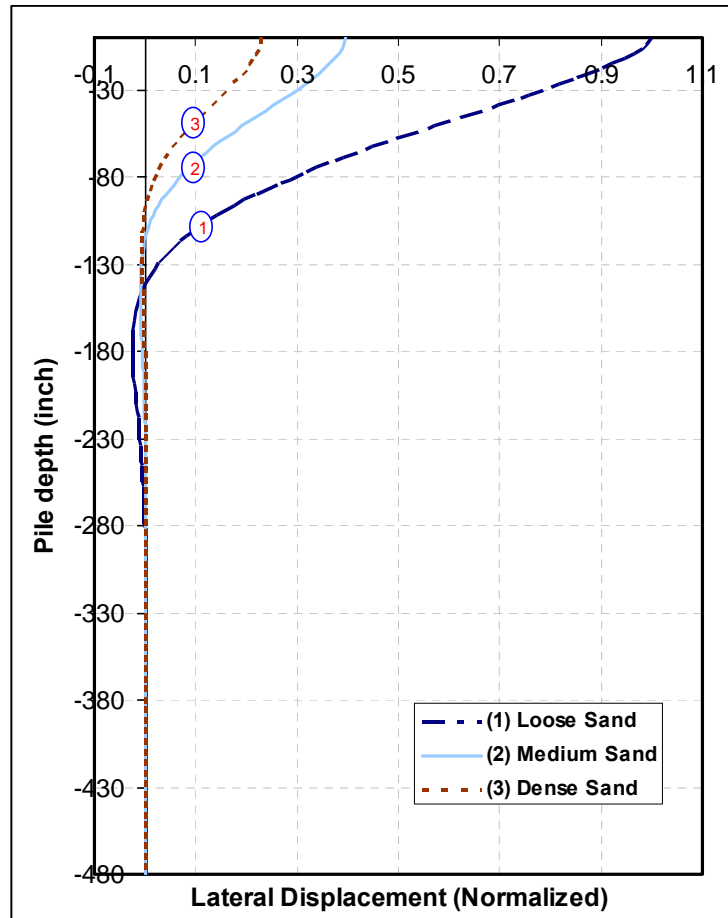


Figure 6-4: Effect of soil density on the deflected shape under the same loading.

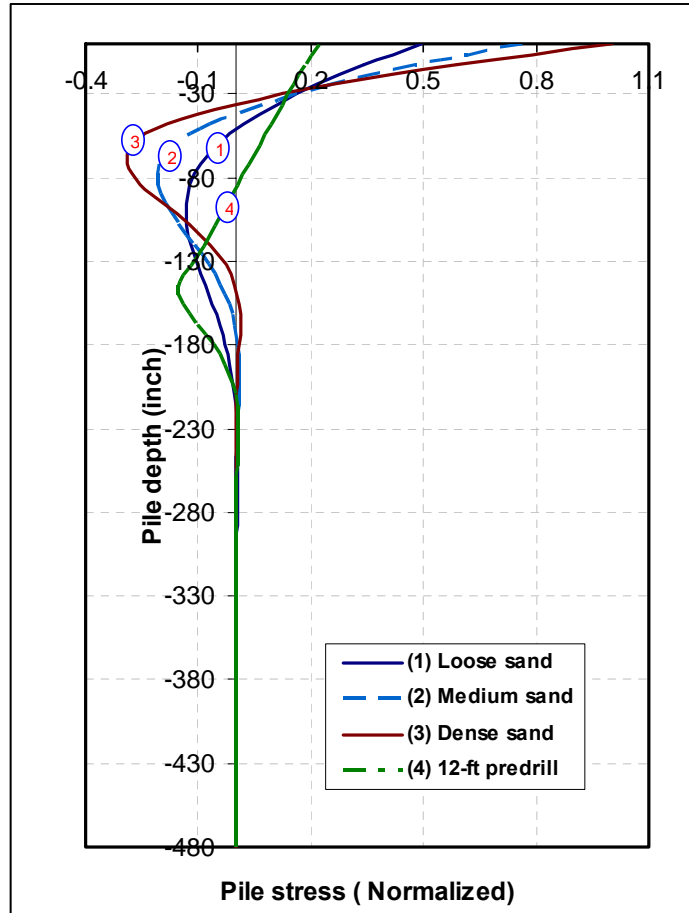


Figure 6-5: Effect of soil density on stress variation.

6.5 STRESS-STRAIN MODELS FOR FRP CONFINED CONCRETE

The behavior of concrete confined with FRP materials has been extensively researched during the last few years. Fiber-wrapping or encasement of plain concrete in FRP shells enhances the strength and ductility of concrete. Concrete members under compressive loading expand laterally as stress increases.

The strength and elasticity of the composite shell has a dramatic effect on the behavior of the encased concrete. The concrete strength is mainly based on the strength of the composite shell. The behavior of FRP confined concrete has been studied by many researchers. Despite the extensive research effort spent on studying the FRP confined

concrete, a proper analytical tool to predict such behavior has not yet been established. Early investigation attempts tried to extend the models developed for steel confined concrete to be used for FRPs but later investigations showed that such assumption leads to inaccurate results.

Most studies employed the well-known equation by Popovic and used by Mander (1988) for the confined concrete. The stress-strain model is illustrated in Figure 6-6 and based on equation (6-1).

$$f_c = \frac{f'_{cc} \left(\frac{\epsilon_c}{\epsilon'_{cc}} \right)^r}{r - 1 + \left(\frac{\epsilon_c}{\epsilon'_{cc}} \right)^r} \quad (6-1)$$

Where

$$r = \frac{E_c}{E_c - E_{sec}}; E_{sec} = \frac{f'_{cc}}{\epsilon'_{cc}}$$

and f'_{cc} and ϵ'_{cc} = confined peak strength and the corresponding strain, respectively.

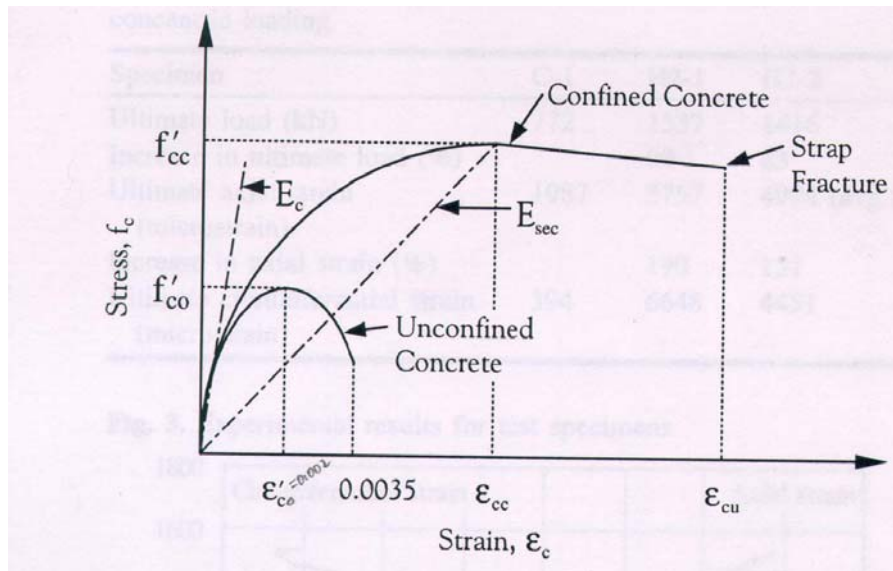


Figure 6-6: Stress-strain model for concrete confined by FRP (Bogdanovic 2002).

The peak stress of the FRP confined concrete is mainly dependent on the lateral confinement pressure. For cylindrical columns the peak value is given by

$$f'_{cc} = f'_c + k_1 f_l \quad (6-2)$$

$$\varepsilon'_{cc} = \varepsilon'_c \left(1 + 5k_1 k_3 \frac{f_l}{f'_c} \right) \quad (6-3)$$

$$k_1 = 6.7 f_l^{-0.17}; \quad k_3 = \frac{40}{f'_c} \leq 1$$

and for rectangular columns, the peak stress is given by

$$f'_{cc} = f'_c (1 + 0.0572 f_l)$$

$$\varepsilon'_{cc} = \varepsilon'_c (1 + 0.280 f_l)$$

When the experimental values of E_c and ε'_c are not available, the values can be calculated theoretically from the following formulas

$$E_c = 3320 \sqrt{f'_c} + 6900 \quad (6-4)$$

$$\varepsilon'_c = \frac{f'_c}{E_c} \frac{n}{n+1} \quad (6-5)$$

Where all values are given in Mega Pascal.

The lateral confinement pressure for cylindrical shapes was derived by (Marques et al 2004) as follows:

$$f_l = \frac{2t}{D} f_j \quad (6-6)$$

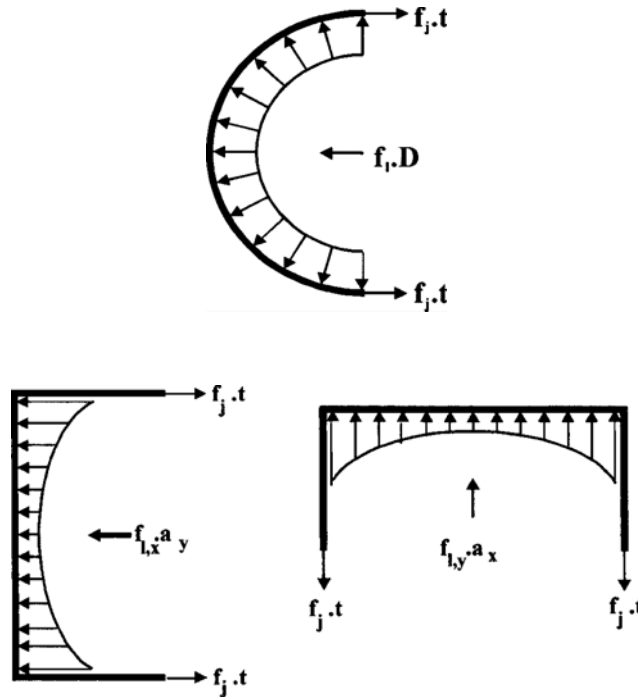


Figure 6-7: Lateral forces produced by confinement with rectangular and circular jackets (Marques 2004).

And for rectangular shapes is given as

$$f_{l,x} = 2 \frac{t}{a_y} f_j \quad (6-7)$$

$$f_{l,y} = 2 \frac{t}{a_x} f_j \quad (6-8)$$

$$f_{l,y} = 2 \frac{t}{a_x} f_j \quad (6-9)$$

$$f_l = \frac{f_{l,x} a_y + f_{l,y} a_x}{a_x + a_y} \quad (6-10)$$

The lateral pressure of confinement in circular and rectangular sections is shown in Figure 6-7.

Based on test results from concrete-filled FRP tubes, Samaan and Mirmiran (1998) utilized the four-parameter relationship of Richard and Abbott (1975) to develop and calibrate their FRP-confined concrete model. The model represents the bilinear response of FRP-confined concrete with equation (6-11).

$$f_c = \frac{(E_1 - E_2)\varepsilon_c}{\left[1 + \left(\frac{(E_1 + E_2)\varepsilon_c}{f_o}\right)^n\right]^{\frac{1}{n}}} + E_2\varepsilon_c \quad (6-11)$$

Where ε_c and f_c are the axial strain and stress of concrete, respectively; E_1 and E_2 are first and second slopes, respectively; f_o is the reference plastic stress at the intercept of the second slope with the stress axis; and n =curve-shaped parameter that mainly controls the curvature in the transition zone (Samaan 1998). Figure 6-8 shows the basic parameters equation (6-11) expression.

$$E_1 = 47.586\sqrt{1000f'_c} [ksi] \quad (6-12)$$

$$E_2 = 52.411f'_c{}^{0.2} + 1.3456\frac{E_j t_j}{D} [ksi] \quad (6-13)$$

$$f_o = 0.872f'_c + 0.371f_r + 0.908 [ksi] \quad (6-14)$$

$$f'_{cu} = f'_c + 3.38f_r{}^{0.7} \quad (6-15)$$

$$\varepsilon_{cu} = \frac{f'_{cu} - f_o}{E_2} \quad (6-16)$$

$$f_r = \frac{2f_j t_j}{D} \quad (6-17)$$

Where

D = Core diameter

E_j = Modulus of elasticity of jacket in hoop direction

f_j = Jacket's hoop strength

f_r = Confining pressure

t_j = Tube thickness

f'_{cu} = Ultimate strength of FRP-confined concrete

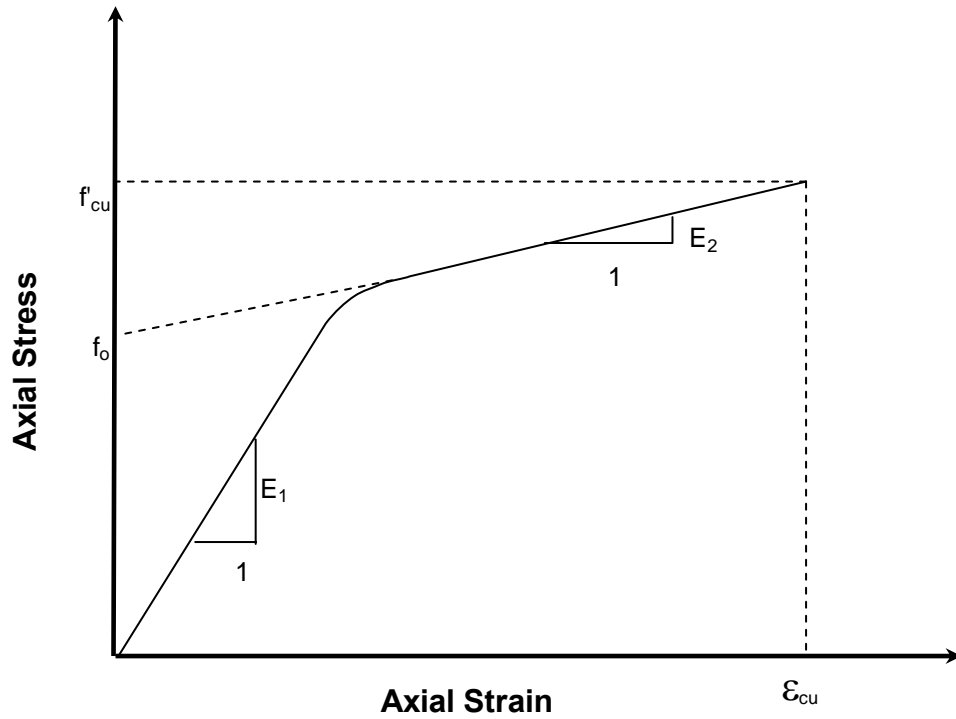


Figure 6-8: Parameters of bilinear confinement model.

Figure 6-9 shows a comparison of the two confinement models through several stress-strain curve plots. As can be seen, Mirmiran's bilinear model always has its second part ascending. Changing the curve parameters will only affect its slope. On the other hand, Mander's model is non-linear and it can have its second portion descending when the confining jacket has low hoop strength. Also, it can be seen that the confinement strength strongly depends on the fiber directions in the composite shell. The confined concrete will show higher strength as the fiber goes towards the hoop direction.

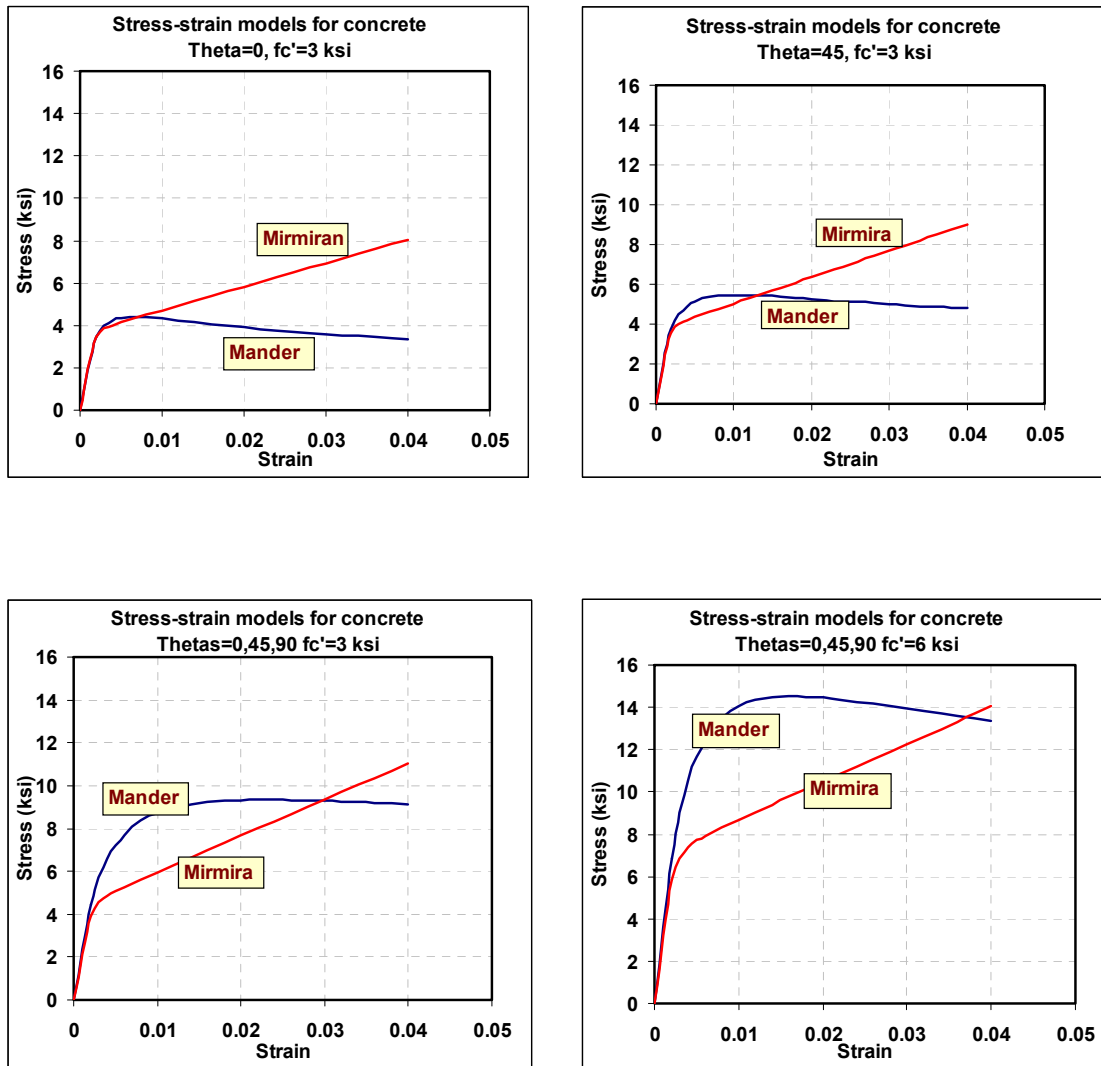


Figure 6-9: Stress-Strain curves for FRP confined concrete.

6.6 STRESSES IN FRP COMPOSITES

The directional strengths have a similar scenario to that of elastic modulus in which the highest value is in the fiber direction and the lowest is in the perpendicular direction. According to the maximum strength theory, the off axis strength can be calculated

$$\sigma_1 = \sigma_x \cos^2 \theta \quad (6-18)$$

$$\sigma_2 = \sigma_x \sin^2 \theta \quad (6-19)$$

$$\tau_{12} = -\sigma_x \cos \theta \sin \theta \quad (6-20)$$

$$-\frac{X'}{\cos^2 \theta} < \sigma_x < \frac{X}{\cos^2 \theta} \quad (6-21)$$

$$-\frac{Y'}{\sin^2 \theta} < \sigma_x < \frac{Y}{\sin^2 \theta} \quad (6-22)$$

$$-\frac{S'}{\cos \theta \sin \theta} < \sigma_x < \frac{S}{\sin \theta \cos \theta} \quad (6-23)$$

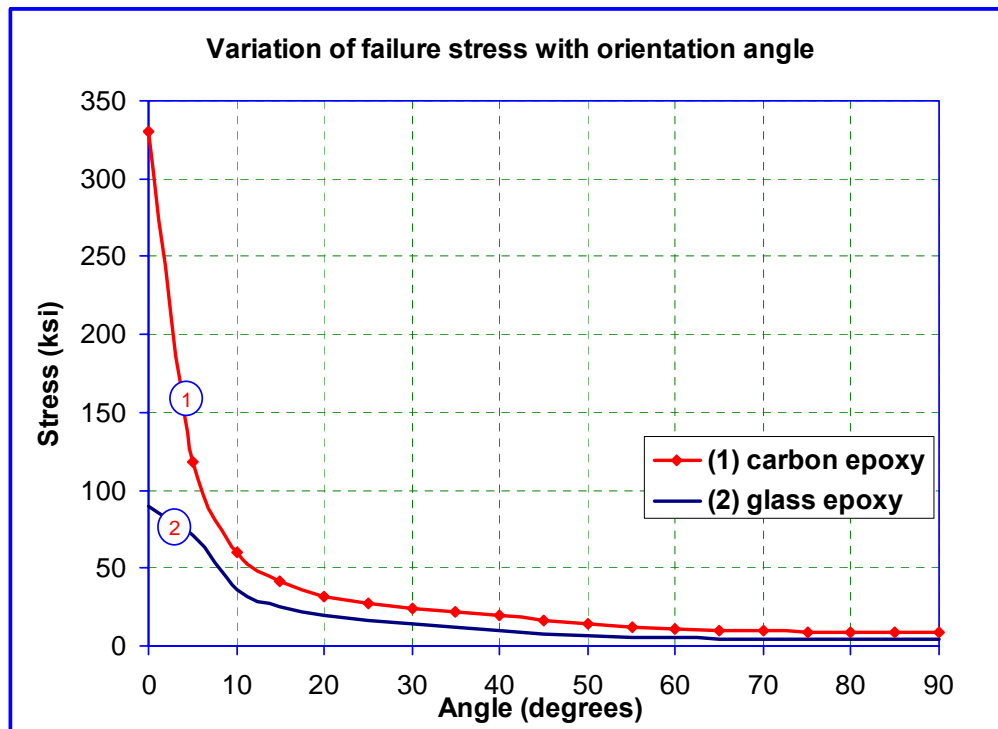
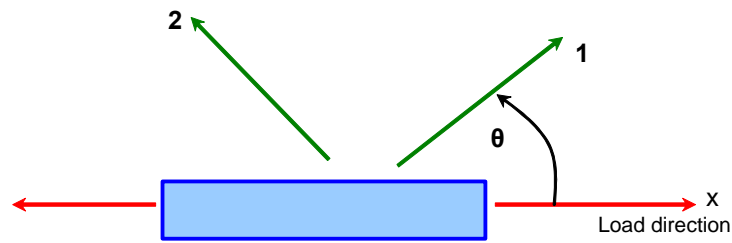


Figure 6-10: Variation of failure stress with fiber orientation angle for glass and carbon epoxy.

When the stresses on the principal material directions exceed a pre-defined value (failure criteria), then the failure has occurred to that layer. The failure criteria should be

defined for each material and in all directions. Figure 6-10 shows the variation of the failure stress with the fiber orientation angle θ . Any stress value above the lowest curve exceeds the allowable stress for the particular orientation. Hence, the design should be performed such that the stress in any material direction will be in the allowable zone.

To accommodate the different types of stresses in a loaded FRP composite pile, the pile shell has to be designed with multiple layers with different fiber orientations. Since the pile is an axial compression member normally designed to carry axial compressive loads, the composite fibers should be oriented to provide the highest strength and stiffness. From the previous graphs, it has been shown that a unidirectional composite layer has its highest mechanical properties at a 0-degree angle with respect to the loading direction. Laying up all layers to have their fibers in the direction of pile axis will improve its axial properties in terms of composite carrying capacity but, on the other hand it will weaken the confinement pressure on the concrete core.

Failure in composites has different mechanisms than that in isotropic materials such as metals. In isotropic materials, the failure is predicted by comparing the stresses to the strengths or the allowable stresses. In this case there is no principal material direction and the material has the same properties in all directions. For orthotropic composite materials, such a method is not adequate because the failure mechanism and strength properties change with the fiber direction for any composite lamina. The failure stresses should be checked in all major directions for each layer. There are many different modes of failure and the number of material strengths required depends on the failure criteria to be applied. Usually 9 strength properties are required; tensile, compressive and shear strengths in the three principal material directions. Since composites are mostly used in

forms of thin layers, 2D stresses states are often sufficient for most applications which reduces the number from 9 to 5. Failure usually does not occur by yielding but rather by sudden fracture.

6.7 BEHAVIOR OF LATERALLY LOADED COMPOSITE PILES

Stiffness and flexibility are very important factors which have to be considered when designing piles for integral abutment bridges. The goal is always to minimize the resistance against the lateral movement of the bridge super structure. The lower the resistance against lateral movements, the less stress is induced on the bridge deck and the supporting piles.

Piles according to their load-transfer method can be categorized in two types: friction piles, and bearing piles. Both types are assumed to have the same function, which is to support the structure and accommodate the vertical and lateral loadings. Several factors usually affect the lateral behavior of driven piles and will be discussed in the following sections of this chapter.

6.7.1 FRICTION PILES

Piles that develop their carrying capacity by side shear are called friction piles. The pile gains its resistance to settlement through the direct contact between the shaft and the surrounding soil. The ultimate friction capacity of a pile in a specific soil depends on the size of the contact area with the soil. The larger the contact area, the higher skin friction will be gained. As a result, skin friction piles should be designed with larger contact surface area than other types of piles. The ultimate load capacity of a friction pile under axial loading is the lesser of the compressive strength of the pile material and the

maximum load capacity of the soil-pile interface. In integral abutment bridges, where piles are subjected to combined axial and lateral loads, the pile may fail laterally as a result of surrounding soil failure.

Maximum lateral flexibility in piles is desired to accommodate the lateral bridge movements; the pile section should be selected to provide an adequate surface friction area with an acceptable amount of flexibility.

6.7.2 END-BEARING PILES

End bearing piles are piles that transfer their load through direct contact between the pile tip and the layer of hard strata located at a considerable depth below the base of the structure. This type of pile gains its carrying capacity from the penetration resistance of the soil at the pile tip. A model illustration of end-bearing piles is shown in Figure 6-11.

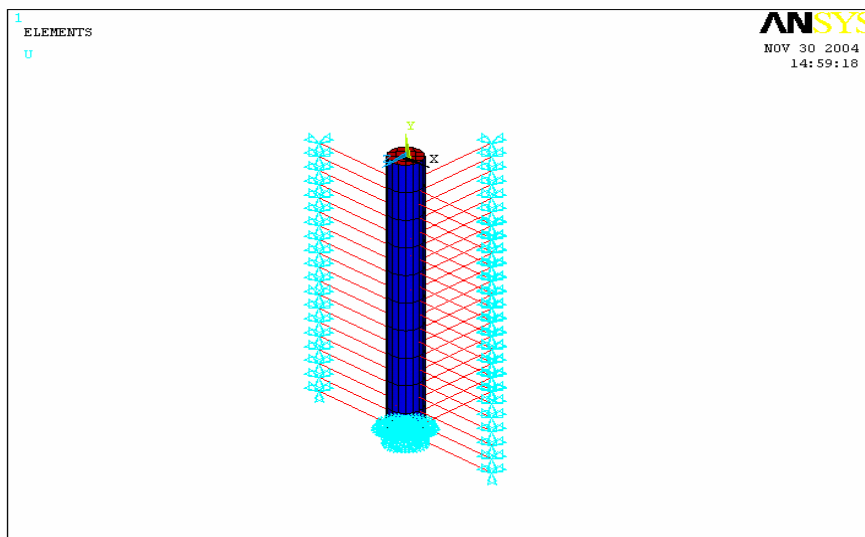


Figure 6-11: End-bearing pile model.

6.8 AXIAL STRESSES AND DEFORMATIONS

Vertical pile deformations under increasing loads are of major concern in bridge structures. The combined deformations that result from dead loads, live loads, and creep should be taken into consideration when designing pile foundations. The amount of bridge settlement should remain within the allowable design range so that the bridge surface stays leveled with the road elevation. The amount of deformation depends on the pile axial stiffness, i.e. the pile cross-sectional area and its material properties. Figure 6-12 shows the load-deformation curves for several piles of similar cross sections and different lengths subjected to the same loading scheme.

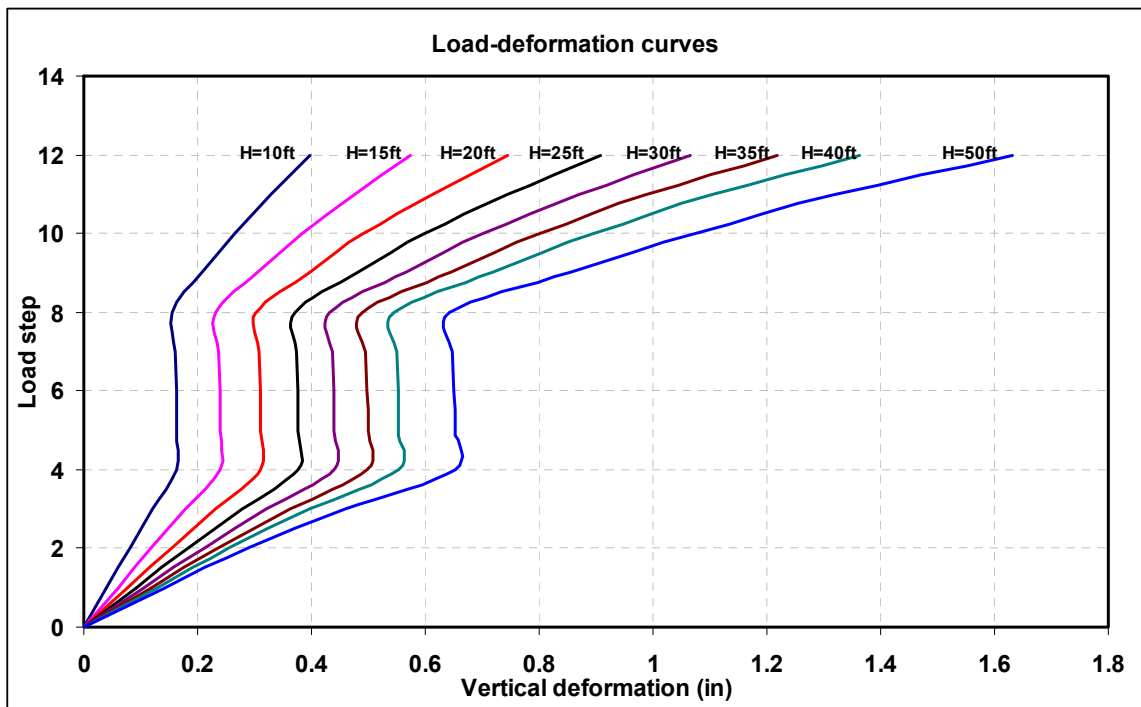


Figure 6-12: Load-deformation curves for different pile lengths.

Stresses in piles of integral abutment bridges are a combination of axial and bending stresses. Axial stresses are resulting from dead and live loads of the bridge structure. Dead load stresses are permanent and usually applied as soon as the super structure is installed. Axial load stresses are usually uniform and cover the whole length of the pile as shown in Figure 6-13.

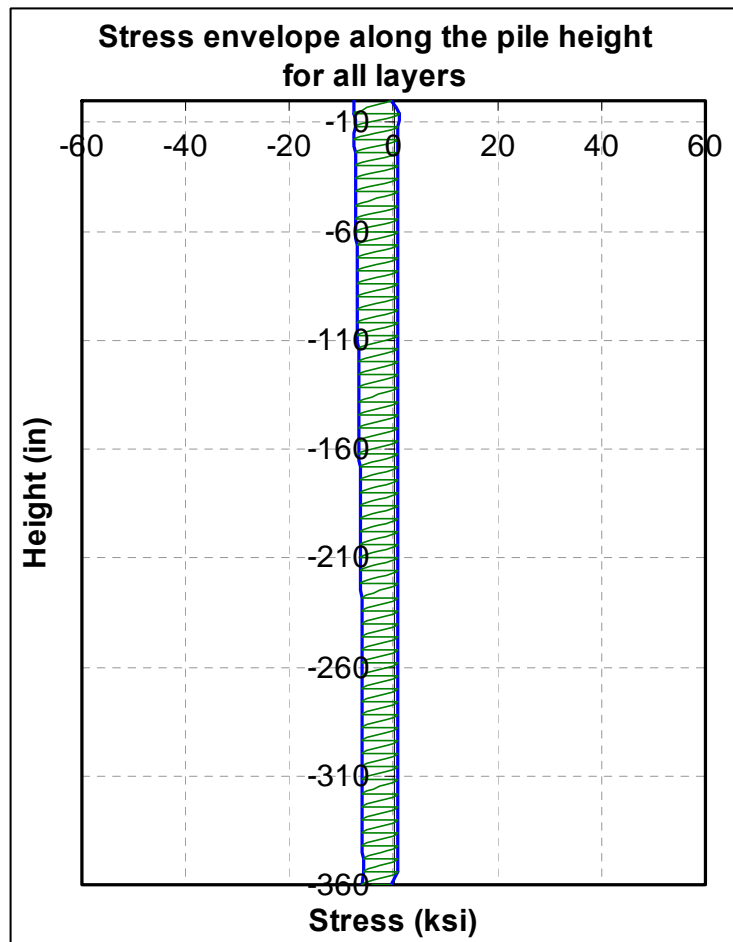


Figure 6-13: Stress envelope for a pile under axial compression.

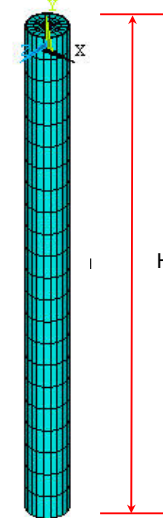
6.9 BENDING STRESSES

Bending stresses result from the lateral movement of the pile head due to thermal expansion and contraction of the bridge deck. The stress magnitude depends on several factors which include: the pile lateral stiffness, amount of lateral displacement and soil stiffness. A pile with a circular cross-section filled with concrete as described in the following information sheet was analyzed under lateral head displacement only. The three major stresses in all layers are plotted and illustrated in Figure 6-14 through Figure 6-16. The bending stresses are not as uniform along the pile length as those of axial stresses. They vary from maximum at the pile head and decrease with depth, and then vanish at a certain depth. Figure 6-17 and Figure 6-18 also show the variation of bending stress at a point with different depths along the pile shaft. As can be seen, the stress behavior varies along the depth of the point in consideration.

Pile information sheet:

Composite type: Glass epoxy

Property	ksi	Property	ksi
E_x	4500	X_t	90
E_y	1100	Y_t	3.9
G_{xy}	550	X_c	-80
V_{xy}	0.26	Y_c	-17.5
		S	6.2



Number of layers: 12

Layer thickness: 0.025 in.

Radius, $R=4.88$ in.

Laminate structure:[0,0,90,90,0,0,0,0,90,90,0,0]

Filling: Plain concrete $f_c'=4$ ksi

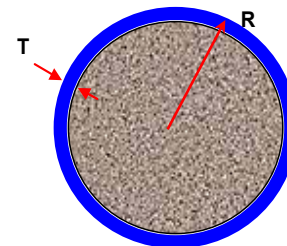
Height = 20 ft

Soil type: Very stiff clay

Loading:

Axial dead load: No axial load

Lateral head movement: 2 in. [steps 1 to 12]



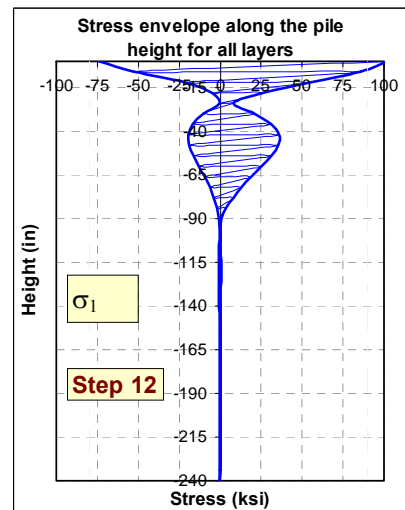
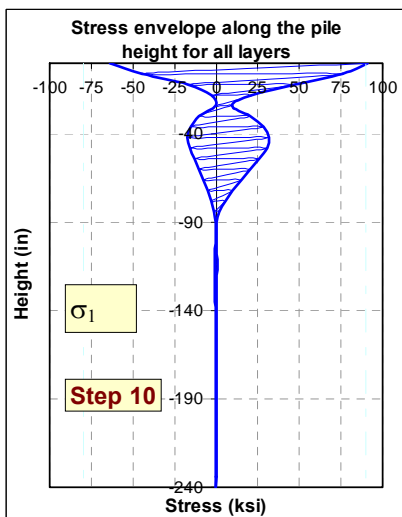
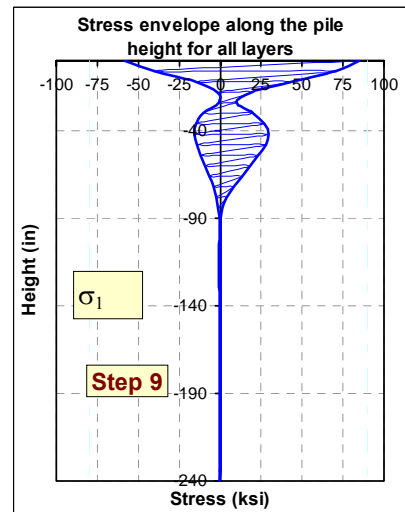
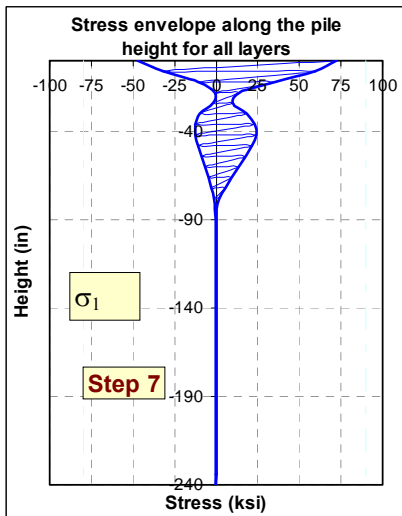
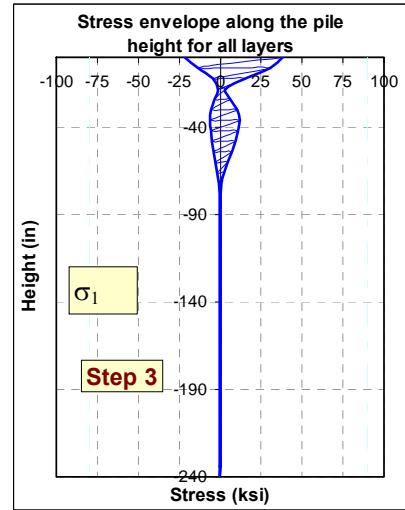
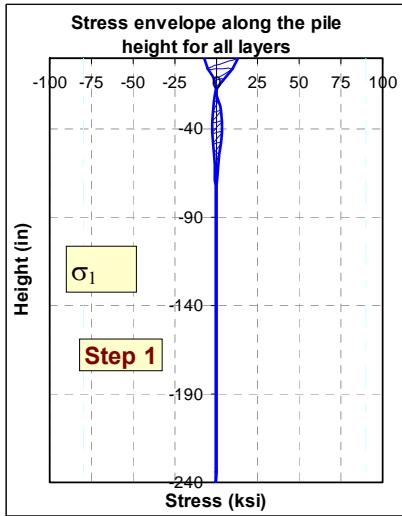


Figure 6-14: Development of the stress (σ_1) due to lateral pile movement (bending only).

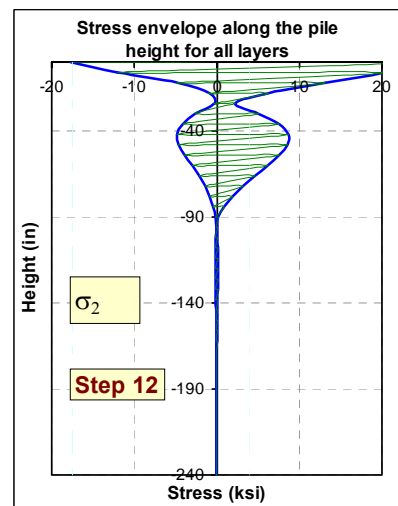
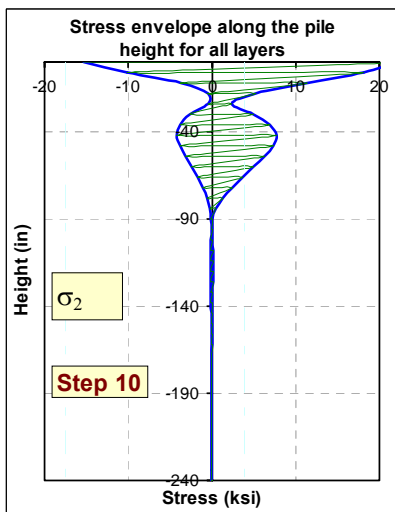
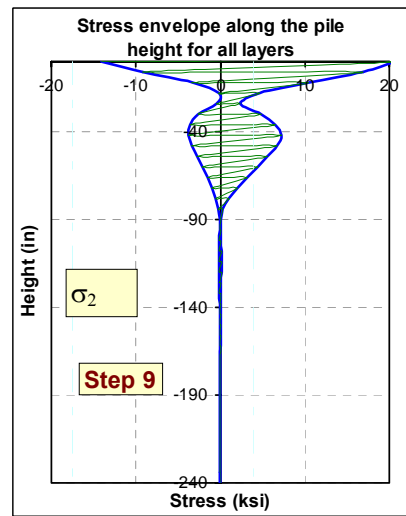
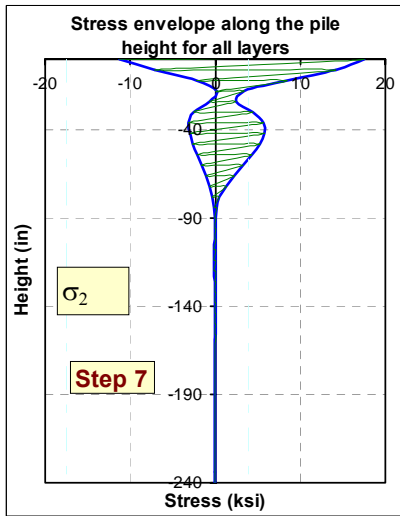
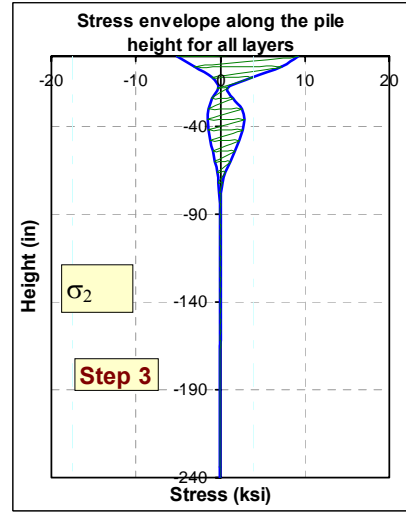
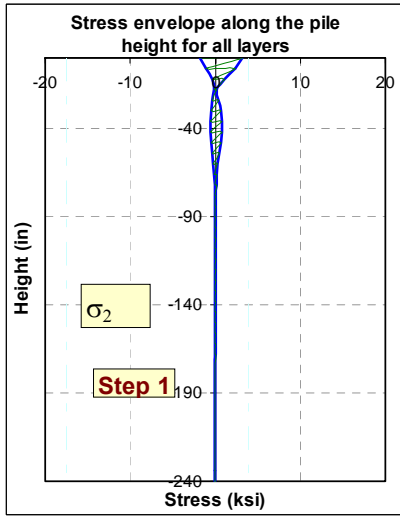


Figure 6-15: Development of the stress (σ_2) due to lateral pile movement (bending only).

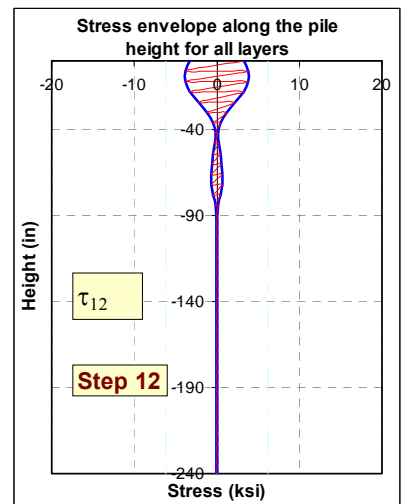
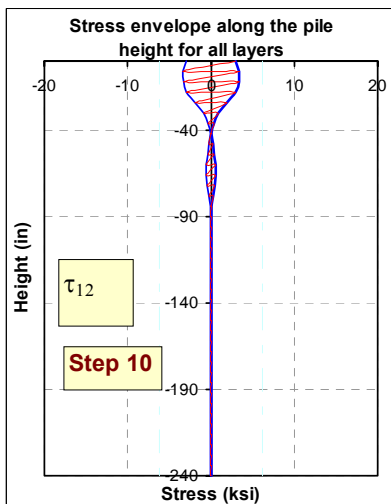
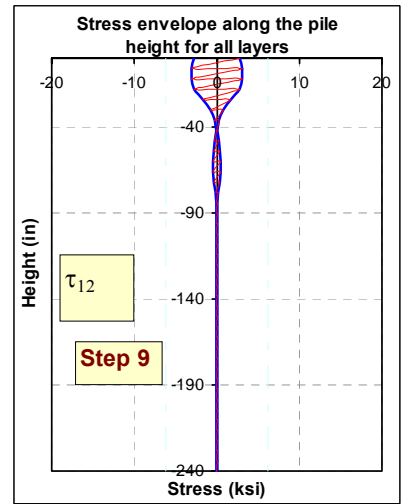
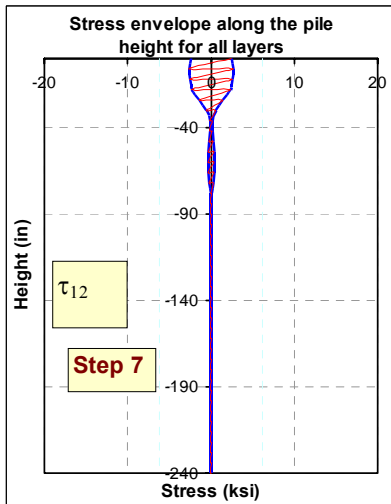
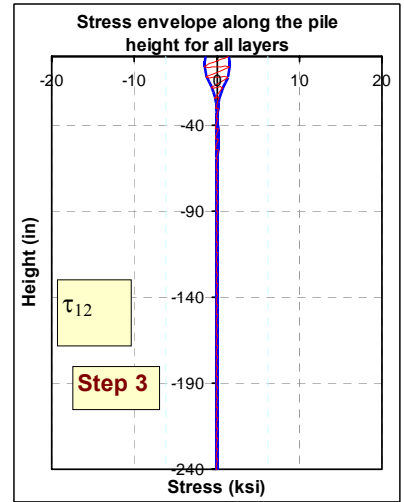
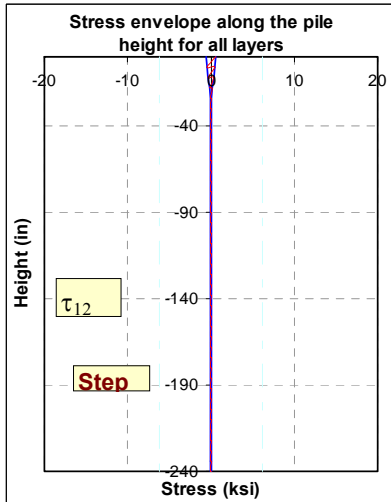


Figure 6-16: Development of the shear stress (τ_{12}) due to lateral pile movement (bending only).

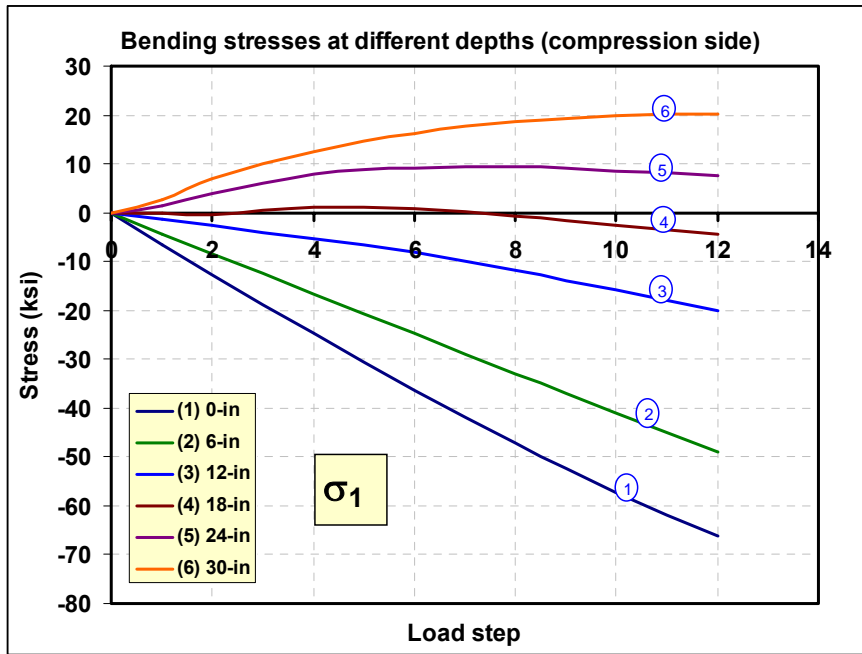


Figure 6-17: Bending stresses (σ_1) at different depths of the pile shaft due to lateral head movement (Compression side).

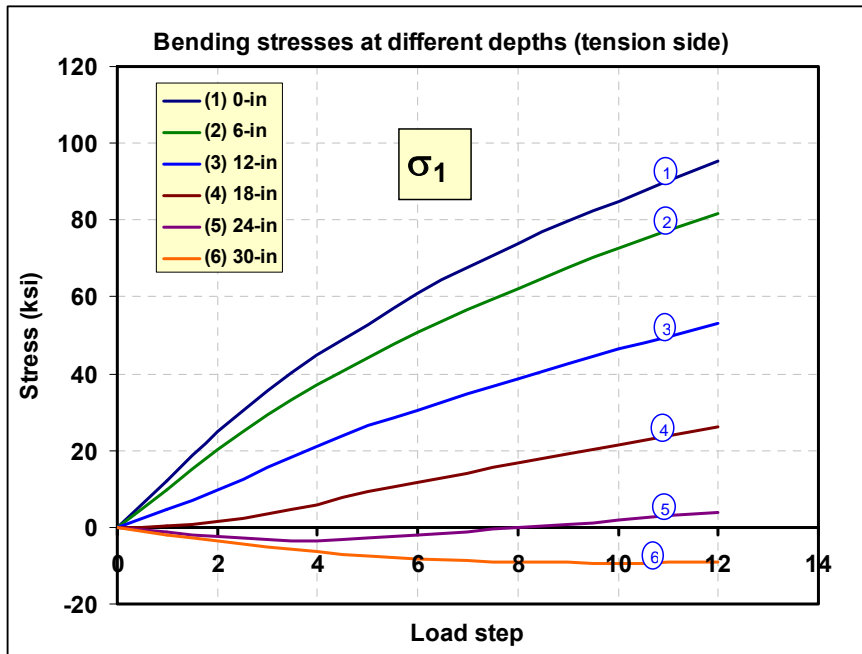


Figure 6-18: Bending stresses (σ_1) at different depths of the pile shaft due to lateral head movement (Tension side).

NUMERICAL INVESTIGATION OF THE FRP PILE-SOIL INTERACTION

This chapter presents the findings of finite element analyses on a series of FRP pile-soil models that were performed to investigate the behaviors of FRP piles under combined axial compression and bending moments. The investigation utilized all numeric parameters that may have effect on the pile-soil behavior.

7.1 OBJECTIVES OF THE NUMERICAL INVESTIGATION

The objectives of the study are to investigate the following:

- The behaviors of fiber reinforced composites as a piling material.
- The different types of stresses developed in the composite shell through out the different stages of loading.
- The effect of the following parameters on stresses and pile behaviors:
 1. Soil type
 2. Concrete filling
 3. Material type
 4. Layer orientations

5. Cross-sectional area
6. Predrilled hole
7. Section geometry
8. Dead load magnitude

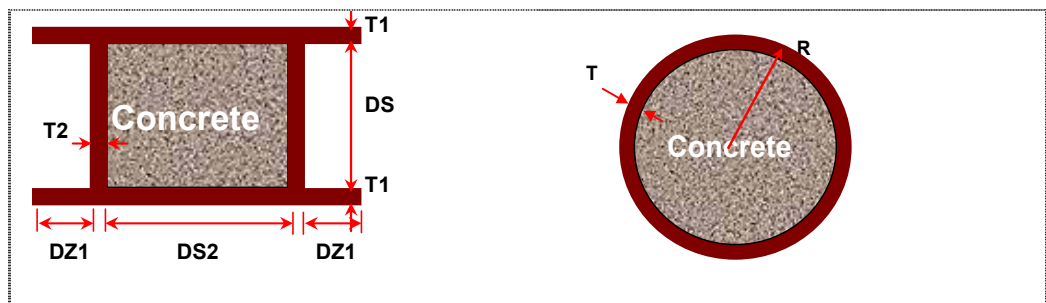
7.2 THE SOIL-PILE MODEL

The computer model was developed using the ANSYS Parametric Design Language (APDL). APDL is a scripting language that one can use to automate common tasks or even build a model in terms of parameters (variables). APDL also encompasses a wide range of other features such as repeating a command, macros, if-then-else branching, do-loops, and scalar, vector and matrix operations.

The model was built with maximum flexibility that allows all the necessary parameters to be changed for each single run. The following parameters were set to be variables:

1. Pile height, H
2. Pile dimensions;
 - DS: web height
 - DS2: middle flange width
 - DZ1: edge flange width
 - T1: flange thickness
 - T2: web thickness
3. Soil type
4. Concrete strength and stress-strain model.
5. Number of FRP layers in each segment.

6. Layer thickness
7. Mesh size in all directions for all segments.
8. Composite material type
9. Predrilled hole depth
10. All loads and deformations.
11. Cross-section geometry



7.3 MAXIMUM LOAD CAPACITY

The carrying capacity of a load bearing pile can be dictated by several factors based on the provisions of its design. Pile failure may occur in different scenarios; material failure in which the pile materials reach its ultimate capacity, geometric failure (buckling) in which the pile becomes unstable to withstand any additional loads, and finally, excess pile deformations above the allowable design limits.

In jointed bridges, lateral movements that result from thermal expansion and contraction of the bridge deck do not have a direct effect on the supporting piles. The expansion joints and bearings allow the bridge deck to move freely over the piers and abutments. The supporting piles in such systems will carry axial load only.

In integral abutment bridges the expansion joints and bearings will be eliminated for engineering purposes. Thermal movements of the bridge deck will transfer through the abutments to the supporting piles. As a result, the pile heads will move laterally to accommodate that movement.

The dead loads of the bridge structure are permanent and will be the first loads to be applied on the piles. As a result, the piles will be uniformly prestressed initially. The amount of the stress depends on the applied loads and the pile cross sectional properties.

Moments resulting from pile head movement will produce bending stresses at the pile head. These stresses will be added to the existing compressive stresses resulting from bridge dead loads which are already applied on the pile. Addition of the two stresses will result in an increase at the compression stresses at the compression side of the bending and a decrease at the tension side of the bending as illustrated in Figure 7-1.

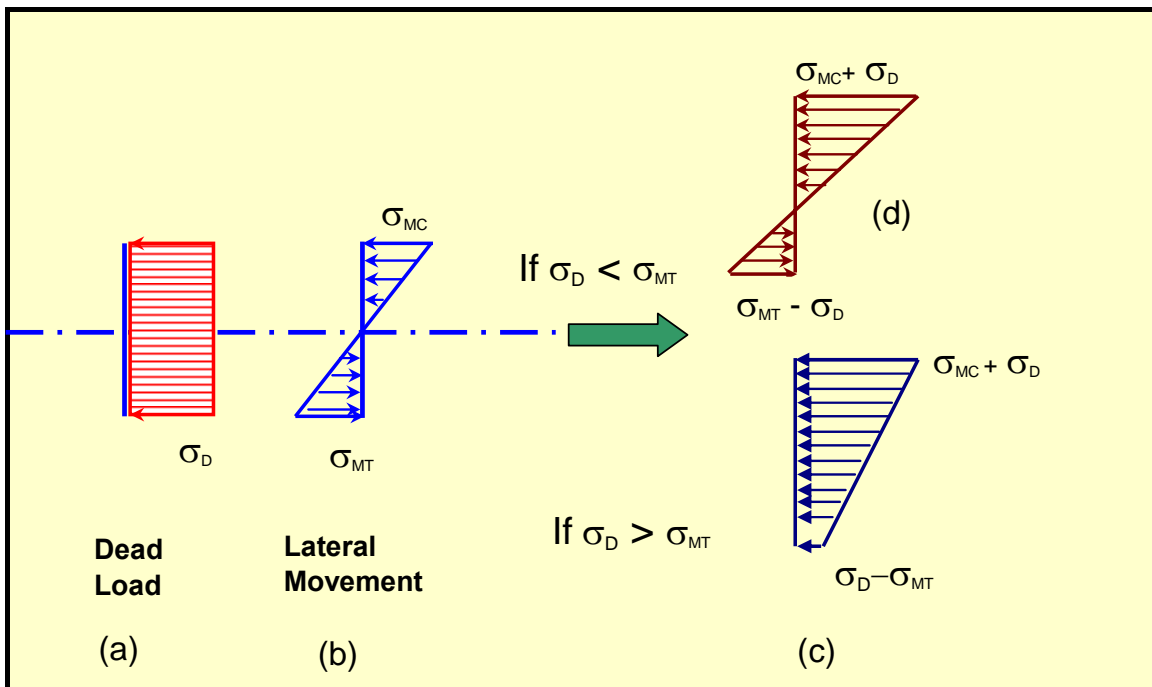
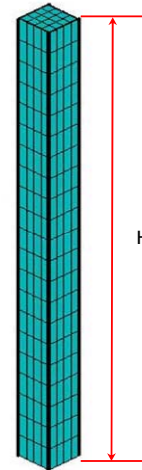


Figure 7-1: Combined stresses in a pile under dead loads and lateral movements.

Pile information:

Composite type: Glass epoxy

Property	ksi	Property	ksi
E_x	4500	X_t	90
E_y	1100	Y_t	3.9
G_{xy}	550	X_c	-80
V_{xy}	0.26	Y_c	-17.5
		S	6.2



Number of layers: 12

Layer thickness: 0.0208 in.

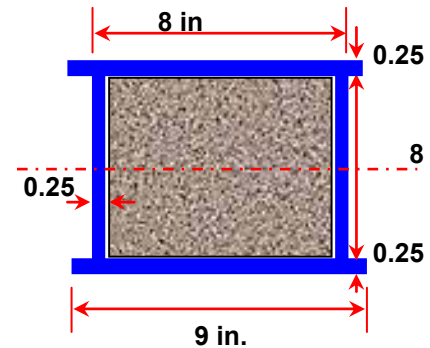
Laminate structure:[0,0,90,90,0,0,0,0,90,90,0,0]

Filling: Plain concrete $f_c'=3$ ksi

Height = 20 ft

Soil type: Dense sand

Loading:



Case 1:

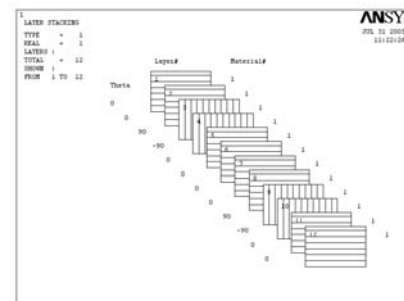
Axial load: 900 kips [steps 1 to 12]

Case 2:

Axial dead load: 300 kips [steps 1 to 4]

Lateral load: 50 kips [steps 5 to 8]

Axial live load: 200 kips [9 to 12]



As can be seen in Figure 7-1, the axial dead loads will produce the compressive stress σ_D on the pile shaft. The lateral movements will produce bending stresses with values of σ_{MT} and σ_{MC} at the tension and compressive sides of the pile head respectively. If the bending tensile stress σ_{MT} is greater than the axial compressive stress σ_D , portions of the pile shaft will be subjected to tensile stresses, Figure 7-1(d). If σ_{MT} is less than σ_D then the pile shaft will stay under non-uniform compressive stresses, Figure 7-1(c).

The same scenario will be repeated after applying the axial live loads. The pile may end with either two stress zones (tension and compression) or one non-uniform compression zone as shown in Figure 7-1 (d) and Figure 7-1 (c) respectively.

According to the maximum stress failure criterion, the stresses in each layer should remain within the allowable stress limits during and after all load applications. Any stress value exceeding the allowable limit will lead to a layer failure. Therefore, the pile's maximum load capacity can be defined as the amount of load a pile can carry before any stress component exceeds the assigned criteria.

Structural elements made of composite materials do not have standard mechanical properties because of the variety of composite properties and different architecture for each element. Therefore, the maximum load capacity of a composite pile can be determined based on the geometrical, mechanical and architectural properties of the pile in consideration.

To investigate the effects of lateral head movement on the axial capacity of load bearing piles, a pile model with the configuration described in the pile information sheet can be analyzed under two cases of loading: pure axial load up to failure, and axial load

plus lateral head movement up to 2 inches. The effects of all design parameters on the pile's maximum load capacity will be discussed in the following sections.

Figure 7-2 presents an illustration for the envelopes of the three major stress components in all 12 layers at 900 kips axial compression load. It can be seen that the second stress component, σ_2 , has reached the allowable limit in one or more layers. The other two stress components, σ_1 and τ_{12} , did not reach any of the limits bounded by the failure criteria zone.

Since the stress-strain behavior of the fiber reinforced composites is linearly elastic, then the stresses resulting from the different types of loading can be added using the principle of superposition. Therefore, the pile that reached the allowable stress limit at 900 kips (shown in Figure 7-2) will not be able to take any more loading or bending. Any additional stresses from either the axial loading or the lateral movement will be added to the current stress values. An excess in the stresses beyond the allowable limit will lead to a pile failure.

To accommodate the stresses from both the axial load and the lateral movements, the pile should be designed such that all stress components at any loading stage should stay within the allowable region. Figure 7-3 through Figure 7-5 show the stress envelopes for the three stress components in all layers at an axial load of 300 kips and lateral displacement up to 2.0 inches. Each graph has two envelopes: the first envelope is for the axial load and usually has a uniform shape over the length of the pile. The second envelope is for bending from the lateral movement which does not have a constant or uniform shape. It can be seen that the stresses at the upper portion of the pile increase as the lateral movement increases while the axial load remains constant. From 0 up to 1.5

inches of lateral movement, all stress components are still in the allowable zones, but, at 2.0 inches the second stress component, σ_2 , exceeds the allowable limit at the tension side as can be seen in Figure 7-4. According to the “first layer failure” approach, the pile will have failed and will not be able to take any more loads.

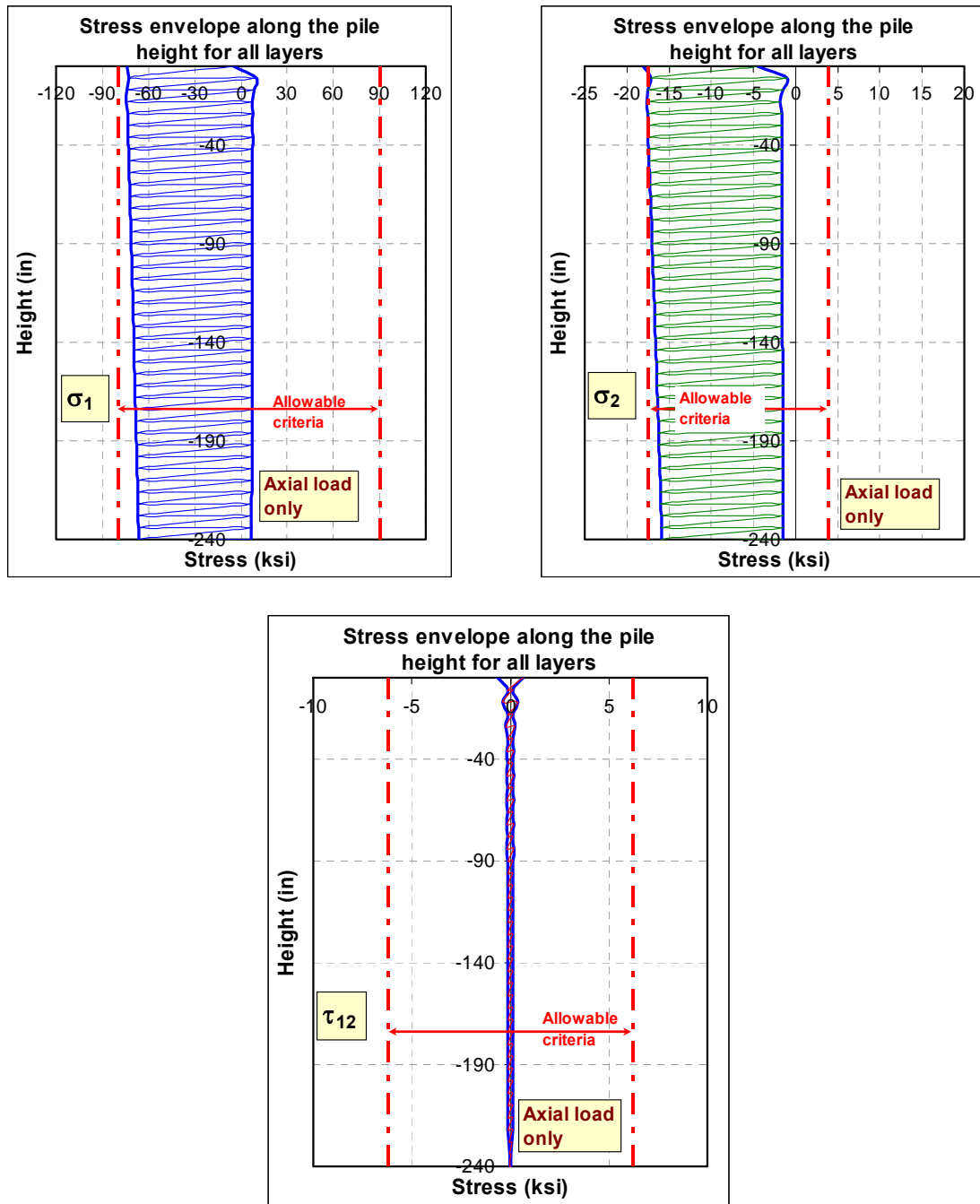


Figure 7-2: Stress envelopes for a pile under axial compression only (Load=900 kips).

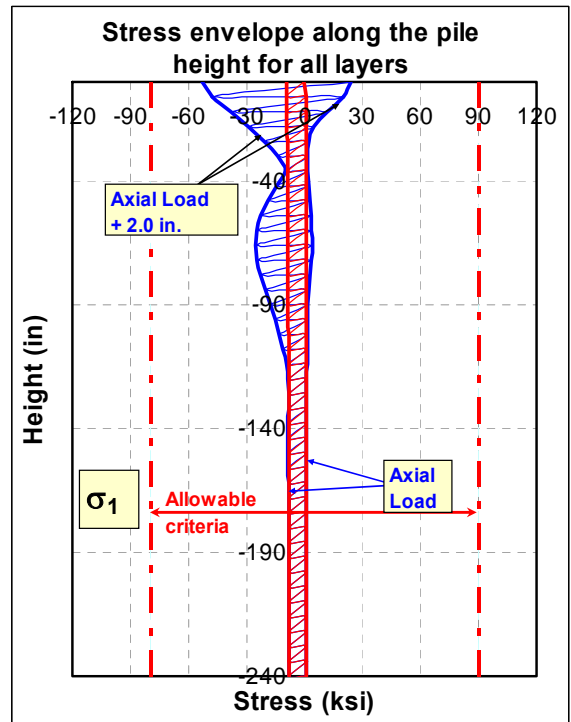
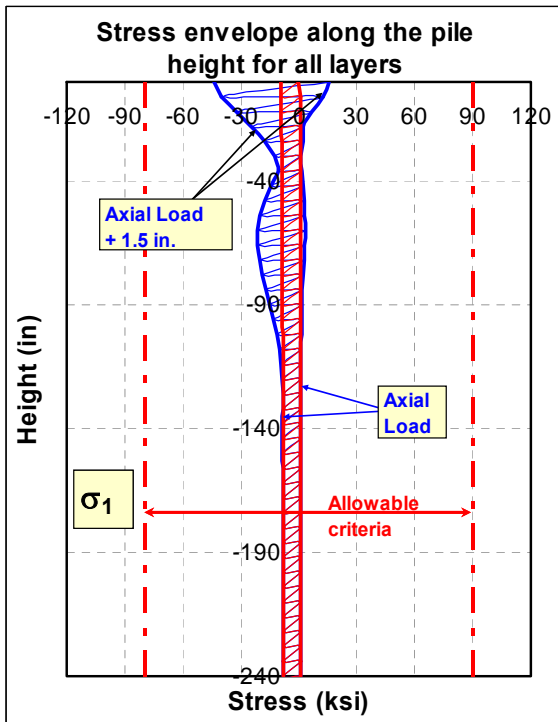
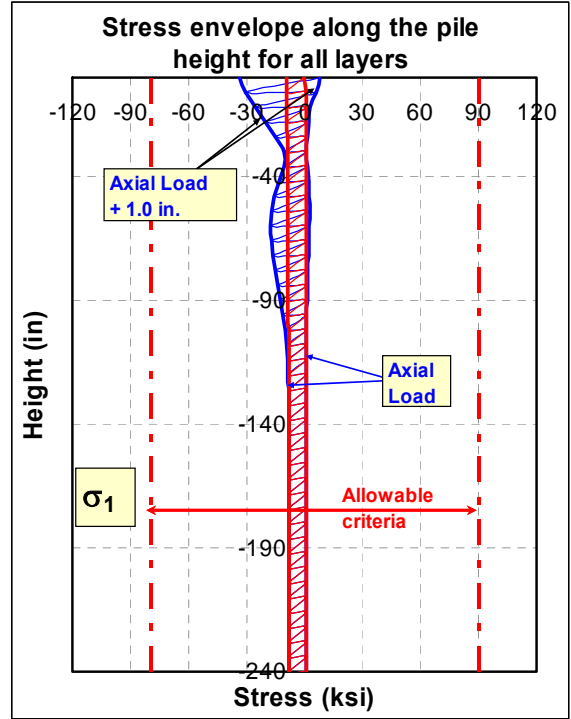
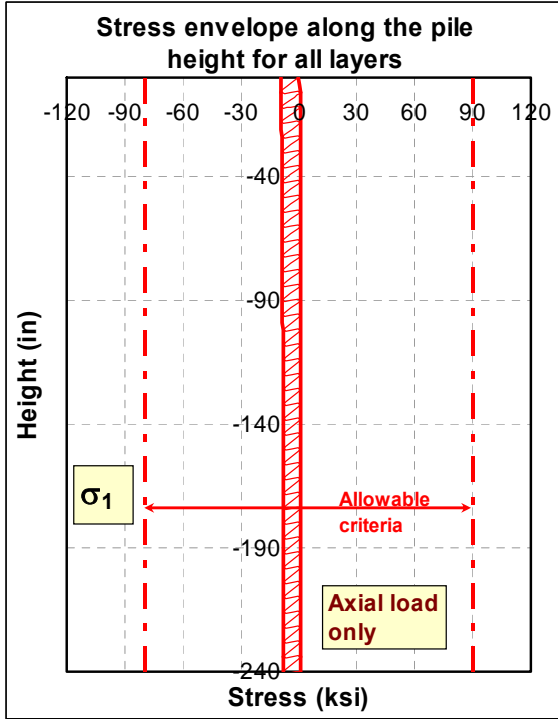


Figure 7-3: Effect of lateral movement on axial capacity, stress σ_1 .

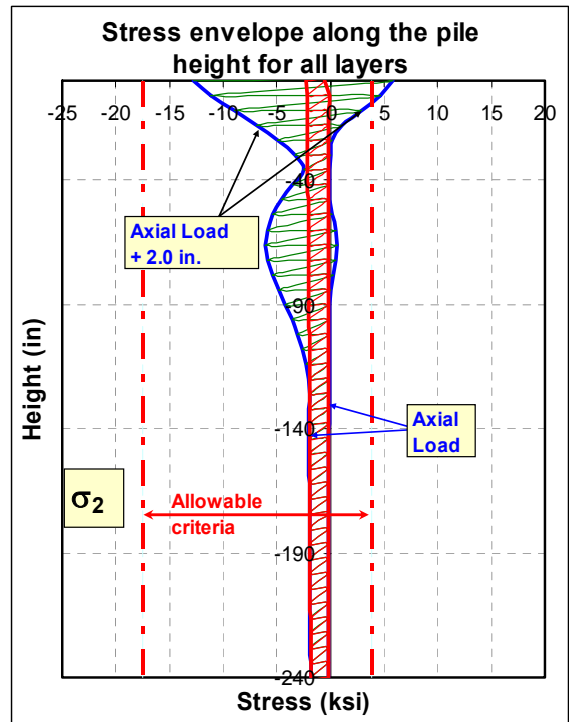
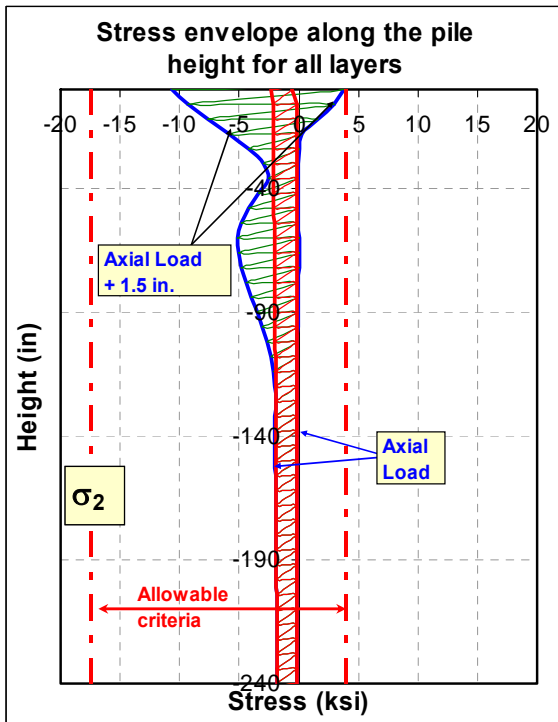
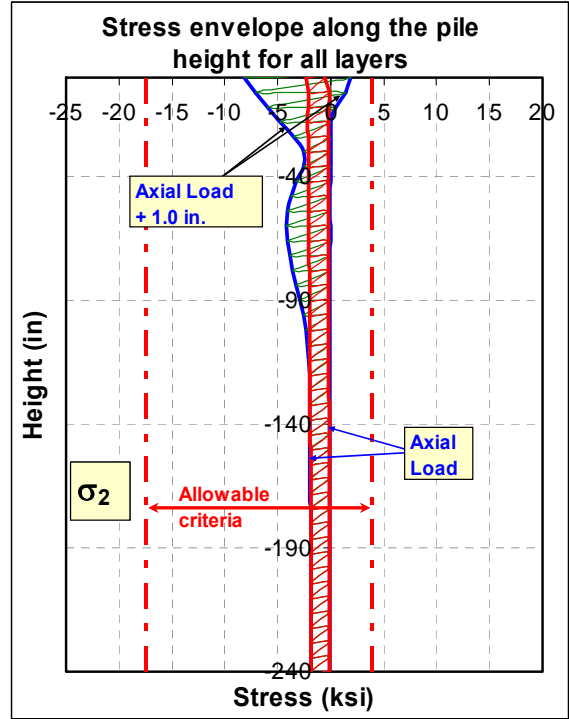
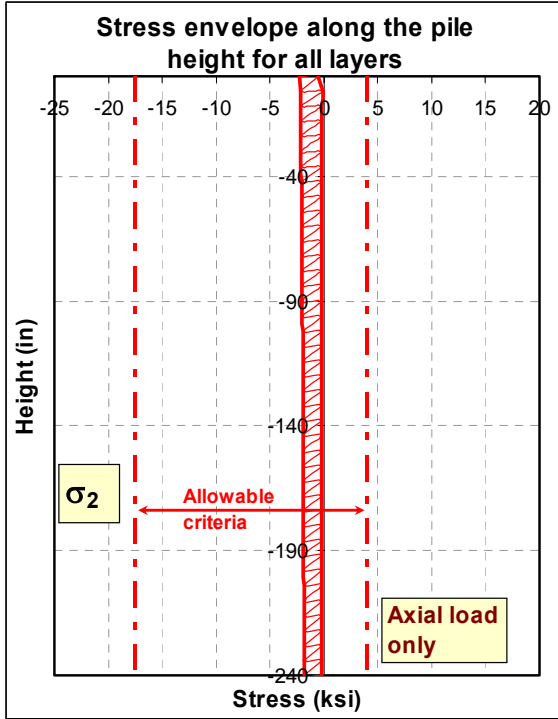


Figure 7-4: Effect of lateral movement on axial capacity, stress σ_2 .

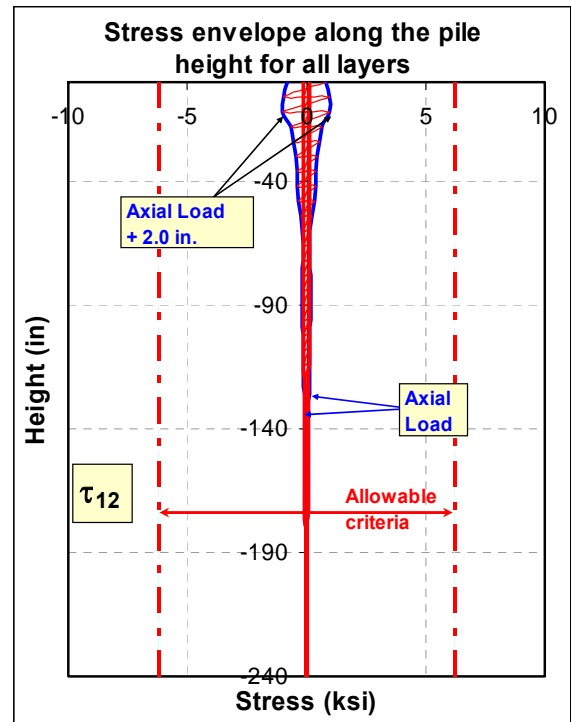
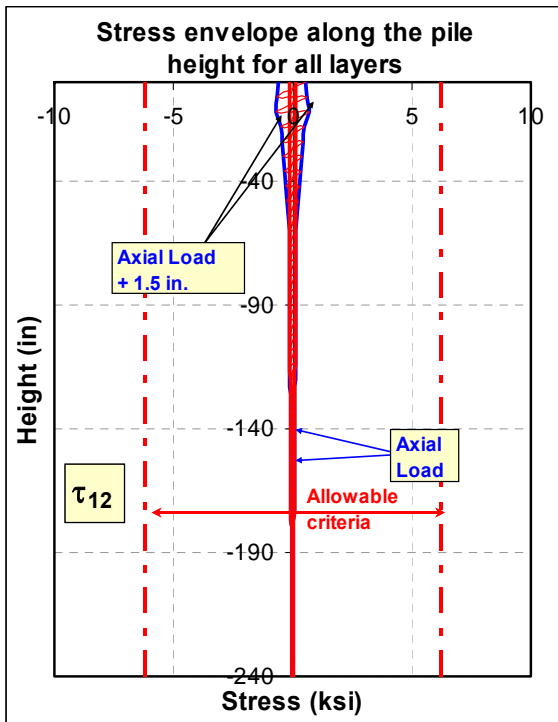
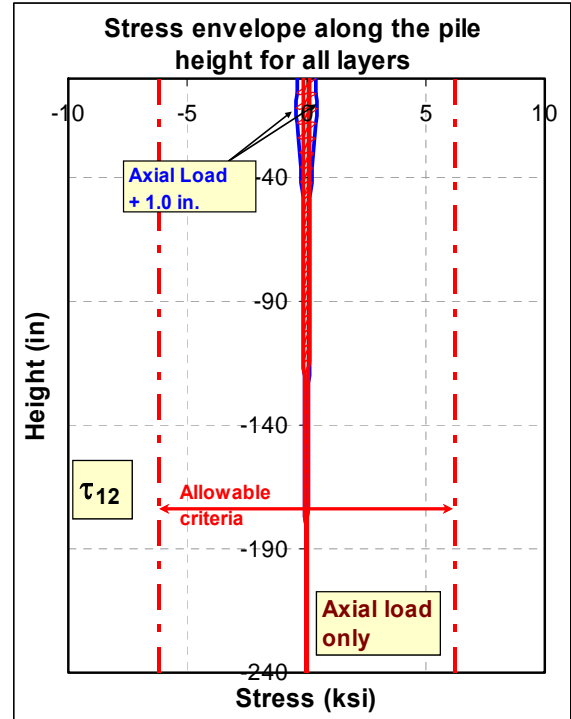
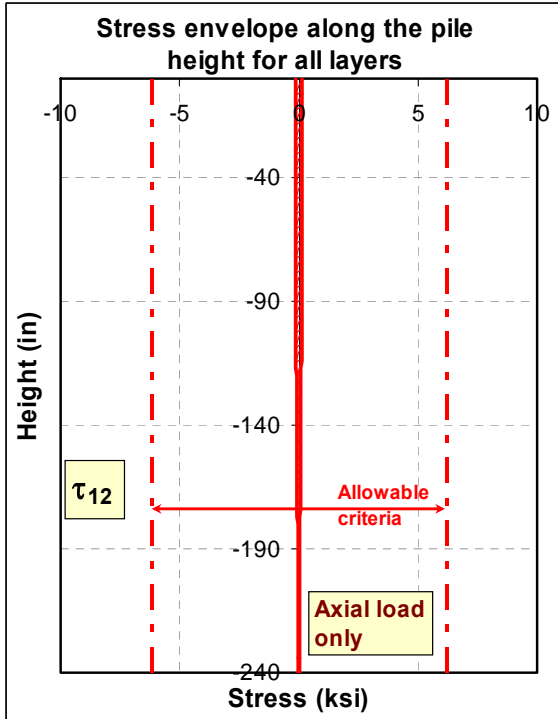


Figure 7-5: Effect of lateral movement on axial capacity, stress τ_{12} .

The stress variation at a point for the two cases of loading is plotted for two different layers in the pile shell, as shown in Figure 7-6 and Figure 7-7. In the first figure, it can be seen that all stresses are within the allowable stress criteria and the layers are still capable of handling more loads. In the latter figure, the stresses in the pile with 900 kips pure compression are still within the criteria, while the other pile of 300 kips axial load and 2 inches lateral movement has its layer number 9 exceeding the allowable stress.

Stresses resulting from lateral movement of the pile head have a major effect on the axial capacity of an integral bridge pile. As soon as the pile head starts to move laterally, stresses begin to increase dramatically at the upper portion of the pile. The pile will be capable of carrying more axial loads as long as the stresses in all layers are within the allowable limits. If a stress component in one or more layers exceeds the allowable stress criterion, then the pile has failed.

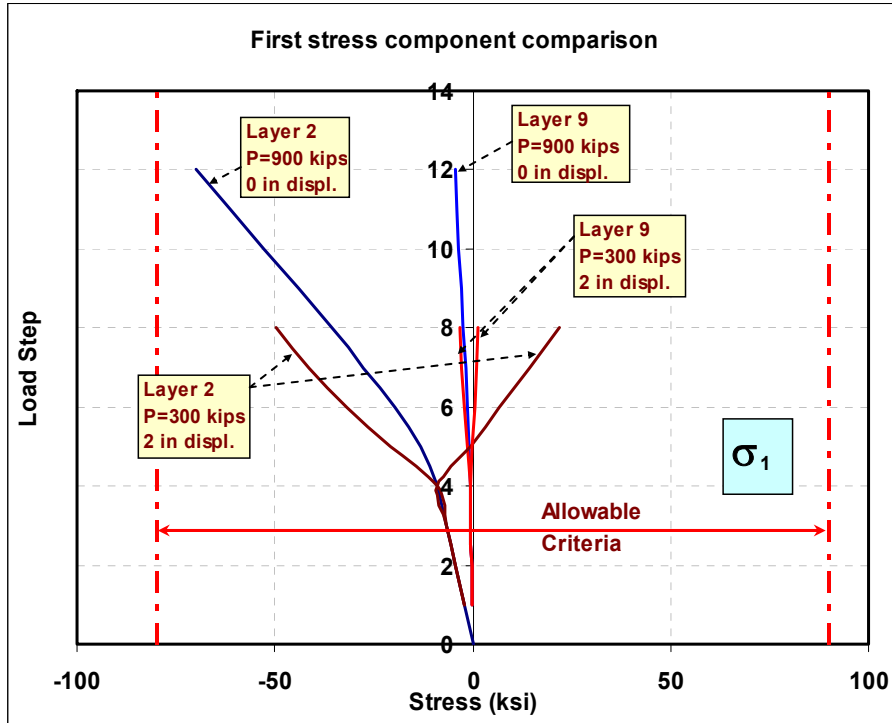


Figure 7-6: Stress (σ_1) development with time.

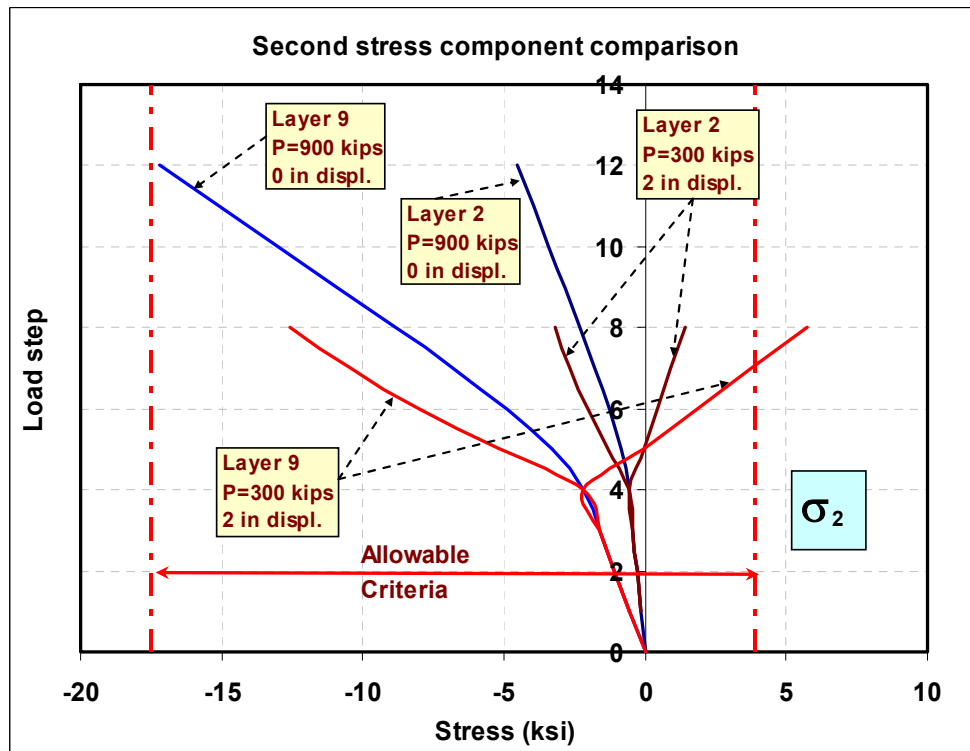


Figure 7-7: Stress (σ_2) development with time.

7.4 EFFECT OF THE DIFFERENT PARAMETERS ON THE BEHAVIOR OF LATERALLY LOADED PILES

The behavior of driven piles under axial loading and bending moments depends on several factors that are related to the pile itself, the soil medium and the loading conditions. In the following sections a discussion of the effect of each parameter (factor) will be presented.

7.4.1 SOIL TYPE

Soil profile is one of the crucial factors that have major effects on the lateral behavior of piles in integral abutment bridges. Soil properties are represented by load-displacement ($P-\Delta$) curves to simulate the vertical and lateral behavior of the soil-pile system. Generally, three factors have the most influence on the $P-\Delta$ curves that control the soil-pile interaction: the soil properties, the pile's flexural rigidity, and the nature of loading.

To study the effects of soil type on the soil-structure interaction, four different piles in different soil profiles were investigated. Two load configurations were utilized: (1) a combination of axial and lateral loads, and (2) a combination of axial load and a specified lateral head displacement. Figure 7-8 shows different plots of lateral deformation curves for identical piles driven in cohesion and cohesionless soils. The piles were assumed to be fully driven in each soil profile and were subjected to a specified vertical axial load as a dead load. After the application of the full dead load, the piles were subjected to an incremental (multi-step) lateral load at its top to represent the thermal expansion and contraction of the bridge deck. The pile heads were left free to move laterally for the purpose of measuring lateral stiffness of the soil-pile system. As

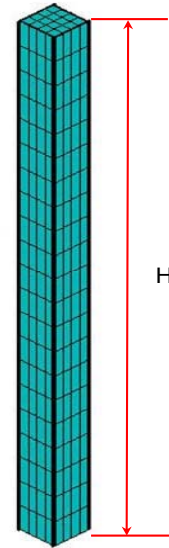
can be seen, the responses of the piles (which were subjected to the same load conditions) are different for each soil profile. The pile in the very stiff clay experienced higher lateral resistance than those in the other soils. The pile in the soft clay showed response to the lateral deformations at greater depth compared to the pile in stiff clay. A wider comparison of the same pile in other soils is presented in Figure 7-9. In this figure, the lateral responses of identical piles under similar loading conditions are plotted along the pile depth for different types of soils. The plots show clearly the effect of soil stiffness on the deflected shape of the pile. It has to be noted that the curves do not have the same x-scale.

Figure 7-10 shows the lateral deformation curves for the same piles subjected to axial load and lateral movements up to 2 inches. As can be seen from the curves, the piles' responses to the lateral movement are not the same. The pile in the soft clay experienced the highest lateral deformation with the deepest point of fixation. The pile in the very stiff clay experienced the lowest lateral deformation and shallowest point of fixation.

Pile information:

Composite type: Glass epoxy

Property	ksi	Property	ksi
E_x	4500	X_t	90
E_y	1100	Y_t	3.9
G_{xy}	550	X_c	-80
V_{xy}	0.26	Y_c	-17.5
		S	6.2



Number of layers: 12

Layer thickness: 0.0208 in.

Laminate structure:[0,0,90,90,0,0,0,0,90,90,0,0]

Filling: Plain concrete $f_c'=3$ ksi

Height = 40 ft

Soil type: Soft clay, Stiff clay, very stiff clay
and dense sand

Loading:

Case 1:

Axial dead load: 300 kips [steps 1 to 6]

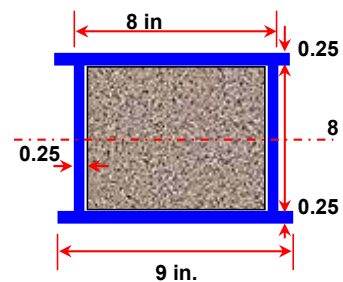
Lateral load: 50 kips [steps 7 to 12]

Case 2:

Axial dead load: 300 kips [steps 1 to 4]

Lateral displacement: 2 in. [steps 5 to 8]

Axial live load: 200 kips [steps 9 to 12]



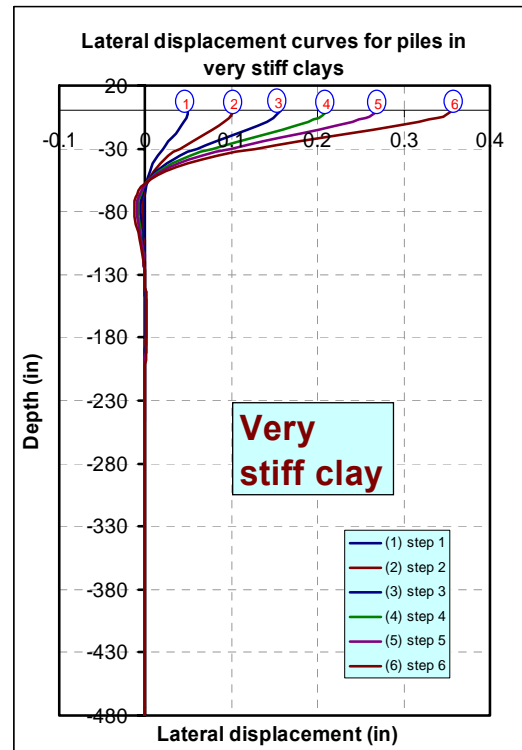
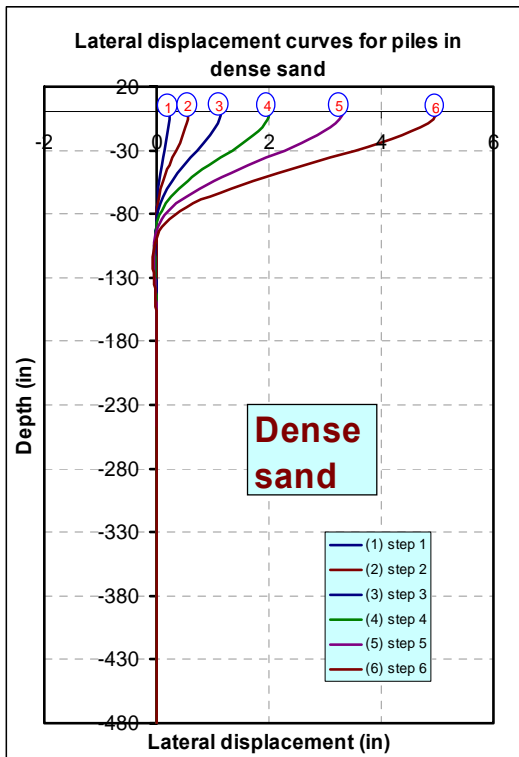
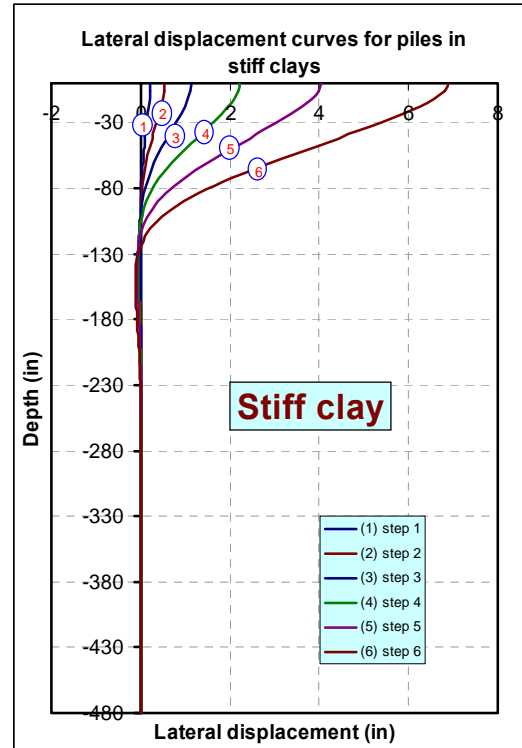
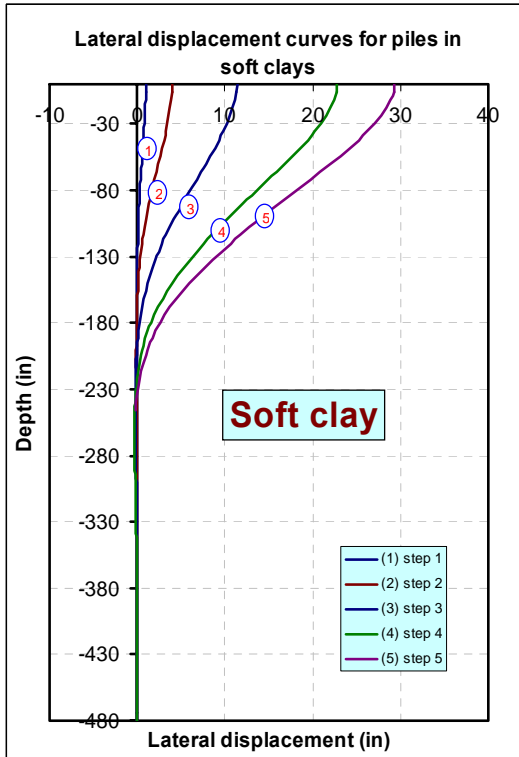


Figure 7-8: Lateral displacement curves for a pile in different soil profiles under lateral load.

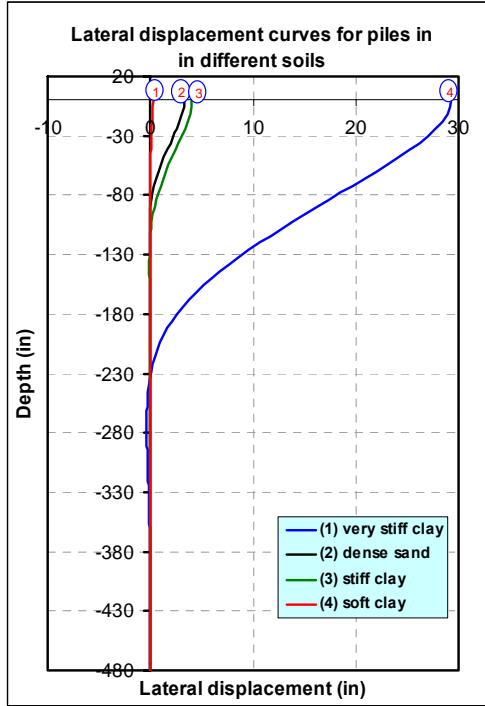


Figure 7-9: Lateral displacement curves for a pile under horizontal force in different soil profiles.

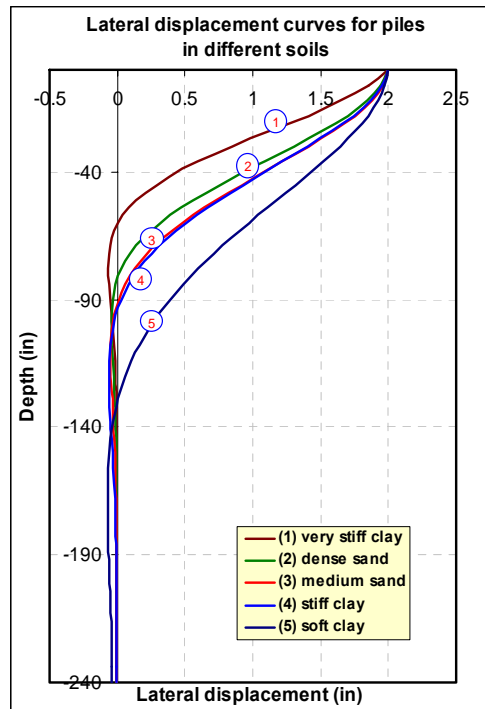
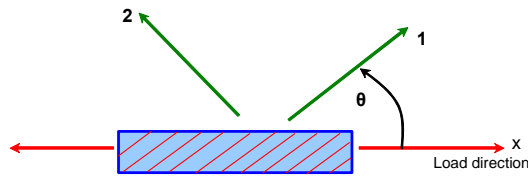


Figure 7-10: Lateral displacement curves for a pile under constant displacement in different soil profiles.

The soil properties also have a major effect on the stresses developed on the deformed pile, mostly bending stresses. The deflected shape always gives an indication as to how large the resulting stresses will be in the pile shaft. The following figures present the stress variation profiles of a pile in different soils. The pile consists of a 12-layer composite shell with multiple orientation angles and is subjected to axial dead load and gradual lateral displacement at its top.

Due to the massive output of the stress analysis of the multi-layered multi-directional fiber reinforced composites, it will be difficult to present all output results. Instead, sample curves will be selected to show the behavior of the desired entity at some extreme locations; then an envelope curve will show the entire range of extreme values at all nodes in the finite element mesh. Each pile model has several hundreds of nodes and each node has multiple stress values; three of them are of interest. In addition, the composite shell consists of multiple layers with each layer having its own material directions. As a result, for each node we will have (12 layers x 3 directions = 36 stress values) at each load step.

In Figure 7-11 and Figure 7-12 the actual and the normalized stress variations with time (load is time-dependent and increases with time) are plotted for two points at the extreme compression and tension locations of the pile section respectively. The two points are selected at the top of the pile (0-ft deep); the conjunction with the abutment usually has the highest stress values. The stress curves are plotted in the major material direction σ_l for a single layer (0-degree) which has its fibers in the direction of the pile axis.



Each curve of the set consists of three parts based on the load application sequence: dead load (DL), lateral movement (LM), and live load (LL), respectively, in the order of load application. As can be seen, the behavior of each portion of any of the curves is different for each loading stage. For illustration, if we consider the very stiff clay curve #1 in Figure 7-12, the dead load stresses are about 10% of the total compression stress at that point. Bending stresses from lateral movement of the pile head form about 70% and the remaining 20% are due to the live load effect.

The break contribution to stress for each type of loading is not the same for all soil types. As can be seen, all piles showed equal dead load stresses at each soil profile because the dead load was applied as a pure axial compression before any lateral movement occurs. Stresses resulting from lateral movements show variable behavior for each soil profile. Stiffer soils showed higher bending stress rates compared to soft soils. This is because the bending stress is highly dependent on the stiffness of the soil medium around the pile. Also the concrete filling begins to develop cracks as soon as the bending moments reach the rupture moment. The bending stress behavior is not constant along the depth of the pile shaft. The stress value and rate at a point change with the depth and location of that point at the pile. Figure 7-13 shows the stresses along a series of points along the depth of the pile shaft for all soil profiles. It can be seen that each point has a different stress value from the other within the region in which bending moments have

effect. In the region where the bending moment starts to vanish, the stresses are about the same.

Figure 7-14 through Figure 7-16 show the stress variation at three different locations along the pile depth. The stresses in the FRP shell are smaller at lower depth. Bending effects disappear gradually with depth until they reach a state of steady compression. Therefore, pile stresses in all soil profiles are very close in value at 10-ft depths as can be seen in Figure 7-16.

Concrete stresses at a point and at a line over the pile length were also investigated as shown in Figure 7-17 and Figure 7-18 respectively. As can be seen, the stresses in concrete are directly proportional to the soil stiffness. Stiff soils, such as very stiff clays produced the highest concrete stresses in both tension and compression zones (curves #5). On the other hand, the lateral soil resistance for the piles in soft clays is the lowest and the bending stresses in the pile are very small, such that the concrete did not experience any tension cracks.

The stress curve representation at a point is not adequate to reflect the actual behavior of the pile in analysis of multi-directional layered composite material structures. Each single layer has its own failure criteria based on the material type. All major stresses in each layer should be checked against failure.

Figure 7-19 shows a group of stress envelopes for the major stress components along the pile depth for the different soil profiles. The stresses are plotted for all layers at each node and at load step 8 which includes the total dead load and the 2 in. lateral movement. It can be seen that all three stress components, σ_1 , σ_2 , and τ_{12} , are increasing in the bending zone as the soil stiffness increases. The effect of soil stiffness on the crack

patterns in concrete is shown in Figure 7-20. The piles in stiff soils experienced major cracks in all directions of the upper portion, while the piles in medium soils had fewer cracks.

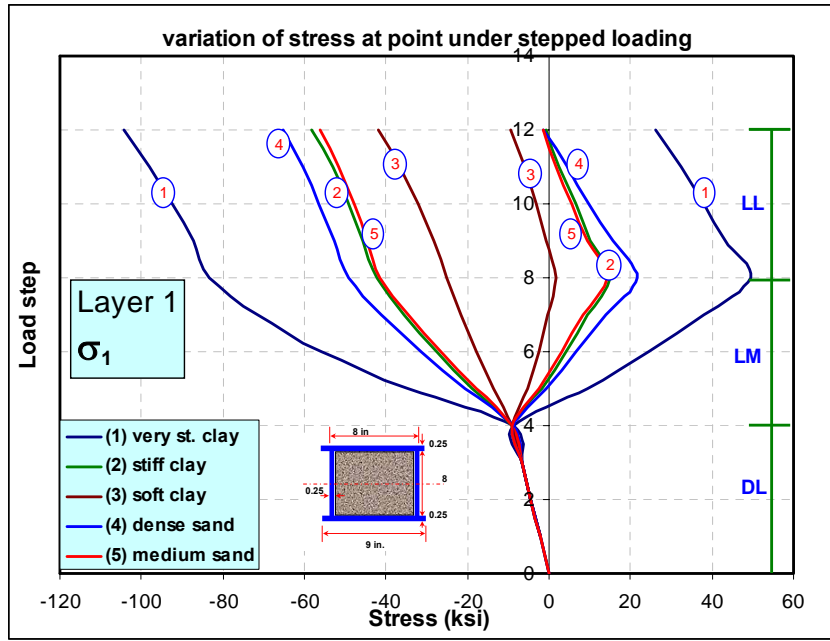


Figure 7-11: Stress variation with time at a point located at 0-ft from the top.

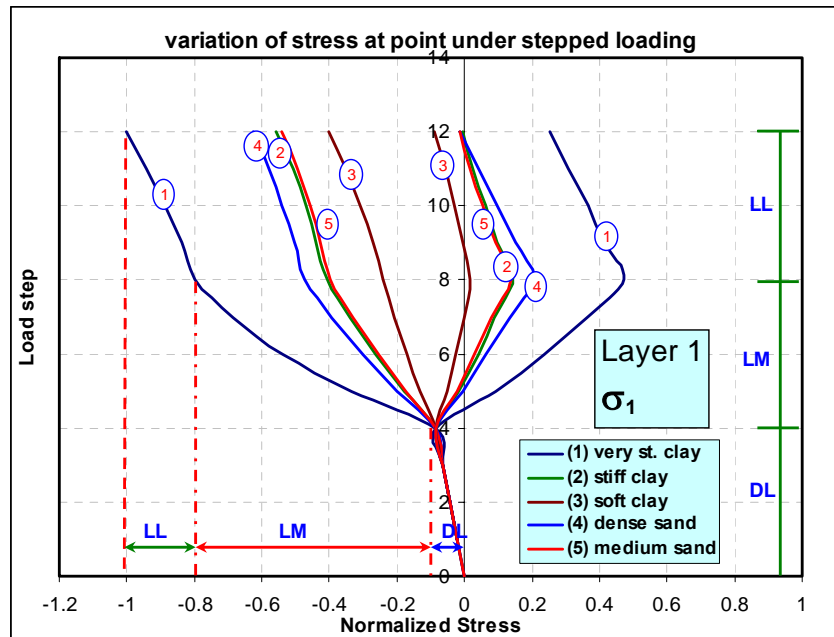


Figure 7-12: Normalized stress variation with time at a point located at 0-ft from the top.

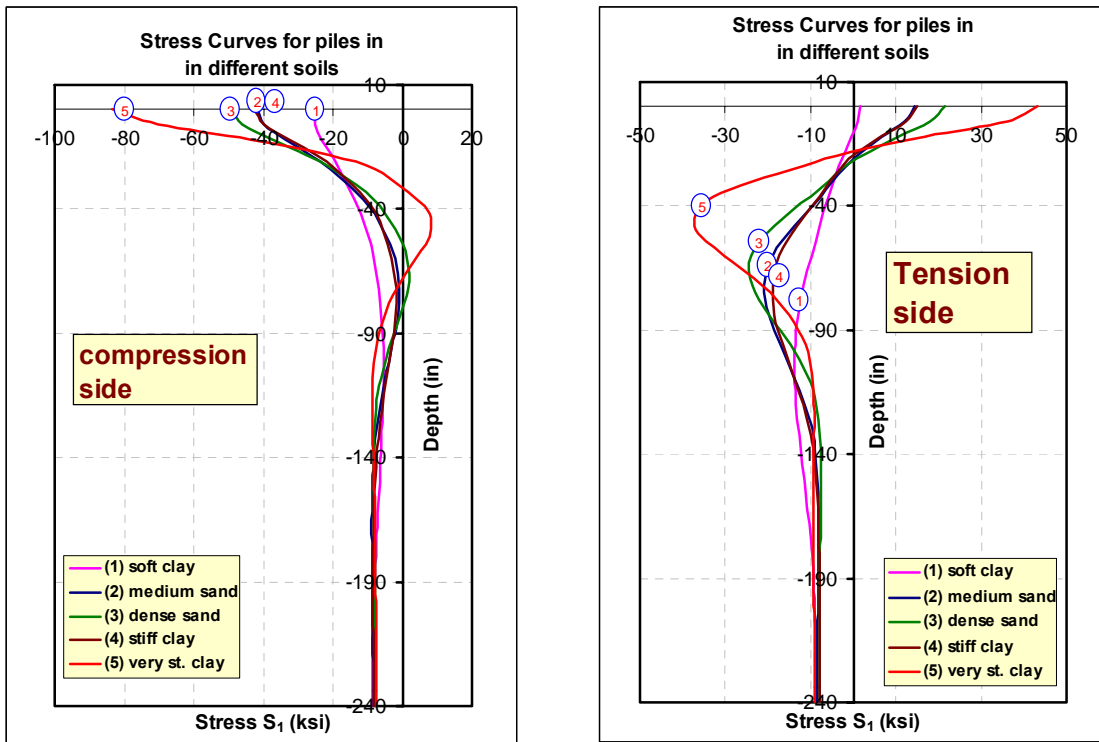


Figure 7-13: Stress variation along the depth of the pile shaft in both tension and compression sides.

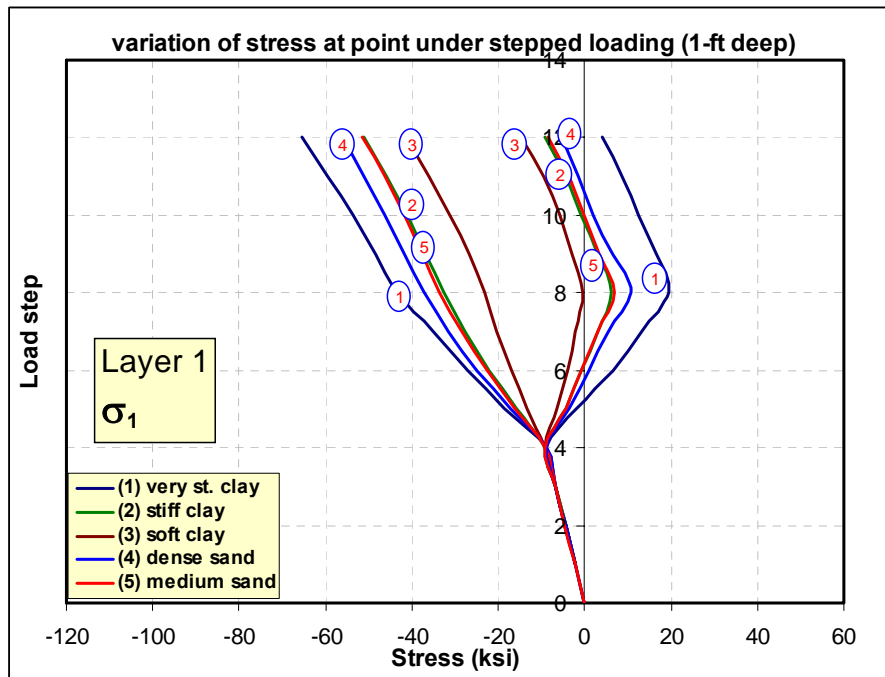


Figure 7-14: Stress variation with time at a point located at 1-ft from the top.

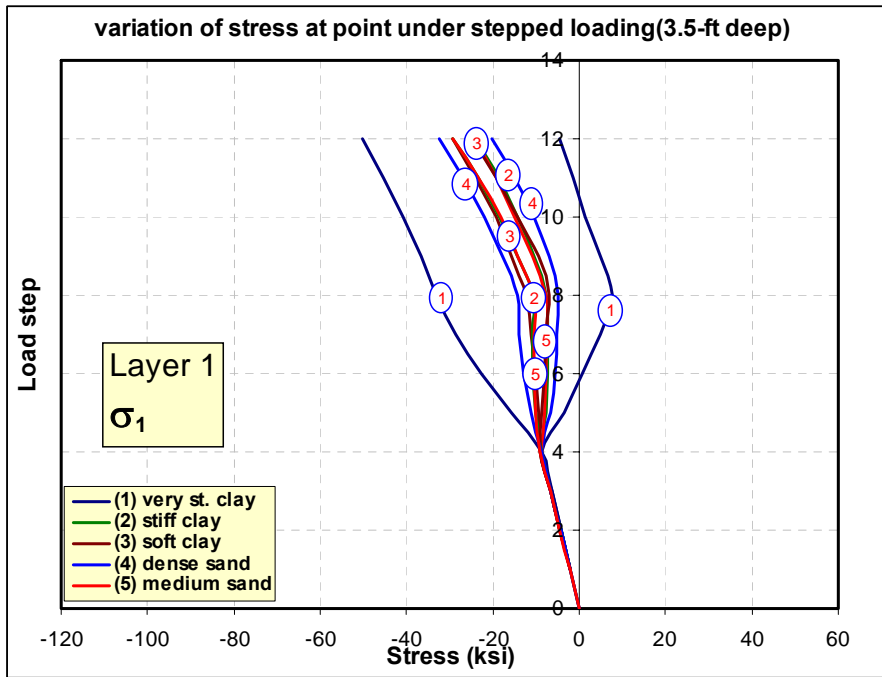


Figure 7-15: Stress variation with time at a point located at 3.5-ft from the top.

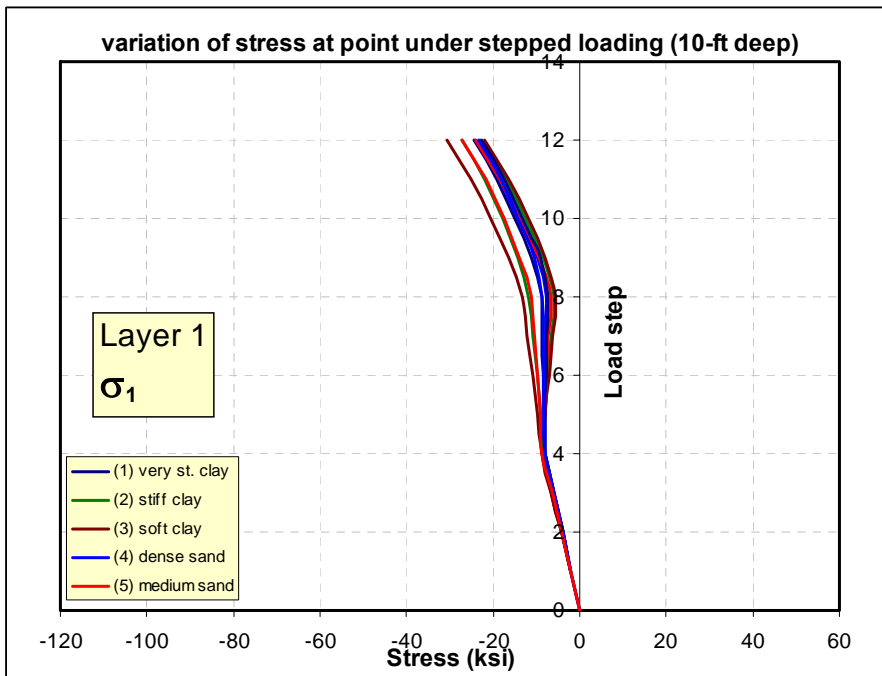


Figure 7-16: Stress variation with time at a point located at 10-ft from the top.

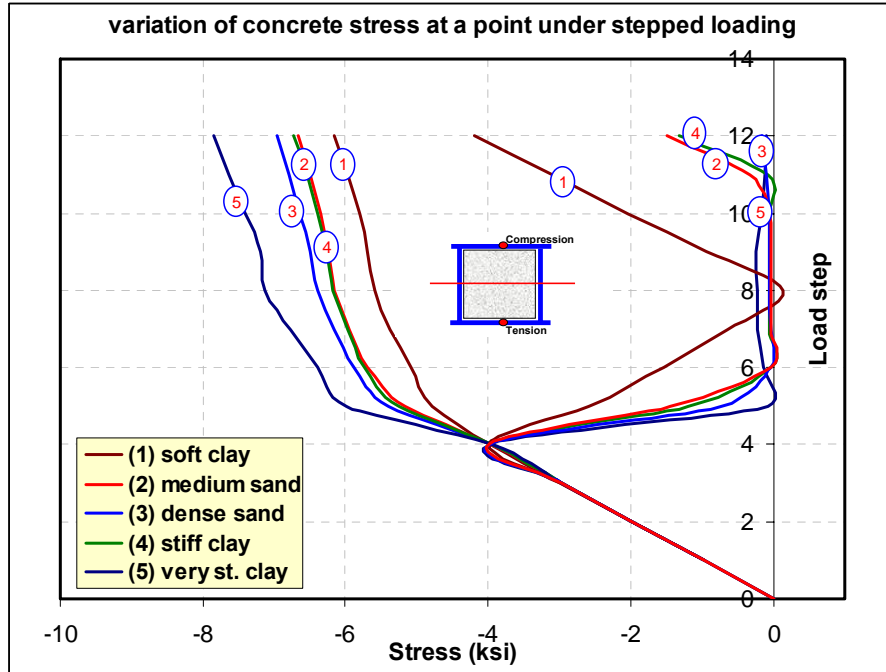


Figure 7-17: Stress variation with time in concrete at a point located at 0-ft from the top.

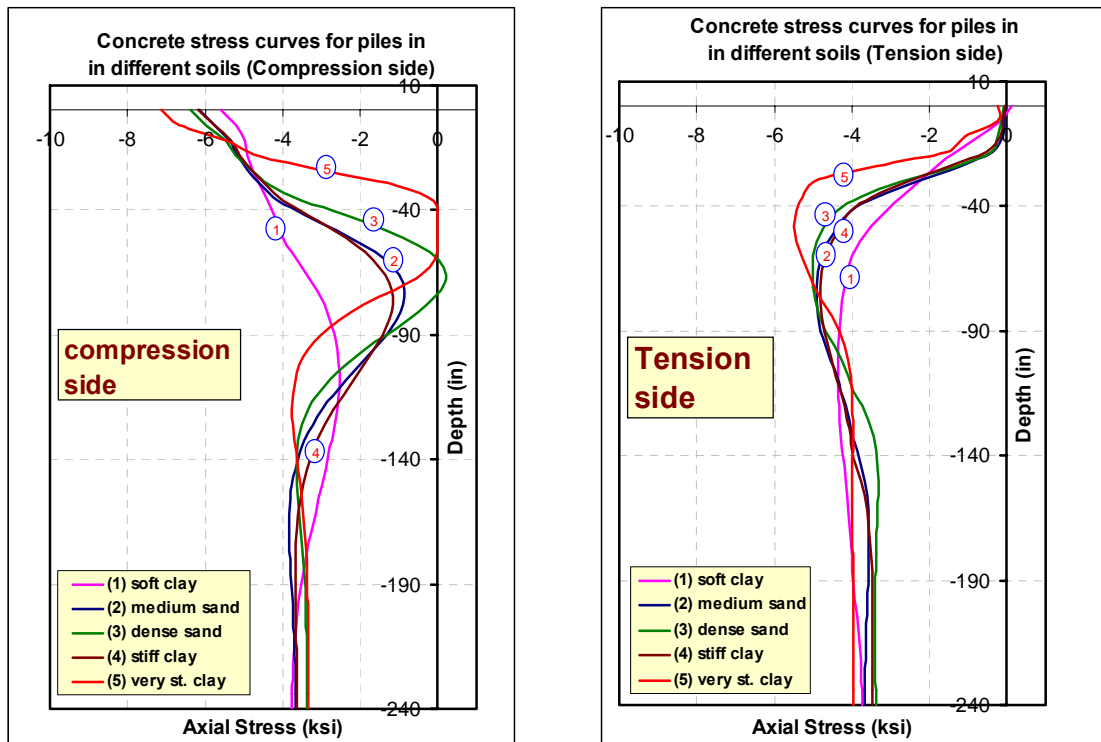


Figure 7-18: Stress variation in concrete along the depth of the pile shaft in both tension and compression sides.

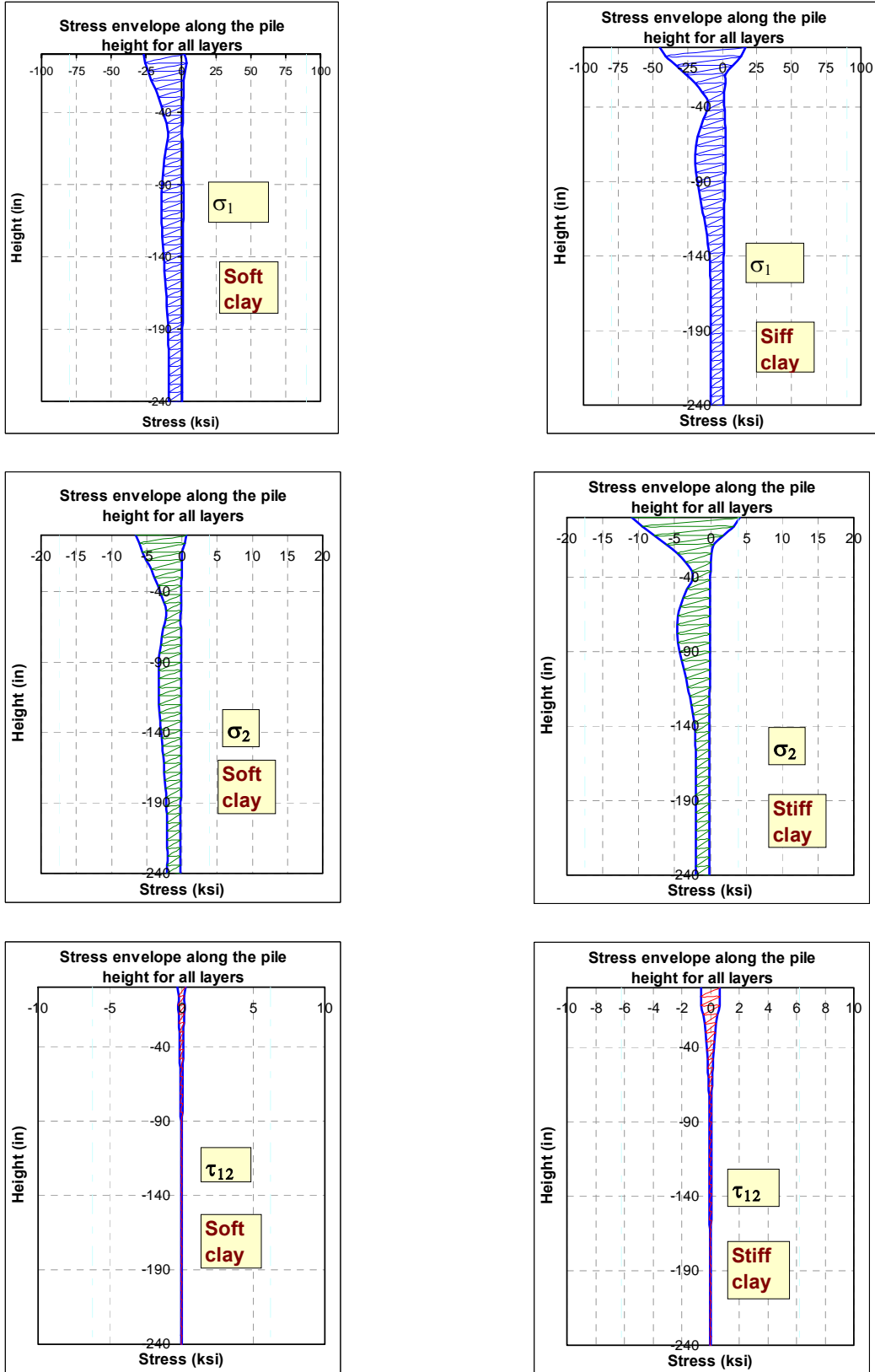


Figure 7-19: Stress envelopes along the pile length for all layers at load step 8.

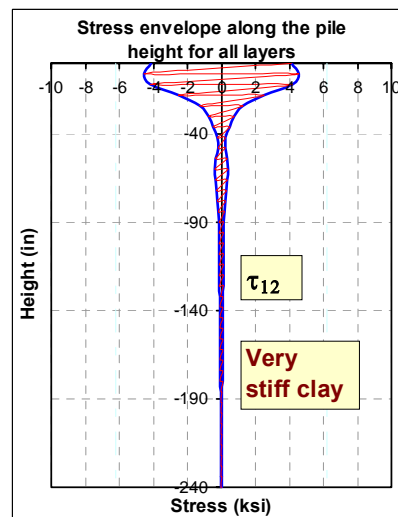
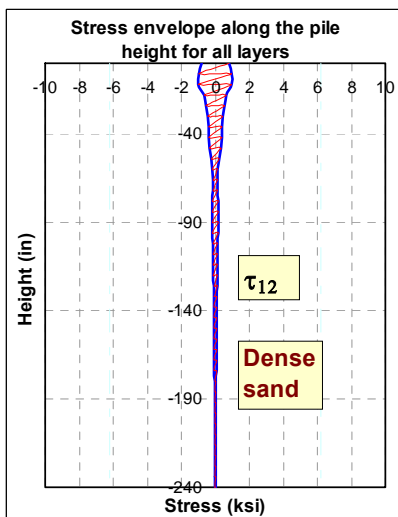
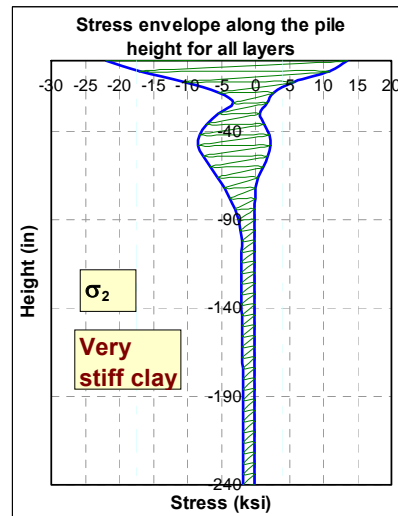
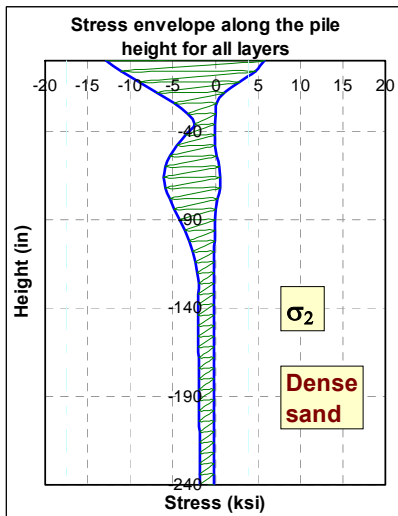
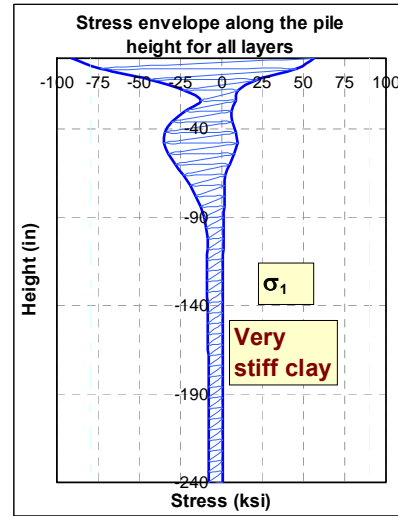
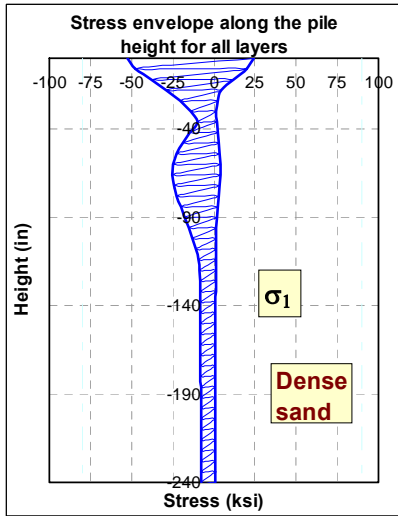
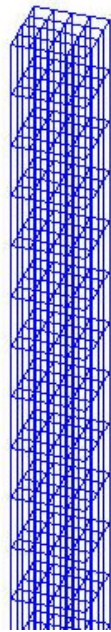
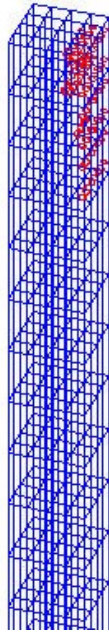


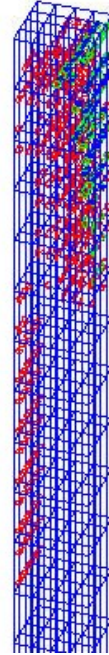
Figure 7-19: Stress envelopes along the pile length for all layers at load step 8 (cont'd).



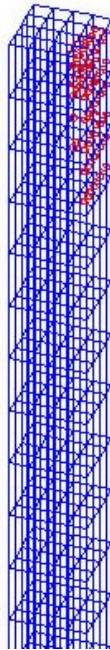
Soft clay



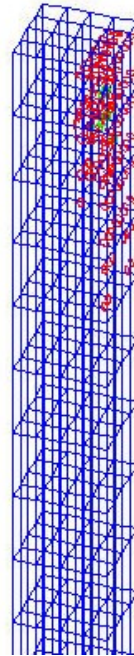
Stiff clay



Very stiff clay



Medium sand



Dense Sand

Figure 7-20: Concrete crack patterns for piles in different soils.

7.4.2 CONCRETE FILLING

Concrete is a stiff material when used in bulk volumes. Concrete stiffness is correlated to its strength. Concrete also is price competitive when compared to other construction materials such as steel. It can be used in conjunction with FRP materials in pile construction. Composite materials have a wide range of stiffness depending on the type and volume fractions of its constituents. It may range from the stiffness of the softest material to the stiffness of high strength steel. Price based comparison shows that concrete has much lower costs than FRP composites on volume or weight basis. For economical considerations, hybrid piles such as concrete-filled FRP tubes can provide very effective solutions for special types of applications.

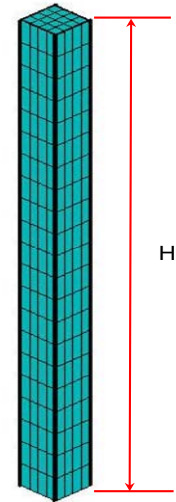
Designing piles for jointless bridges requires some coordination between the axial and lateral stiffnesses of the pile. While higher stiffness is always desirable in the pile axial direction, more flexibility is desired in the lateral direction. Axial stiffness of a compression member depends on its cross-sectional area and the stiffness of its constituent materials. On the other hand, lateral stiffness of a bending member depends on its moment of inertia in addition to the stiffness of the constituent materials.

To investigate the effect of the concrete filling on the behavior of laterally loaded piles, three pile configurations were considered. The three piles have cross-sections as shown in the following pile information sheet. All of them have the same FRP cross-sectional area and the same fiber structure. After subjecting all piles to the axial dead load, an incremental lateral displacement was applied allowing them to bend about their x-axes, as shown in the figure. The live load was then applied in an incremental process.

Piles information:

Composite type: Glass epoxy

Property	ksi	Property	ksi
E_x	4500	X_t	90
E_y	1100	Y_t	3.9
G_{xy}	550	X_c	-80
V_{xy}	0.26	Y_c	-17.5
		S	6.2



Number of layers: 12

Layer thickness: 0.0208 in.

Laminate structure: [0,0,90,90,0,0,0,0,90,90,0,0]

Filling: Plain concrete $f_c' = 3, 4, 5, 6,$ and 7 ksi

Height = 20 ft

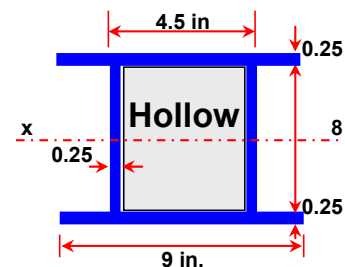
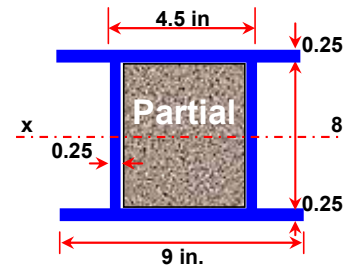
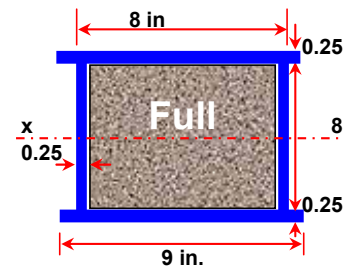
Soil type: very stiff clay

Loading:

Axial dead load: 300 kips [steps 1 to 4]

Lateral displacement: 2 inches [steps 5 to 8]

Axial live load: 200 kips [steps 9 to 12]



The following figures show a comparison between hollow and concrete-filled piles in very stiff clay soil. All piles have the same size of composite shell but with different shape configurations for concrete filling purposes. The first pile is without filling, the second is half-filled with concrete and the third is totally filled as shown in the previous illustration.

Figure 7-21 and Figure 7-22 show a comparison between the load-deformation curves of the three piles under identical loading conditions. The hollow pile experienced higher vertical deformation and fewer lateral deformations than those with the concrete filling. The vertical deformation is twice as much or more than that in the concrete filled pile. The concrete filling increased both the axial and lateral stiffness of the pile.

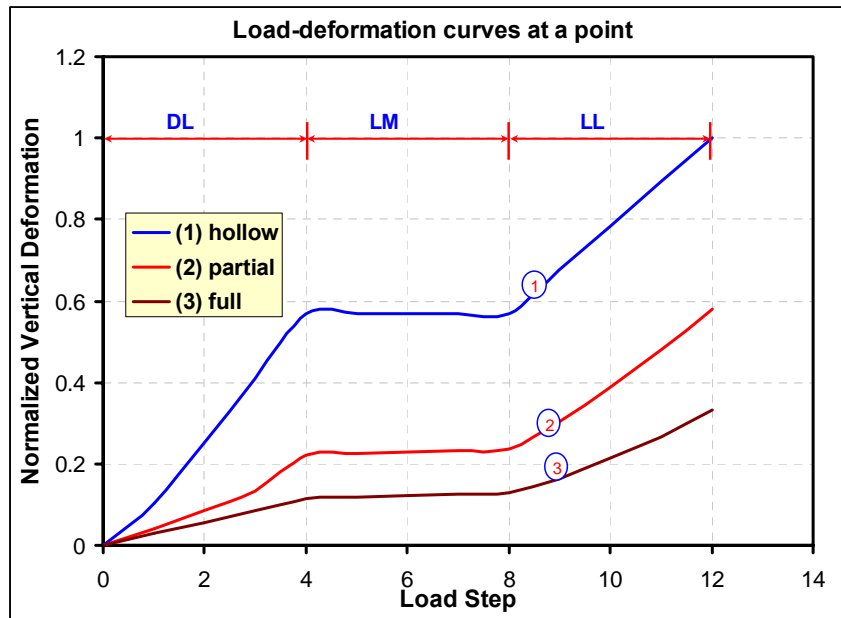


Figure 7-21: Load-deformation curves for a composite shell with different sizes of concrete fillings.

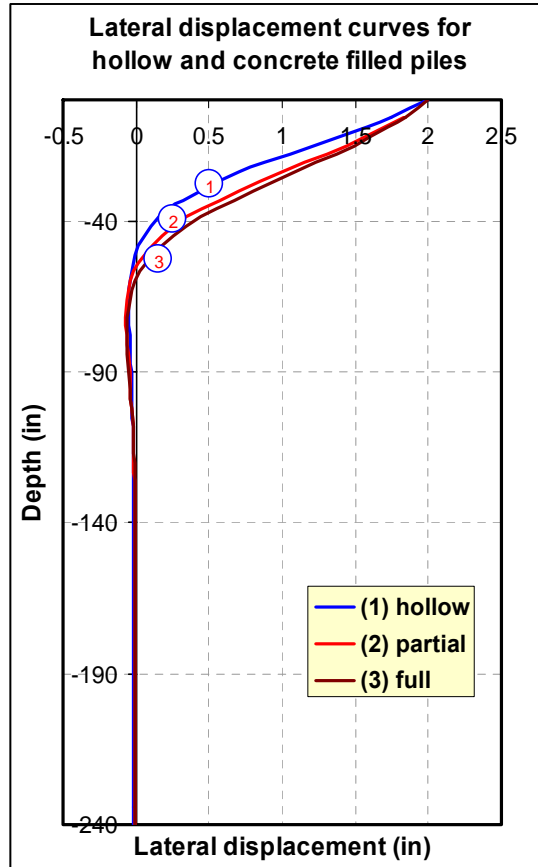


Figure 7-22: Lateral displacement curves for hollow and concrete-filled piles.

Concrete filling also has an effect on the load capacity of the pile and on the stresses developed in the FRP shell. Because of the change in both the axial and the lateral stiffness of the pile shaft, FRP stresses will vary with the size and the strength of the concrete filling. Figure 7-23 through Figure 7-25 show the variations of the three stress components at a point for the three piles after being subjected to the specified loading. As can be seen, the dead load compression stresses in the FRP layers decrease with the increase of the size of the concrete filling (load steps 1 to 4). In the lateral movement stage (load steps 5 to 8) the FRP stresses in the compression side of the pile decrease while the tension side stresses are increased. The increase in the axial stiffness of the pile shaft, as a result of concrete filling, increased the axial load capacity of the pile

shaft. The concrete filling also contributed in the load sharing with the FRP shell which explains the stress reduction in the compression side of the FRP layers.

The concrete filling also increased the bending stiffness of the pile as well as the stresses in the FRP composite shell (compare curve 3b with 1b in Figure 7-23). The increase in bending stiffness should affect the stresses in both the tension and the compression sides in a similar manner.

Figure 7-26 shows a group of stress envelopes for the three major stress components in the FRP shell along the length of the pile shaft. It can be seen that the concrete filling increased the tensile stresses and reduced the compressive stresses in the FRP layers. It is also can be noticed that the concrete filling did a significant reduction in the layers shear stresses τ_{12} .

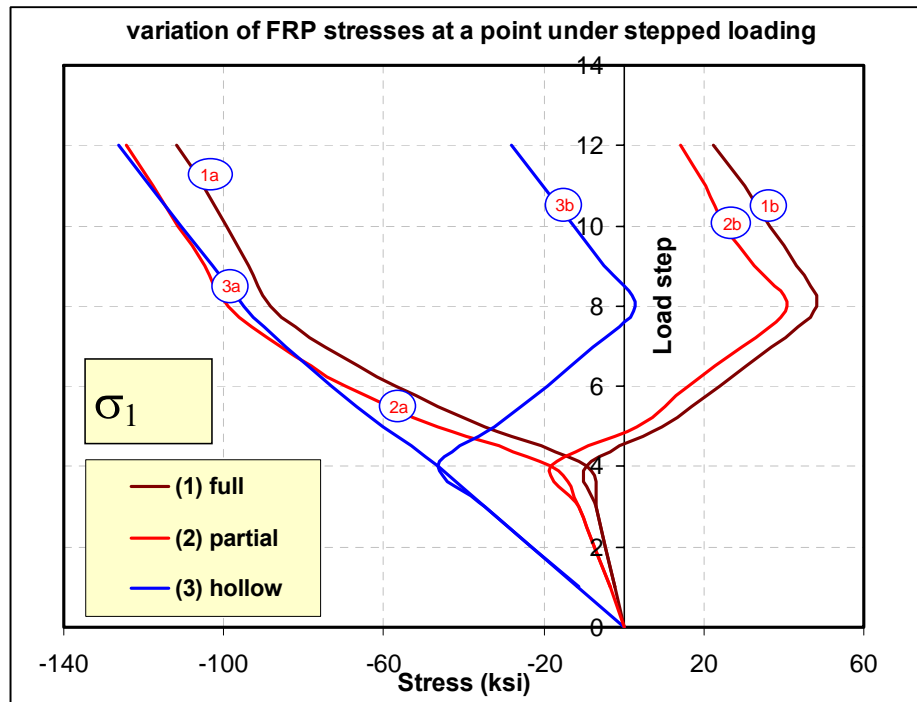


Figure 7-23: Variation of stress (σ_1) at point for hollow and filled piles.

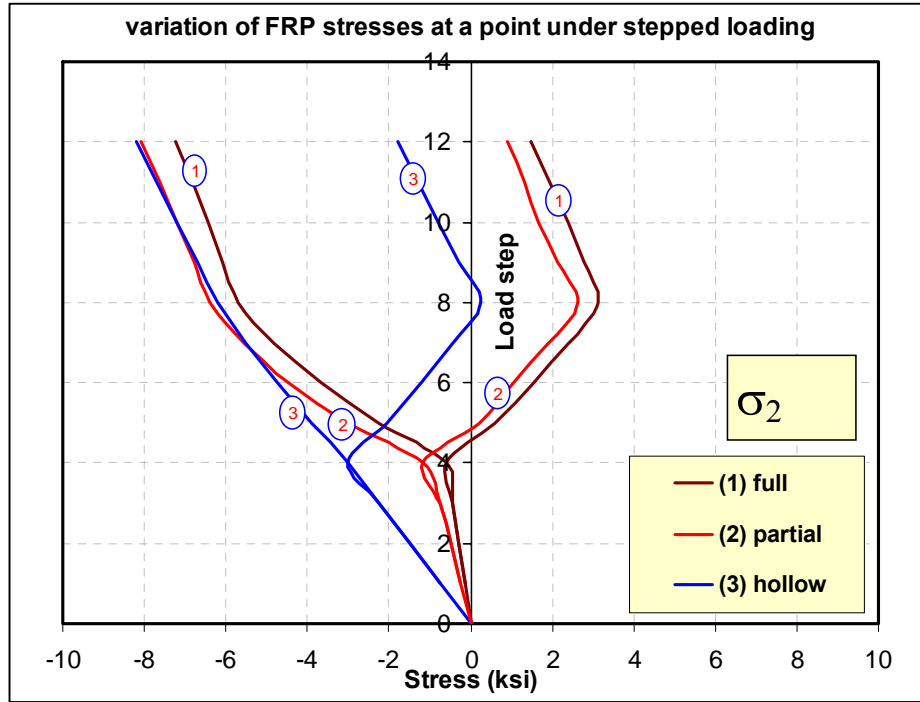


Figure 7-24: Variation of stress (σ_2) at a point for hollow and filled piles.

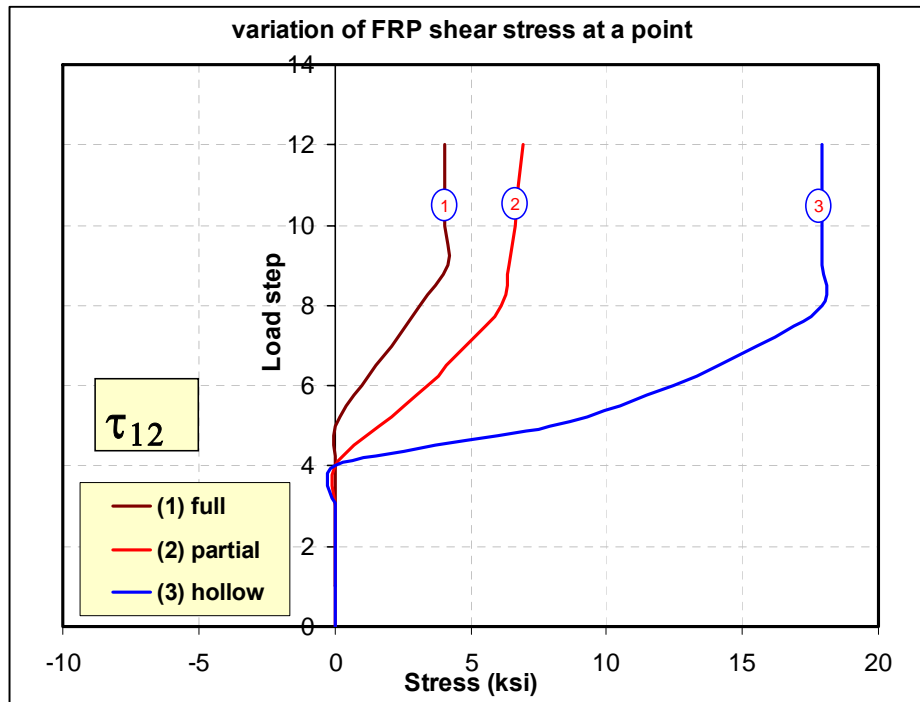


Figure 7-25: Variation of shear stress (τ_{12}) at a point for hollow and filled piles.

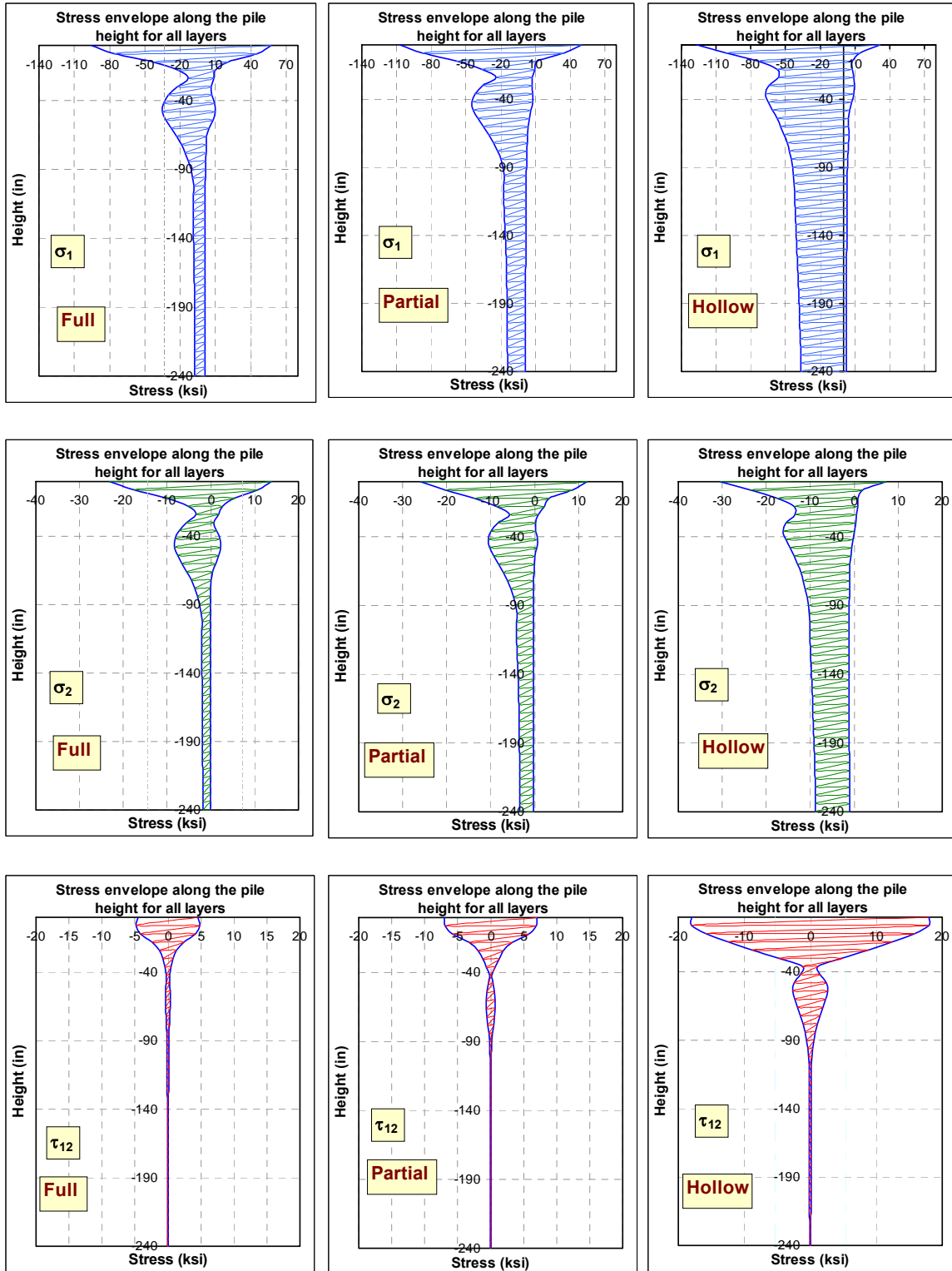


Figure 7-26: Major stress envelopes for all layers at load step 8.

The effect of concrete filling and its strength on the pile stresses was also investigated and illustrated in the following figures. Figure 7-27 shows the load deformation curves for an FRP composite pile filled with different grades of plain concrete under axial compression only. The curves show an increase in the pile deformation at the same load step as the concrete strength decreases. At the initial load steps, the load-deformation curves are linear and the deformation difference is very small compared to that at higher loads. At the plastic stage the deformation curves behave nonlinearly and the difference becomes larger. As can be seen from the figure, high strength concrete supports higher loads with less deformation.

The variation of the first stress component σ_1 in a 0° -layer node is also compared for the different concrete grades. At the extreme compression and tension sides, the variation in stresses developed in the composite layer is not significant. As can be seen from Figure 7-28 and Figure 7-29, the stresses at the initial 4 steps which represent the dead load application are in a very close range. This range started to get relatively wider as the lateral displacement is applied (steps 5 through 8) because the concrete started to reach its nonlinear deformation phase in which it will not take any more stresses as shown in Figure 7-30. It also shows that higher strength concrete has an advantage in stress capacity over those of lower strengths which results started to appear clearly in the same figure after step 4 of loading and in Figure 7-31 as well.

Figure 7-30 and Figure 7-31 show the concrete stress at a point and at a line along the pile depth respectively, it can be seen that high strength concrete carries more compression loads than low strength concrete. The increase in concrete strength increased its stiffness. Higher stiffness produced higher bending stresses under lateral movements.

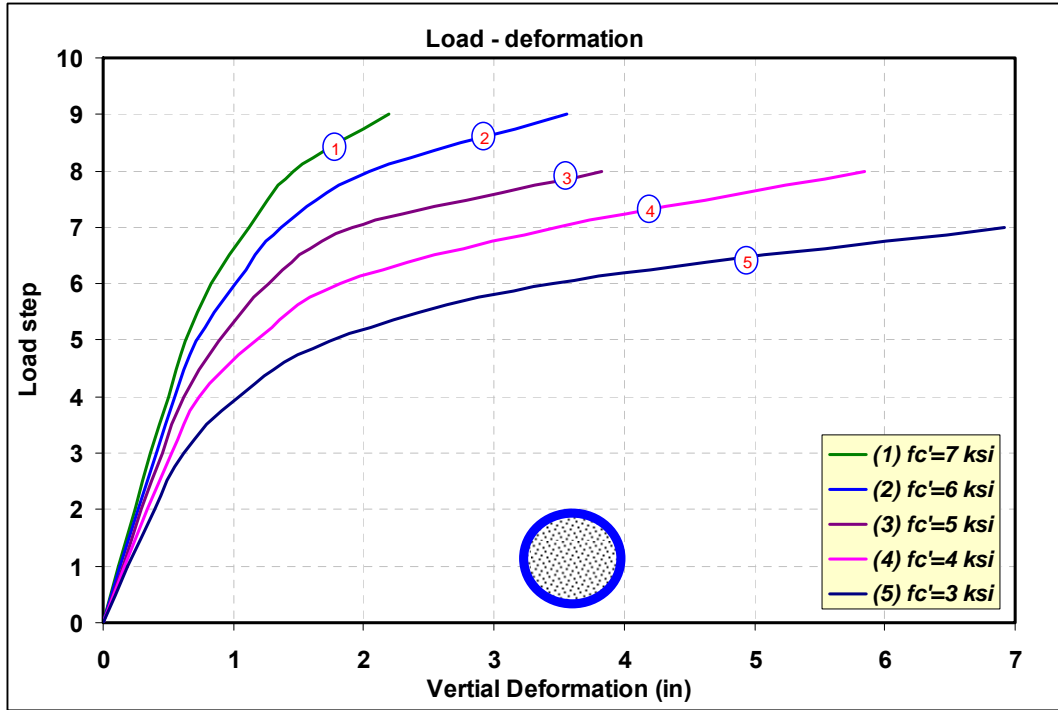


Figure 7-27: Load-deformation curves for an FRP pile filled with different grades of plain concrete under axial compression.

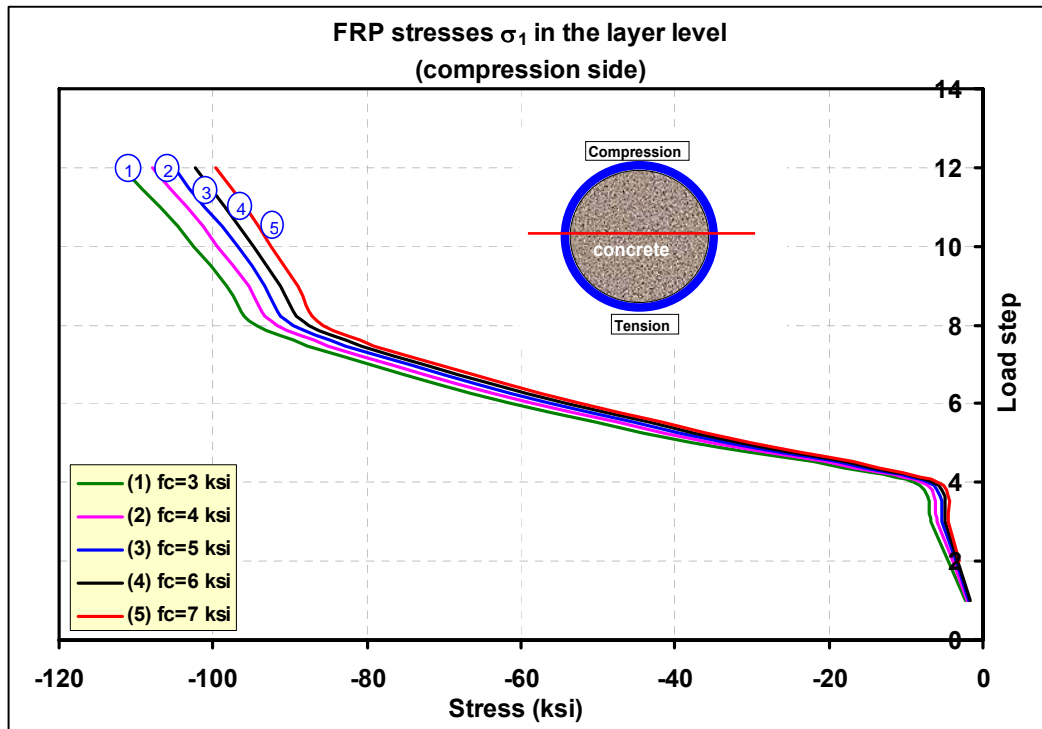


Figure 7-28: Stress variation in the FRP at a point 0-ft from the pile's top.

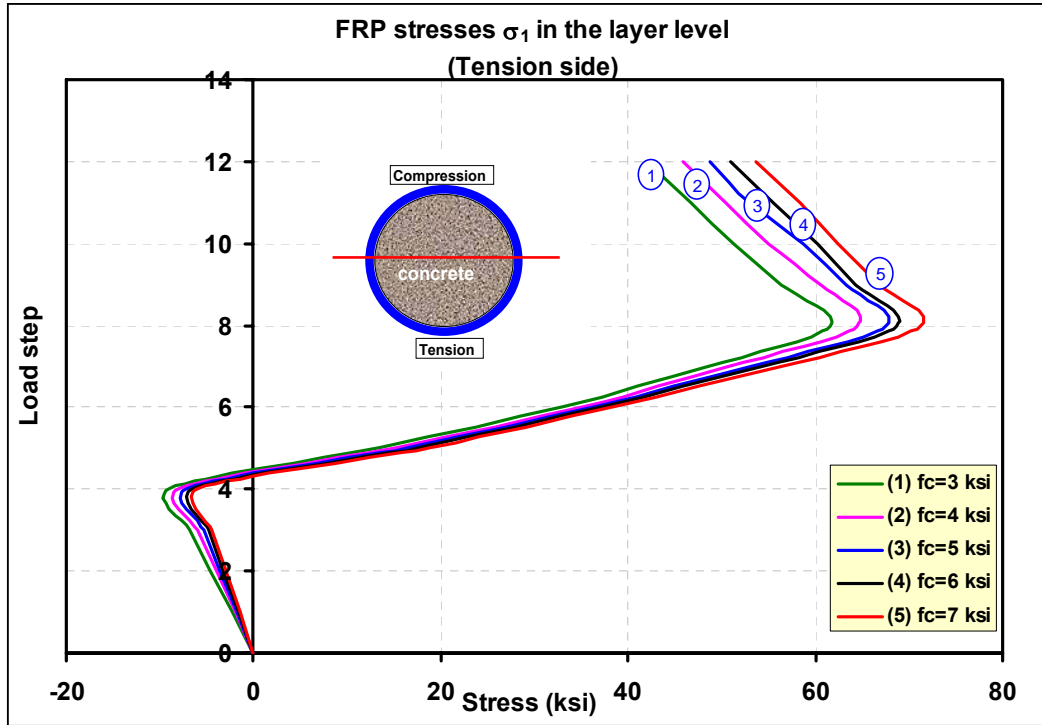


Figure 7-29: Stress variation in FRP at a point 0-ft from the pile's top

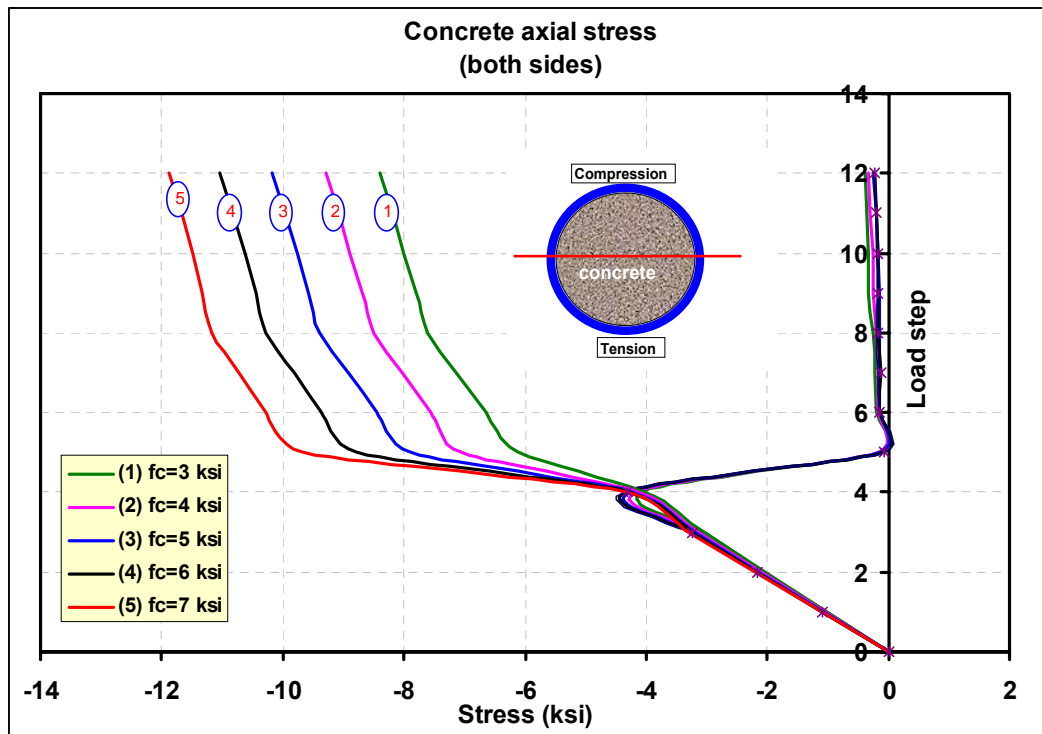


Figure 7-30: Stresses in concrete at a point 0-ft from the pile's top.

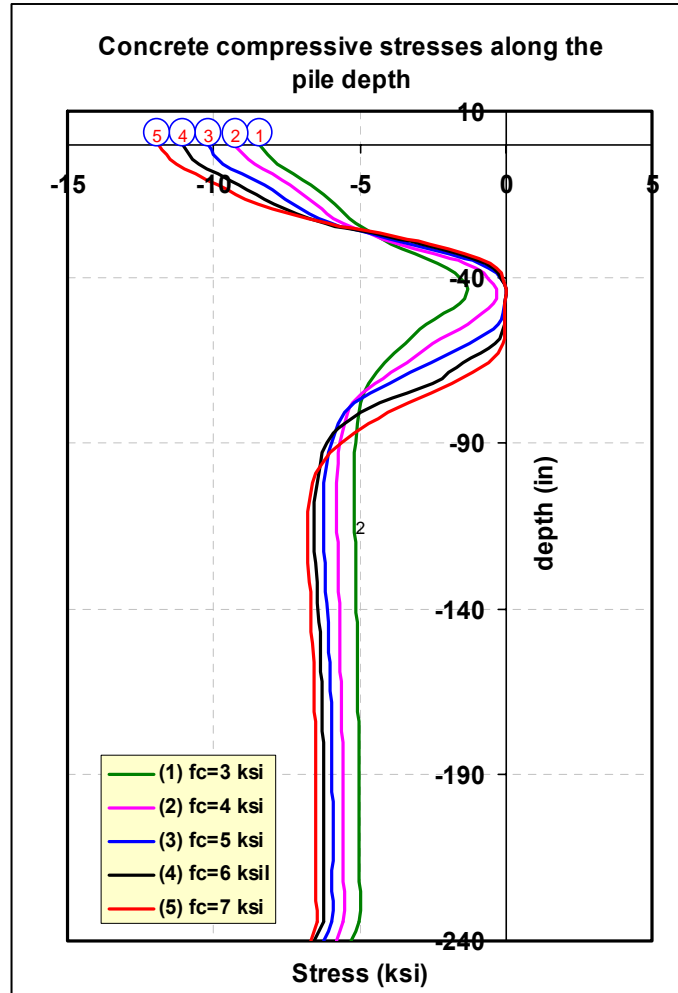


Figure 7-31: Compressive stresses in concrete at a line along the depth of the pile.

7.4.3 MATERIAL TYPE

Fiber reinforced composite materials can be custom manufactured to fit the customer's need. It is usually made of two or more different materials combined in a certain manufacturing process. Due to the wide range of their constituents; resins and fibers, composites can be produced in an infinite number of mechanical properties. Even for the same composite commercial name, we can have products with many different mechanical properties. This implies that using any composite commercial name within this presentation will not assume that the properties of that composite are standard.

The stiffness of neither plain concrete nor fiber glass composites is as high as that of structural steel. As can be seen from the graphical comparison of material stiffness' in Figure 7-32, the elastic modulus of steel is about six times or more than that of concrete and glass composites in the direction of fibers. Also comparing different grades of concrete with some glass composites shows that concrete elastic modulus is in a close range to that of polyester and vinyl ester glass composites. On the other hand, glass epoxy composites have higher values than those of concrete as shown in Figure 7-33.

The minor axis elastic modulus E_y is much less than that of the major axis, E_x . As can be seen in the histogram of Figure 7-34, the elastic modulus in the perpendicular direction to the fibers E_y is very small even for the carbon epoxy. In unidirectional composites, the minor axis modulus reflects the matrix (resin) properties since there are no fibers in that direction.

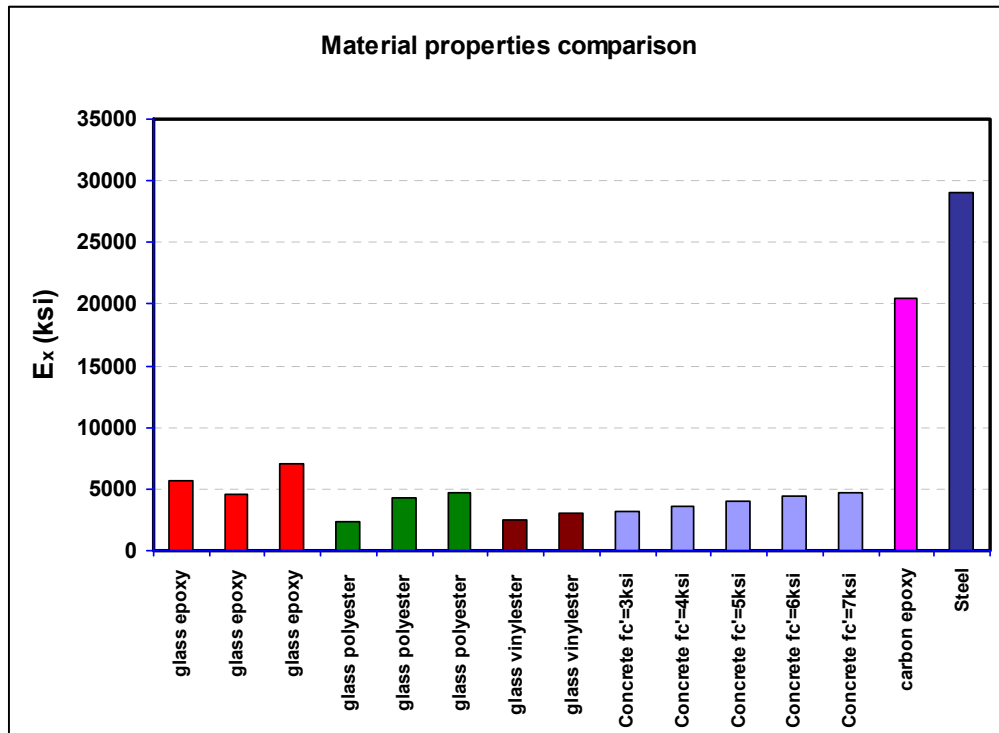


Figure 7-32: Comparison of elastic modulus for composites, concrete and steel.

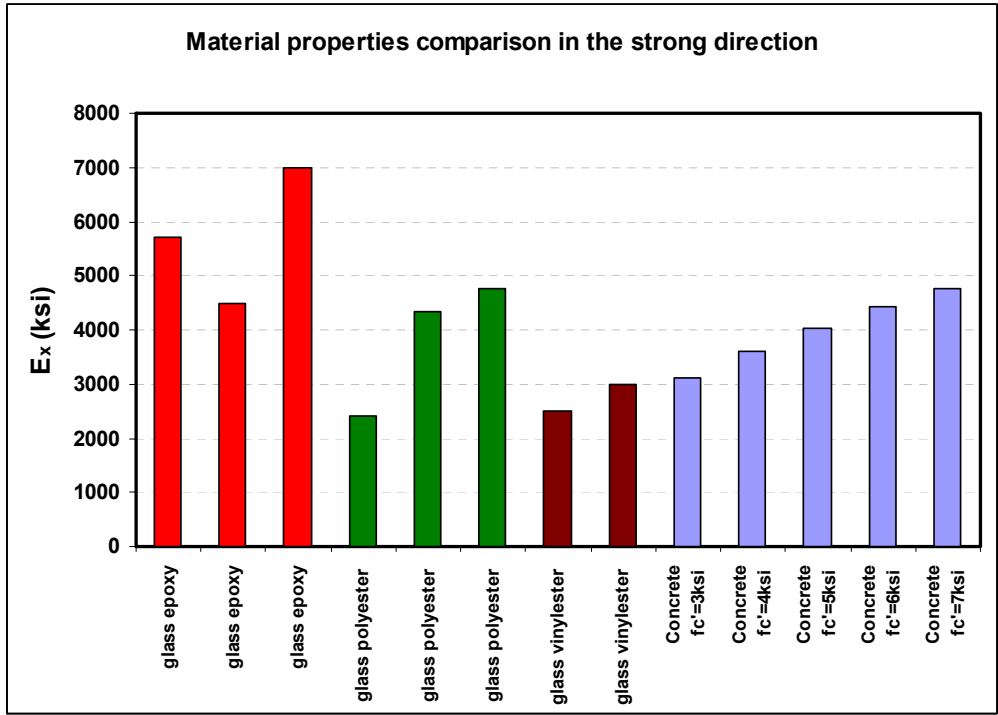


Figure 7-33: Comparison of strong direction modulus of elasticity for different glass composites and plain concrete.

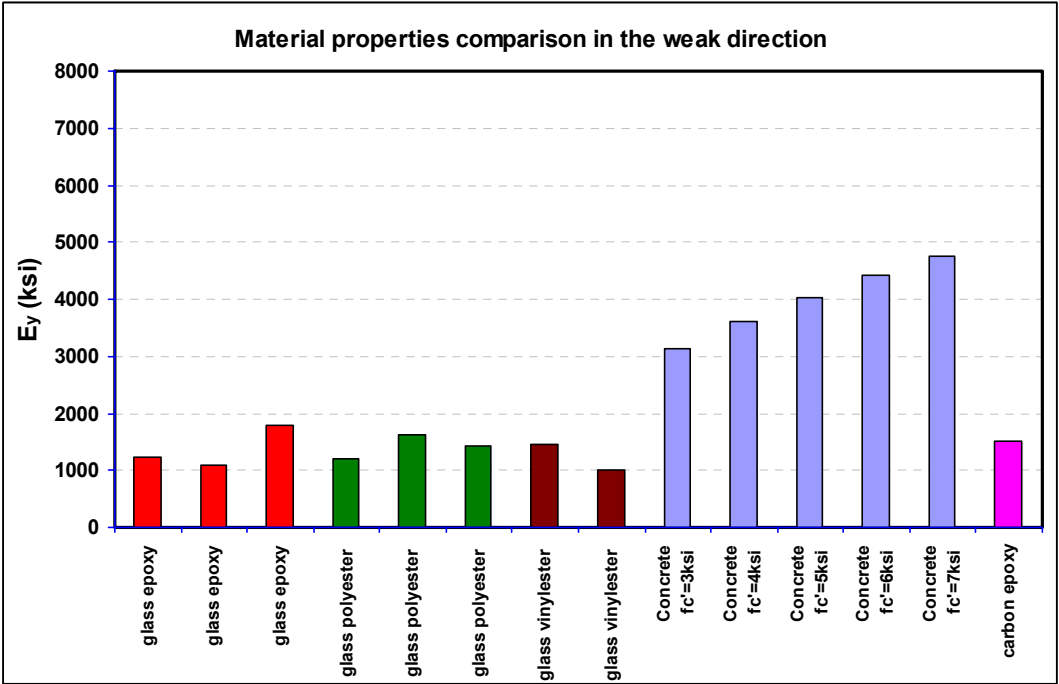


Figure 7-34: Comparison of weak direction modulus of elasticity for different glass composites and plain concrete.

The FRP elastic modulus data presented in the previous two histograms were based on unidirectional specimens measured in the fiber direction and perpendicular to the fiber direction. The elastic modulus in the direction perpendicular to the fiber direction is much less than that of the fibers direction. Figure 7-35 shows the variation of the elastic modulus of the specimen as the angle changes from 0 to 90°. As can be seen, at 0-degree angle (at which the fibers are in the test direction) the composite specimens have a wide variation in the elastic modulus while at a 90-degree angle, the specimens have values within a very narrow range. This indicates that the minor axis modulus of elasticity (at a 90 degree angle) is based on the resin mechanical properties.

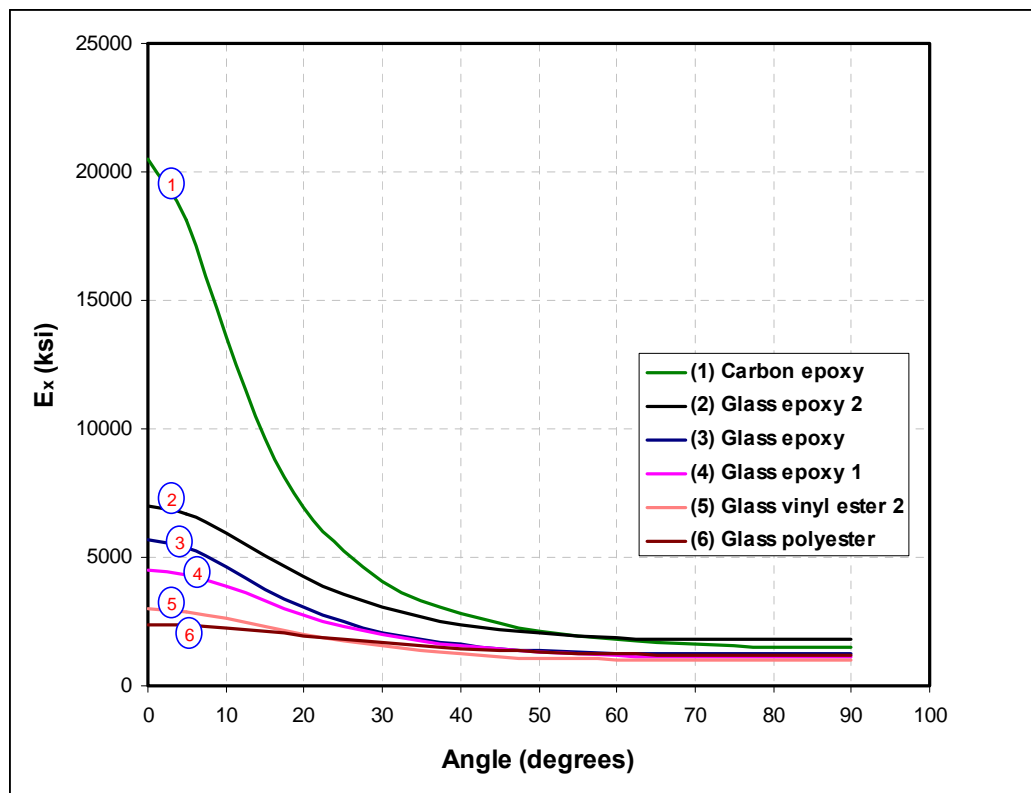


Figure 7-35: Variation of the elastic modulus with fiber orientation angle for different composite materials.

Piles information:

Composite type:

Material	E_x	E_y	G_{xy}	V_{xy}	X_t	Y_t	X_c	Y_c	S
Glass Polyester	2400	1200	520	0.28	39.5	7.	-34.2	-14.6	5.4
Glass vinylester	3000	1000	420	0.35	37.5	8	-37.5	-20	6
Glass epoxy	4500	1100	550	0.26	90	3.9	-80	-17.5	6.2
Carbon epoxy	20500	1500	1040	0.28	330	8.3	-209	-33	10.3

Number of layers: 12

Layer thickness: 0.0208 in.

Laminate structure:[0,0,90,90,0,0,0,0,90,90,0,0]

Filling: Plain concrete $f_c'=3$ ksi

Height = 20 ft

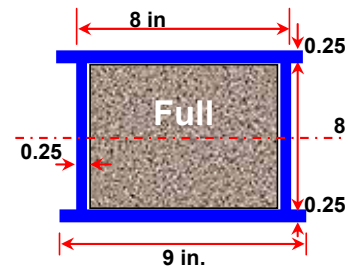
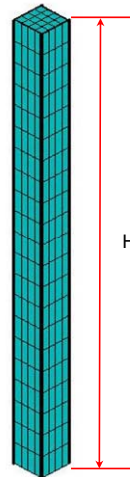
Soil type: dense sand

Loading:

Axial dead load: 300 kips [steps 1 to 4]

Lateral displacement: 2 inches [steps 5 to 8]

Axial live load: 200 kips [steps 9 to 12]



The effects of material type on the deformations of laterally loaded piles are illustrated in Figure 7-36 and Figure 7-37. The two figures show the vertical and lateral deformation curves at a point and at a line along the pile depth respectively. Epoxy and carbon composites are stiffer than polyester and vinylester composites. High stiffness fibers increased both the pile's axial and lateral stiffness. As can be seen, the carbon epoxy pile showed very small vertical deformations compared to the other three piles.

Figure 7-38 and Figure 7-39 show the major layer stresses, σ_1 and σ_2 , development at a point for a pile made of different composite materials in dense sand soil. The high stiffness of the carbon fibers produced higher compressive, tensile, and bending stresses as can be seen in the figures. The major axis modulus E_x for carbon epoxy composites is about 4 to 5 times that of glass composites. On the other hand, the minor axis modulus E_y is equal or less than that of fiber glass composites as shown Figure 7-34. As a result, the minor axis stresses which are shown in Figure 7-39 did not show a similar trend to that of the strong axis. The minor axis stresses in the carbon epoxy pile are the lowest among others made of glass composites.

Figure 7-40 shows two graphs for the stress components at both the tension and compression sides of the pile along its depth. As can be seen, the stresses do not have a constant trend along the pile depth. Stress curves for the different materials keep changing behaviors along the pile's depth even at the same load step. They intersected more than once along the depth.

Material properties also have a dramatic effect on the crack patterns of the concrete filling, Figure 7-41. Stiffer materials such as carbon epoxy will produce higher bending moments under lateral movements which reflect on the tensile and compressive

stresses of the concrete filling. Higher stresses will develop more concrete cracks which weaken the pile section and raise the stresses in the composite shell.

Figure 7-42 shows the stress envelopes of the first stress component, σ_1 , for the different materials piles. It can be seen that the high material stiffness increased both bending and axial stresses in the pile.

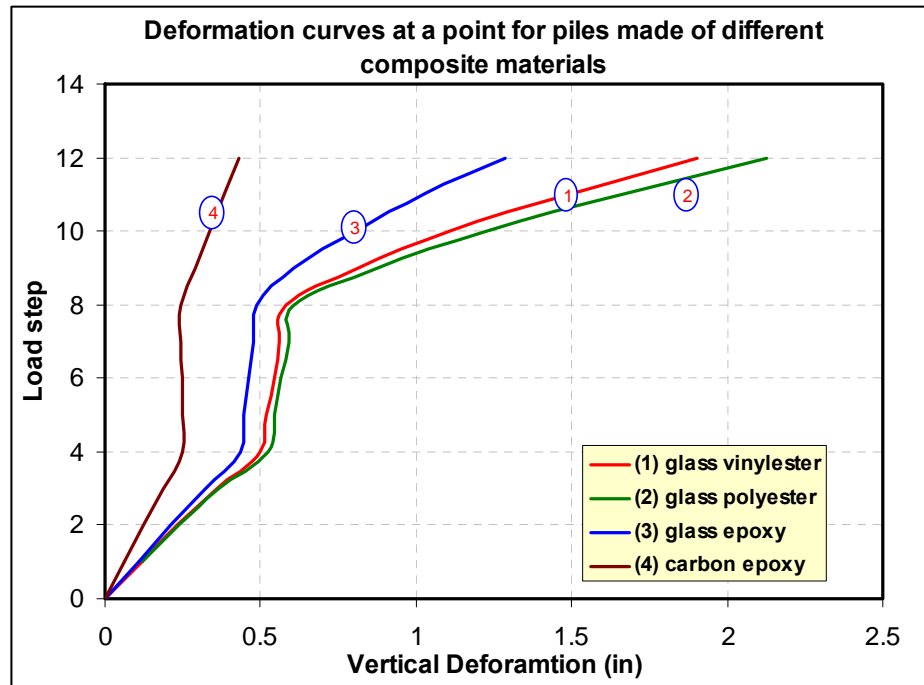


Figure 7-36: Vertical deformation curves for piles made of different composite materials.

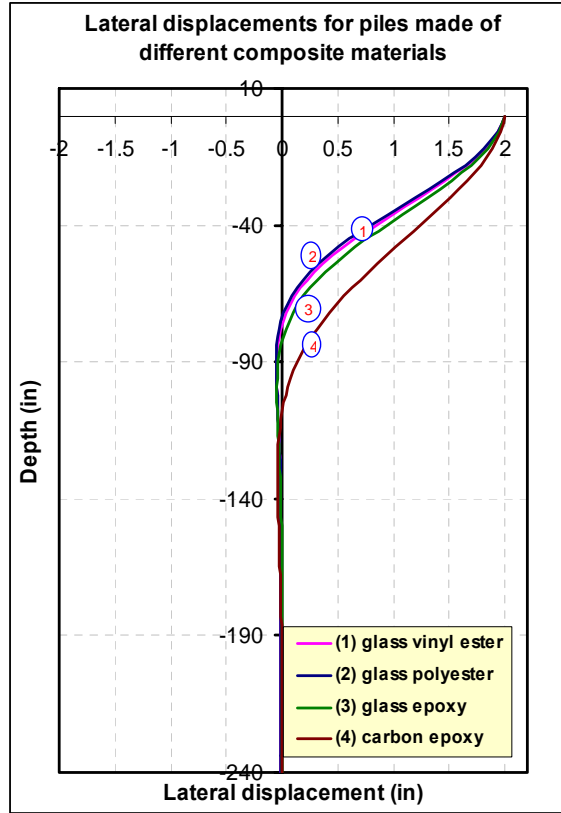


Figure 7-37: Lateral displacement curves for piles made of different composite materials.

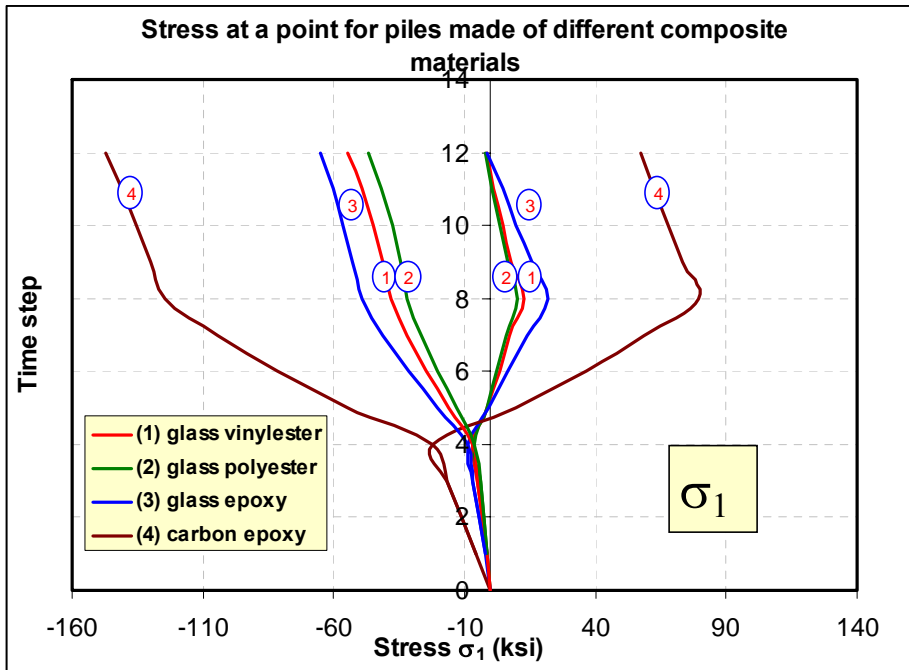


Figure 7-38: Stress variation at a point for a pile made of different composite materials.

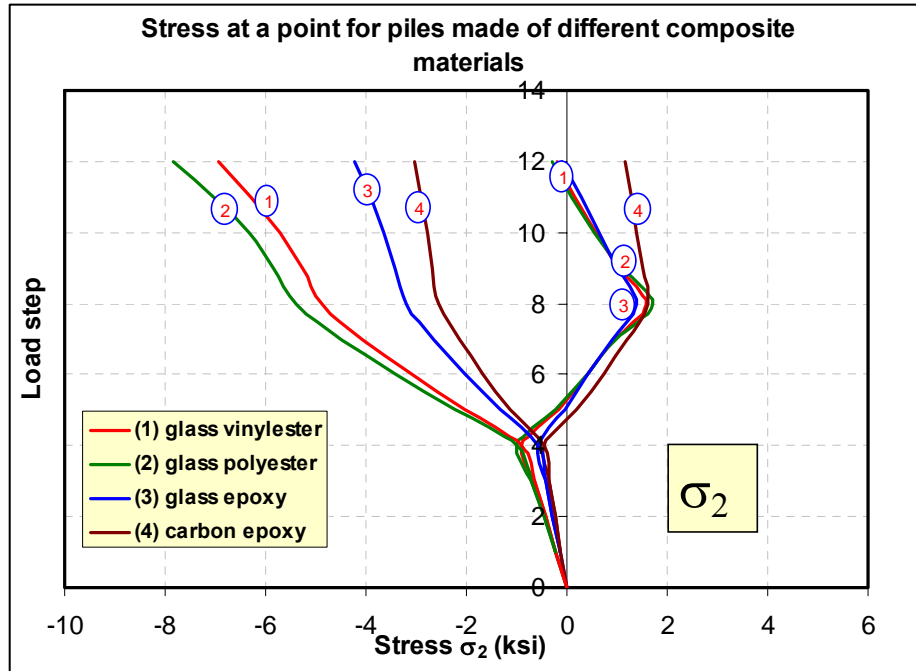


Figure 7-39: Stress variation at a point for a pile made of different composite materials.

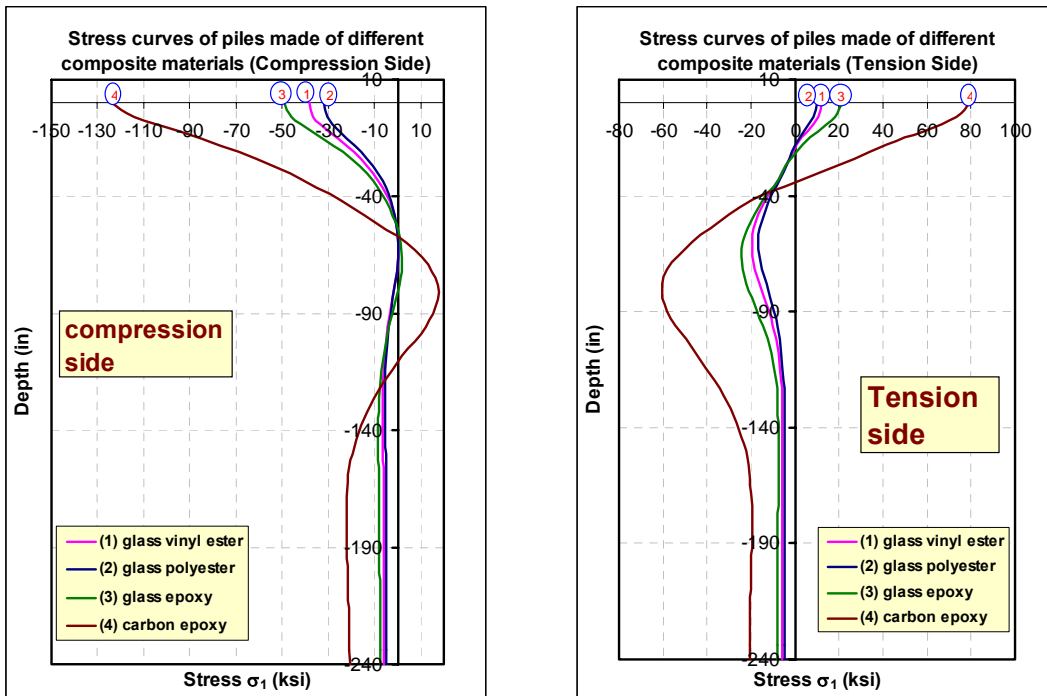


Figure 7-40: Stress variation along the whole depth for a pile made of different composite materials.

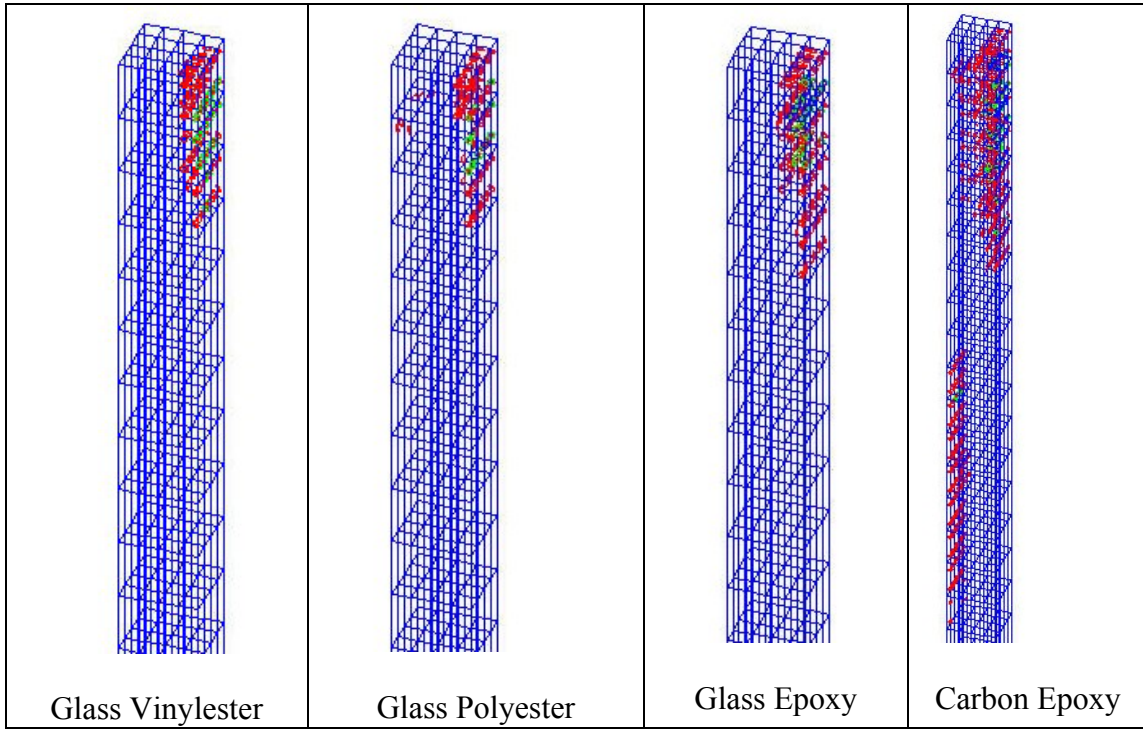


Figure 7-41: Crack patterns for piles with different composite shells.

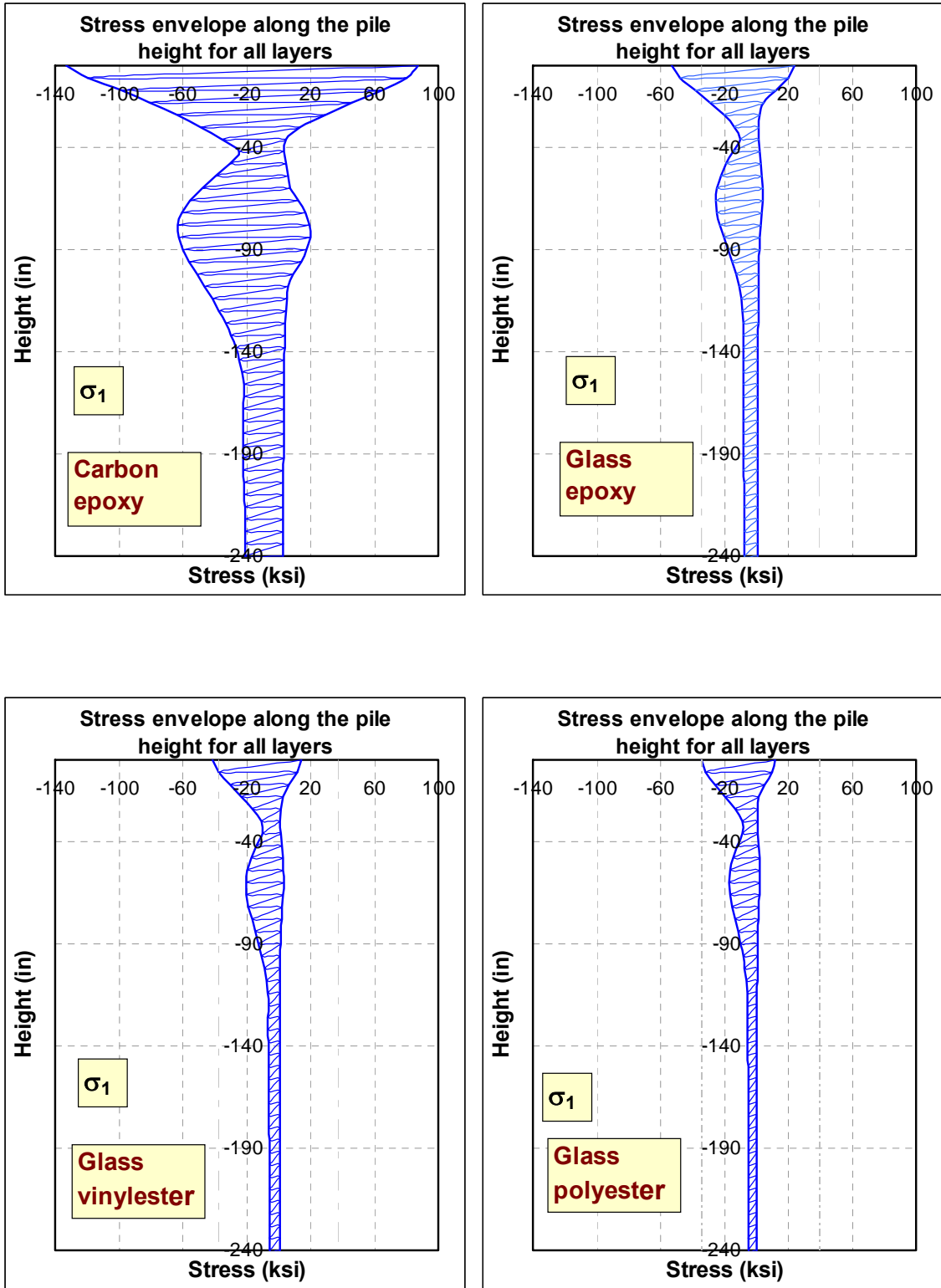


Figure 7-42: Stress envelopes for piles made of different composite materials.

7.4.4 LAYER ORIENTATION

In unidirectional laminas where a single composite layer has its fiber in one major direction, the stacking sequence of multiple layers has a major effect on the final design of the structure. The material properties in the fiber direction have higher magnitudes than those in the transverse direction. The variation between material properties in the fiber direction and the transverse direction depends on many factors such as: fiber type, resin type, and fiber volume fraction in the lamina. The lamina properties in the major x-axis (direction of fibers) usually gain the reinforcement properties and in the minor y-axis (perpendicular to fiber direction) gain the matrix properties.

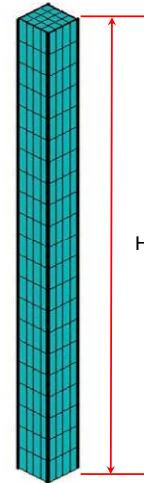
To investigate the effect of fiber orientation on the pile and soil-pile behaviors, a hollow pile model with the configuration and loading described in the pile information sheet 1 was analyzed for vertical deformation comparison purposes. A total of seven models were analyzed with the following fiber structures: $[0,0]_6$, $[15,-15]_6$, $[30,-30]_6$, $[45,-45]_6$, $[60,-60]_6$, $[75,-75]_6$, $[90,90]_6$.

Figure 7-43 shows the load-deformation curves for all seven piles with their composite shells having the $[\theta,-\theta]_6$ fiber structure in each case. The contribution of the composite shell on the stiffness of the pile depends on its fiber volume fraction. The higher the fiber volume in the loading direction, the higher the stiffness will be. As can be seen in the figure, the piles with the 0-degree fibers showed the highest stiffness and those with the 90-degree fibers showed the lowest stiffness. The axial deformations of the pile with the $[90,90]_6$ structure are 10 times or more than that of the $[0,0]_6$ fiber structure.

Pile information sheet 1:

Composite type: Carbon epoxy

Property	ksi	Property	ksi
E_x	20500	X_t	330
E_y	1500	Y_t	8.3
G_{xy}	1040	X_c	-209
V_{xy}	0.28	Y_c	-33
		S	10.3



Number of layers: 12

Layer thickness: 0.01667 in.

Laminate structure: $[0,0]_6, [15,-15]_6, [30,-30]_6, [45,-45]_6,$

$[60,-60]_6, [75,-75]_6, [90,90]_6$

Filling: hollow

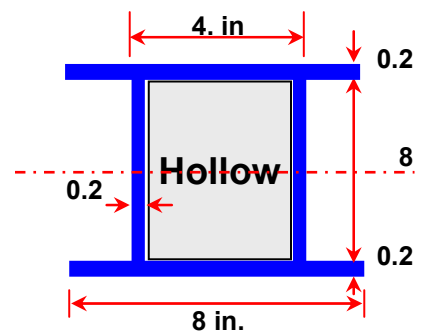
Height = 20 ft

Soil type: Dense sand

Axial dead load: 200 kips [steps 1 to 4]

Lateral displacement: 2.in [steps 5 to 8]

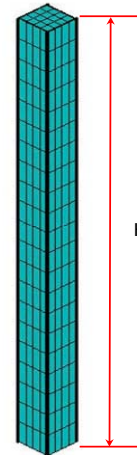
Axial live load: 200 kips [steps 9 to 12]



Pile information sheet 2:

Composite type: Glass epoxy

Property	ksi	Property	ksi
E_x	4500	X_t	90
E_y	1100	Y_t	3.9
G_{xy}	550	X_c	-80
V_{xy}	0.26	Y_c	-17.5
		S	6.2



Number of layers: 12

Layer thickness: 0.0208 in.

Laminate structure: [90,90,75,-75,60,-60,45,-45,15,-15,0,0]

Filling: Plain concrete $f_c' = 3$ ksi

Height = 20 ft

Soil type: Dense sand

Axial dead load: 200 kips [steps 1 to 4]

Lateral head movement: 2 in. [steps 5 to 8]

Axial live load: 200 kips [steps 9 to 12]

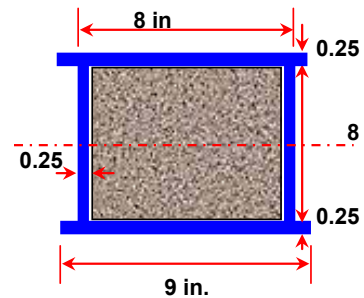


Figure 7-44, Figure 7-45, and Figure 7-46 show the stress envelopes of the three major stress components for the pile with the $[0,0]_6$ fiber structure. The pile in such configuration has the highest axial and lateral stiffness and the least axial deformations. Because all fibers were directed in one single direction, 0-degree, the pile experienced high shear stresses at higher loads as shown in Figure 7-46.

The second model that used to study the variation of stresses in piles with different orientation layers is described in pile information sheet 2. The pile was loaded with the three types of loading in a total of 12 steps. Results of stress analysis at a point and along the pile depth for the different layers are presented in Figure 7-47 through Figure 7-52. Figure 7-47 and Figure 7-50 show the variation of the first stress component σ_1 at a point and along the pile depth, respectively, in some selected layers in the pile shell. As can be seen, the layers with 0-degree orientation angles showed the highest stress values among other layers. That is because the 0-degree fibers are in the direction of loading also the layer has its highest stiffness in this direction. On the contrary, the second stress component σ_2 showed the highest stress values in layers with 90-degree orientation angles as shown in Figure 7-48 and Figure 7-51. The shear stress values are found to be maximum in the layers with 45-degree fiber orientation angles as shown in Figure 7-49 and Figure 7-52.

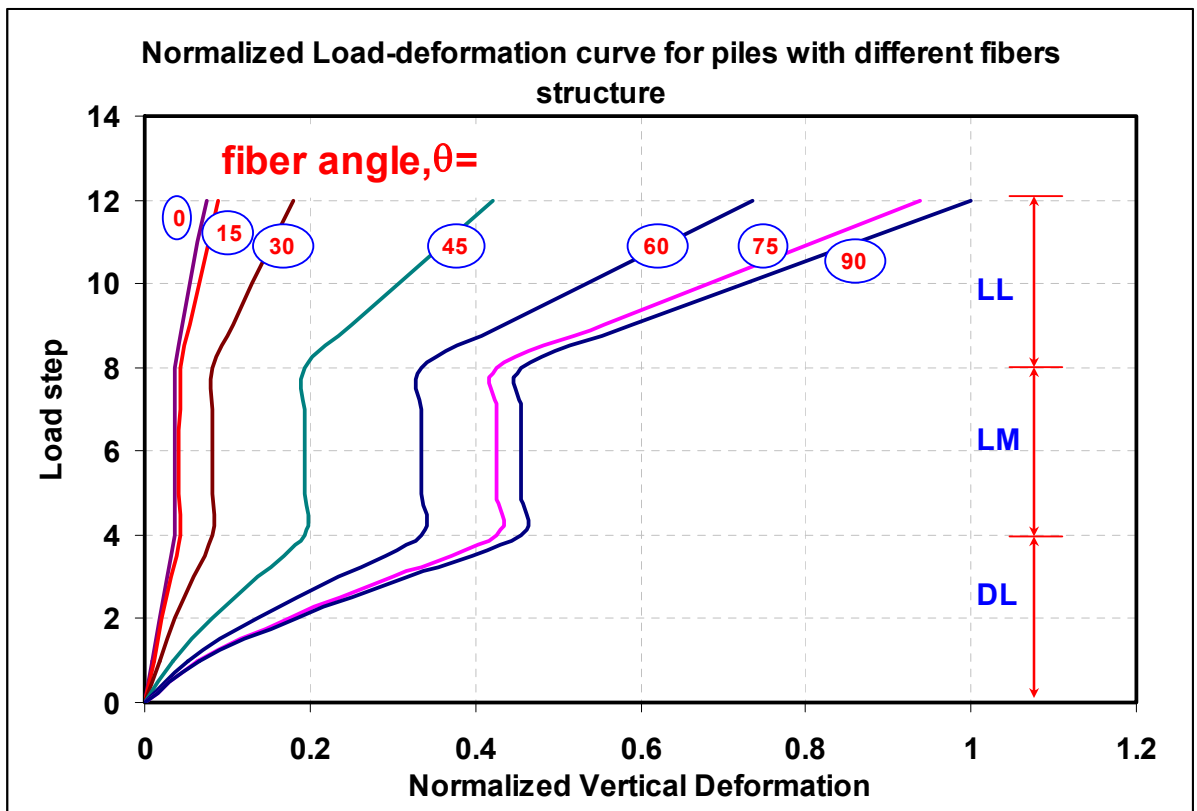


Figure 7-43: Normalized deformation curves for piles with different fibers structure.

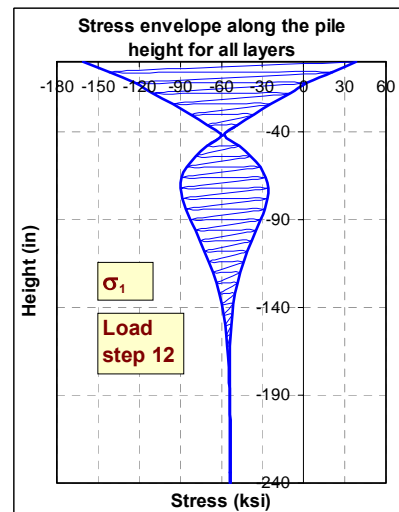
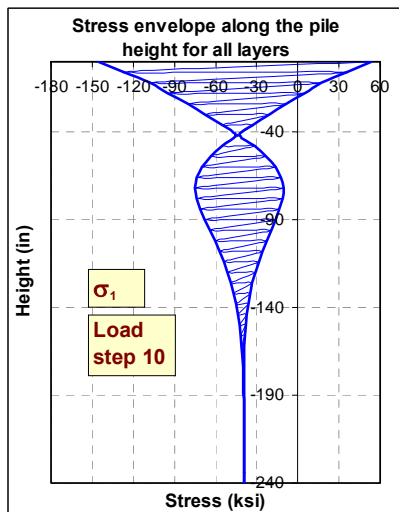
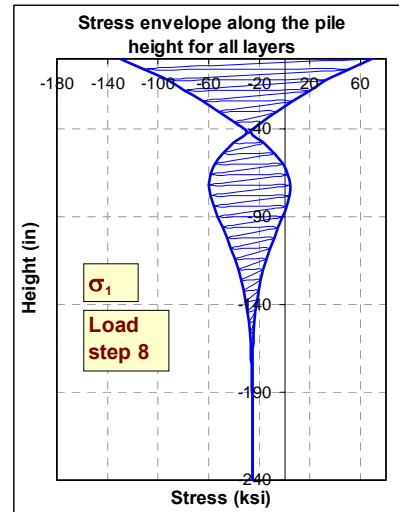
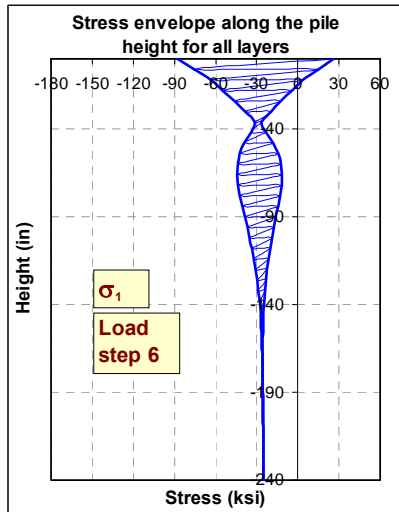
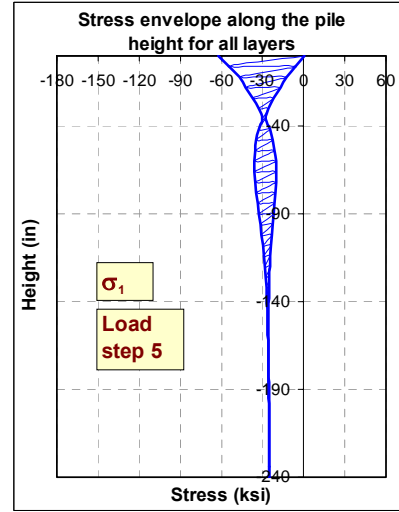
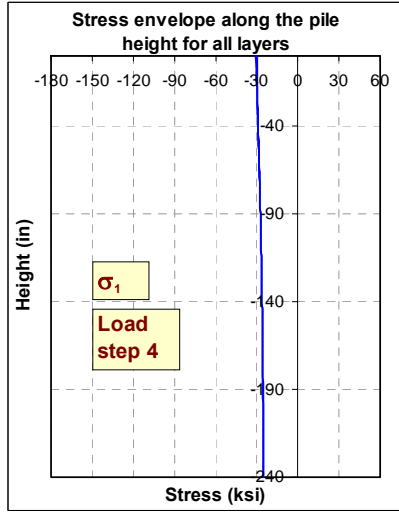


Figure 7-44: First stress component (σ_1) envelopes along a pile made of 0-degree fibers.

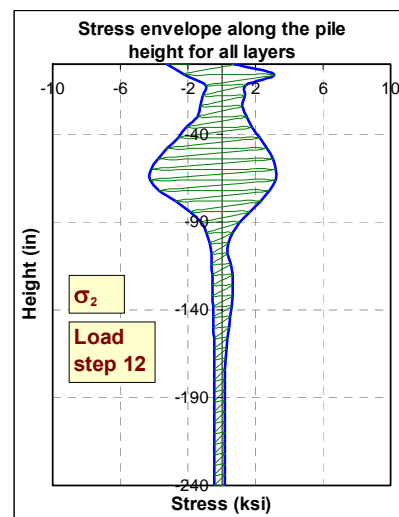
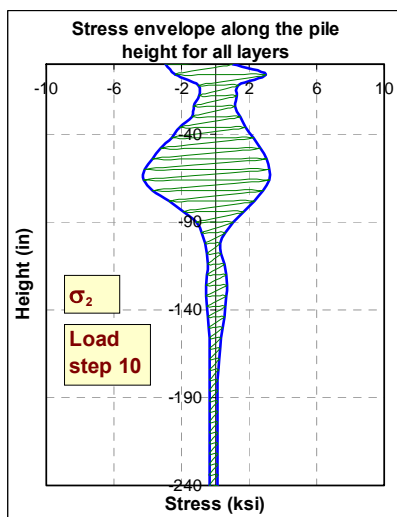
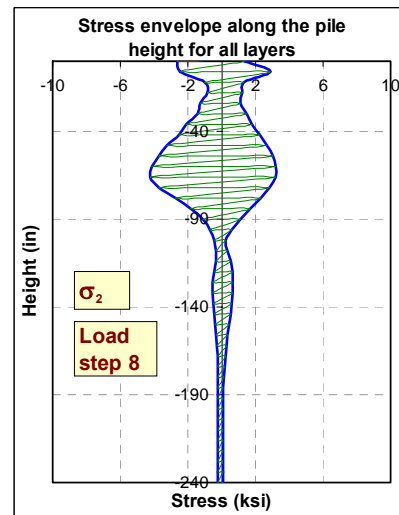
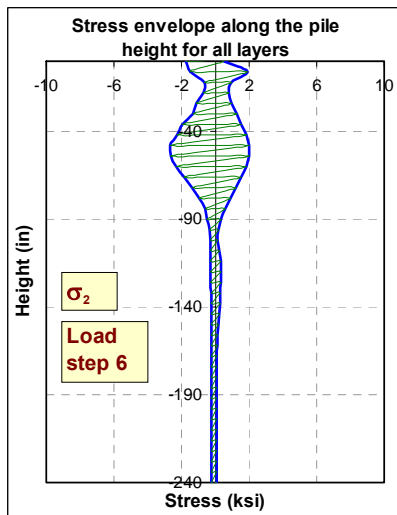
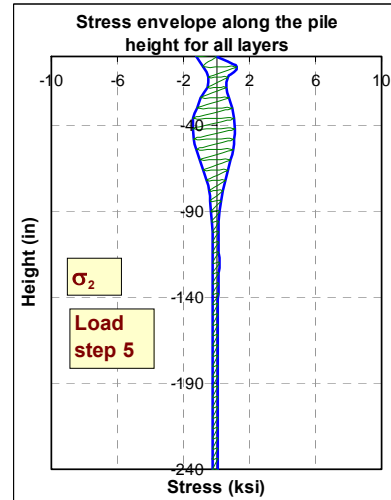
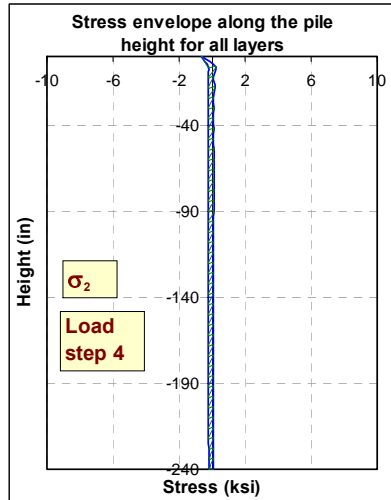


Figure 7-45: Second stress component (σ_2) envelopes along a pile made of 0-degree fibers.

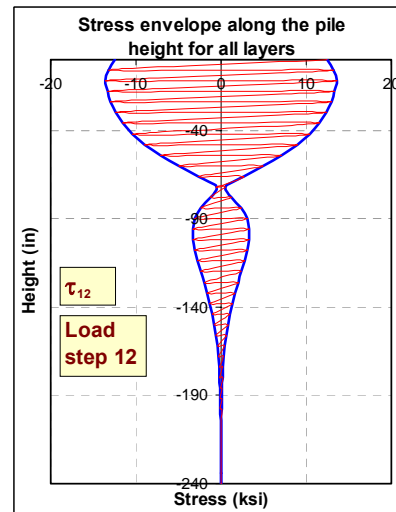
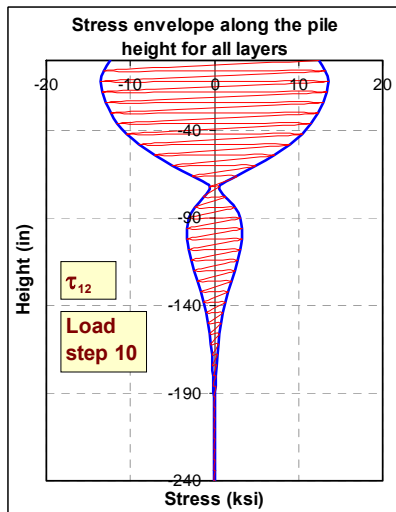
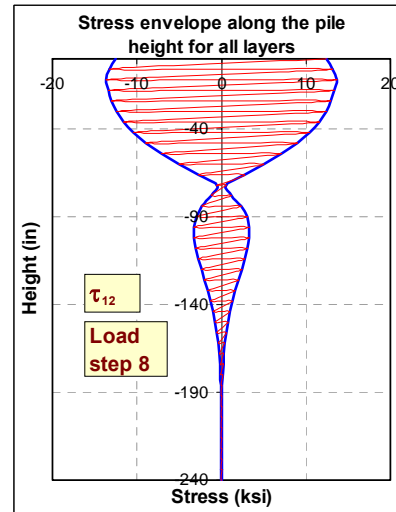
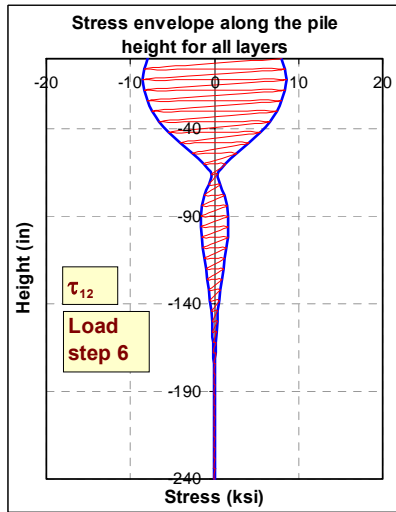
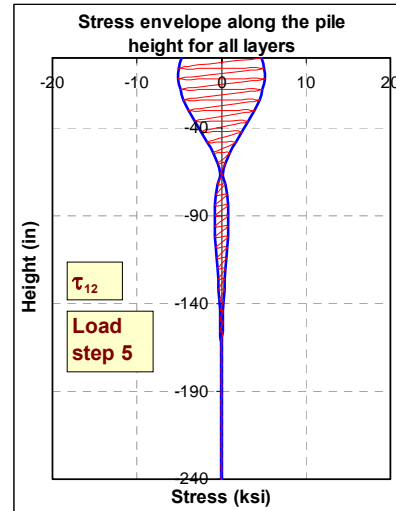
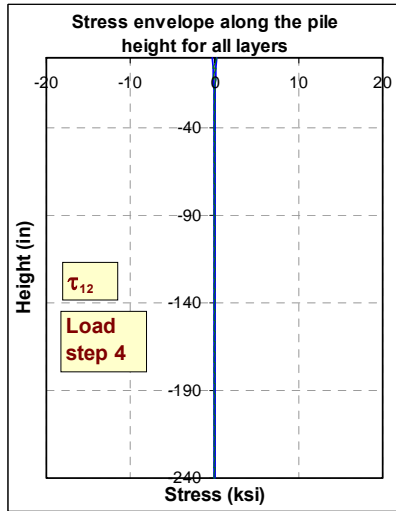


Figure 7-46: Shear stress (τ_{12}) envelopes along a pile made of 0-degree fibers.

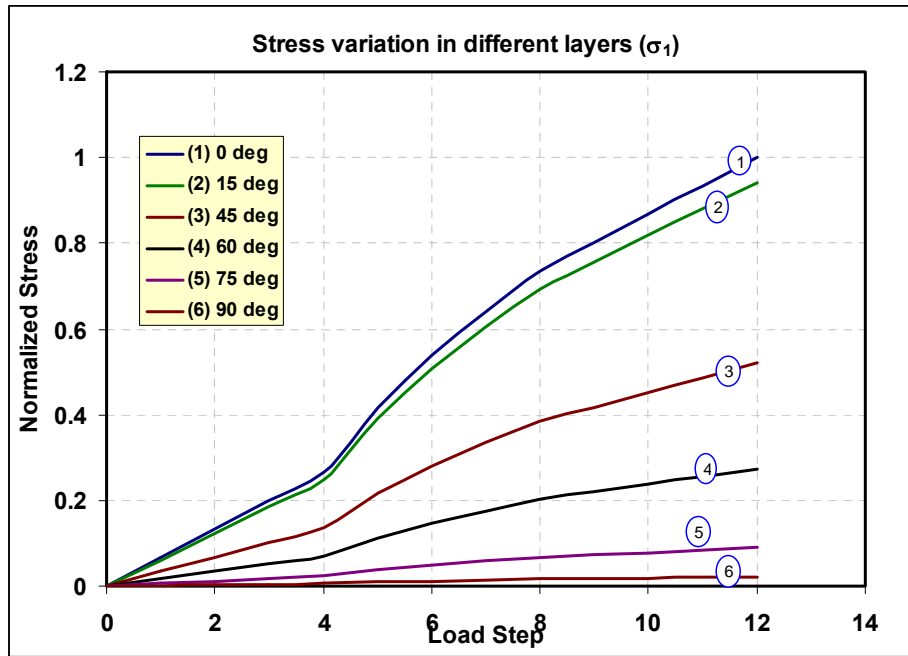


Figure 7-47: First stress component variation in different layers within the same pile.

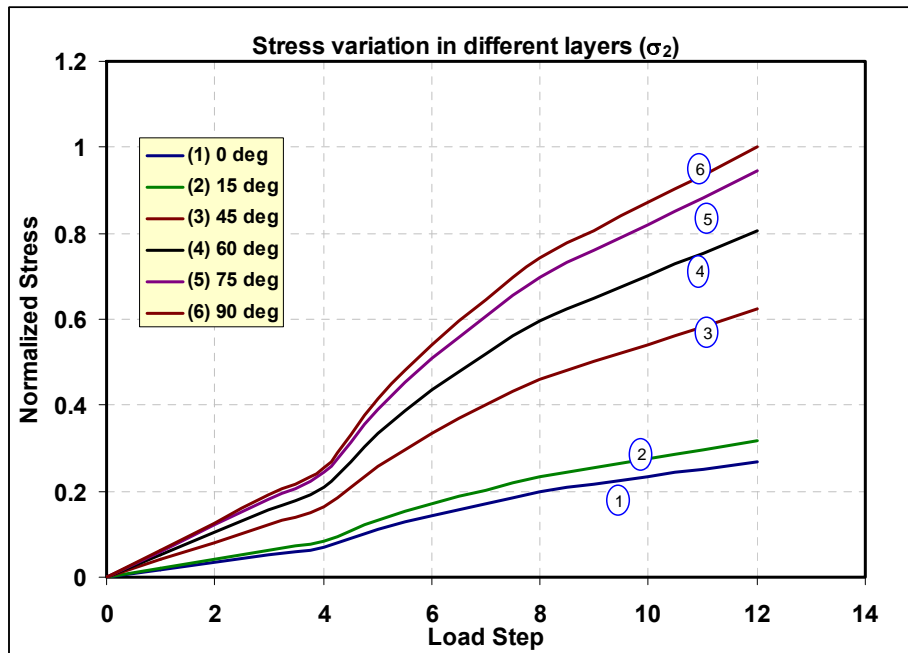


Figure 7-48: Second stress component variation in different layers within the same pile.

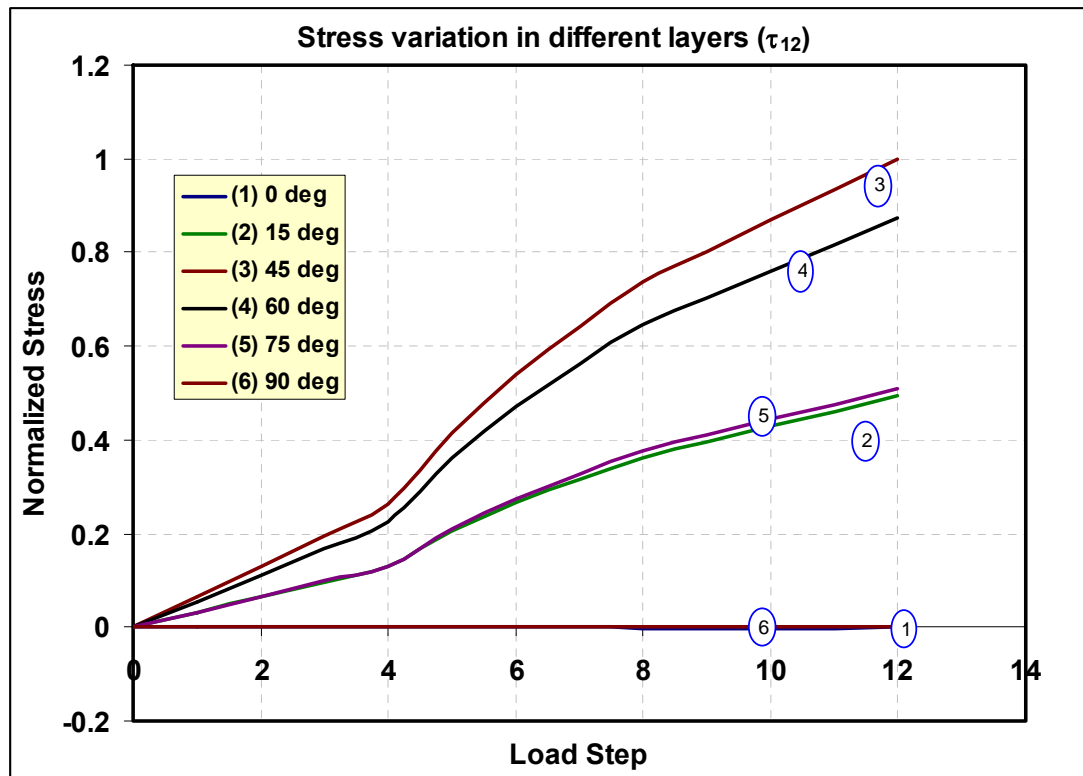


Figure 7-49: Third stress component variation in different layers within the same pile.

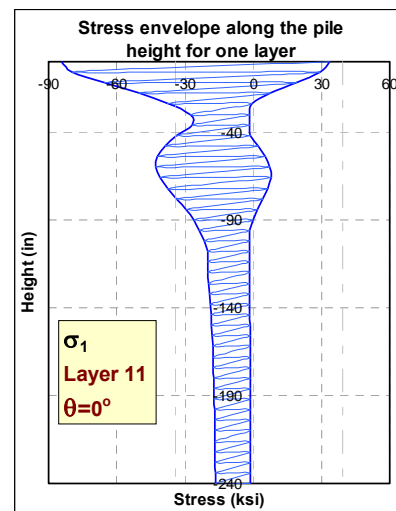
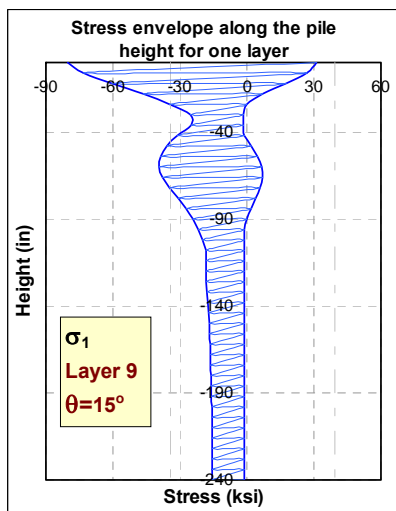
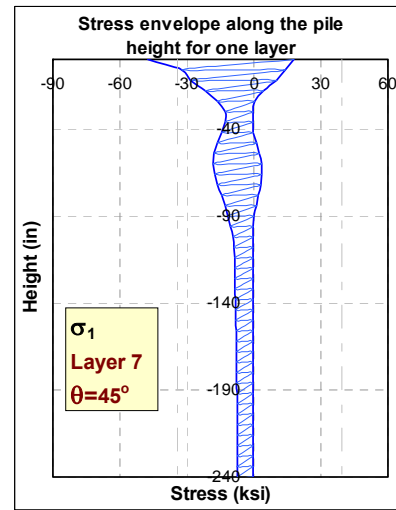
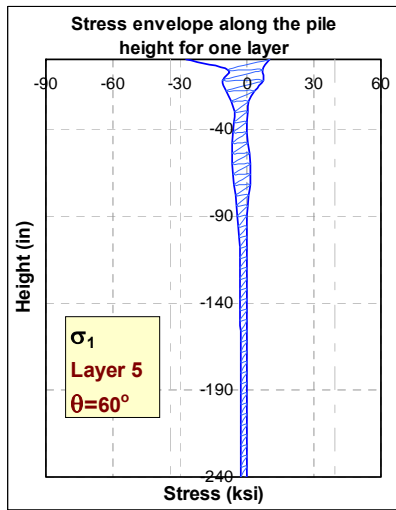
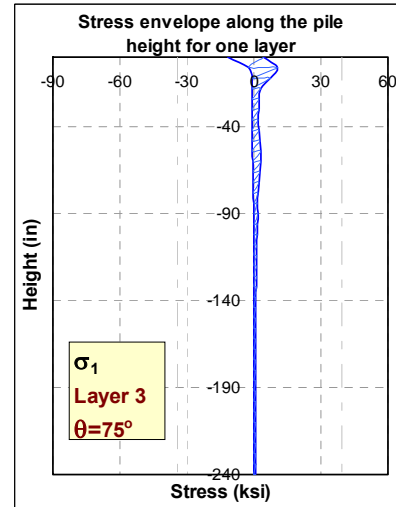
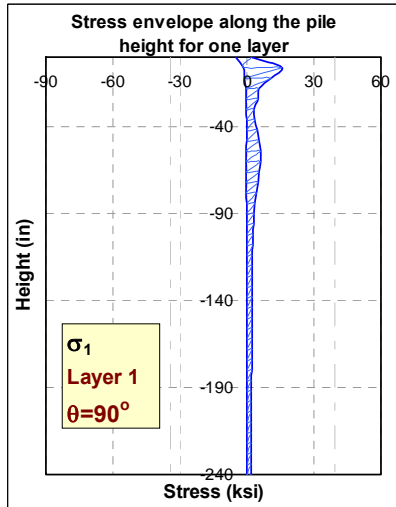


Figure 7-50: Stress (σ_1) envelopes for different layer orientations.

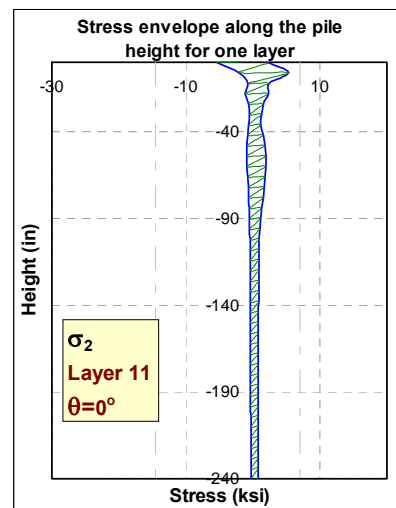
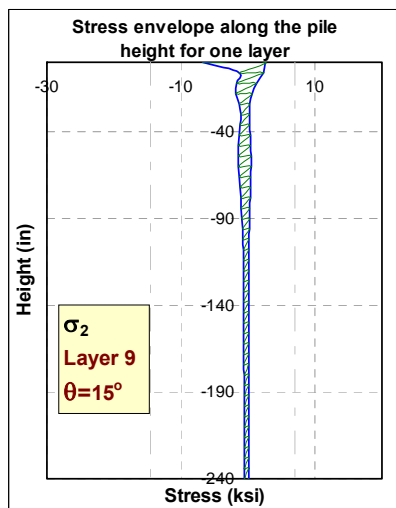
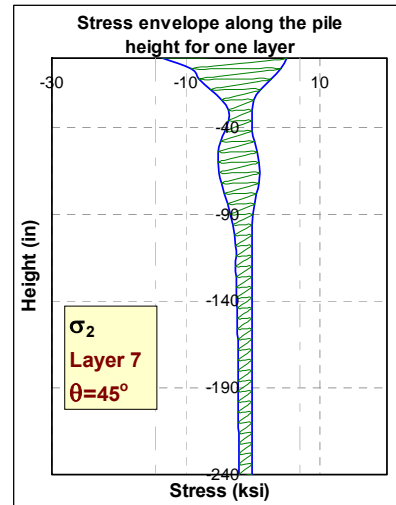
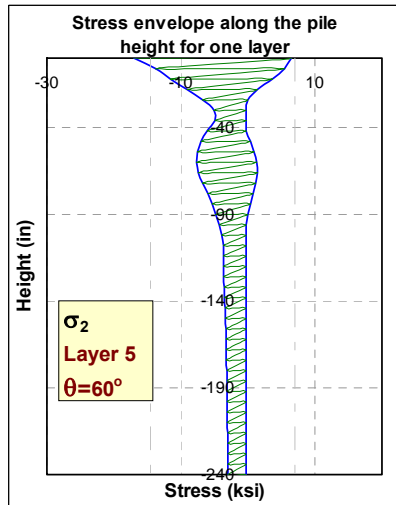
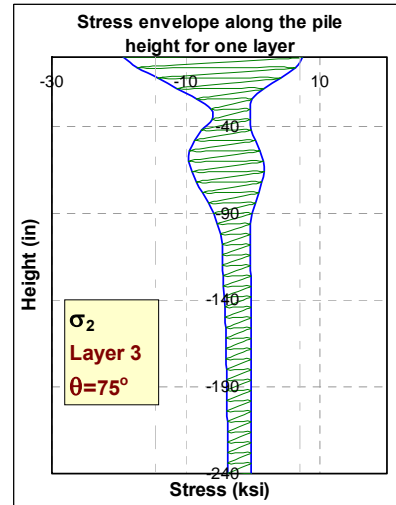
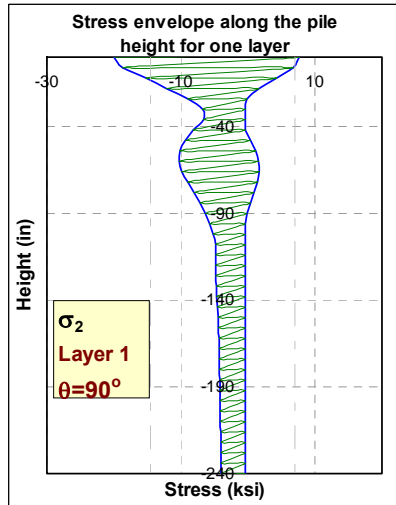


Figure 7-51: Stress (σ_2) envelopes for different layer orientations.

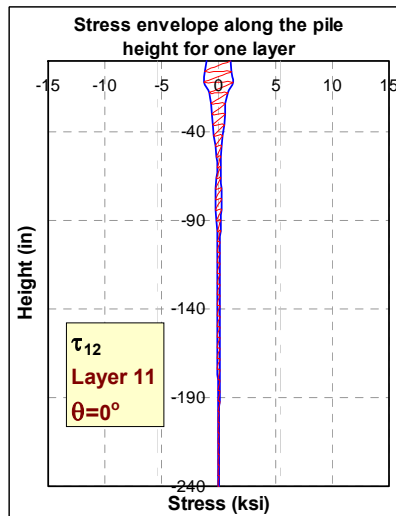
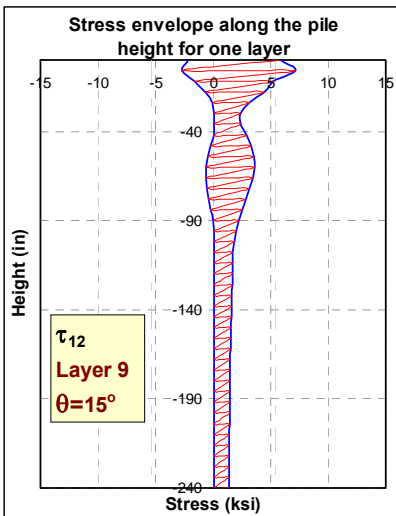
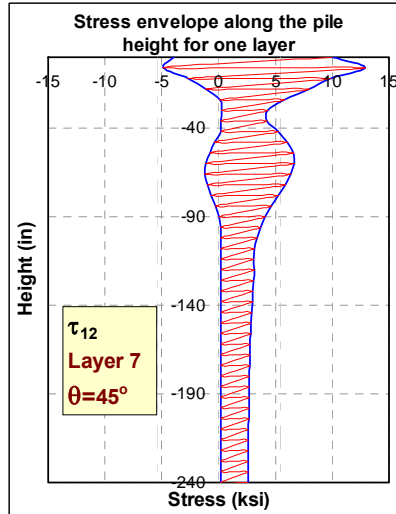
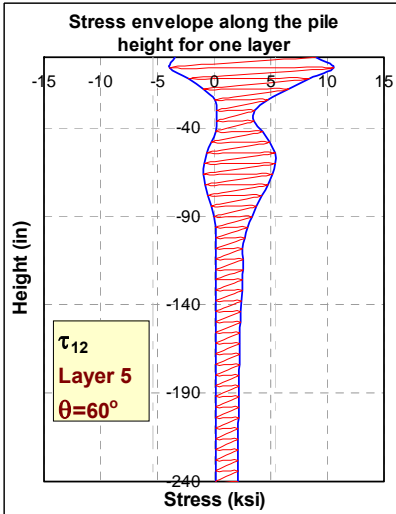
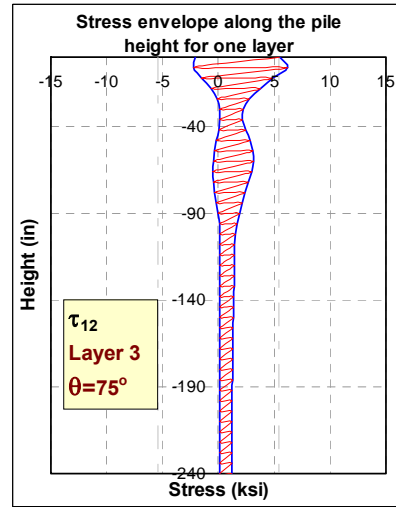
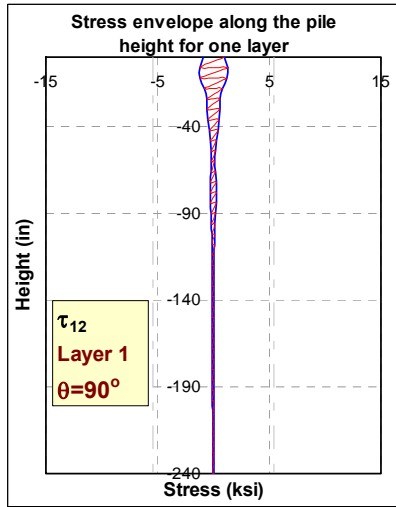


Figure 7-52: Stress (τ_{12}) envelopes for different layer orientations.

Pile information sheet 3:

Composite type: Glass epoxy

Property	ksi	Property	ksi
E_x	4500	X_t	90
E_y	1100	Y_t	3.9
G_{xy}	550	X_c	-80
V_{xy}	0.26	Y_c	-17.5
		S	6.2

Number of layers: 12

Layer thickness: 0.025 in.

Radius, $R=4.88$ in.

Laminate structure:[0,0,45,-45,0,0,60,-60,90,90,0,0]

Filling: Plain concrete $f_c'=4$ ksi

Height = 20 ft

Soil type: Dense sand

Loading:

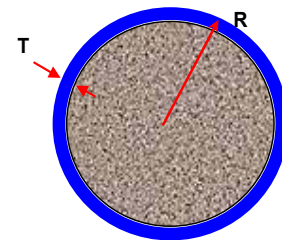
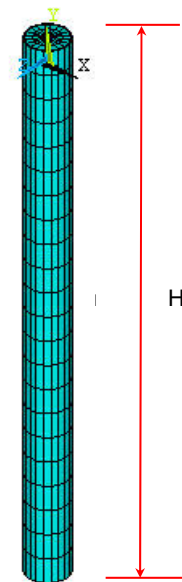
Case 1:

Axial dead load: 1000 kips [steps 1 to 12]

Case 2:

Axial dead load: 400 kips [steps 1 to 6]

Lateral head movement: 2 in. [steps 7 to 12]



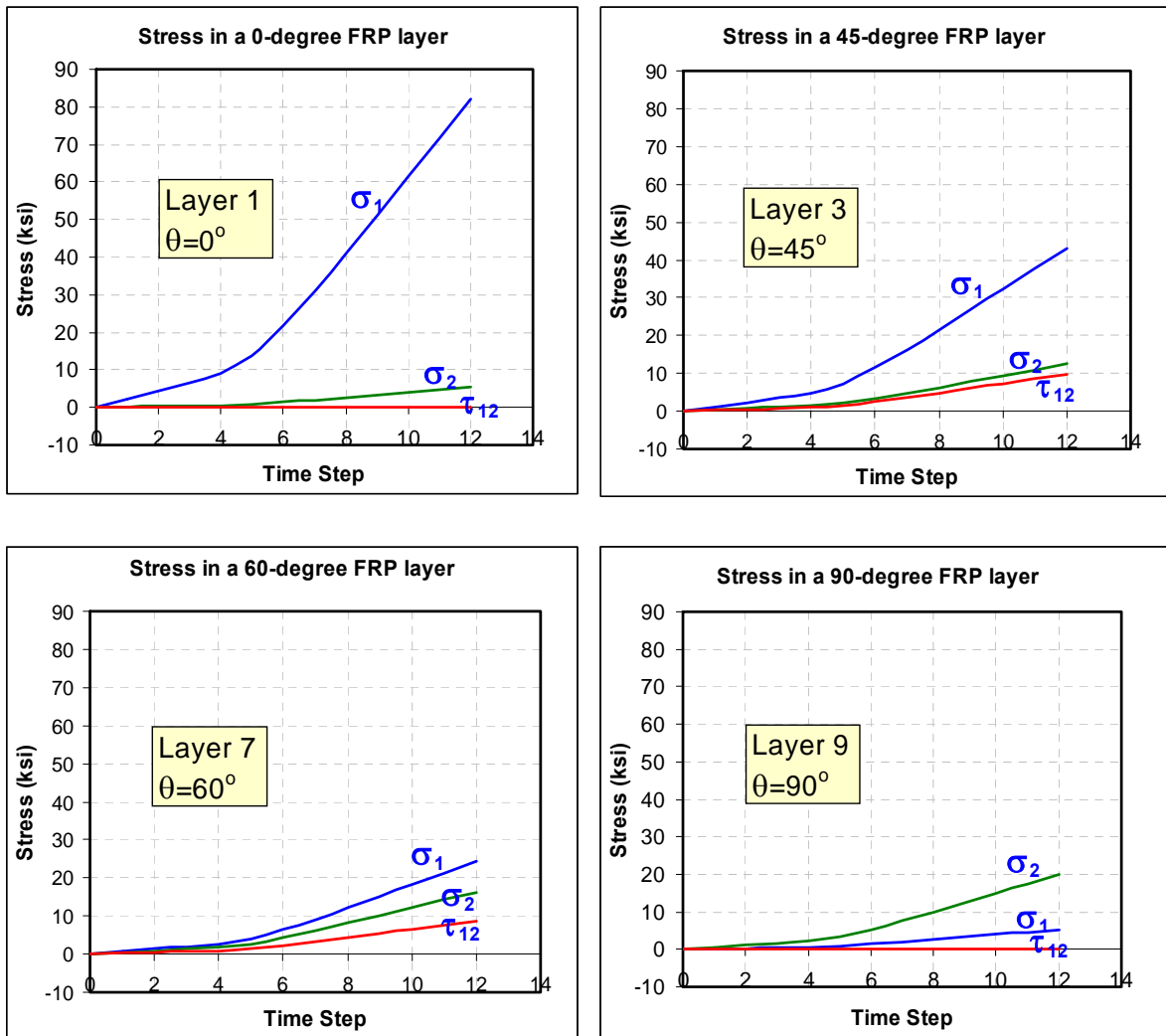


Figure 7-53: Stress variation with time in different FRP layers in a multi-layer pile subjected to axial compression only.

Figure 7-53 and Figure 7-54 show the stress variation with time for a point at the extreme compression side of a pile made of a multi-layer composite shell filled with concrete. The pile has a circular cross section and is subjected to axial compression and lateral head movement as described in pile information sheet 3. The composite shell consists of 12 layers with different fiber orientations that vary between 0 and 90-degrees measured with respect to the pile axis. As can be seen, the layers with small orientation

angles (close to 0) have their first stress component σ_1 higher than those with larger orientation angles. The second stress component σ_2 has its peak values in the layers with high fiber orientation angles (close to 90).

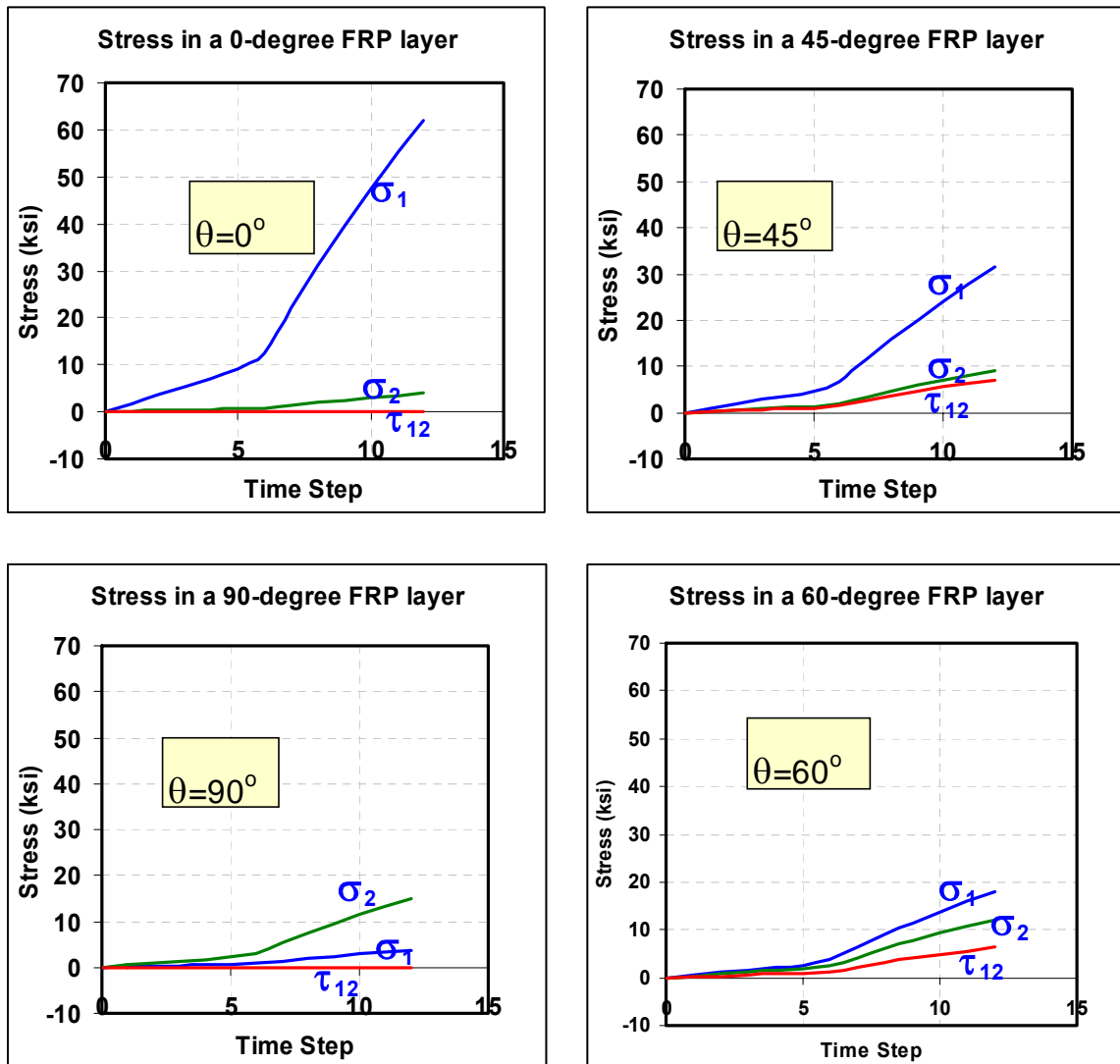


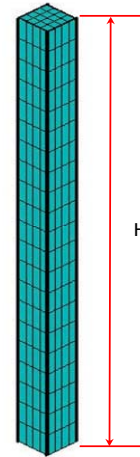
Figure 7-54: Stress variation with time in different FRP layers in a multi-layer pile subjected to axial compression and lateral movement.

The last model in this section will be as shown in the following information sheet

Pile information sheet 4:

Composite type: Carbon epoxy

Property	ksi	Property	ksi
E_x	20500	X_t	330
E_y	1500	Y_t	8.3
G_{xy}	1040	X_c	-209
V_{xy}	0.28	Y_c	-33
		S	10.3



Number of layers: 12

Layer thickness: 0.01667 in.

Laminate structure: [variable]

Filling: Hollow

Height = 20 ft

Soil type: Dense sand

Axial dead load: 200 kips [step 1]

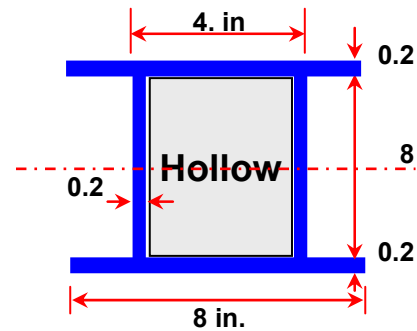
Lateral head movement: 2 in. [step 2]

Laminate structure:

Set 1: [76,-76,41-41,35,-35,62,-62,48,-48,55,-55]

Set 2: [76,-76,90,90,42,-42,29,-29,71,-71,52,-52]

Set 3: [86,-86,0.3,-0.3,9,-9,4.7,-4.7,20,-20,0.85,-0.85]



In this model, only the fiber structure was changed in each single run to monitor the effect of the fiber orientation on the stresses developed during and after loading. All other parameters were kept constant. The three major stress components are plotted at each case and illustrated in Figure 7-55. As can be seen, at a certain fiber orientation angle for each layer in the shell, the stresses are minimized to the lowest values as shown in set 3 graphs. The fiber structure which gives the lowest stress values in all directions is called the optimum design. The designer will have the flexibility to arrange the layers with different reinforcing angles to maximize or minimize the desired properties based on the loading and boundary conditions. Reducing the layer stresses will allow the pile to handle more axial loads and lateral displacements.

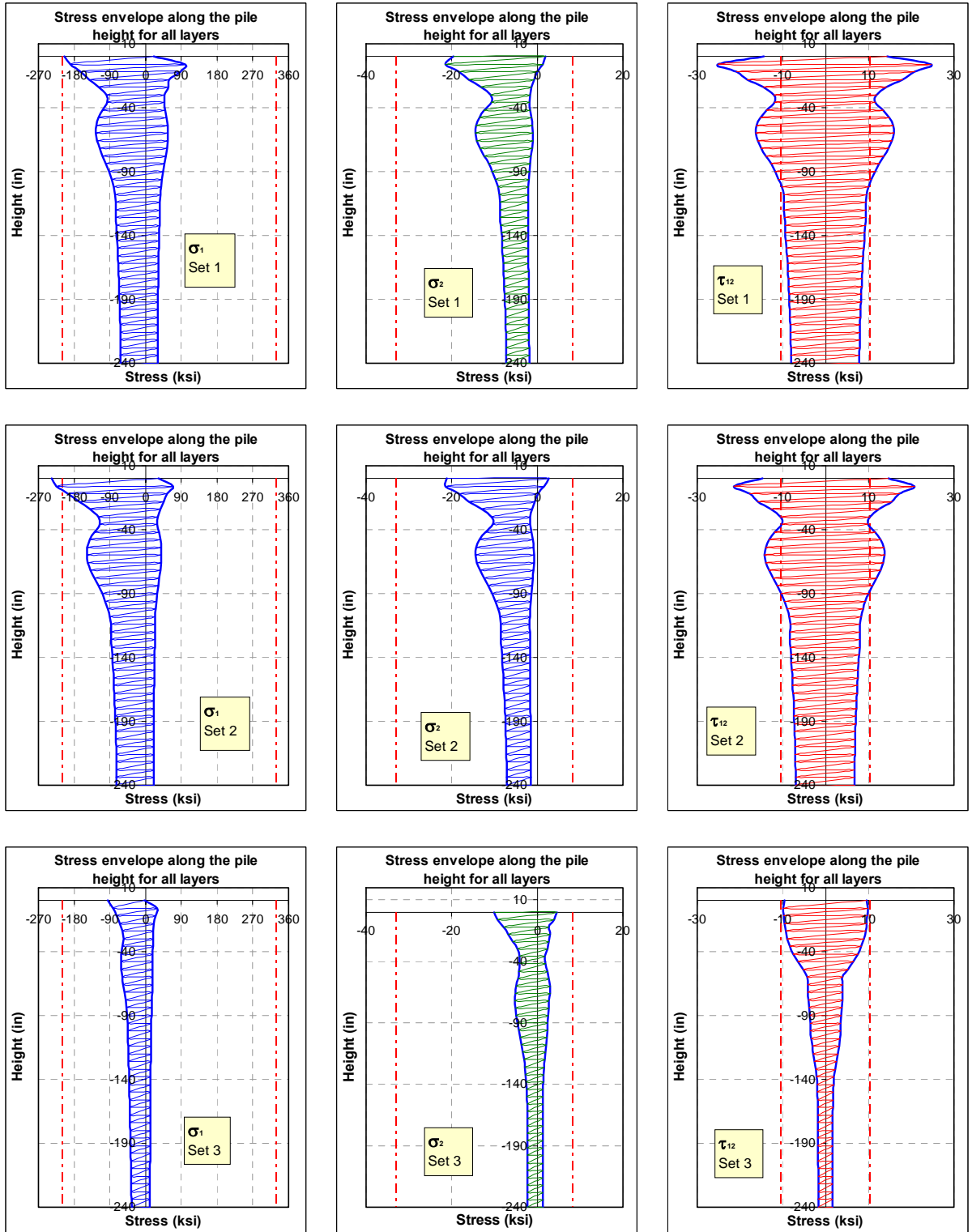


Figure 7-55: Effect of variation of fiber orientations on the different stresses.

7.4.5 CROSS-SECTION AREA

The size of the section is also a point of consideration when designing piles for integral bridges. The size of the pile can be decided by the designer based on the loads and the expected lateral deformations of the bridge super structure. The choice may come to install many piles with small section size or a few piles with larger cross sections. The decision will be based on several factors mostly economical such as manufacturing and installation costs, and practical aspects such as transportation and driving.

As an illustrative example, consider a cylindrical pile of radius R to carry the Load P and the lateral displacement D . For an existing load of $3P$, three piles will be needed or a single pile with triple the section area to replace the 3 piles.

Table 7-1: Effect of the section size on the moment of inertia

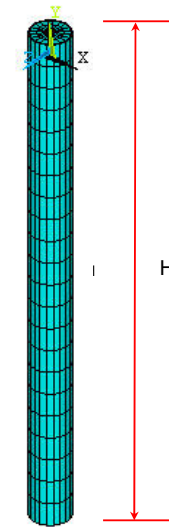
Pile	A	2A	3A
Radius	R	$\sqrt{2} R$	$\sqrt{3} R$
Area	πR^2	$2\pi R^2$	$3\pi R^2$
Inertia	$\frac{\pi R^4}{4}$	$\frac{4.\pi R^4}{4}$	$\frac{9.\pi R^4}{4}$

As can be seen from Table 7-1 a pile with twice the section size, $2A$ has 4 times the moment of inertia and the one with triple the size, $3A$ has 9 times the inertia. On the other hand, multiple piles with the size A set in a row next to each other to bend about one axis will have a moment of inertial of nI where I is the moment of inertia of the pile of the size A and n is the number of piles.

Pile information:

Composite type: Glass epoxy

Property	ksi	Property	ksi
E_x	4500	X_t	90
E_y	1100	Y_t	3.9
G_{xy}	550	X_c	-80
V_{xy}	0.26	Y_c	-17.5
		S	6.2



Number of layers: 12

Layer thickness: 0.025 in.

Laminate structure:[0,0,90,90,0,0,0,0,90,90,0,0]

Filling: Plain concrete $f_c'=3$ ksi

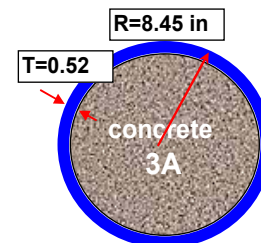
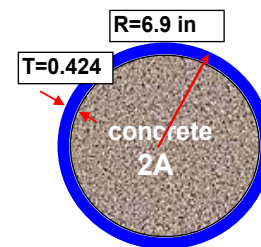
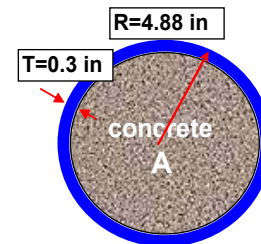
Height = 30 ft

Soil type: Soft clay, very stiff clay

Loading:

Axial dead load: 300,600,900 kips [steps 1 to 6]

Lateral displacement: 2 in. [steps 7 to 12]



To investigate the effect of pile cross-sectional size on the stiffness against lateral movement, one large pile with a cross-section size of 3A is compared with 3 small piles of size A each. The large pile has a concrete and FRP material size equivalent to the three small ones. All piles are assumed to be driven in the same soil and subjected to axial and lateral loading such that the large pile is subjected to 3 times the load of the single small pile. Figure 7-56 and Figure 7-57 show the deformation curves for the two sets of piles in very stiff clay and soft clay environments, respectively, with no predrilled holes. As can be seen, the single large pile experienced larger lateral displacements than the equivalent three small piles. The displacements are as twice of that of the small piles in very stiff clay and much more than that in piles driven in the soft clay. On the contrary, when the two pile sets are driven in very stiff clay but with 6-ft deep predrilled holes at the top, the 3 small piles showed higher lateral displacements than the single large pile as shown in Figure 7-58.

The lateral resistance of a pile is a combination of the stiffness of both the pile shaft and the surrounding soil. In the case of 1 large pile, the area projection that faces the soil is equal to $2\sqrt{3}R$ and in the case of 3 small piles; the total area projection is equal to $6R$. This simple calculation shows that the area projection for the 3 small piles is about 1.7 times that of the single large pile. As a result, the combination of the pile flexural rigidity and the lateral soil resistance will determine the flexibility of the soil-pile system.

In the case of a predrilled hole at the upper portion of the pile Figure 7-58, the total stiffness of the soil-pile system is in the favor of the large pile which ended with fewer lateral displacements than that of the 3 small piles.

Figure 7-59 shows a group of stress envelopes for the three piles of cross sectional areas, A , $2A$, and $3A$ loaded with P , $2P$, and $3P$ axial load respectively and each is subjected to a 2 inches lateral displacement. As can be seen, the stresses in the smallest pile have the highest values and for the largest pile have the lowest values. That can be explained based on the deformed shapes in Figure 7-60, which shows that the piles with the smaller diameters have sharper curvature that increases the bending moments, and then the stresses at the upper portion of the piles.

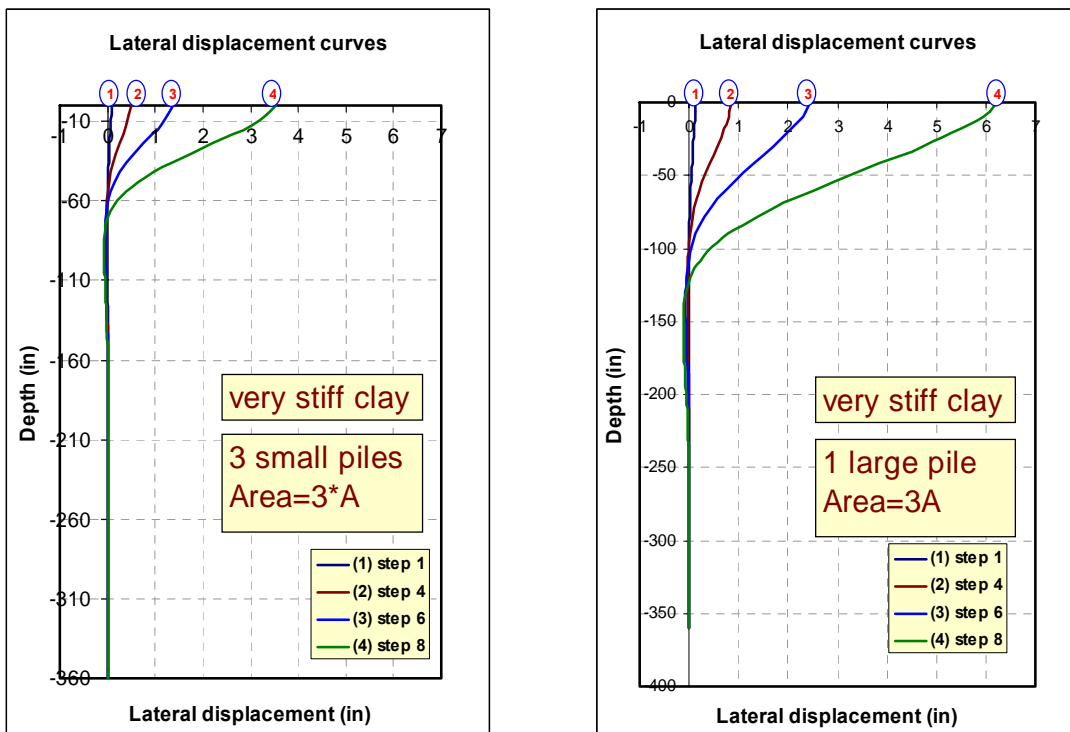


Figure 7-56: Comparison of lateral displacements for different pile sizes in very stiff clay.

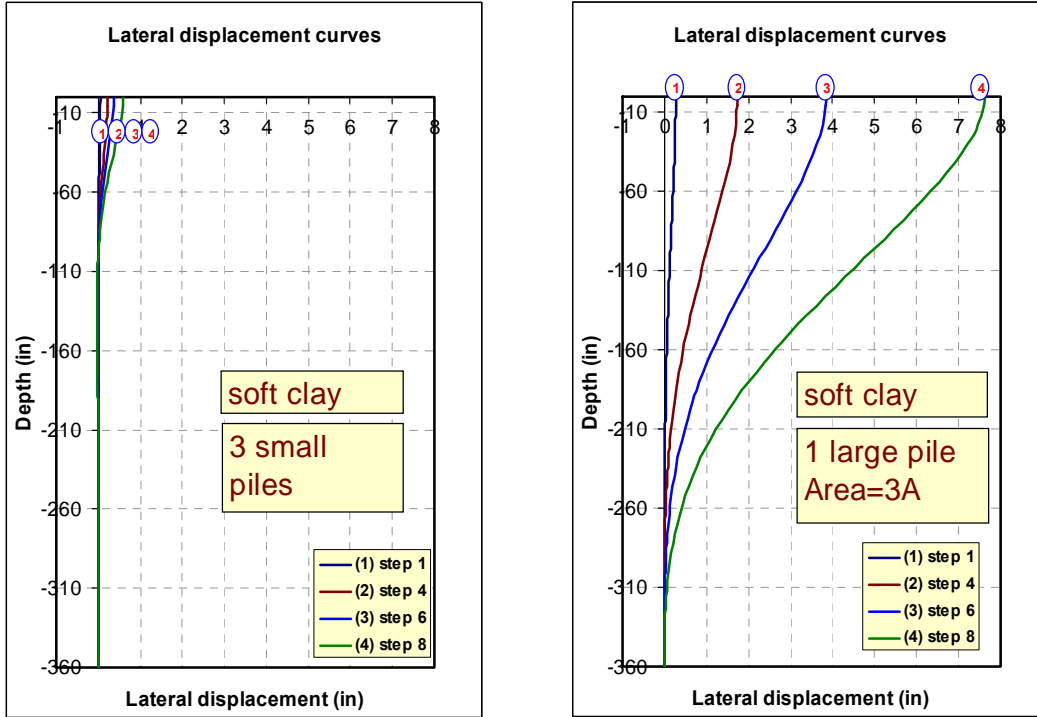


Figure 7-57: Comparison of lateral displacements for different pile sizes in soft clay.

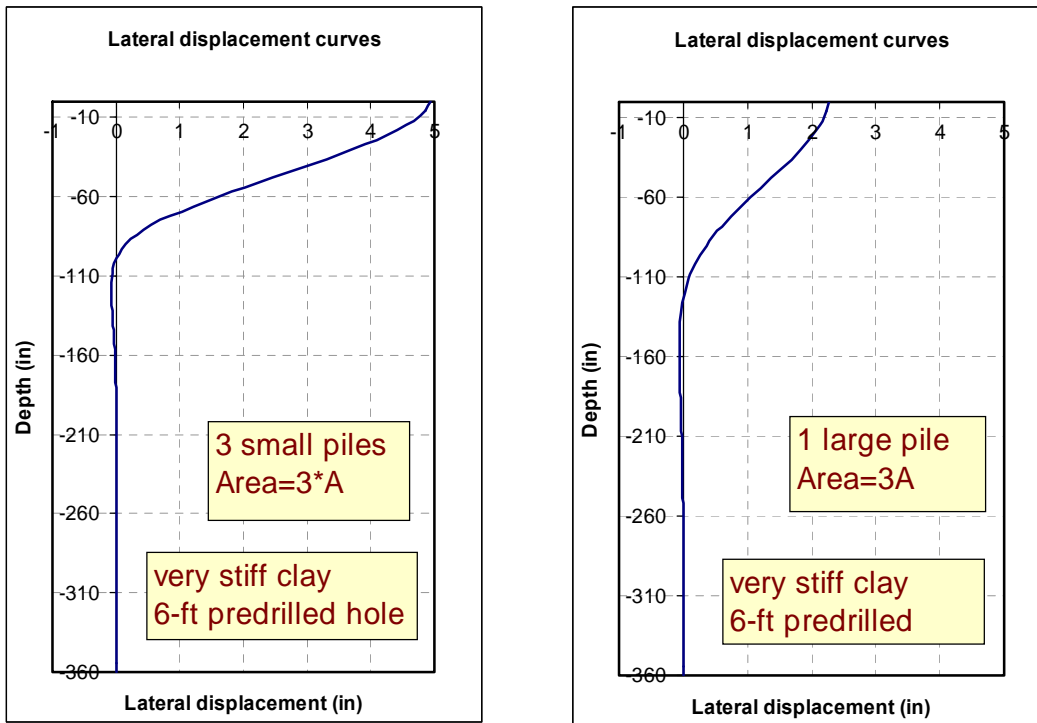


Figure 7-58: Comparison of lateral displacements for different pile sizes in very stiff clay and 6-ft predrilled holes.

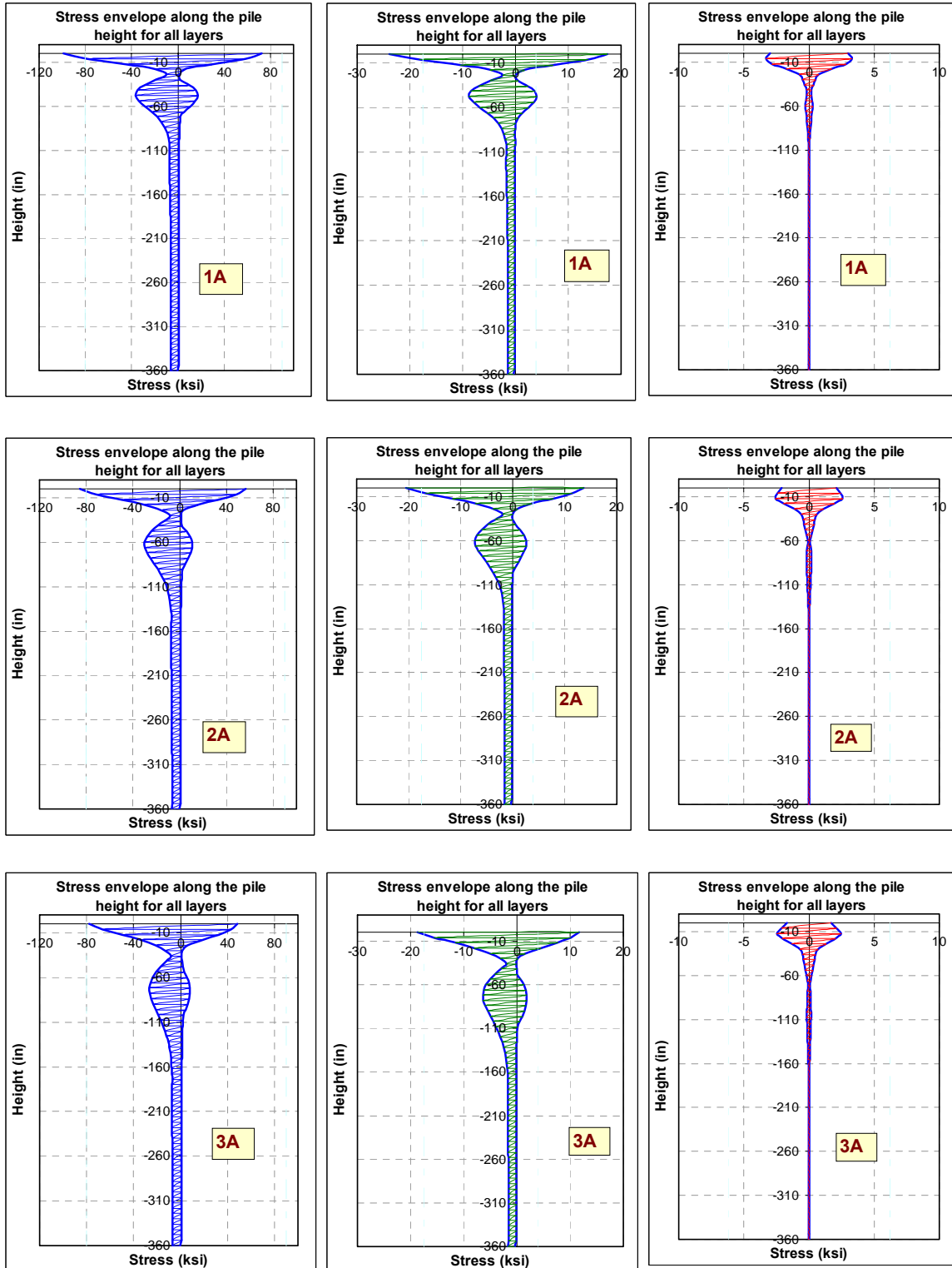


Figure 7-59: Effect of cross sectional area on stresses (no predrilled holes).

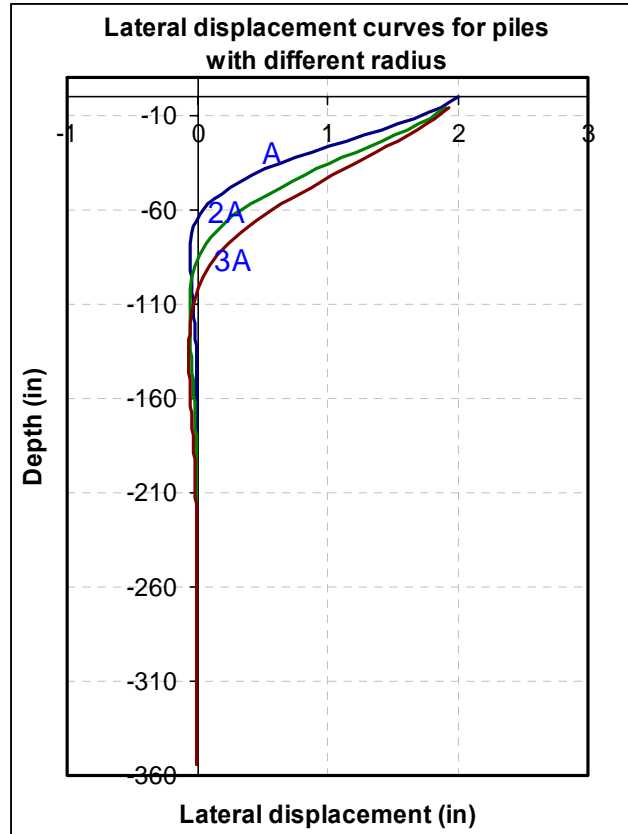


Figure 7-60: Lateral displacement curves for piles with different radius.

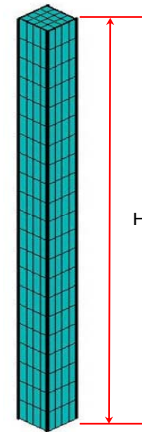
7.4.6 PREDRILLED HOLE

Piles driven in stiff soils such as dense sands and very stiff clays experience higher bending stresses than those driven in medium or soft soils when subjected to lateral head displacements. To reduce the stress magnitude, the upper portion of the pile can be released laterally by removing the surrounding soil or replacing it with loose sand or any other soft soil. This can be done by making a predrilled hole that has adequate depth and diameter around the pile to provide less lateral resistance in the direction of the bridge axis. Predrilled holes are a common technique usually used to reduce pile stresses in jointless bridges.

Piles information:

Composite type: Glass epoxy

Property	ksi	Property	ksi
E_x	4500	X_t	90
E_y	1100	Y_t	3.9
G_{xy}	550	X_c	-80
V_{xy}	0.26	Y_c	-17.5
		S	6.2



Number of layers: 12

Layer thickness: 0.0208 in.

Laminate structure:[0,0,90,90,0,0,0,0,0,90,90,0,0]

Height = 20 ft

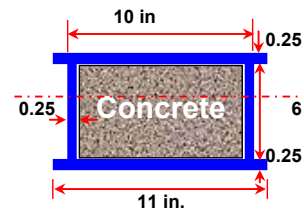
Soil type: very stiff clay

First Model :

Axial dead load: 300 kips [steps 1 to 6]

Lateral load: 130 kips [steps 7 to 12]

Predrilled holes: 0, 2, and 4 ft



Filling: concrete $f_c'=3$ ksi

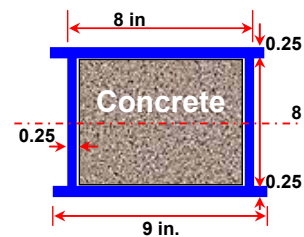
Second Model :

Filling: Plain concrete $f_c'=4$ ksi

Axial dead load: 300 kips [steps 1 to 4]

Lateral displacement: 2 inches [steps 5 to 8]

Axial live load: 200 kips [steps 9 to 12]



Filling: concrete $f_c'=4$ ksi

To study the effect of predrilled holes on the stresses and stiffness of FRP composite piles, two soil-pile models were analyzed with different predrilled-hole depths. The first model was used for lateral stiffness comparison and the second was for stress comparisons. Figure 7-61 shows the normalized load-deformation curves for a point on a pile with different predrilled holes subjected to both axial and horizontal loads to compare the soil-pile stiffness as the hole depth changes. Figure 7-62 also shows the normalized deformed curves along the pile depth for the same three cases of Figure 7-61. As can be seen, the pile with the 4-ft predrilled hole showed very low lateral resistance compared to that of 0-ft predrilled hole. The flexibility of the soil-pile system is directly proportional to the depth of the predrilled hole.

The effect of predrilled hole depth on pile stresses can be investigated by subjecting the pile to a specified axial load and lateral displacement to simulate the actual bridged load. The piles in consideration were subjected to axial compression and then followed by lateral head displacement incremented up to 2 inches. The axial load that represents the live load was then applied. The second model which is described in the pile information sheet will be used for this comparison. As can be seen in Figure 7-63, all pile heads are displaced 2 inches but the rest of the pile lengths have different deformed shapes from each other. Also it can be noted that piles with deeper predrilled holes experienced lateral displacements on longer portions of their shafts compared to those with shallow or without predrilled holes. In other words, the point of fixation depth for a pile is directly proportional to the depth of the predrilled hole.

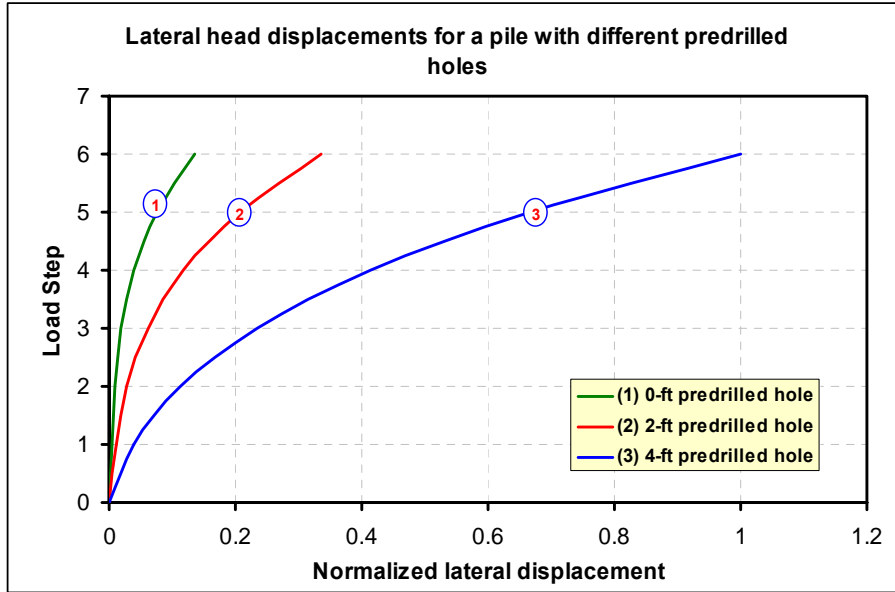


Figure 7-61: Load-displacement curves for a pile with different predrilled holes.

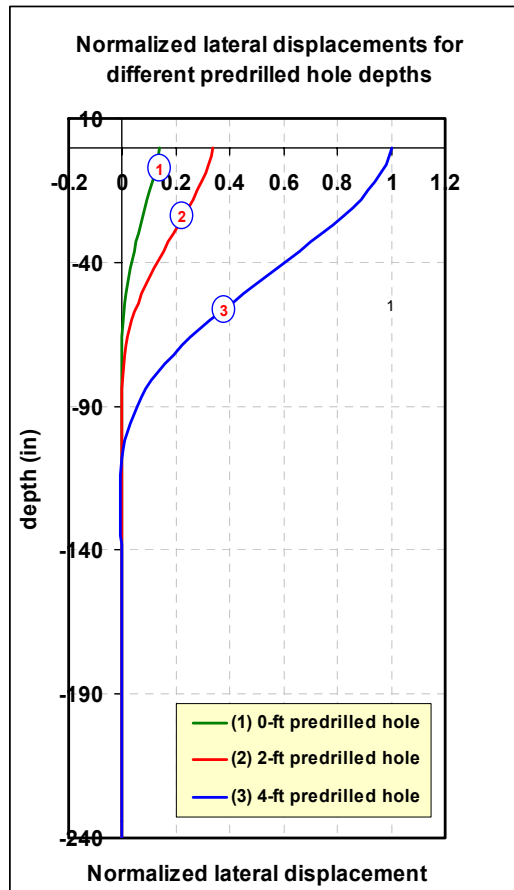


Figure 7-62: Effect of predrilled hole depth on lateral stiffness.

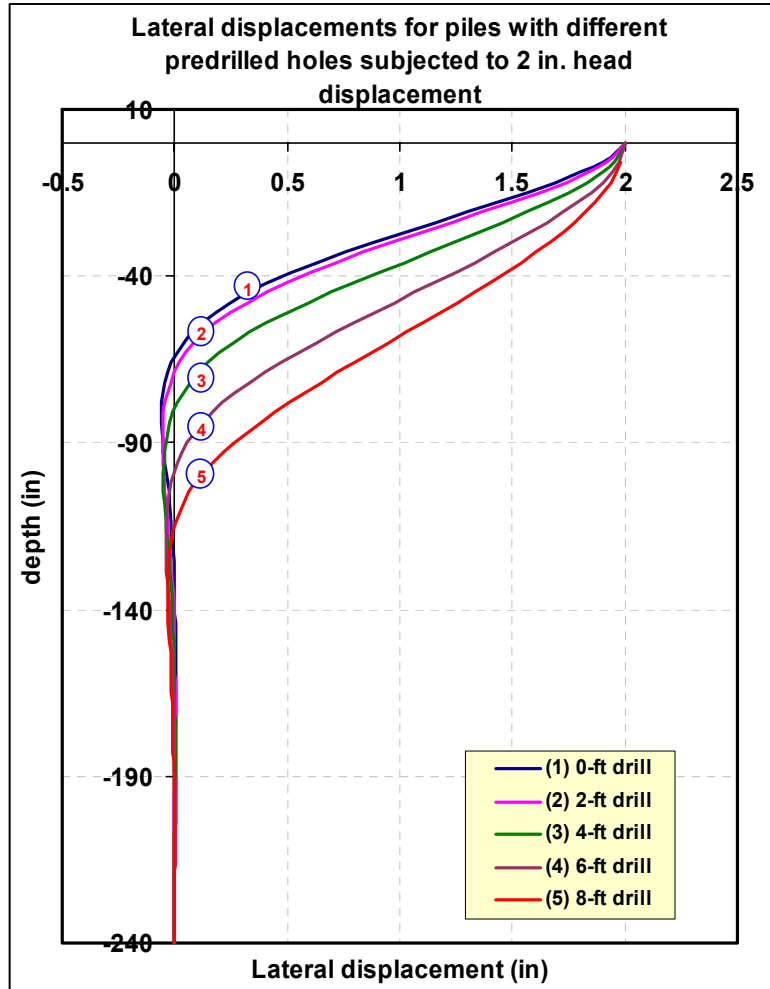


Figure 7-63: Lateral displacements along the pile depth for different predrilled holes.

Figure 7-64 through Figure 7-72 show the effect of predrilled holes on the stresses of concrete-filled FRP composite piles. Each set of curves presents the stress variation from different view. Figure 7-64 shows a stress comparison at point for a pile with different predrilled holes. The point is located at the extreme stress location with 0-ft depth on the pile shaft. The curves illustrate the stress development as the load increases with time. As can be seen, the pile without predrilled hole developed much higher stresses than those with predrilled holes. For this point location, the stress value is inversely proportional to the depth of the predrilled hole.

The stress variations at a point are also illustrated at two other locations; 1-ft depth and 2-ft depth, Figure 7-65 and Figure 7-66 respectively. The stress behavior with the predrilled hole depth did not show the same trend that was noticed in the curves of 0-ft depth location. As can be seen, the pile without a predrilled hole did not show the highest stress value; instead another pile with a predrilled hole experienced the highest stress. The explanation of this change can be seen in Figure 7-67 which shows the stress variation for the same pile over the whole depth. This figure includes illustrations for the tension and compression sides of the pile at selected loading stages. It can be clearly seen that the behaviors of the different curves are not consistent. They are intersecting more than one time over the depth of the pile shaft which means no pile keeps the extreme behavior along its depth.

Another comparison is also shown in Figure 7-68 and Figure 7-69. The curves in these two figures show the stress at a point and its variation with the depth of the predrilled hole. The point located at 0-ft depth on the pile shaft shows a significant stress reduction as the predrilled hole depth increases. The point at 1-ft depth shows a slight decrease in stress while the points at 2 and 4-ft depths show a stress increase as the predrilled hole depth increases.

The stress envelopes for the piles are shown in Figure 7-70 through Figure 7-72. The envelopes of the first stress component, σ_1 , for a single layer in the different piles are plotted in Figure 7-70. The graph numbers show that the maximum stress in the layer reduced from -109 ksi in the pile without predrilled hole to about -45.5 ksi in the pile with 6-ft predrilled hole. A reduction of about 60% in the stress is achieved by using a predrilled hole at the pile top. Figure 7-71 and Figure 7-72 show the envelopes of first

and second stress components; σ_1 and σ_2 respectively for all layers. The stress reduction appears clearly in the 6 and 8-ft predrilled holes envelopes. A stress reduction up to 75% can be achieved when a predrilled hole is used.

The effect of the predrilled holes on the crack patterns in the concrete fill is illustrated in Figure 7-73. As can be seen, the cracks density is very high in the pile without predrilled hole and very low in the pile of 8-ft predrilled hole.

In conclusion it can be said that providing a predrilled hole with adequate depth for piles driven in stiff soils will reduce the stresses resulting from the lateral movement of the pile head. Stress reduction will reduce the crack intensity in the concrete fill which will keep it intact to support more axial loads.

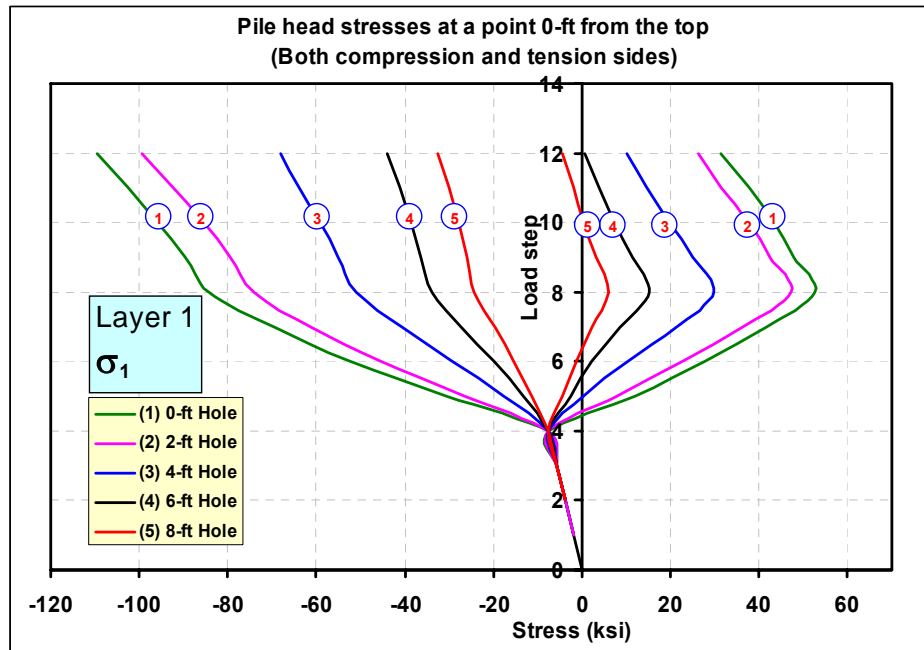


Figure 7-64: Effect of predrilled hole depth on pile stresses (0-ft depth).

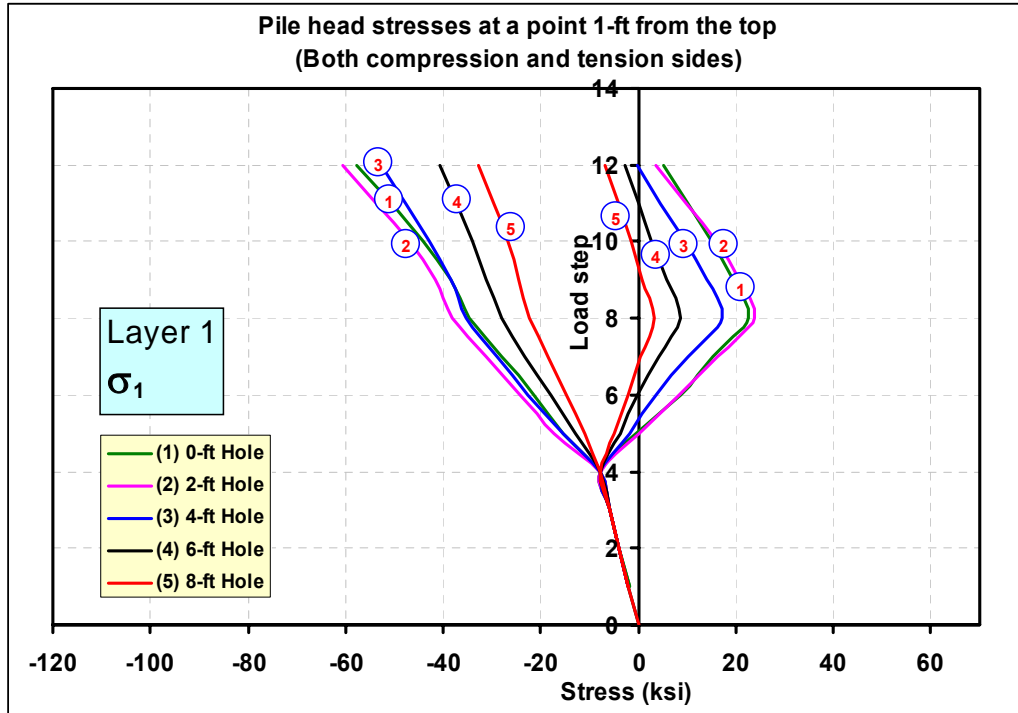


Figure 7-65: Effect of predrilled hole depth on pile stresses (1-ft depth).

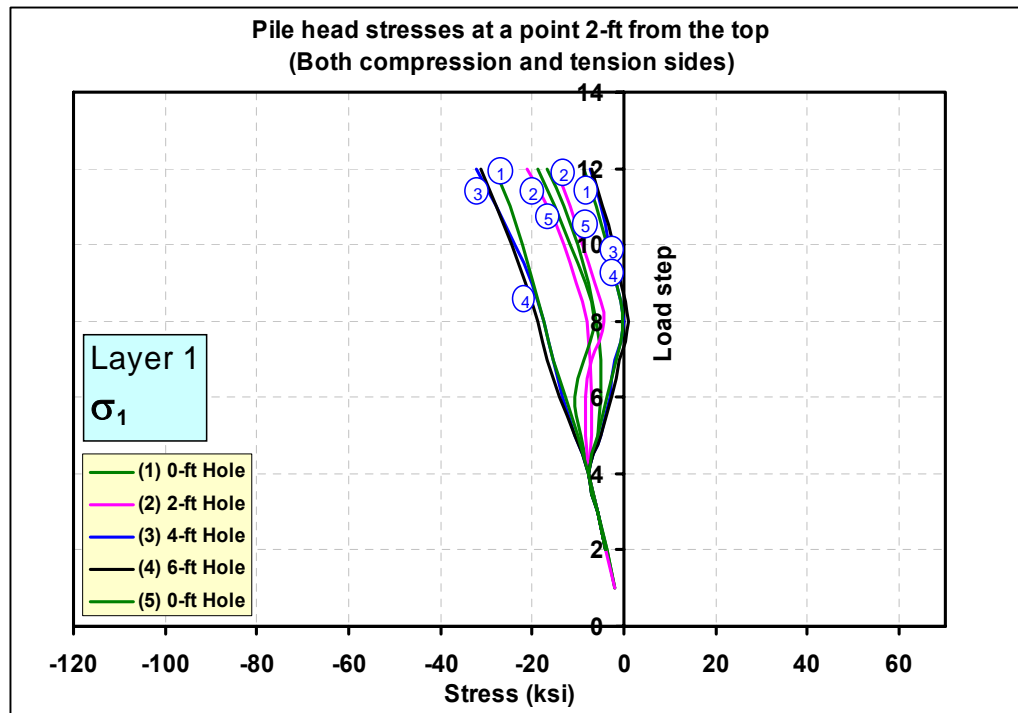


Figure 7-66: Effect of predrilled hole depth on pile stresses (2-ft depth).

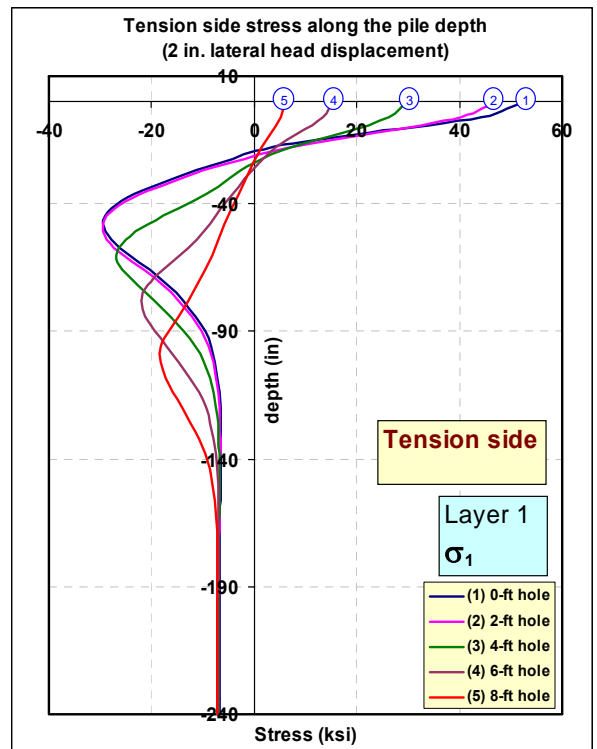
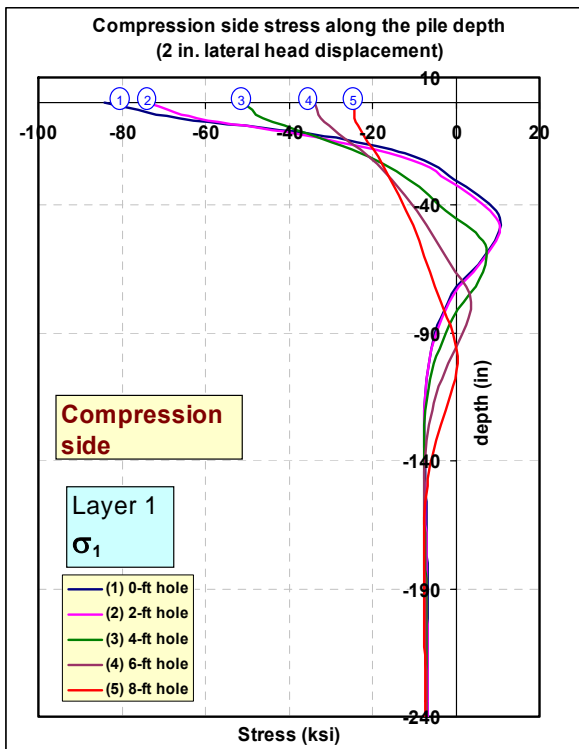
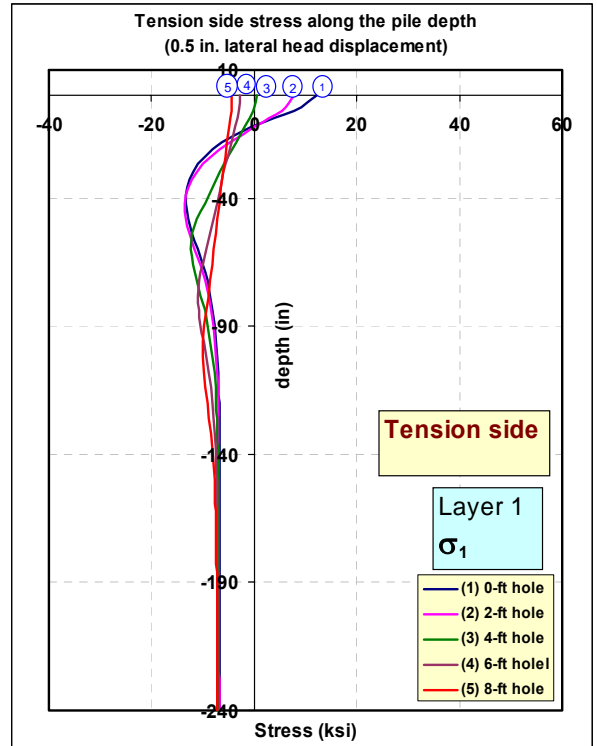
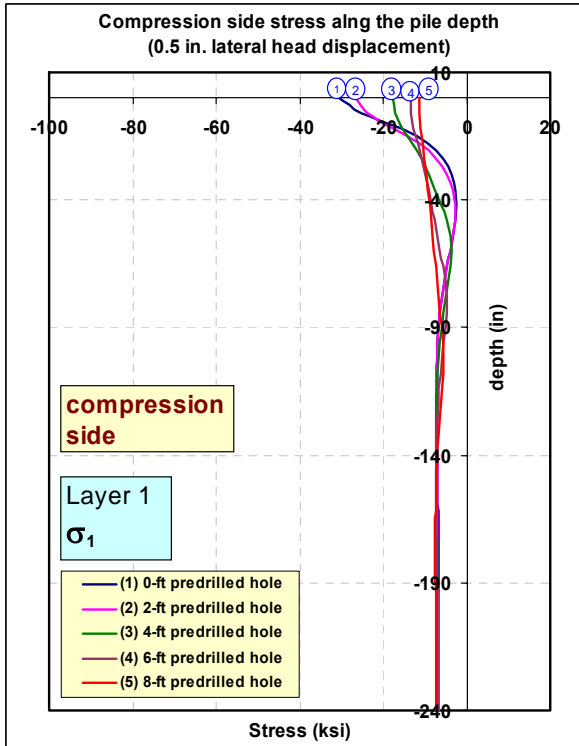


Figure 7-67: Stress variation along the depth of the pile shaft in both tension and compression sides for different predrilled holes.

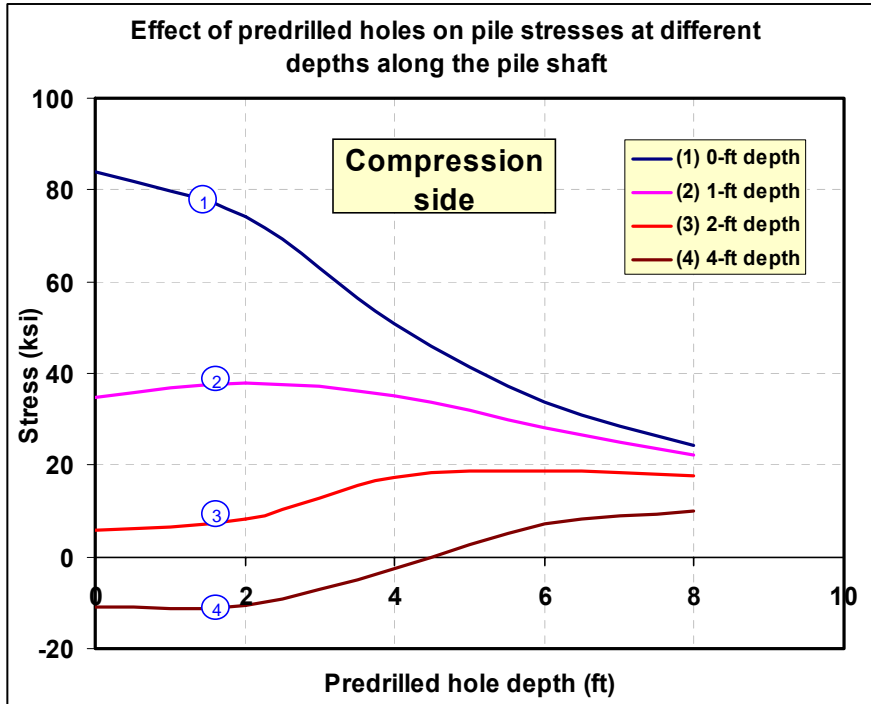


Figure 7-68: Variation of stress at point for a pile with different predrilled holes.

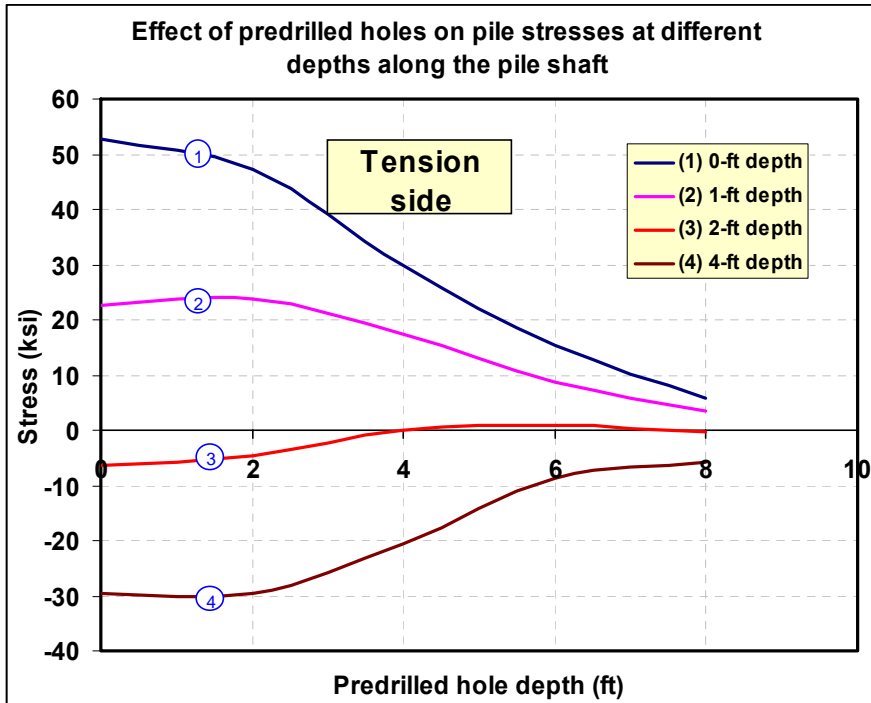


Figure 7-69: Variation of stress at point for a pile with different predrilled holes.

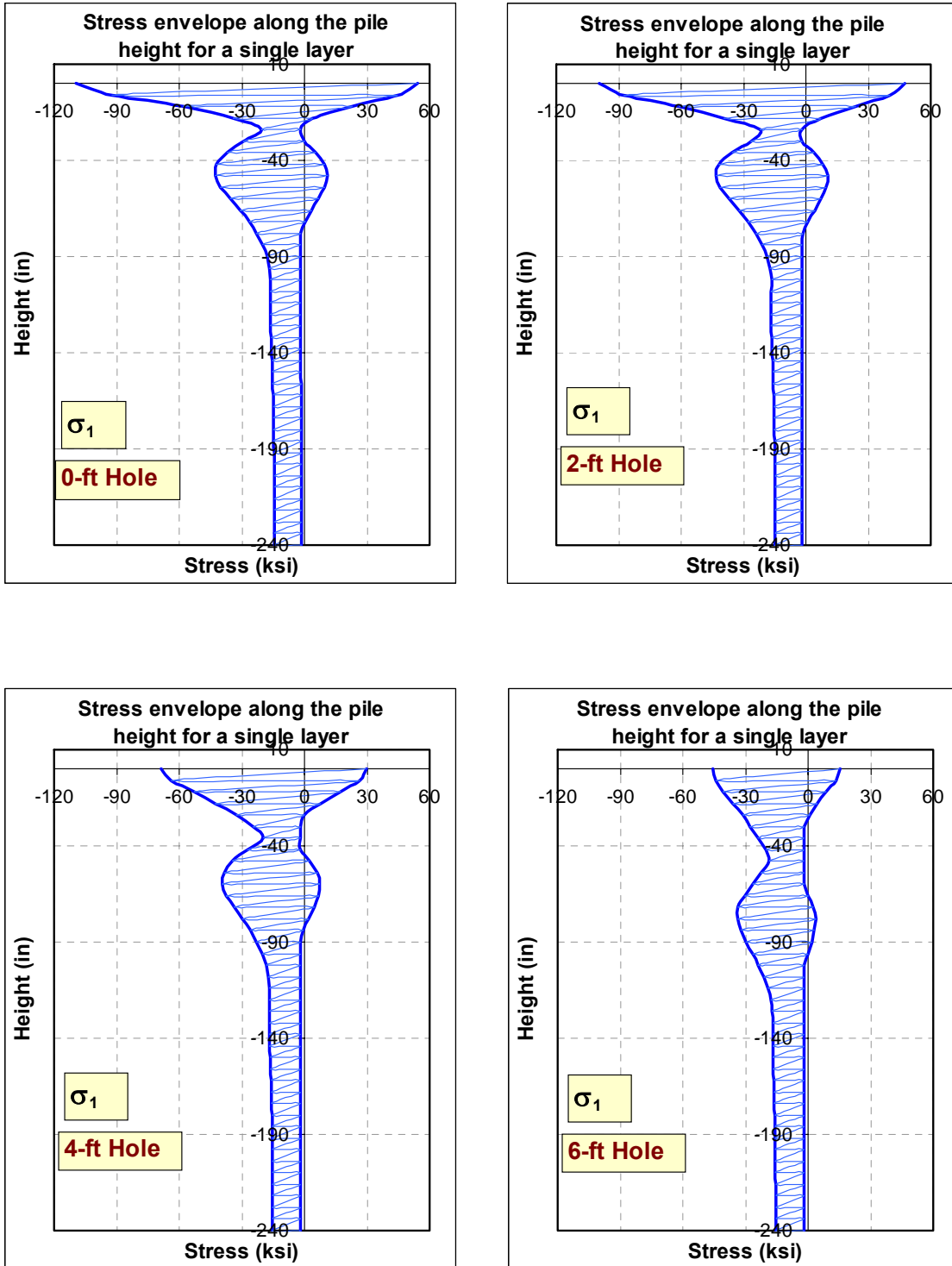


Figure 7-70: Variation of FRP Stress (σ_1) in a single layer with the depth of the predrilled hole.

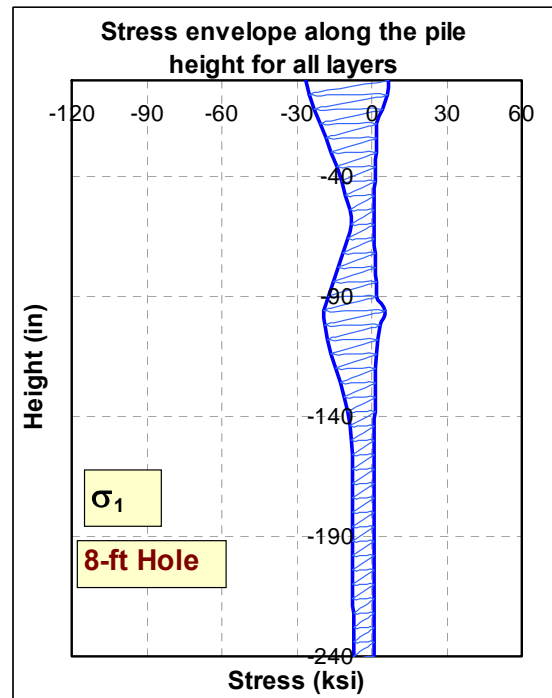
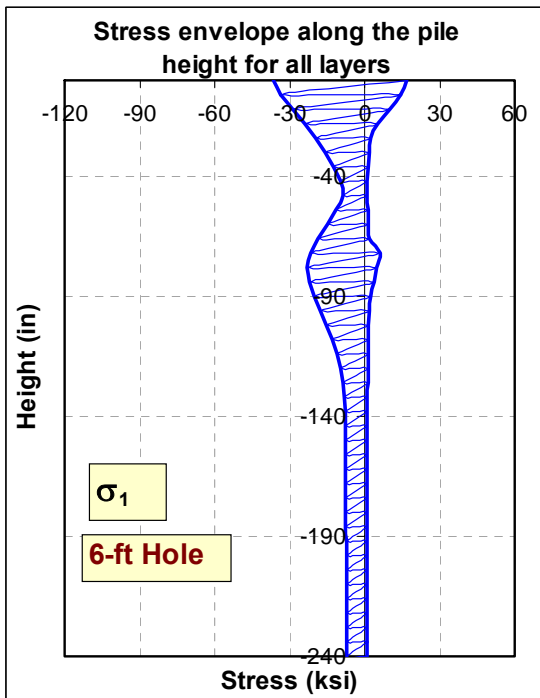
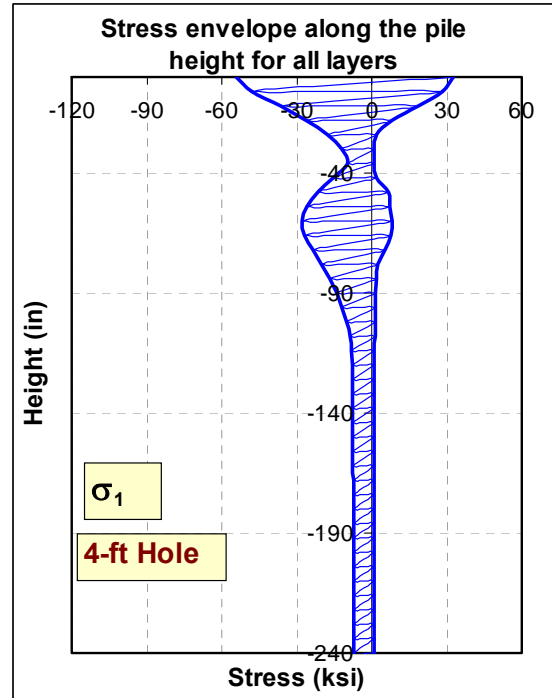
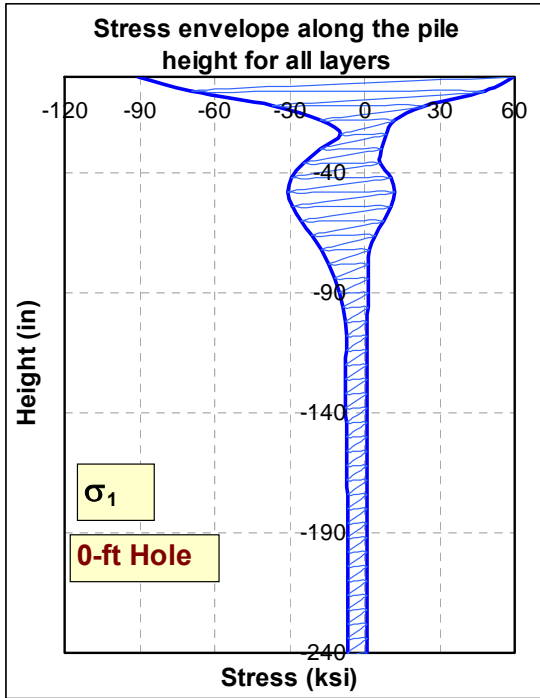


Figure 7-71: Variation of FRP Stress (σ_1) with the depth of the predrilled hole.

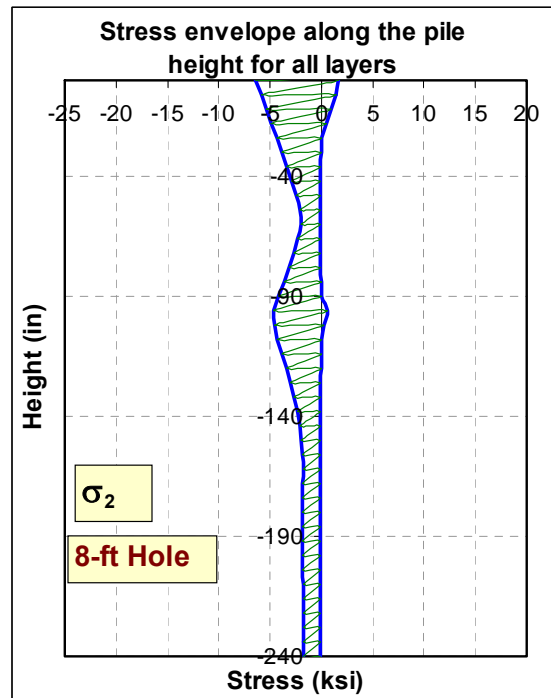
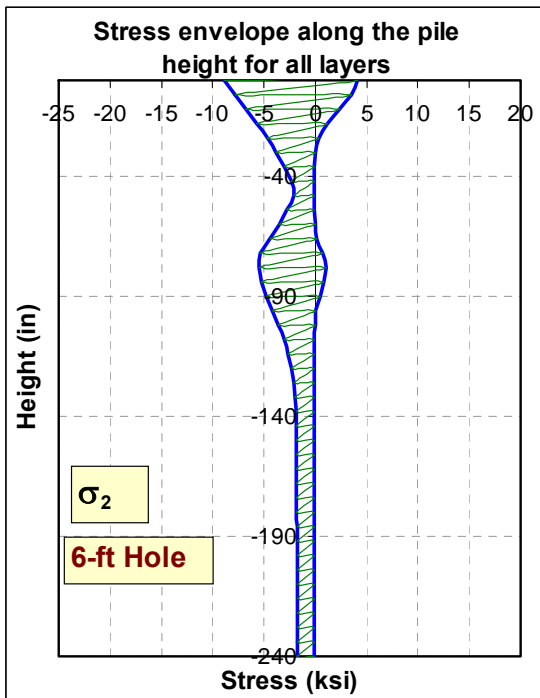
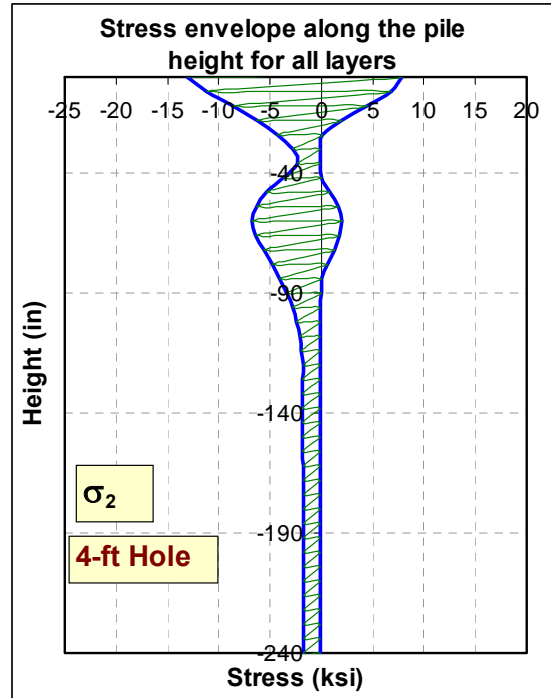
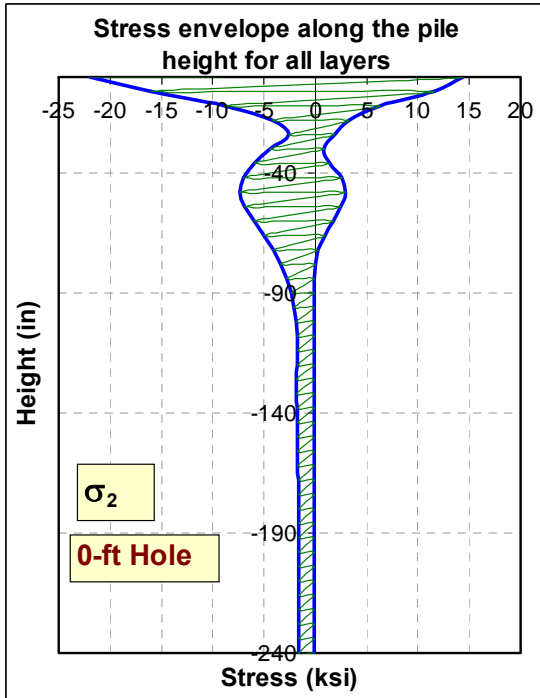


Figure 7-72: Variation of FRP Stress (σ_2) with the depth of the predrilled hole.

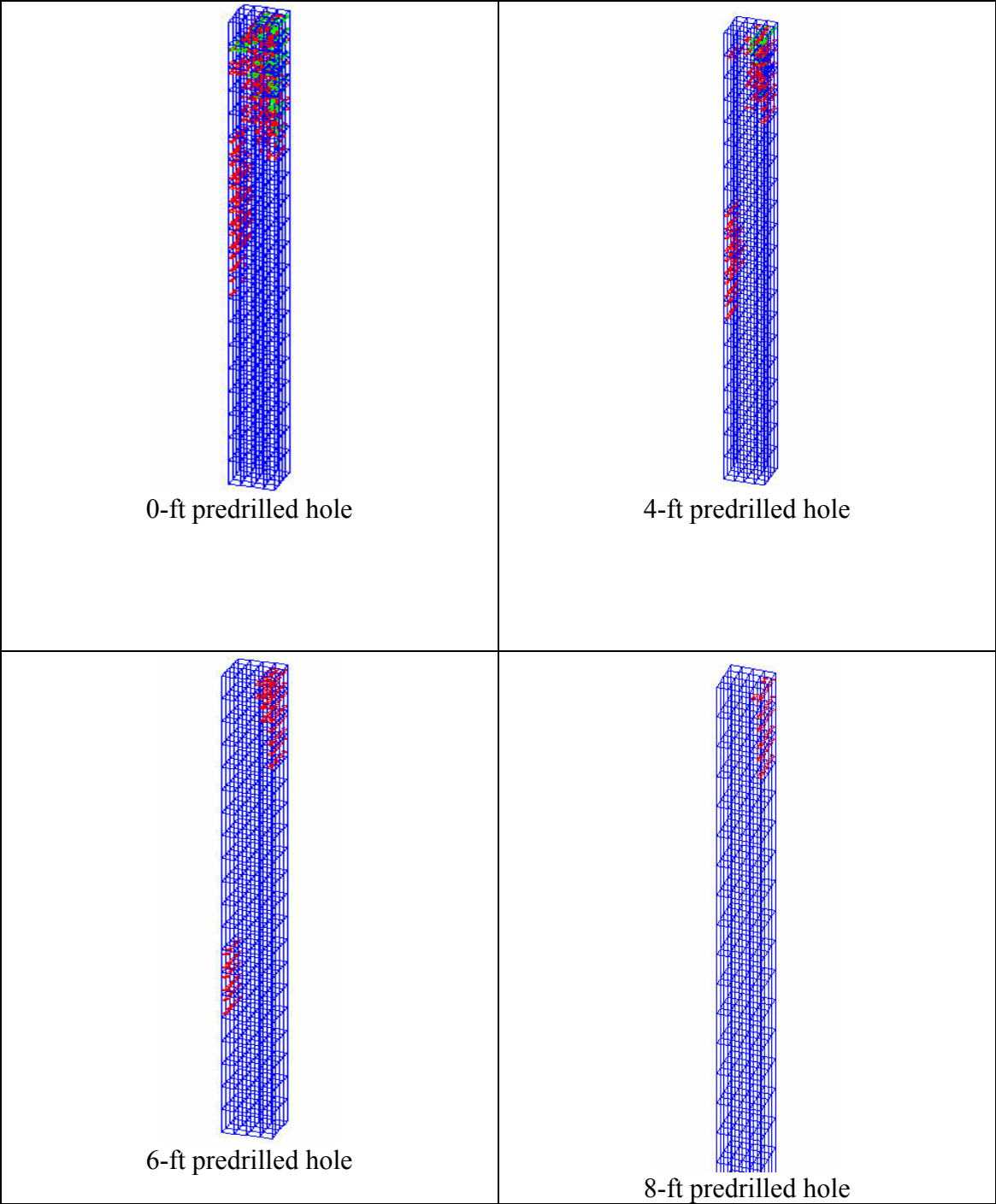


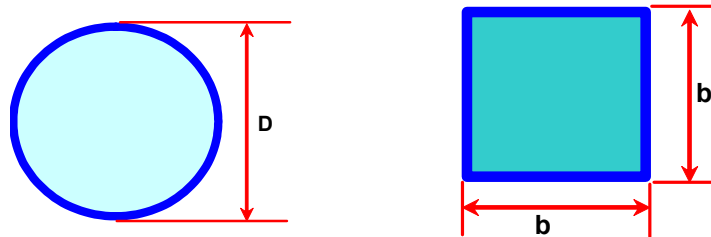
Figure 7-73: Crack patterns in piles with different predrilled holes.

7.4.7 SECTION GEOMETRY

The lateral resistance of a pile group against the lateral displacements of a bridge deck depends on several factors some of which are number of piles, pile geometry, and the stiffness of both the pile's material and soil properties. As discussed earlier, the piles in integral abutment bridges are recommended to be aligned in a single row to minimize their lateral resistance. The pile cross section also has a contribution to the lateral stiffness of the pile group. The section can be chosen to provide minimal stiffness.

Effect of Section Orientation on Pile Flexibility

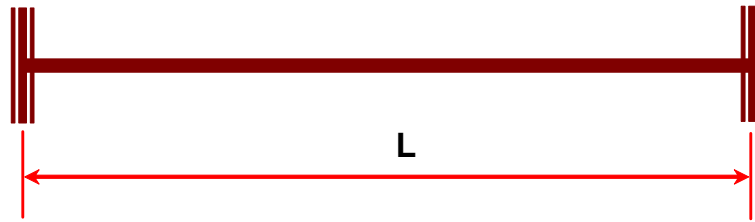
Consider a pile with the basic cross-sectional shape; circular or a square cross section with dimensions given as shown in the figure below.



The square section has a cross sectional area equal to $A=b^2$, where b is the side length of the square. A circle with an equivalent square area will have a diameter of $D=\frac{2b}{\sqrt{\pi}}$. The circle's dimensions can not be modified while maintaining a constant area.

On the other hand, the square section can have its dimensions modified while maintaining either the original area or perimeter. Since our goal is to achieve lower moment of inertia and less stresses, a rectangular section may satisfy that objective.

Again if we consider the same square section that has a side length b to be the cross section of a structural member with a length L and fixed ended at both sides.


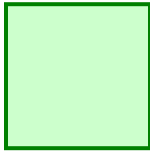


If one end of the member is subjected to a support settlement of magnitude Δ , the resulting moment at each end support will be

$$M = \frac{6EI\Delta}{L^2}$$

This section can be modified to a rectangle with the same area b^2 and with a width to height ratio 2:1.

Table 7-2: Variation of stresses with cross-sectional geometry

Property	h 	
Area	b^2	b^2
Perimeter	$4.24 b$	$4b$
Inertia	$\frac{b^4}{24}$	$\frac{b^4}{12}$
Moment	$\frac{6E(b^4/24)\Delta}{L^2}$	$\frac{6E(b^4/12)\Delta}{L^2}$
Stress	$\frac{3E\Delta b}{\sqrt{2}L^2}$	$\frac{3E\Delta b}{L^2}$

It can be seen from the calculations of Table 7-2 that after modifying the cross sectional dimensions while maintaining the original area, the section moment of inertia is reduced to 50% of the original section. As a result, the moment is also reduced to 50% of

the original moment. The variation of moment of inertia with b/h ratio is shown in the figure below.

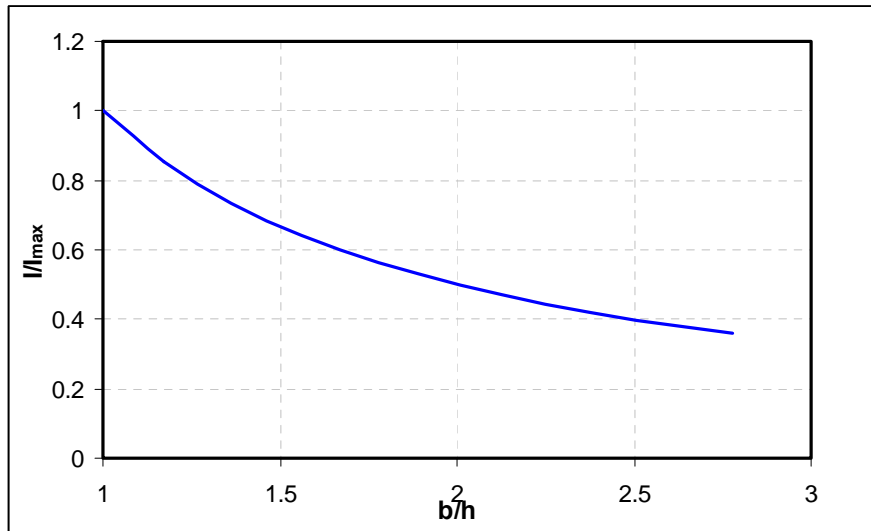


Figure 7-74: Variation of moment of inertia of a rectangular section with variation of (b/h)

Two cases of loading were used to study the effect of the section geometry on the soil-pile behavior. The pile information sheet includes all the information about the pile sections, their properties and cases of loading.

The first case was for stiffness comparison of the different pile sections driven with and without a predrilled hole. All piles are subjected to the axial dead load then followed by the lateral force. Figure 7-75 shows a lateral deformation comparison for all piles that have equal cross-sectional areas but different geometrical shapes. It can be seen that the pile deformations for the different cross-section shapes vary within a narrow range which indicates that the section geometry has a minor effect on the flexibility of the soil-pile system when the pile is fully embedded in stiff soils.

Similar comparison of the same pile sections was also carried out in the same environment but with a 4-ft deep predrilled hole at the top of each pile. The piles were also subjected to axial and lateral loads to compare their lateral stiffness when there is no

soil resistance at a certain depth of the pile. The load-deformation curves for all piles are plotted as shown in Figure 7-76. As can be seen, the piles' responses are different from the previous case, which did not have a predrilled hole. The pile that has the smallest moment of inertia, DS=6 in., showed the maximum flexibility compared to the rest. The pile that has the highest moment of inertia, DS=10 in., showed the highest stiffness and as a result experienced the lowest lateral displacements under the same loading conditions.

The two soil-pile models showed different behaviors when a predrilled hole was provided at the top of the pile. In the first case when the piles were fully embedded in the soil, the lateral stiffness was a combination of both the pile and the soil stiffness. As the pile geometry was modified to minimize the moment of inertia about its bending axis, the area of lateral soil resistance increased. The increase in the lateral stiffness depends on both the pile width and the soil stiffness. If the amount of the stiffness (gained from an increase in the lateral soil resistance when the cross-section geometry changed) is less than that lost because of the reduction in the pile's moment of inertia, then the soil-pile system will be more flexible and vice versa.

Reducing the flexural rigidity of a fully embedded pile by modifying its geometrical shape does not guarantee a reduction in the stiffness of the soil-pile system. This can be true if the cross-sections are moving freely without any additional resistance other than their stiffness. But in the case of driven piles, the soil stiffness provides additional resistance to the lateral displacements. The p - y curves which represent the lateral stiffness of the soil are generated based on several parameters one of which is the projected area on contact with the soil when the deformation takes place. Because of the

combined stiffness, the pile section should be proportioned to provide the least resistance for both soil and inertia.

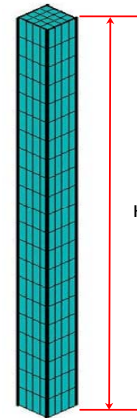
The second case was for stress comparison when the piles were subjected to axial load and lateral head movement as described in case 2 of the pile information sheet. Both pile groups, with and without predrilled holes were investigated. Figure 7-77 shows a comparison of the first and second stress components' envelopes for the four piles without predrilled holes. The different pile sections showed very close stress profiles with no significant difference to be noticed. Figure 7-78 and Figure 7-79 also show a comparison of the first stress component at a point and at a line respectively along the pile depth for all piles. As can be seen, the pile with the circular cross-section showed the highest stress values and the pile with the lowest moment of inertia showed the lowest stress values. This does not imply that the circular section pile is the stiffest, because a stress comparison at a point is not adequate to describe the whole pile behavior. The stress envelopes are more global and reflect the behaviors of all nodes.

Figure 7-80 and Figure 7-81 show the stress variations at a point and at a line respectively along the piles' depths for piles with 6-ft predrilled holes. It can be seen that the pile with the largest moment of inertia, $DS=10\text{in.}$ experienced the highest stress values and the pile with the smallest moment of inertia, $DS=6\text{in.}$ experienced the lowest stress values. The stress envelopes in Figure 7-82 also show a reduction in the stress values as the moment of inertia of the section reduced.

Piles information:

Composite type: Glass epoxy

Property	ksi	Property	ksi
E_x	4500	X_t	90
E_y	1100	Y_t	3.9
G_{xy}	550	X_c	-80
V_{xy}	0.26	Y_c	-17.5
		S	6.2



Number of layers: 12

Layer thickness: 0.0208 in.

Laminate structure: [0,0,90,90,0,0,0,0,90,90,0,0]

All sections have the same FRP and concrete area

Filling: Plain concrete $f_c' = 3$ ksi

Height = 20 ft

Soil type: very stiff clay

Loading:

Case 1:

Axial dead load: 300 kips [steps 1 to 6]

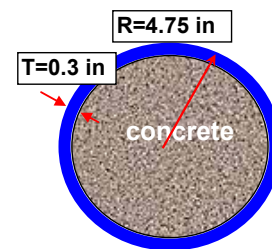
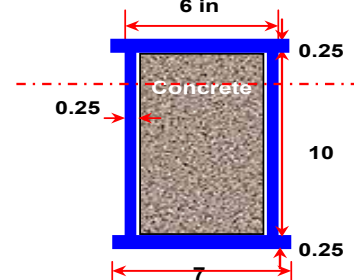
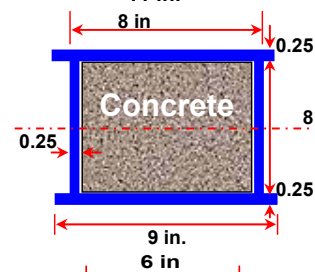
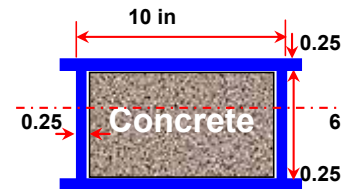
Lateral force: 130 kips [steps 7 to 12]

Case 2:

Axial dead load: 300 kips [steps 1 to 4]

Lateral displacement: 2 inches [steps 5 to 8]

Axial live load: 200 kips [steps 9 to 12]



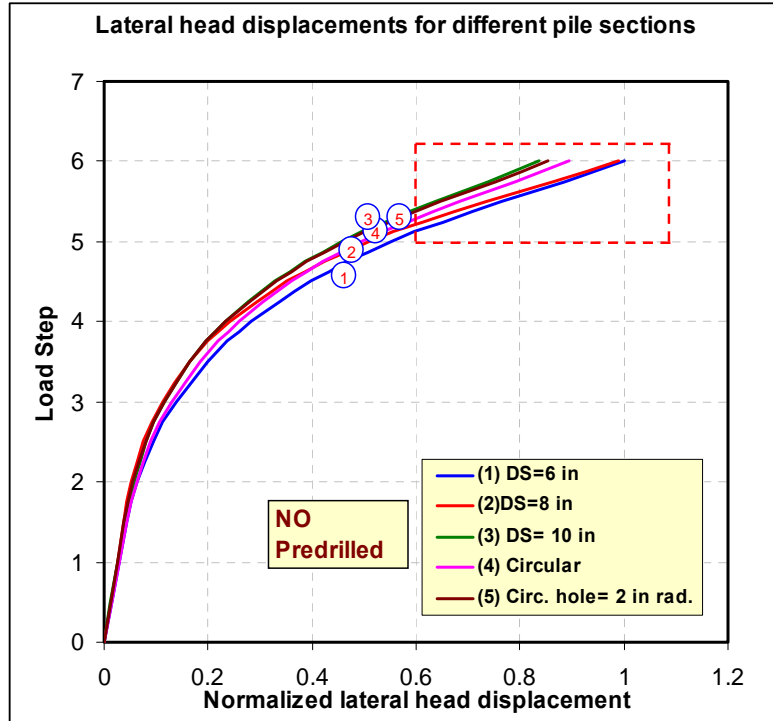


Figure 7-75: Normalized lateral head displacements for different section geometries with no predrilled hole.

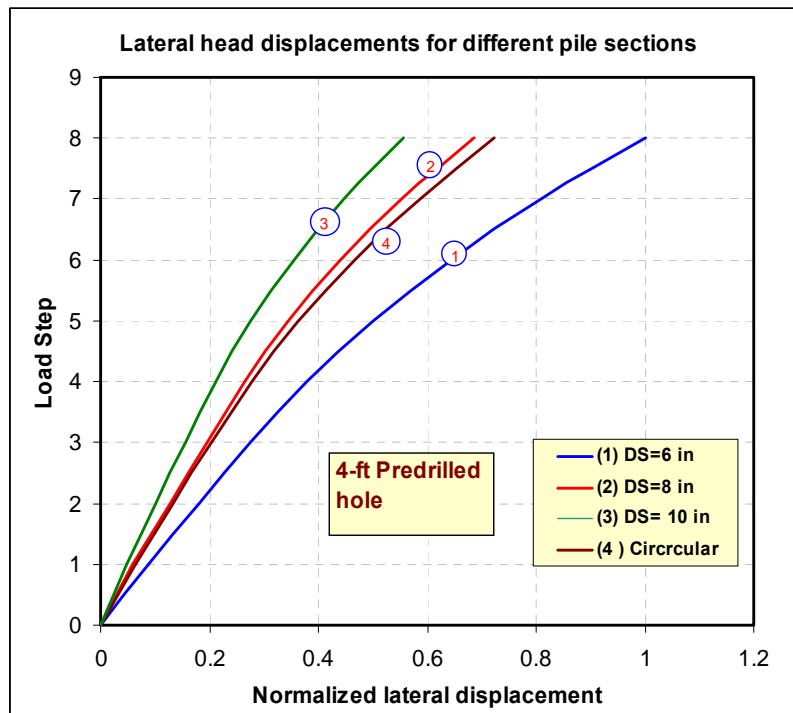


Figure 7-76: Normalized lateral head displacements for different section geometries with 4-ft predrilled hole.

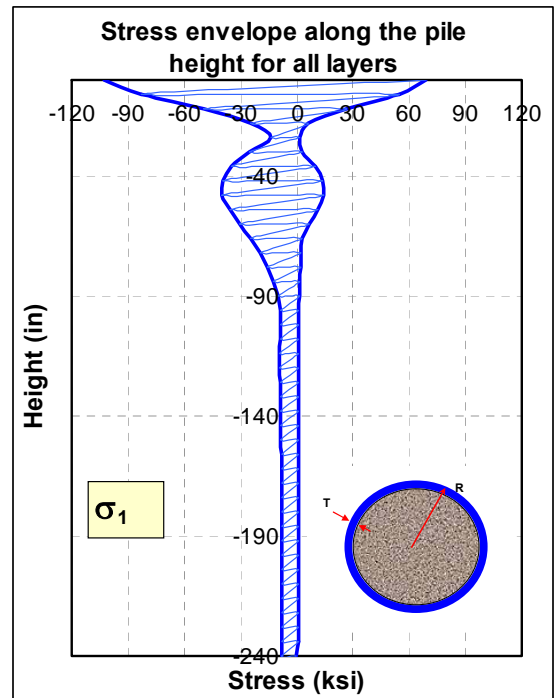
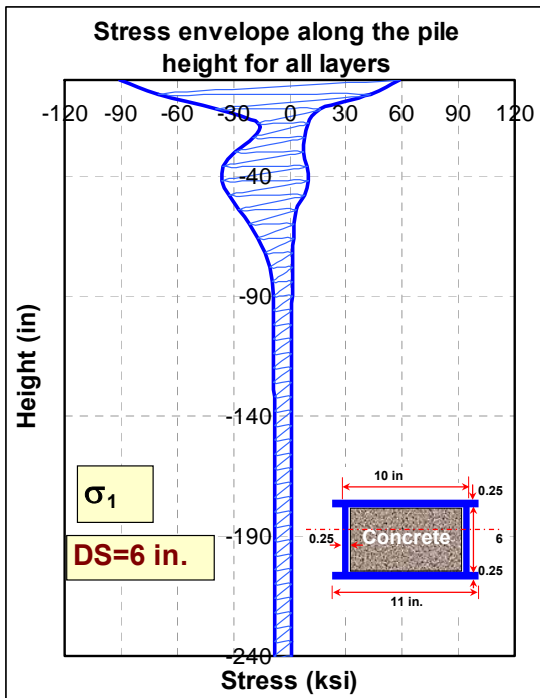
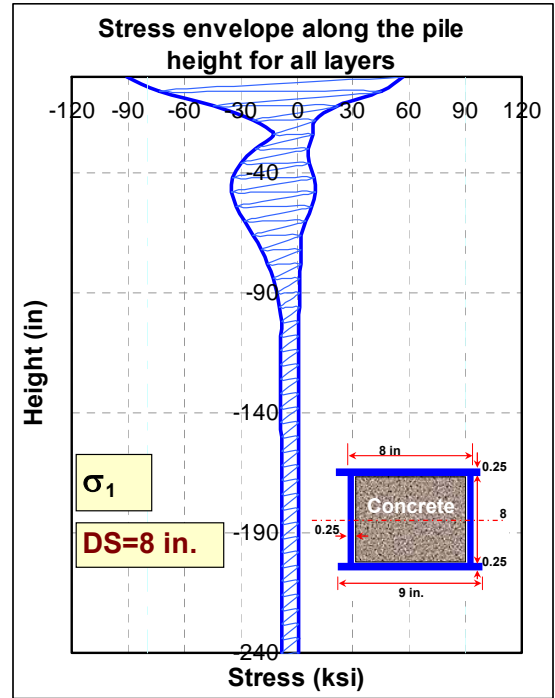
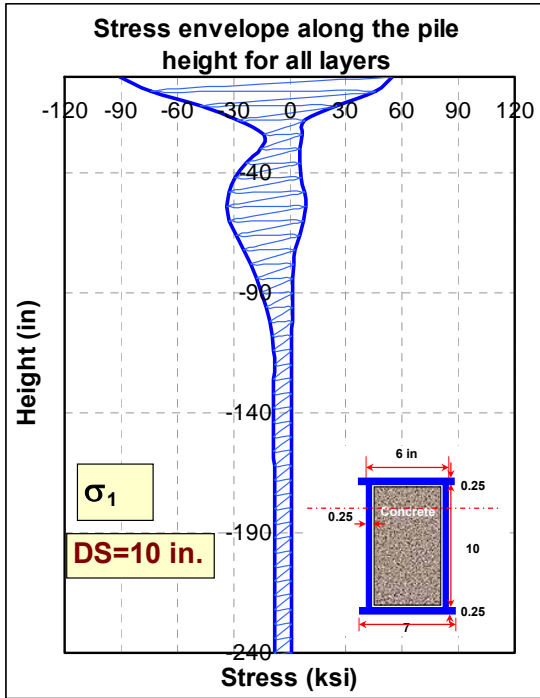


Figure 7-77: Stress envelopes for piles with different section geometries.

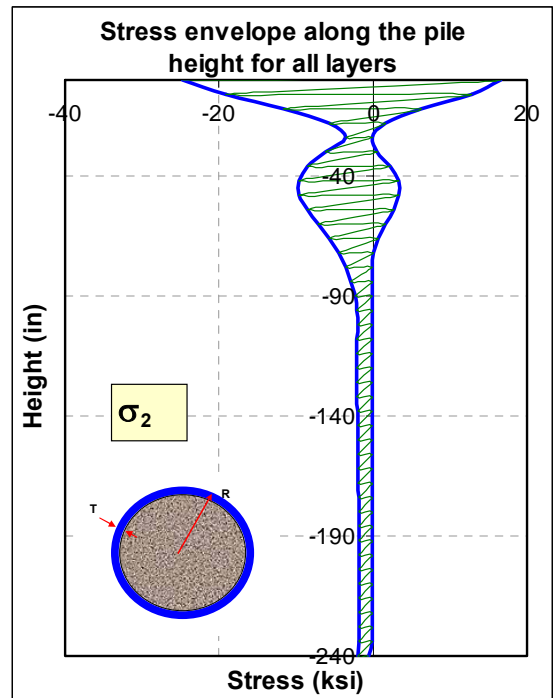
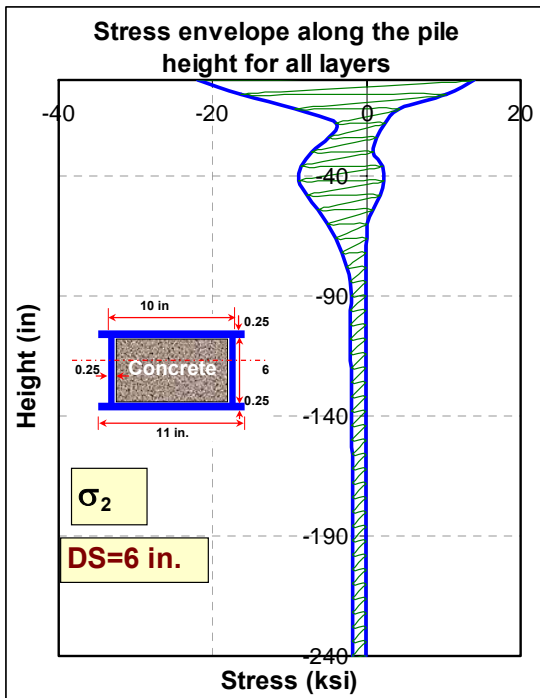
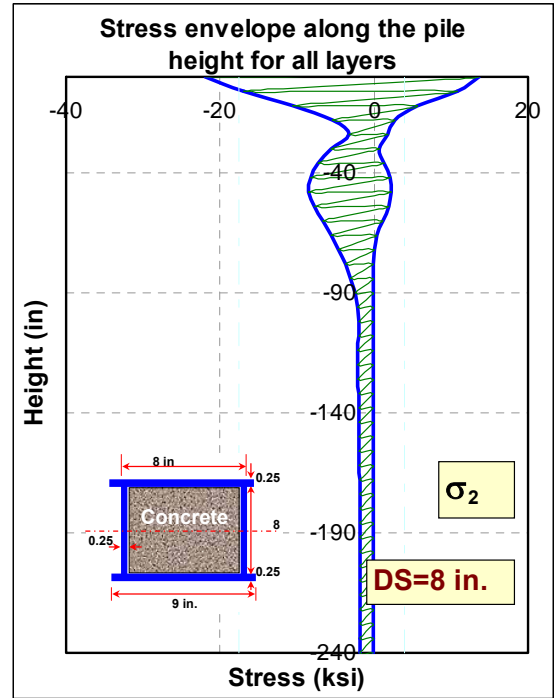
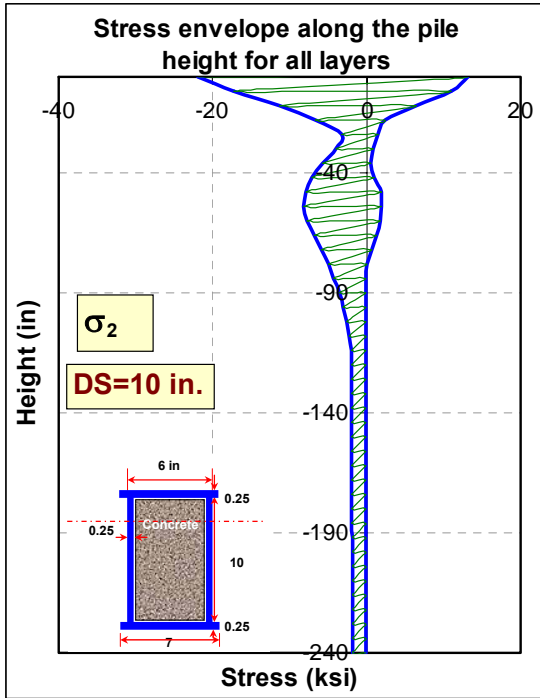


Figure 7-77: Stress envelopes for piles with different section geometries (cont'd).

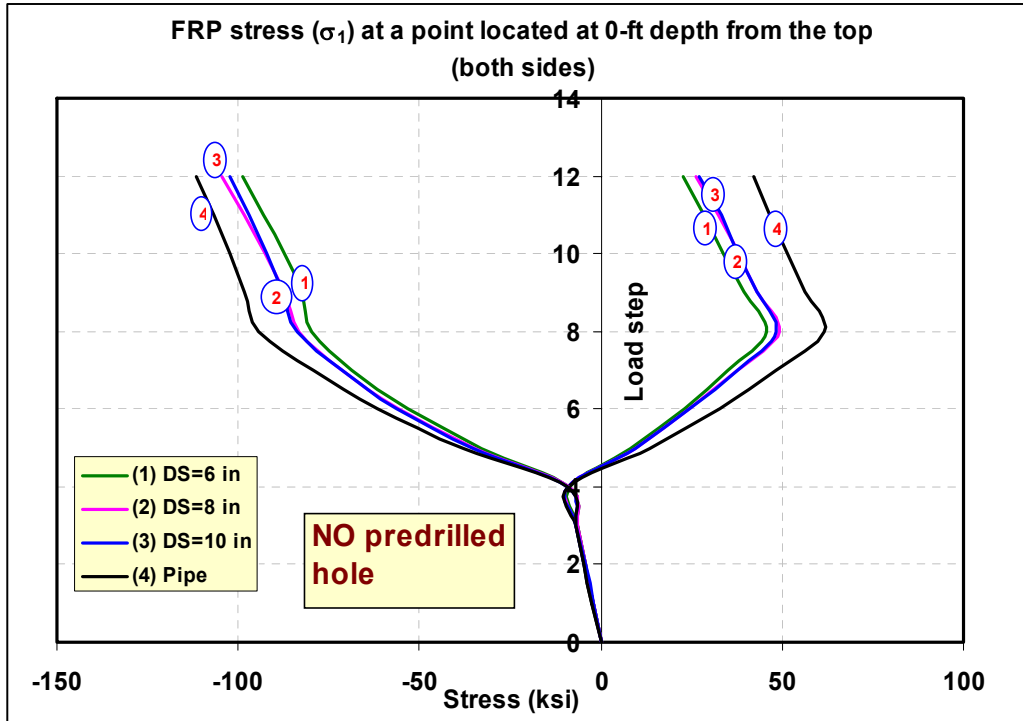


Figure 7-78: Stress variation at a point located at 0-ft from the top (0° - layer).

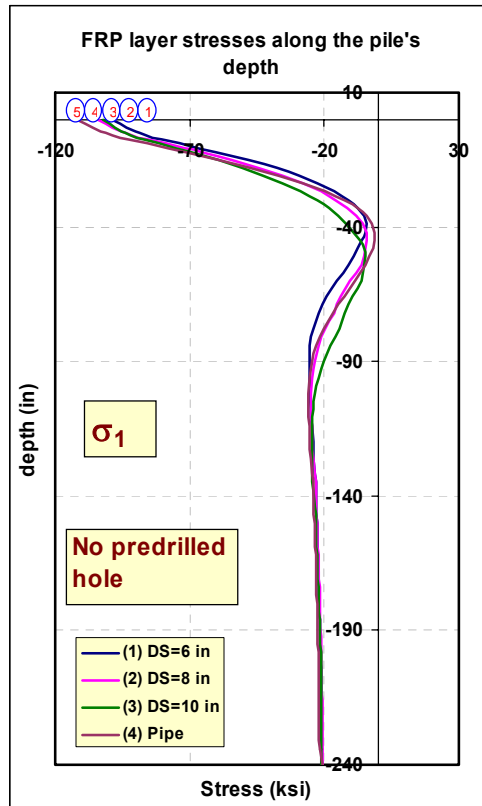


Figure 7-79: Stress variation along the pile's depth at the compression side.

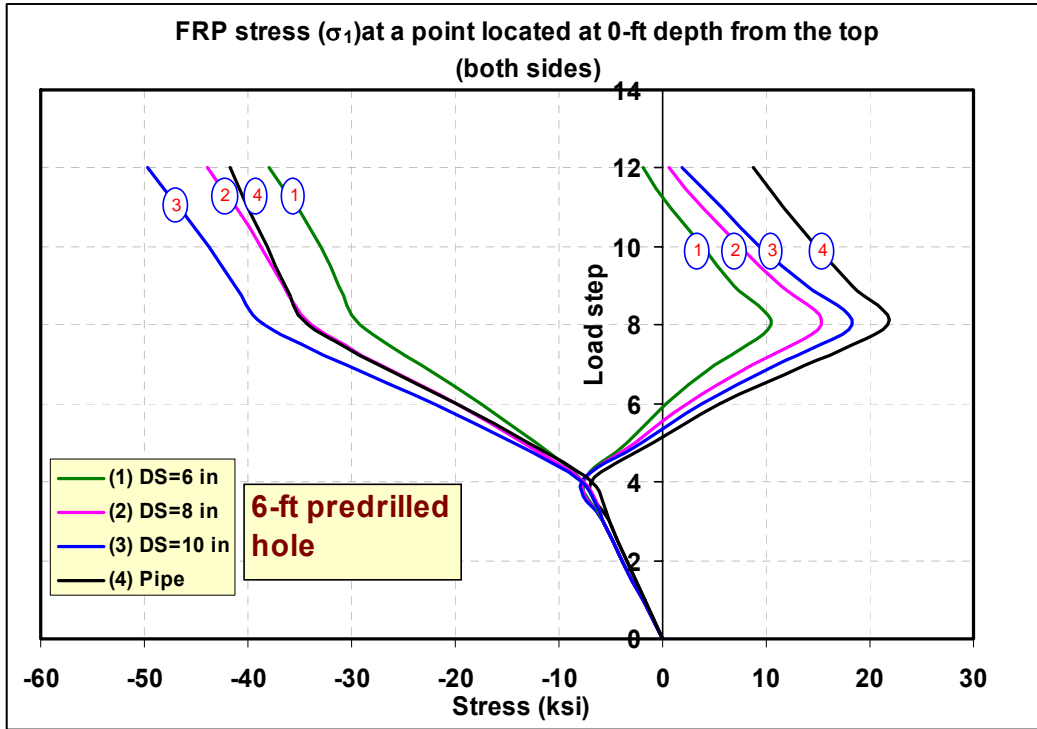


Figure 7-80: Stress variation at a point for located at 0-ft from the top (0° - layer).

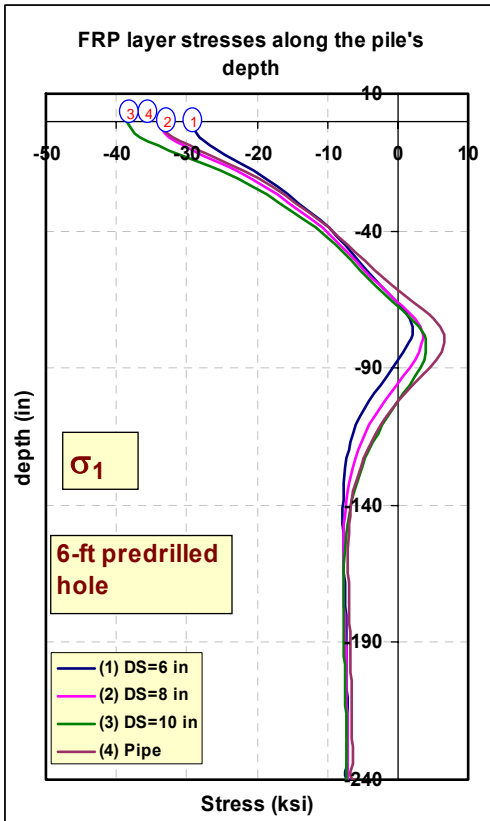


Figure 7-81: Stress variation along the pile's depth at the compression side.

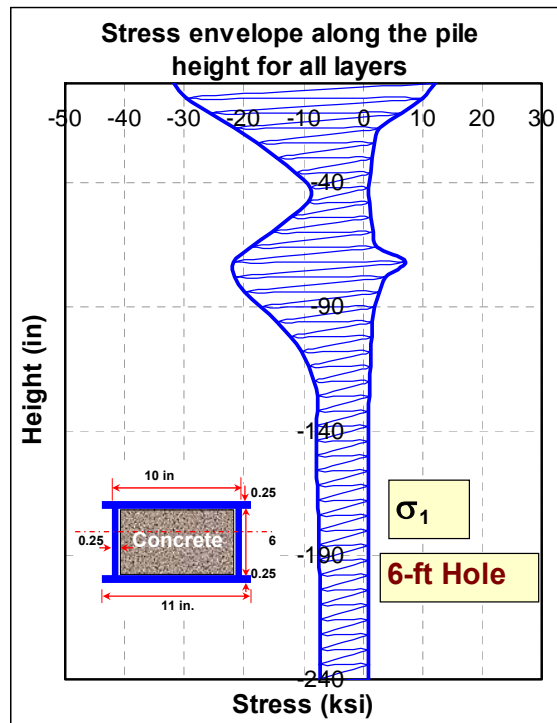
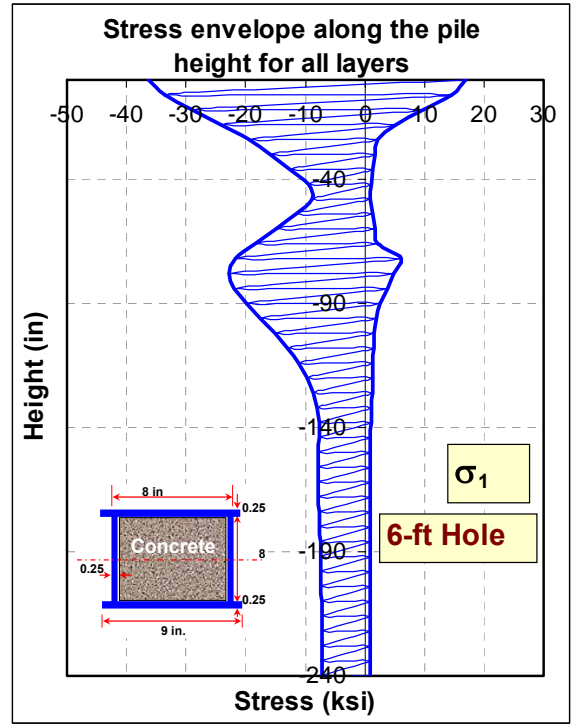
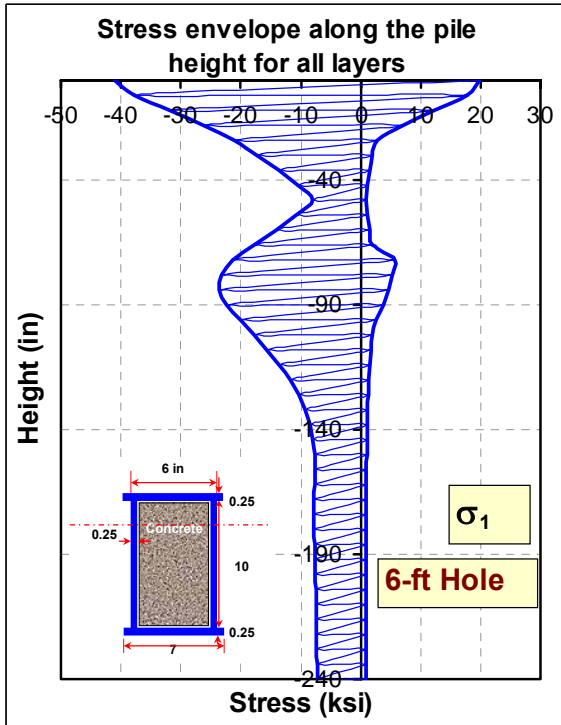


Figure 7-82: Stress envelopes for piles with different cross-sectional shapes and 6-ft predrilled hole.

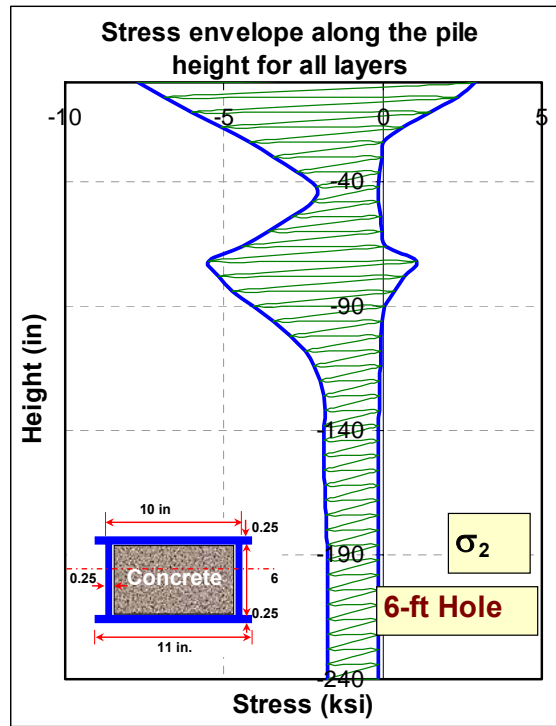
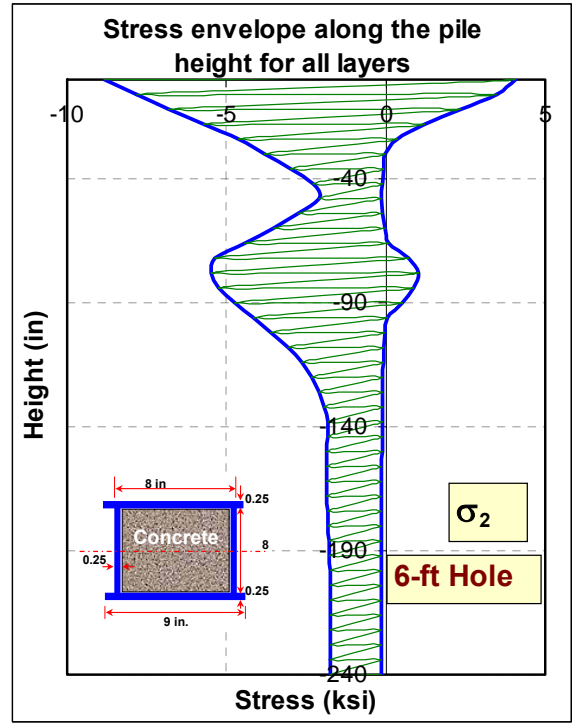
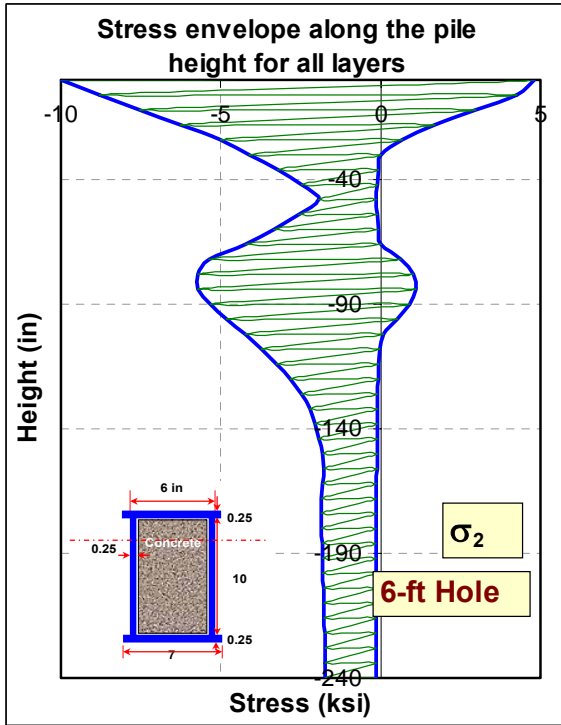


Figure 7-82: Stress envelopes for piles with different cross-sectional shapes and 6-ft predrilled hole (cont'd).

OPTIMIZATION OF COMPOSITE PILES

The goal of a designer is to get the best performance with the minimum cost for his design. There is always a continuous demand on design engineers to reduce production costs and raise efficiency to withstand the increasing market competitions. Optimization techniques have reached a remarkable point in the past few years with the continuous advancement in computers and computer programming. Optimization is a searching technique to find the best results under certain conditions. It is a process to find the conditions that give the maximum or minimum value of a function. The optimum seeking method is a part of *operation search* which is a branch of mathematics that usually is concerned with applying scientific method and techniques in decision making matters (Rao 1996). This method is also known as mathematical programming techniques.

8.1 COMPOSITE MATERIALS OPTIMIZATION

Optimization is a mathematical procedure by which the best configuration to fit certain requirements can be achieved. In structural design, optimization is needed to satisfy functional requirements such as strength and stiffness. Structural members can be configured for optimum strength and stiffness within the cost margin. The constituent

materials can be arranged or proportioned in a way such that the member will have higher performance.

Like other construction materials, composite materials also have the advantage of being optimized through different combinations of the constituent materials; fibers, resins and cores. They can be proportioned to produce sections with variable stiffness and strength. Another advantage of composites over isotropic materials is that strength and stiffness can also be optimized by changing the fiber architecture in the composite matrix. The fibers can be oriented such that they will provide the optimum section property in the desired direction. The properties of a composite are a function of its fiber content and direction. The stiffness and strength for composites can be maximized per unit weight. The mechanical properties in the fiber direction are different from those in the transverse direction. For a unidirectional layer, the longitudinal direction provides the highest strength and stiffness. Other direction properties can be improved by using multiple layers in different directions. A composite section may have multiple layers with different fiber orientations.

Many publications have pointed out that fiber composites may be designed for optimal performance by identifying the optimal laminate configuration. Onada (1985) tried to find the optimum laminate configuration for laminated cylindrical shells under axial compression. Based on his numerical results, he derived semi-empirically, his optimal laminate configuration. One of the best configurations that he found is [when an infinite number of layers are arranged so that the shell becomes quasi-isotropic in the shell surface and quasi-homogenous through the shell thickness. Nshanian (1983) proposed a method for optimal ply angle design through the thickness of symmetric

angle-ply shells of uniform thickness. He applied a special mathematical programming (MP) algorithm to determine the optimal ply angle. The ply angle distribution was approximated by means of continuous piecewise-linear functions or discontinuous piecewise-constant functions. His new configuration showed good results on maximizing buckling loads of thin shell structures.

Computational studies on optimizing laminated cylindrical shells for buckling using uni and multi-dimensional formulations has been reported by Smerdov (2000). He conducted a comparison on one, two and multi-dimensional optimization formulations for shells. Also he found that there is maximum buckling load to be reached after a certain number of layers of different orientation. Increasing the number of layers after that will not increase the buckling load.

It can be seen that composites have the potential to be optimized and manufactured to achieve certain structural requirements. A structural member can be custom designed to handle any structural behavior. The goal of the designer is to find the minimum number of layers and the ply orientation angles that will result in the best performance of the structure for the desired loading conditions.

8.2 ELEMENTS OF OPTIMIZATION PROBLEM

Optimization process in ANSYS utilizes three types of variables that characterize the design process: design variables, state variables, and the objective function. These variables are represented by scalar parameters in ANSYS Parametric Design language (APDL).

8.2.1 DESIGN VARIABLES

Design variables are those parameters that describe the design space of the system to be optimized. They are independent quantities which vary within defined intervals with a specified range of values. The intervals have an upper and lower limit to serve as constraints on the design variables. The vector of the design variables is defined by:

$$X = \begin{Bmatrix} x_1 \\ x_2 \\ \vdots \\ x_n \end{Bmatrix} \quad (8-1)$$

The upper and lower limits of the design constraints are:

$$\underline{x}_i \leq x_i \leq \overline{x}_i \quad (i = 1, 2, 3, \dots, n) \quad (8-2)$$

where: n is the number of design variables.

The design variable constraints are often referred to as side constraints and define what is commonly called feasible design space (Ansys5.7).

Now, minimize

$$f = f(x) \quad (8-3)$$

subject to

$$g_i(x) \leq \underline{g}_i \quad (i = 1, 2, 3, \dots, m_1) \quad (8-4)$$

$$h_i(x) \leq \underline{h}_i \quad (i = 1, 2, 3, \dots, m_2) \quad (8-5)$$

$$w_i(x) \leq \underline{w}_i \quad (i = 1, 2, 3, \dots, m_3) \quad (8-6)$$

where:

f = objective function

g_i, h_i, w_i = state variables containing the design, with underbars and overbars representing lower and upper bounds respectively.

$m_1+m_2+m_3$ = number of state variables constraints with various upper and lower limit values

8.2.2 DESIGN CONSTRAINTS

Design constraints which are referred by ANSYS as *state variables* are response quantities that constrain the design. They are dependent on the design variables and must have a defined minimum and maximum value.

8.2.3 OBJECTIVE FUNCTION

The objective function is the quantity that the designer is trying to minimize or maximize in the optimization processes.

8.3 DESIGN SETS

A *design set* is simply a unique set of parameter values that represents a particular model configuration. Typically, a design set is characterized by the optimization variable values; however, all model parameters (including those not identified as optimization variables) are included in the set (Ansys). The number of design sets for any optimization process is usually assigned in the optimization data file.

8.4 OPTIMAL LAMINATE CONFIGURATIONS

Laminate configurations have a great effect on the structural capacity of the composite element. For composite shells with layers of small thickness, the problem of searching for optimum structural configuration for maximum capacity is formulated as a problem of mathematical programming. In such problems, design parameters are usually the reinforcing angles of each individual layer in the laminate while the objective is to

maximize the section capacity and flexibility. Such an objective is distributed in a complicated manner in the multi-dimensional search space.

The following presentation deals with full size thin-walled composite piles consisting of several unidirectional layers with equal number of fibers in the $-\theta$ and $+\theta$ directions. All layers have the same thickness and are made of the same composite material. All angles are given in degrees which vary between 0 and 90° and measured from the pile axis.

As the number of layers increases, the number of variable parameters increases, which gives more space to search for optimum design. Increasing the dimensionality of the search space complicates the process and may not reach one unique solution. Results may show different angle combinations that lead to the same optimum design. For manufacturing simplifications, Zimmermann (1995) considered the optimization of the shells including only standard orientation angles, namely 0, -45, +45, and 90 degrees. This limited selection reduced the number of variables in the design space. He sought for optimum structures including from two to four different groups of the layers (axial, circumferential, and angle-ply).

8.5 FAILURE CRITERIA

Failure criteria are used to assess the possibility of failure of a material. This allows the consideration of orthotropic materials, which might be much weaker in one direction than another (ANSYS). In analyzing unidirectional layered composite structures, ANSYS considers the material properties of each layer to be orthotropic in the plane of the element. The material X-direction corresponds to the local layer x-direction. Failure criteria are used to learn if a layer has failed due to the applied loads. The criteria

are orthotropic, so the failure stress or failure strain values should be provided for all directions.

According to the maximum stress criterion, for a failure not to occur, all the following conditions have to be satisfied:

$$\begin{aligned} \sigma_1 &\leq X_t & \sigma_2 &\leq Y_t \\ \sigma_1 &\geq X_c & \sigma_2 &\geq Y_c \\ & & |\tau_{12}| &\leq S \end{aligned}$$

Where

σ_1 = Stress in the fiber direction

σ_2 = Stress perpendicular to the fiber direction

τ_{12} = Shear stress

X_t = Tensile strength in the fiber direction

X_c = Compressive strength in the fiber direction

Y_t = Tensile strength in the transverse direction

Y_c = Compressive strength in the transverse direction

S = Shear strength

This definition implies that the *stress ratios* should be maintained as follows for the failure not to occur:

$$\begin{aligned} \frac{\sigma_1}{X_t} &\leq 1 & \frac{\sigma_2}{Y_t} &\leq 1 \\ \frac{\sigma_1}{X_c} &\leq 1 & \frac{\sigma_2}{Y_c} &\leq 1 \end{aligned}$$

$$\frac{|\tau_{12}|}{S} \leq 1$$

Based on this, the stress ratio for all stresses in each layer should be maintained less than or equal to 1 to avoid layer failure. Through the analysis, the maximum stress ratio for all stresses in all layers will be considered the failure criterion of the structure.

8.6 OPTIMIZATION OF LAYER ORIENTATIONS

For laminated shells with layers of finite thickness, the process of searching for optimum structures for a desired behavior can be formulated as a problem of mathematical programming. Consider a laminate with a fixed total given thickness T . In such a problem, the variable parameters are usually the reinforcing angles of the individual layers while the objective function is maximum load capacity. Such an objective function is distributed in a complicated manner in the multi-dimensional search space and it may end with many extreme values. Formulation of such an optimization problem leads to many difficulties. The multi-dimensional search space can not be studied in detail. To minimize the dimensionality of the search space (the number of variable parameters) uni-dimensional optimization can be utilized in which a single parameter will be variable and the rest will be assigned fixed values. This approach in optimization will not be accurate enough to give the best design set of parameters because only one layer will be assigned a variable and the rest will be assigned fixed values. The difficulty here will be in picking the right values for the fixed parameters especially when there are multiple layers in the pile shell.

8.6.1 OPTIMIZATION OF THE HOLLOW DOUBLE-WEB PILE

In this model the pile is made of carbon epoxy composite and is assumed to be hollow. It is subjected to axial load then followed by lateral deformation at the abutment location. The combination of the axial and bending stresses will cause the pile to develop different types of stresses which mainly include: compression, tension, and shear stresses. Excess of any of these stresses above the allowable criteria will cause the pile to fail according to the “first layer failure” approach. The objective here is to arrange the fibers in each layer so that the resulting stresses will be at a minimum.

For the optimization process, the fiber orientation angles are considered as design variables (DVs), the failure criteria for the different types of stresses are considered the state variables (SV's), and the axial deformation which has to be minimum is set as the objective function (OBJ).

The composite pile properties including the shell total thickness will be kept fixed over the whole process. The number of layers will be changed to increase the number of parameters in the design space.

$$\text{Layer thickness} = \frac{T}{NL}$$

Where

T: is the total thickness of the composite shell

NL: is the number of layers in the shell

Piles information:

Composite type: Carbon epoxy

Property	ksi	Property	ksi
E_x	20500	X_t	330
E_y	1500	Y_t	8.3
G_{xy}	1040	X_c	-209
V_{xy}	0.28	Y_c	-33
		S	10.3

Number of layers: variable [NL= 2 up to 12]

Layer thickness: 0.2 in./NL

Laminate structure:[to be determined by optimization]

Filling: Hollow

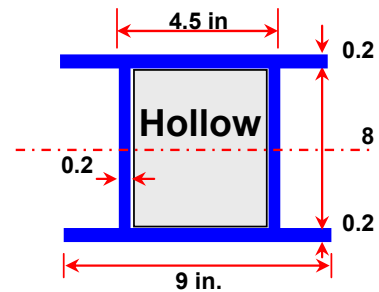
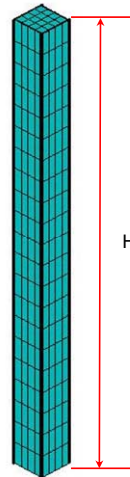
Height = 20 ft

Soil type: dense sand

Loading:

Axial dead load: 200 kips [step 1]

Lateral displacement: 2 inches [step 2]



2-Layer Optimization

The simplest form of layer lay-up of the form $[\theta, -\theta]$ configuration is a 2-layer laminate composite shell. This is a case of uni-dimensional optimization with no fixed angles. Instead, both angles are variables. The laminate will be designed for minimal stresses and minimal axial deformations. As discussed in section 8.5, all stress values should remain within the allowable limits (failure criteria) such that the stress ratios are always equal to or less than 1. During the optimization process, the fibers' orientations (DVs) will continue to change until the objective function is satisfied. The optimization process usually produces many output sets, each of which has new values of the objective function based on the change in the design variables. Figure 8-1 shows a plot of the variation of stress ratio values with fiber orientation angle θ . The curve shows two extremes: a minimum value close to 10 degrees and a maximum value located between 50 and 60 degrees. The maximum value indicates that the stress values at certain locations in the composite shell are very high compared to limits provided by the failure criteria. The values in the curve may represent any of the six stress values indicated earlier in this chapter.

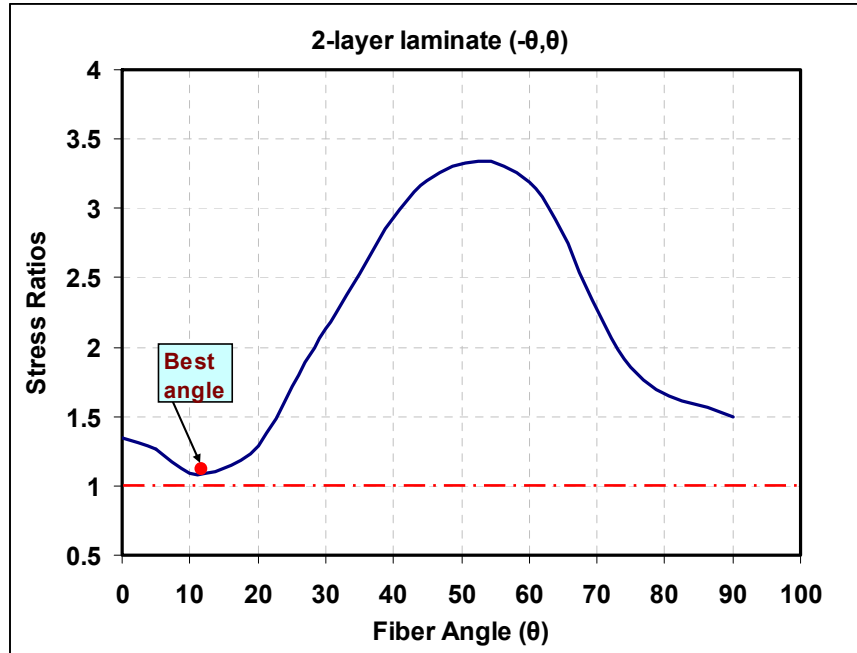


Figure 8-1: Variation of stress ratios with the fiber angles for a 2-layer laminate (1-variable).

4-Layer Optimization

The second step in this process is to use a 4-layer composite laminate with the following laminate structure: $[0, \theta, -\theta, 0]$. In this case the two outer layers were assigned fixed and the inner two layers were variables. The fibers in the two outer layers were set to 0 degrees such that they align with the pile axis for maximum axial and bending strength as well as stiffness. The inner two layers were allowed to vary between 0 and 90 degrees searching for the lowest stress ratios. As can be seen from Figure 8-2 the fiber angle that gave the lowest stress with the combination of the existing 0-degree layers was around 75 degrees. Other angle combinations are also shown in Figure 8-3 and Figure 8-4 in which the outer layers of the pile shell are assigned fixed to a specific orientation, θ_1 and the interior layers, θ_2 are varying between 0 and 90 degrees. As can be seen, the best

results were with those layers that have orientation angles that range between (0 to 20) degrees and (70 to 90) degrees.

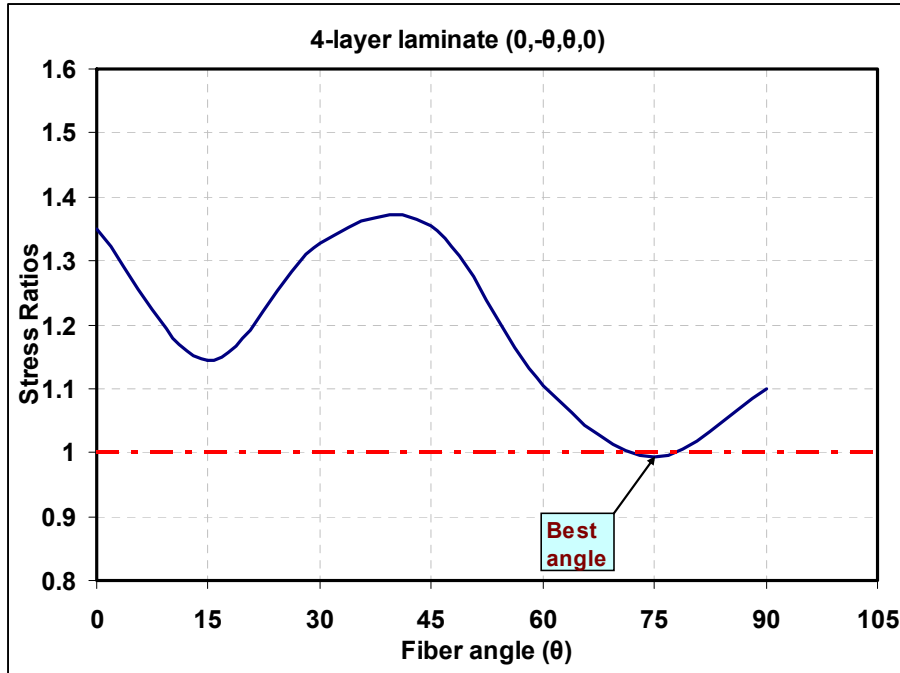


Figure 8-2: Variation of stress ratios with the fiber angles for a 4-layer laminate (1-variable).

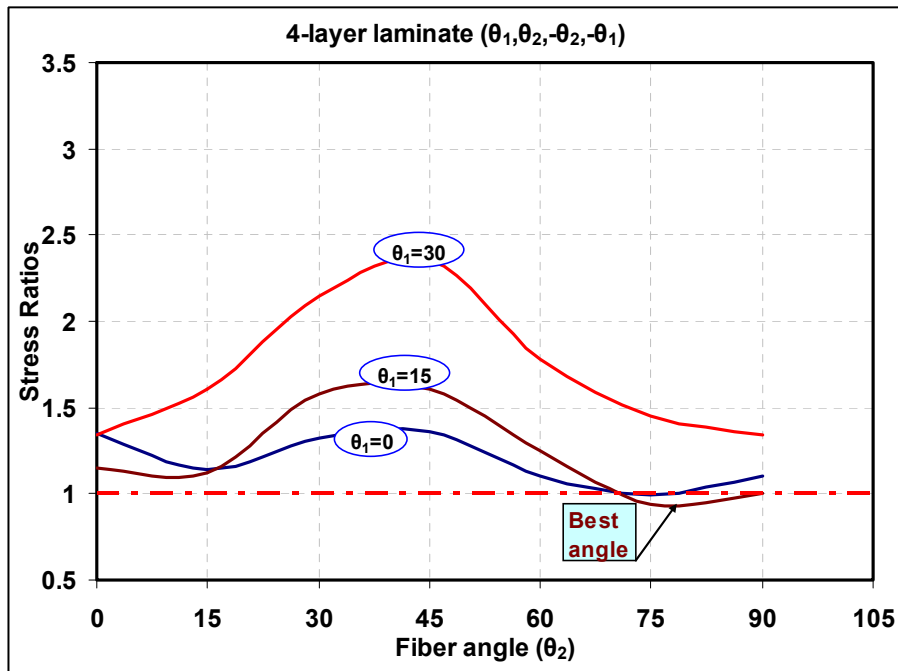


Figure 8-3: Variation of stress ratios with the fiber angle for a 4-layer laminate (2-variables).

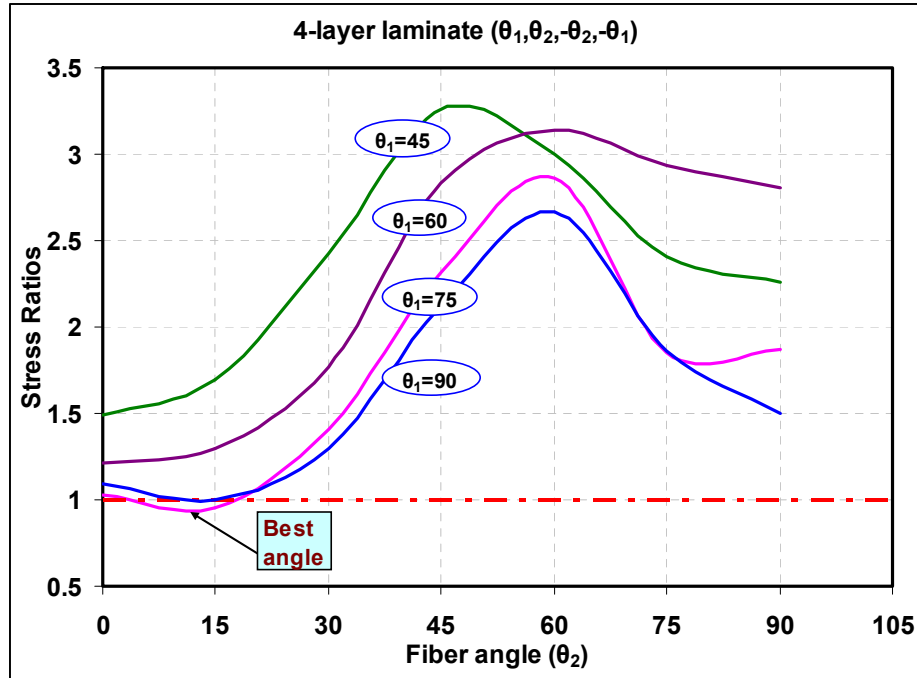


Figure 8-4: Variation of stress ratios with the fiber angles for a 4-layer laminate (2-variables).

6-Layer Optimization

For the 6-layer laminate, one, two and three variable optimization processes were performed. In the first run, the outer layers were set to 0-degrees, the intermediate layers were set to 90-degree and the inner two layers were allowed to vary from 0 to 90-degrees. As can be seen in Figure 8-5, the variable angle was found to be very close to 20-degrees. The best layer lay-up for this optimization loop was found to be the [0,90,-20,20,90,0] structure.

In the second run, the outer two layers were set to 0-degrees and the inner four layers were set to vary between 0 and 90 degrees. The variation of stress ratios with the angle θ for the two variable angles is shown in Figure 8-6. As can be seen from the figure, the best layer lay-up was found to be the [0,-88,-20,20,88,0] structure.

The last run was with all three orientation angles for the 6-layer shell set to vary from 0 to 90-degrees. The best layer lay-up was found to be in the form: [-86,-14,-16,16,14,86] structure. The variation of the stress ratios with the three orientation angles is shown in Figure 8-7.

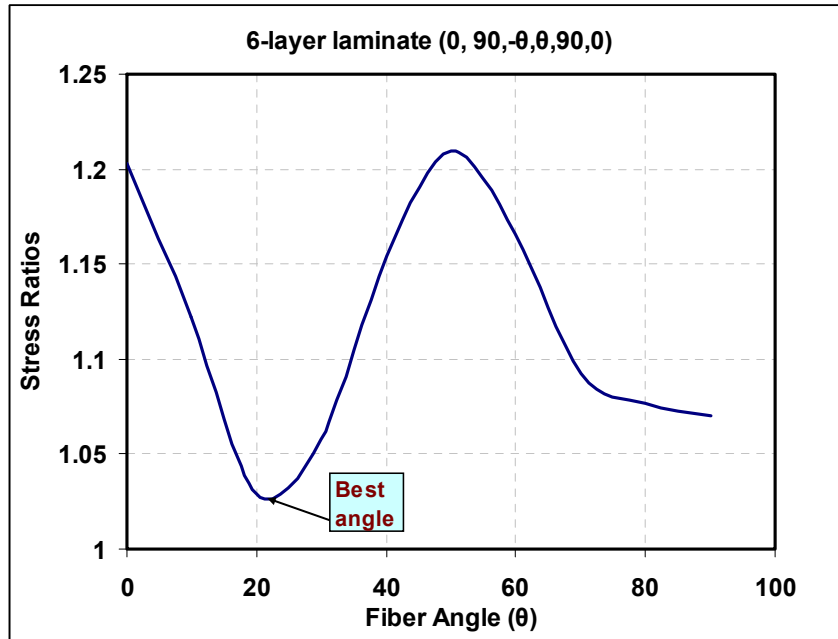


Figure 8-5: Variation of stress ratios with the fiber angles for a 6-layer laminate (1-variable).

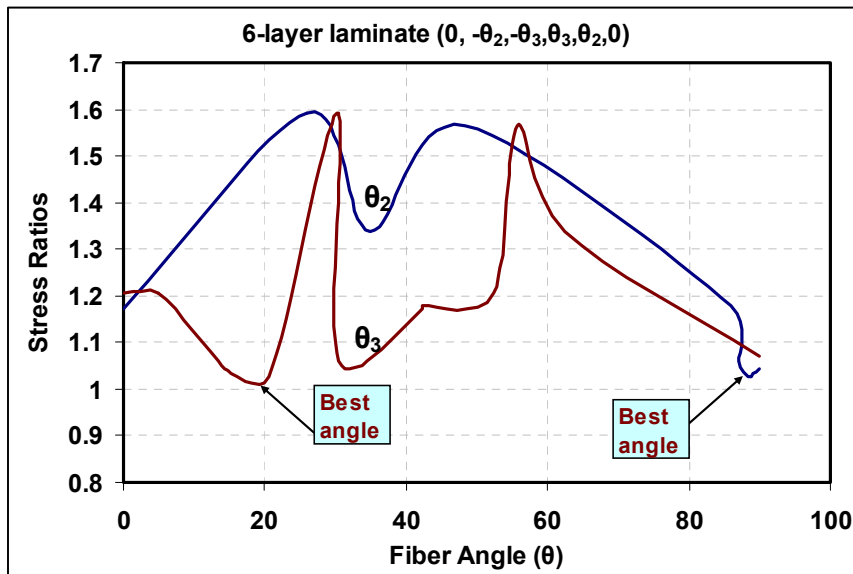


Figure 8-6: Variation of stress ratios with the fiber angles for a 6-layer laminate (2-variables).

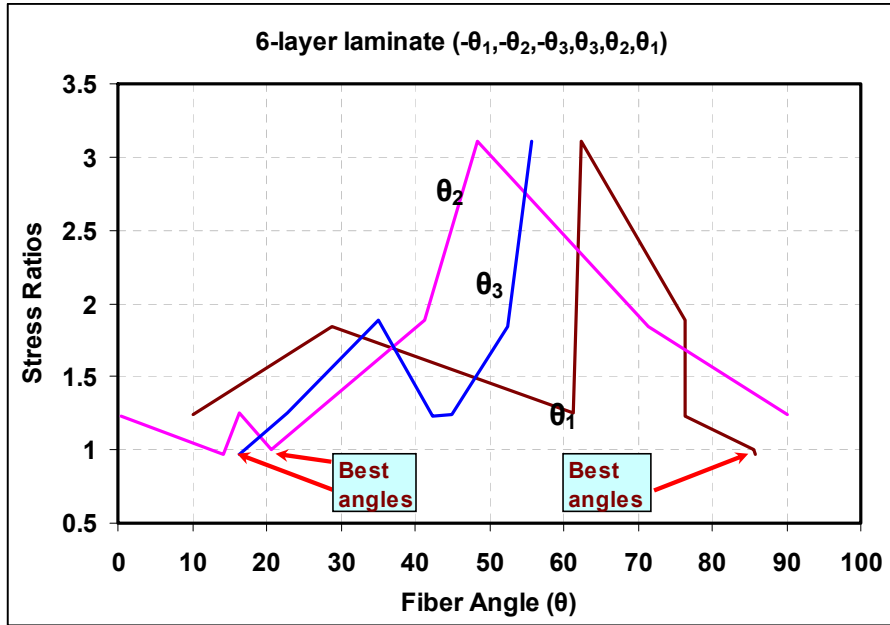


Figure 8-7: Variation of stress ratios with the fiber angles for a 6-layer laminate (3-variables).

8-Layer Optimization

Several optimization runs were performed for an 8-layer laminate. The four orientation angles were also used as the design variables. The first run was with a single variable and the other three were assigned fixed. The second run was with two variables, the third with three variables and the last run was with all four orientation angles were assigned variables.

Figure 8-8 shows the graph for the first case in which the layers lay-up has the $[0,90,30,-\theta_4,\theta_4,-30,90,0]$ structure. The orientation angle for the inner two layers ($-\theta_4,\theta_4$) was allowed to vary between 0 and 90 degrees. The minimum stress ratio obtained for this case was at $\theta_4=0$, but it was greater than 1 which means that the stresses in some layers were above the allowable limit. The second case has the $[0,90,-\theta_3,-\theta_4,\theta_4,\theta_3,90,0]$ structure with the inner four layers allowed to vary between 0 and 90 degrees.

Figure 8-9 shows the variation of stress ratios with respect to the layers' orientations. The best angle lay-up was found to be in the following structure: [0,90,0,-35,35,0,90,0]. The third case was of the $[0, -\theta_2, -\theta_3, -\theta_4, \theta_4, \theta_3, \theta_2, 0]$ structure in which three variables were used to search for the best orientations. Figure 8-10 shows the variation of the stress ratios with the angles' orientations for the three variables. The best layer lay-up was found to be of the [0,-76,90,-15,15,90,76,0] structure.

The last case was performed with the orientations of the 8 layers varying during the optimization process, allowing for maximum flexibility in the search for the best lay-up. The best layer lay-up was of the [-77,-89,-13,-5,5,13,89,77] structure. The variation of the angles versus the stress ratios for the four variables is illustrated in Figure 8-11 .

Figure 8-12 shows the stress envelopes of the three major stress components for some selected sets of the 8-layer optimization results, including the best set. As can be seen in sets 1 and 4, the shear stresses exceeded the allowable limits, while in set 16 all stresses were within the allowable limits, a condition which is already defined in each graph.

Figure 8-13 shows the maximum stress ratios for all FRP elements in the pile for some selected optimization sets. It can be seen that the optimization process was able to reach an optimum configuration for the layers orientation angles that satisfies the design requirements.

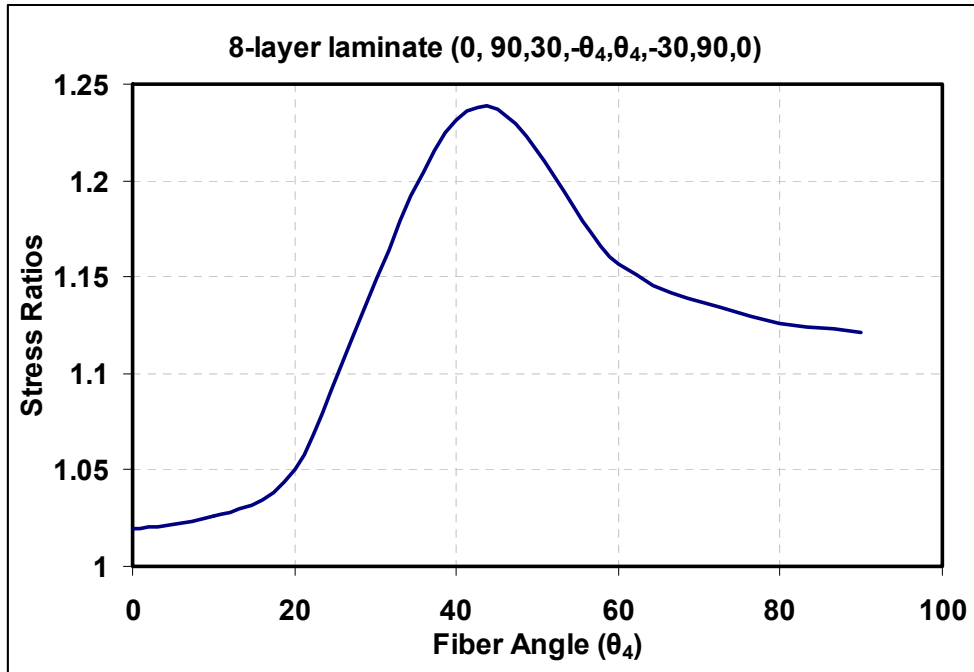


Figure 8-8: Variation of stress ratios with the fiber angles for an 8-layer laminate (1-variable).

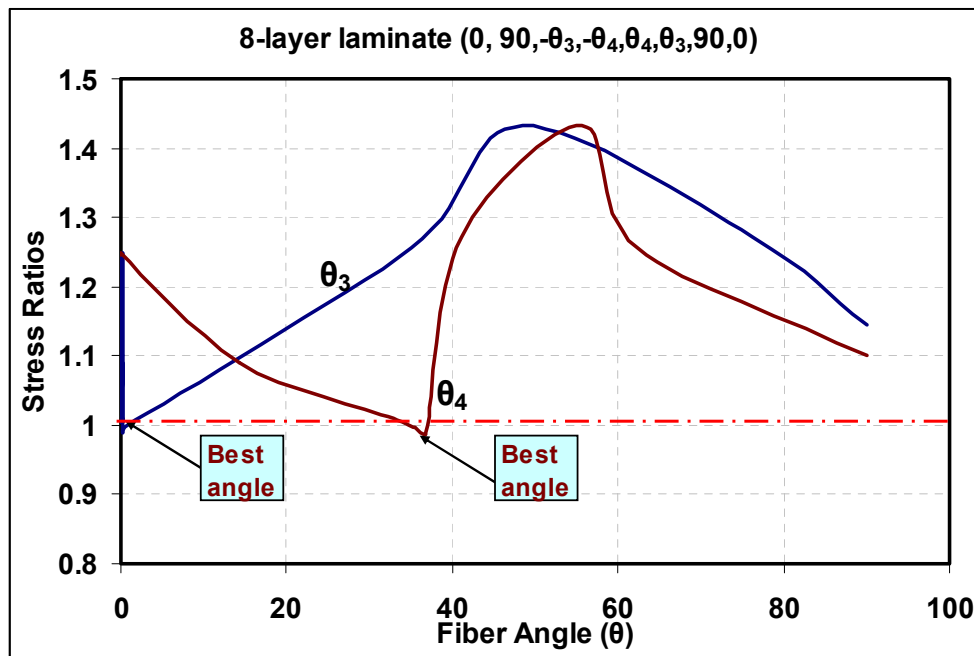


Figure 8-9: Variation of stress ratios with the fiber angles for an 8-layer laminate (2-variables).

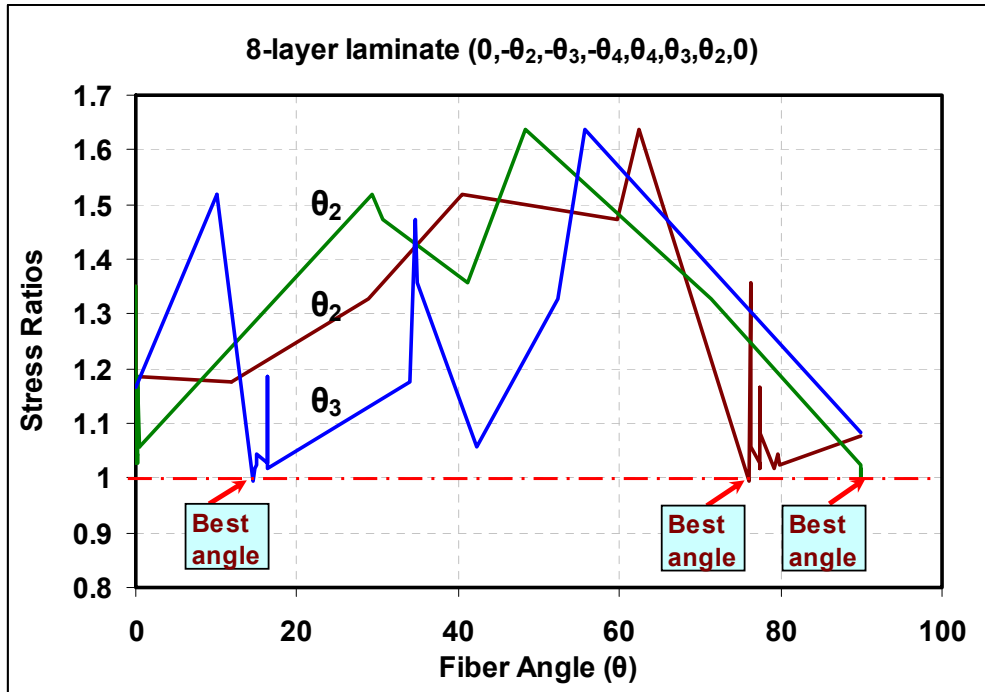


Figure 8-10: Variation of stress ratios with the fiber angle for an 8-layer laminate (3-variables).

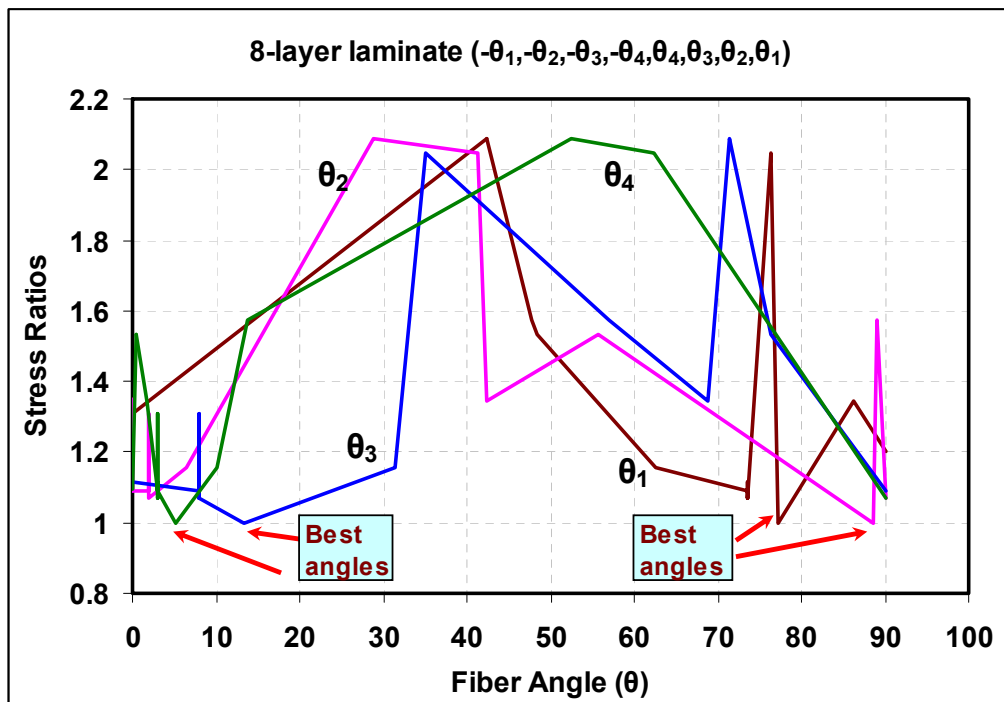


Figure 8-11: Variation of stress ratios with the fiber angles for an 8-layer laminate (4-variables).

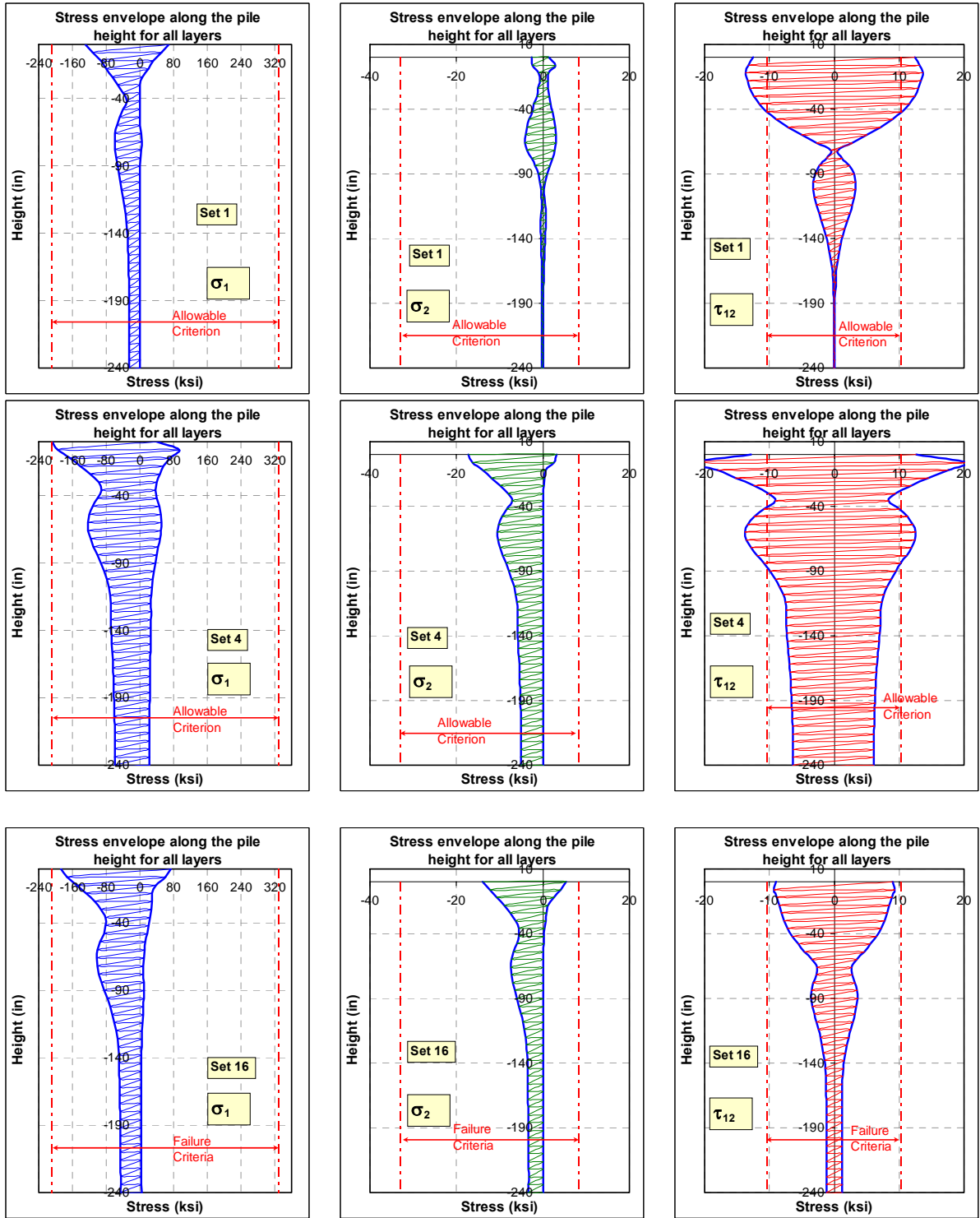


Figure 8-12: Effect of layer-orientation's optimization on pile stresses.

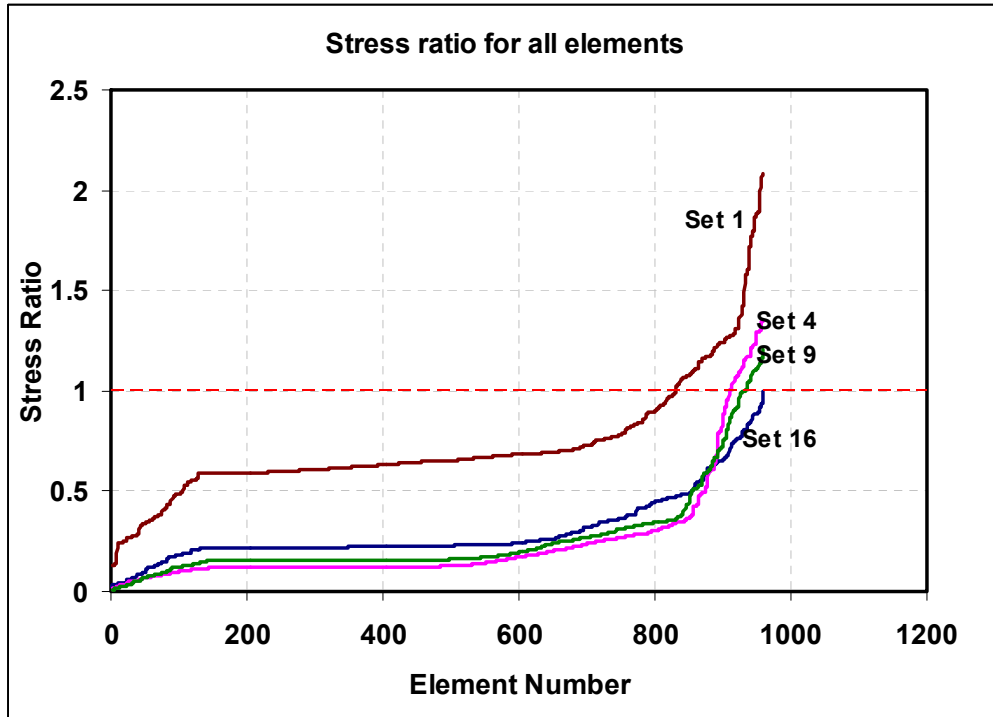


Figure 8-13: Variation of element stresses during optimization.

12-Layer Optimization

To study the effect of the number of layers on the optimization process, the same pile was analyzed using a 12-layer composite shell of the $[-\theta, \theta]_6$ structure. All layer orientations were allowed to vary between 0 and 90 degrees during the optimization process. After several optimization loops, the best set of angles was found to be of the $[-14, 90, 0, -12, -76, -14, 14, 76, 12, 0, 90, 14]$ structure. The variation of stress ratios versus the orientation angles is shown in Figure 8-14. As can be seen, the figure gets very congested as the number of variables increases which makes the graphic representation of such processes not very clear.

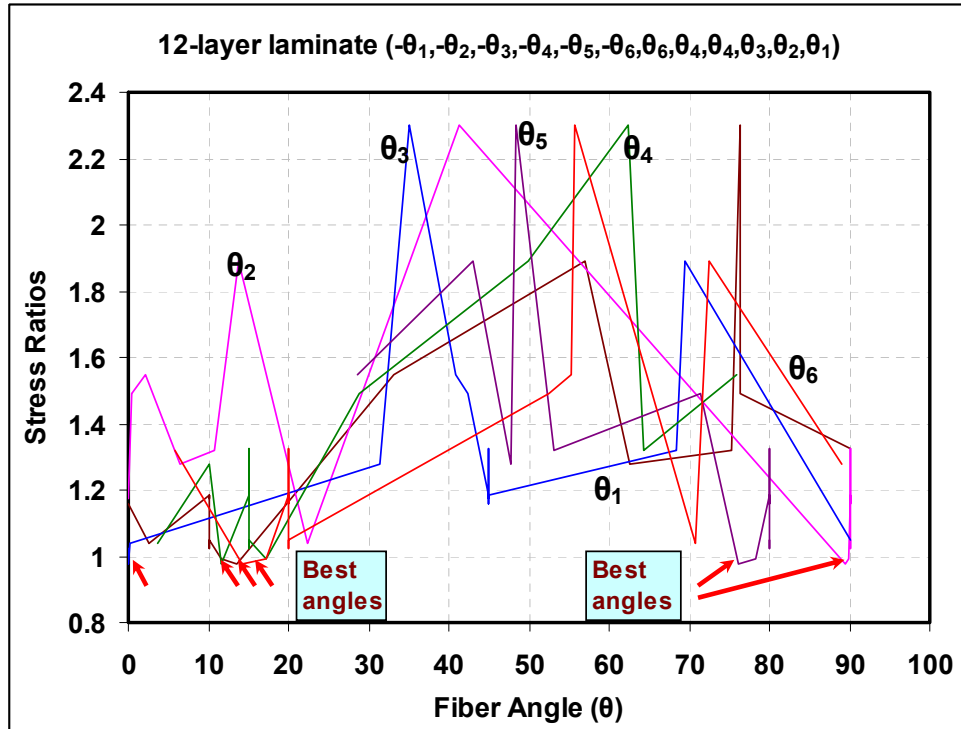


Figure 8-14: Variation of stress ratios with the fiber angles for a 12-layer laminate (6-variables).

In this optimization process, several configurations were used trying to reach the best and fastest optimization approach to satisfy our goals. The 2-layer approach did not give good results because the number of variables was limited to 1. In the 4-layer approach, several runs were performed trying to reach the best laminate structure. The 4-layer approach gave better results than those of the 2-layer approach. As the number of variable increased, the search for the best design set got more complicated and time consuming. Each variable was searching in a complex manner within a wide domain. The sensitivity of the optimum design to the variations of the reinforcing angles decreased as the number of layers exceeded 4 layers. Similar results were obtained for 4, 6, 8, and 12-layer optimizations. Results collected from the different approaches showed similar patterns in which orientation angles for the reinforcing fibers were found in the [0 to 20]

and [70 to 90] degrees intervals. It can be concluded that optimum solutions can be found among the fiber architecture composed of axial and hoop reinforcing angles.

8.7 OPTIMIZATION OF THE SECTION GEOMETRY FOR MINIMUM STRESSES

Rectangular sections have advantages over circular sections in that their dimensions can be proportioned to obtain a specific moment of inertia while maintaining a fixed cross-sectional area. These advantages give flexibility to the designer to optimize the pile cross-section for best performance of the desired properties.

In this section, the design variables are the section's dimensions; DS , $DS2$, DZI and the concrete filling area A_c . The FRP stresses were set as the design constraints (the state variables) such that the stresses should not exceed the allowable limits. The pile vertical deformations were set as the objective function. The rest of the parameters were not changed. The pile was assumed to be in a dense sand environment.

In this optimization process, the goal was to minimize the pile's flexural rigidity through the cross-section geometry and the size of the concrete filling. The size of the FRP shell and the configuration of the layers lay-up were assigned fixed to reduce the number of the design variables. The design variables were allowed to vary within a limited domain so that the pile cross-sectional dimensions remain reasonable. Also the size of the concrete filling was allowed to vary within a limited range during the optimization to maintain a minimum size that satisfies the objective function.

Figure 8-15 shows a group of curves that represent the maximum stress ratios for the pile as the geometry and the concrete volume changes during the optimization process. As can be seen, the stress ratios were more than 1.0 in all curves except for set 7

in which the stresses were reduced to fall within the allowable ratio. This set can be considered as the best design set.

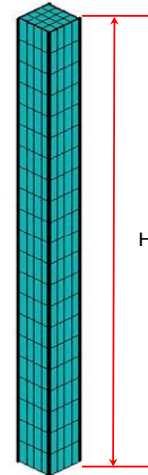
The cross-section that satisfied the best design had a width-to-height ratio greater than 2.0 as shown in set 7 graph of Figure 8-15. The cross-sections with width-to-height ratios less than 2.0 showed higher stress ratios, exceeding the allowable criteria.

However, these results can not be generalized to include every FRP concrete-filled pile in an integral abutment bridge. The pile behaviors are not unique and are usually depending on many factors already discussed in the previous chapter. The soil profile is the factor that has the most influence on the pile behaviors. The term soil-pile is used to describe the pile behaviors because the pile is one part of the soil-pile system and the soil is the other part.

Pile information:

Composite type: Glass epoxy

Property	ksi	Property	ksi
E_x	4500	X_t	90
E_y	1100	Y_t	3.9
G_{xy}	550	X_c	-80
V_{xy}	0.26	Y_c	-17.5
		S	6.2



Number of layers: 8

Shell thickness: $T_1=T_2=0.3$ in.

FRP volume: [assigned to be fixed]

Concrete volume: [variable]

Layer thickness: 0.025 in.

Laminate structure:[0,0,90,90,0,0,0,0]

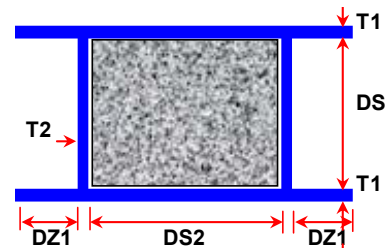
Filling: Plain concrete $f_c'=3$ ksi

Height = 20 ft

Soil type: Dense Sand

Axial dead load: $P=300$ kips [step 1]

Lateral displacement: 2 in. [steps 2 to 3]



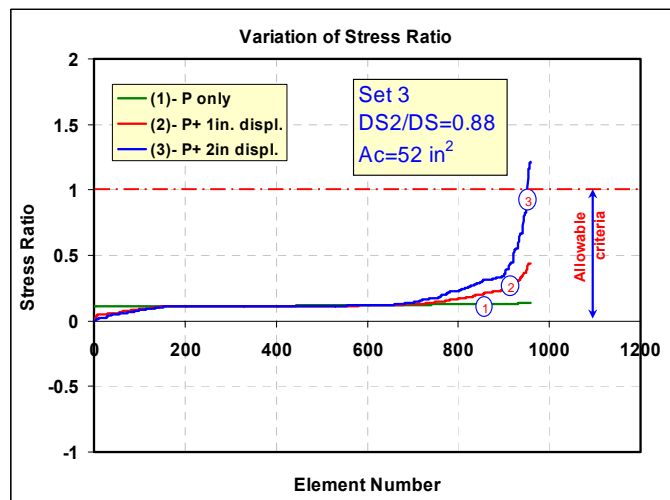
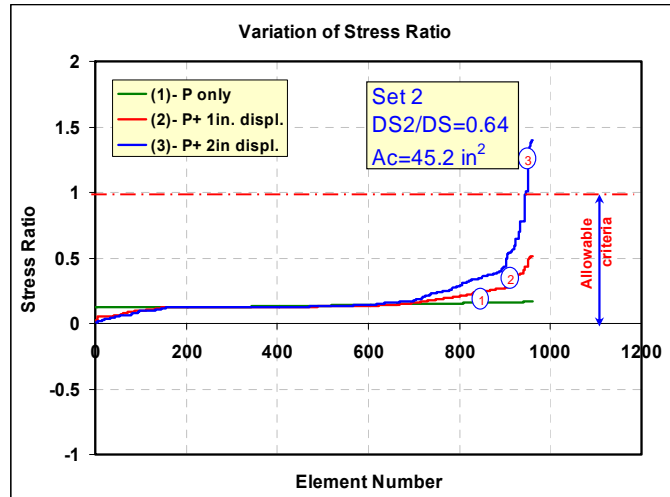
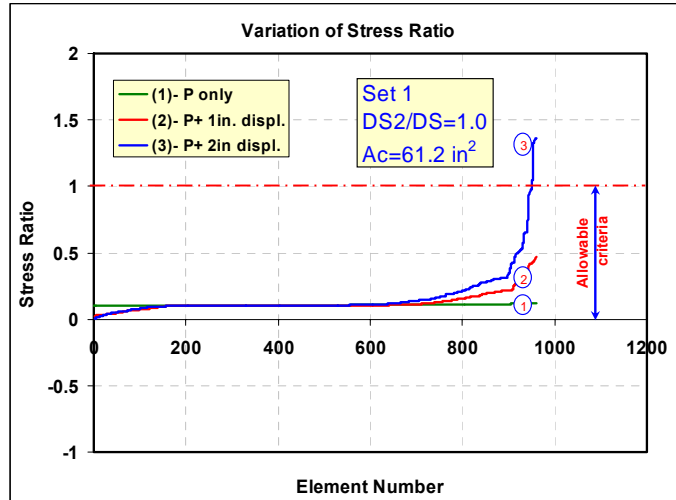


Figure 8-15: Effect of section geometry and concrete filling size on stresses developed after lateral displacements.

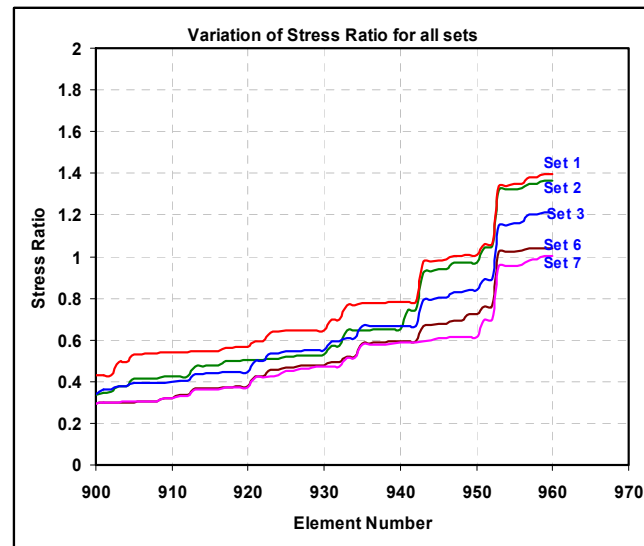
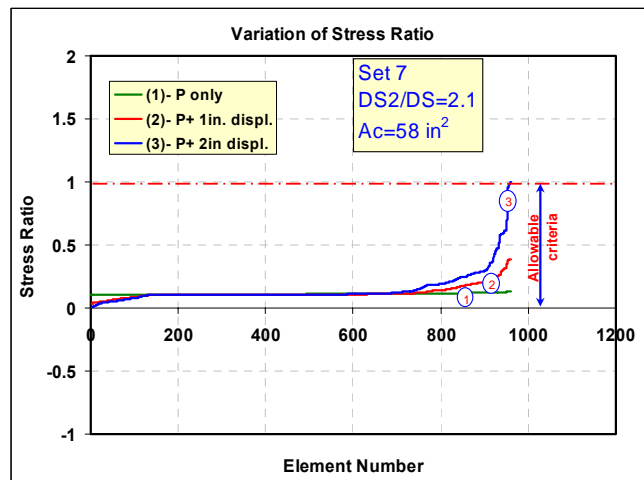
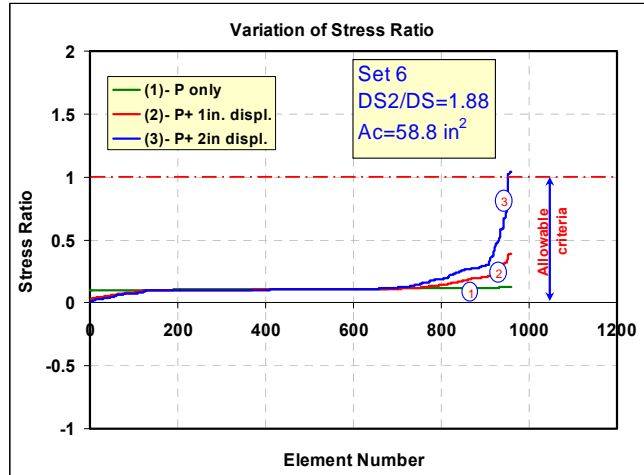


Figure 8-15: Effect of section geometry and concrete filling size on stresses developed after lateral displacements. (cont'd).

8.8 OPTIMIZATION OF THE PILE SECTION FOR BEST AXIAL LOAD

Effect of the Dead Load on the Behavior of FRP Concrete Filled Piles

The sequence of load application on an integral bridge pile has a dramatic effect on the resulting stresses after the lateral deformations. This is caused by the bridge deck expansion or contraction. The dead loads are permanent and they will be active as soon as the super structure is installed. This load will keep the pile under constant and permanent axial compressive stresses.

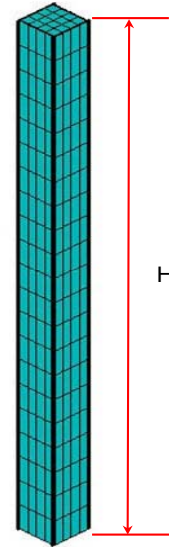
As soon as a significant change in temperature occurs, the pile head will experience a lateral deformation as a result of the expansion or contraction. This deformation will develop bending moments at the pile head and will increase as the temperature increases. Since the pile is initially stressed in compression, the application of bending moment will cause additional compressive stresses at some portions of the pile section and a reduction in the compressive stresses at the rest of the pile section as described earlier in section 7.3. Based on this, the pile should be designed such that the total stresses at any point after all loads application are within the allowable criteria

Figure 8-16 and Figure 8-17 show a group of curves that represent the maximum stress ratios for all FRP elements in a pile subjected to dead load and lateral deformation respectively. The pile was assumed to be in a dense sand environment and subjected to an axial load then followed by lateral deformations. The load was increased from 0 kips up to 500 kips and all stress results were recorded. As can be seen in Figure 8-16 and, Figure 8-17, the pile shell experienced higher stresses at smaller dead loads. As the dead load increased, the stresses started to get lower up to a certain value of loading then started to increase again.

Pile information:

Composite type: Glass epoxy

Property	ksi	Property	ksi
E_x	4500	X_t	90
E_y	1100	Y_t	3.9
G_{xy}	550	X_c	-80
V_{xy}		Y_c	-17.5
		S	6.2



Number of layers: 8

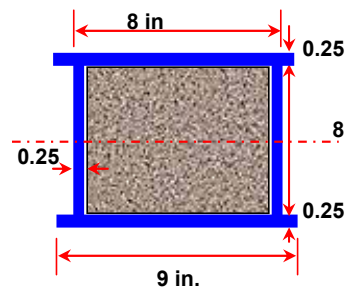
Layer thickness: 0.0314 in.

Laminate structure:[11, -11, 65, -65, 21, -21, 66, -66]

Filling: Plain concrete $f_c'=3$ ksi

Height = 20 ft

Soil type: Dense sand



Loading:

Axial dead load: [0 to 500] kips [step 1]

Lateral displacement: 2 in. [steps 2 to 3]

The graphs for the 300 kips dead load showed the least stress values among other loads. This concludes that the pile has an optimum value of dead load to be applied so that the pile stresses will be minimal. Figure 8-17 shows a comparison for the peaks in all load cases. The case with the 300 kips dead load appears to have the lowest stress values.

Figure 8-18 includes a set of stress envelopes for all load cases for comparison purposes. The curves show the variation of the 3 stress components; σ_1 , σ_2 , and τ_{12} as the axial load changes. This concludes that an increase in the axial dead load does not always lead to an increase in stresses. In this case which includes a combination of axial compression and bending, the stresses reached their optimum at a certain value of axial load. Any change to this value, either increase or decrease, will lead to an increase in the stress values.

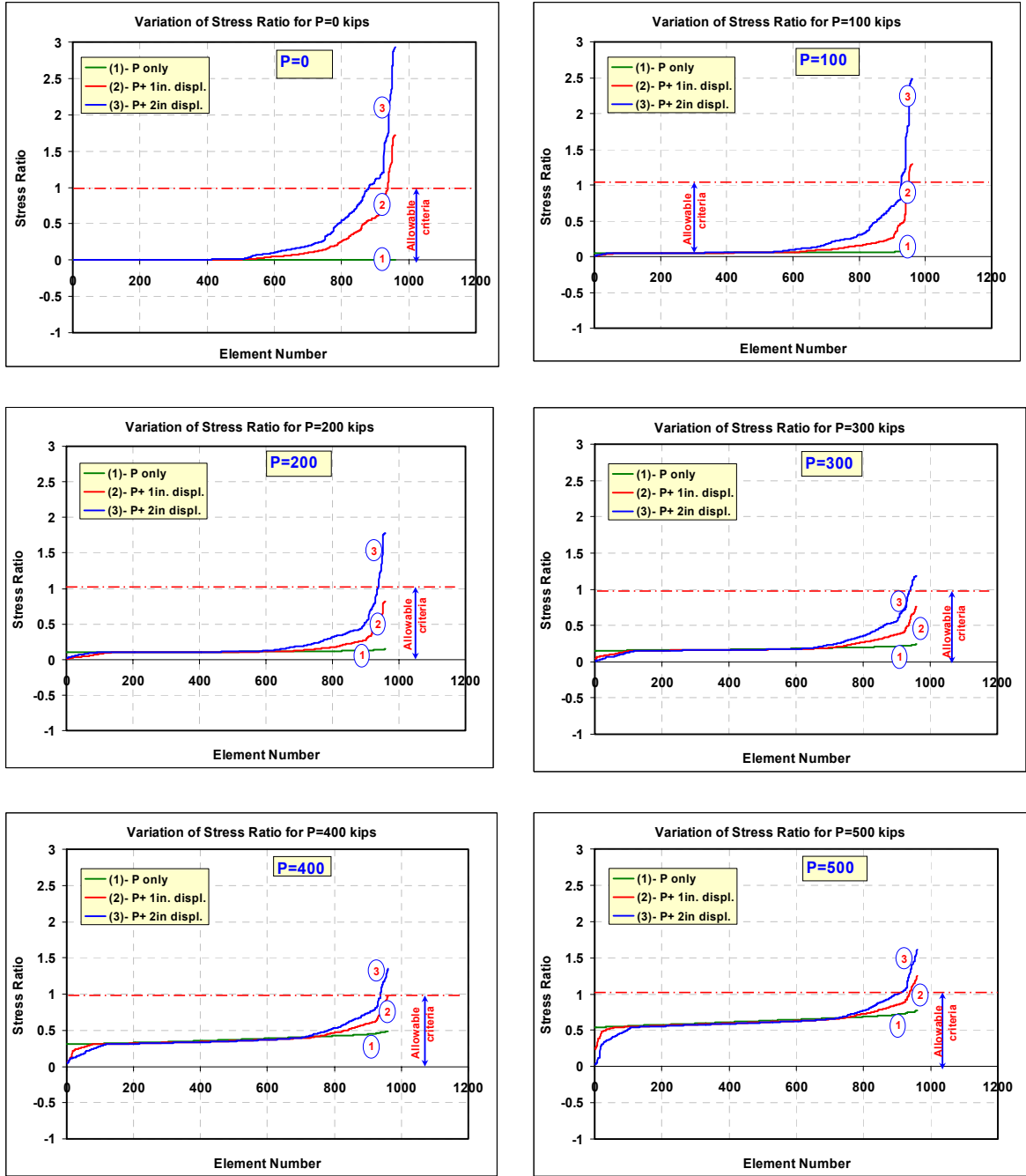


Figure 8-16: Effect of dead load value on stresses developed after lateral deformations.

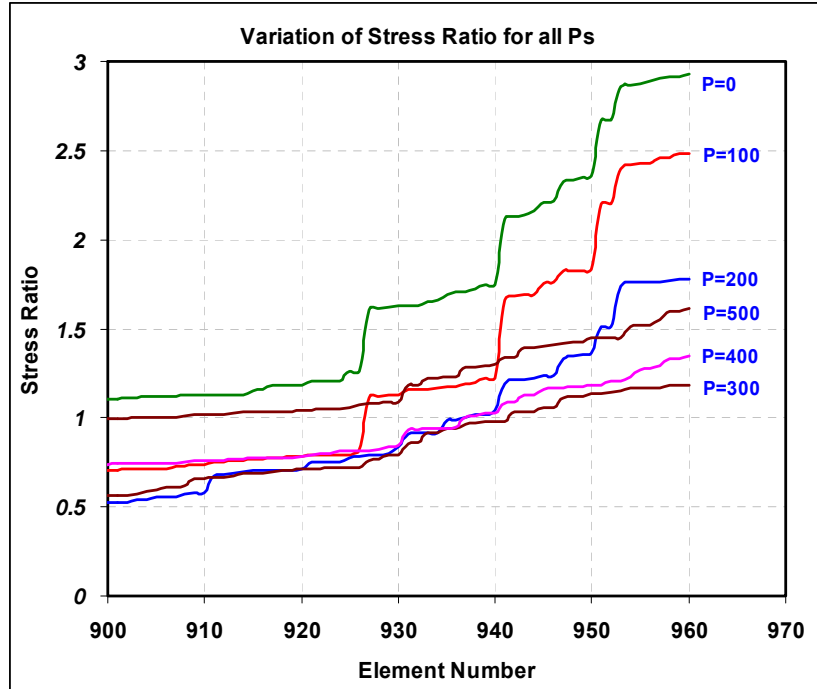


Figure 8-17: Comparison of stress ratios in the pile shell for different dead load values.

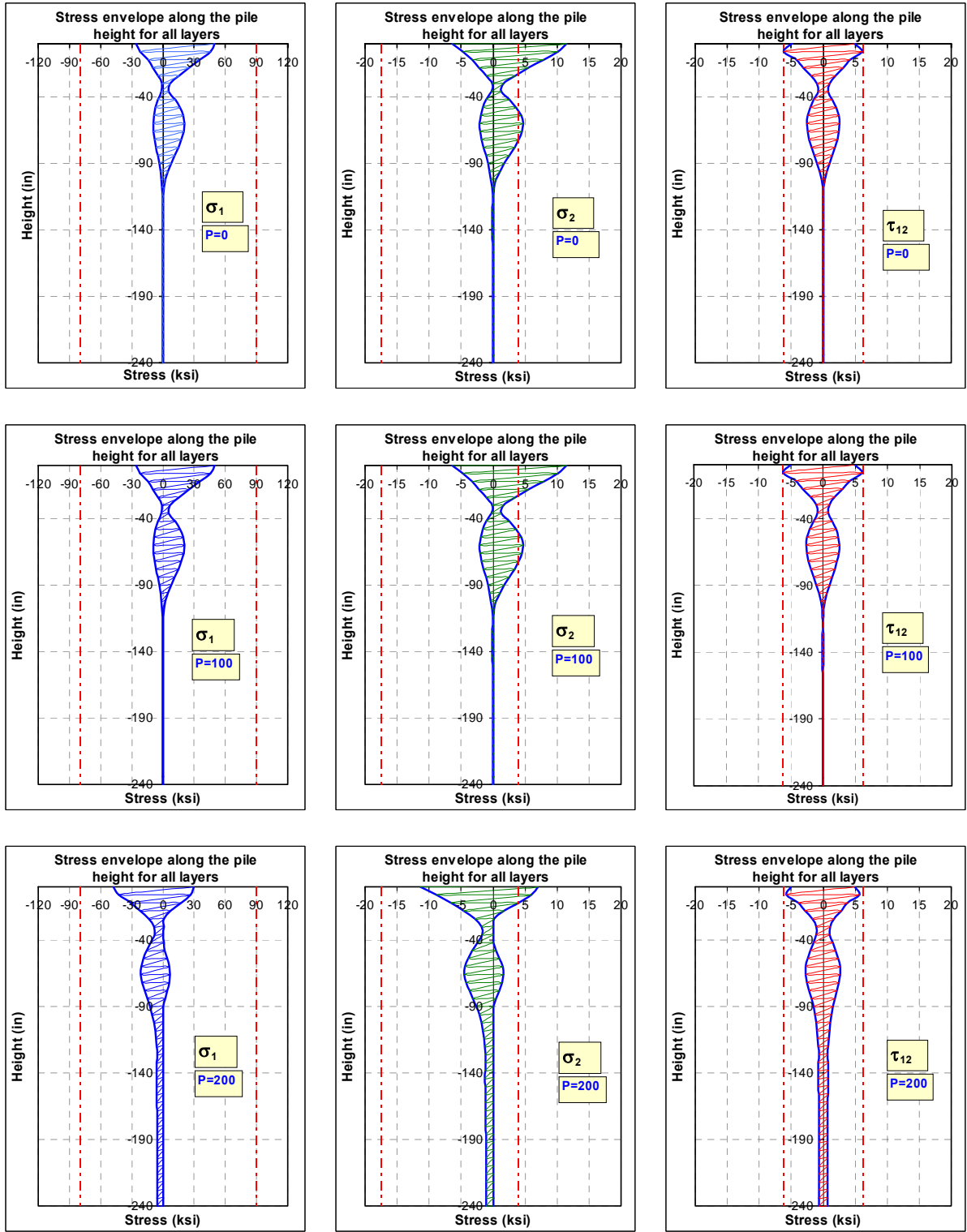


Figure 8-18: Stress envelopes for axial load optimization.

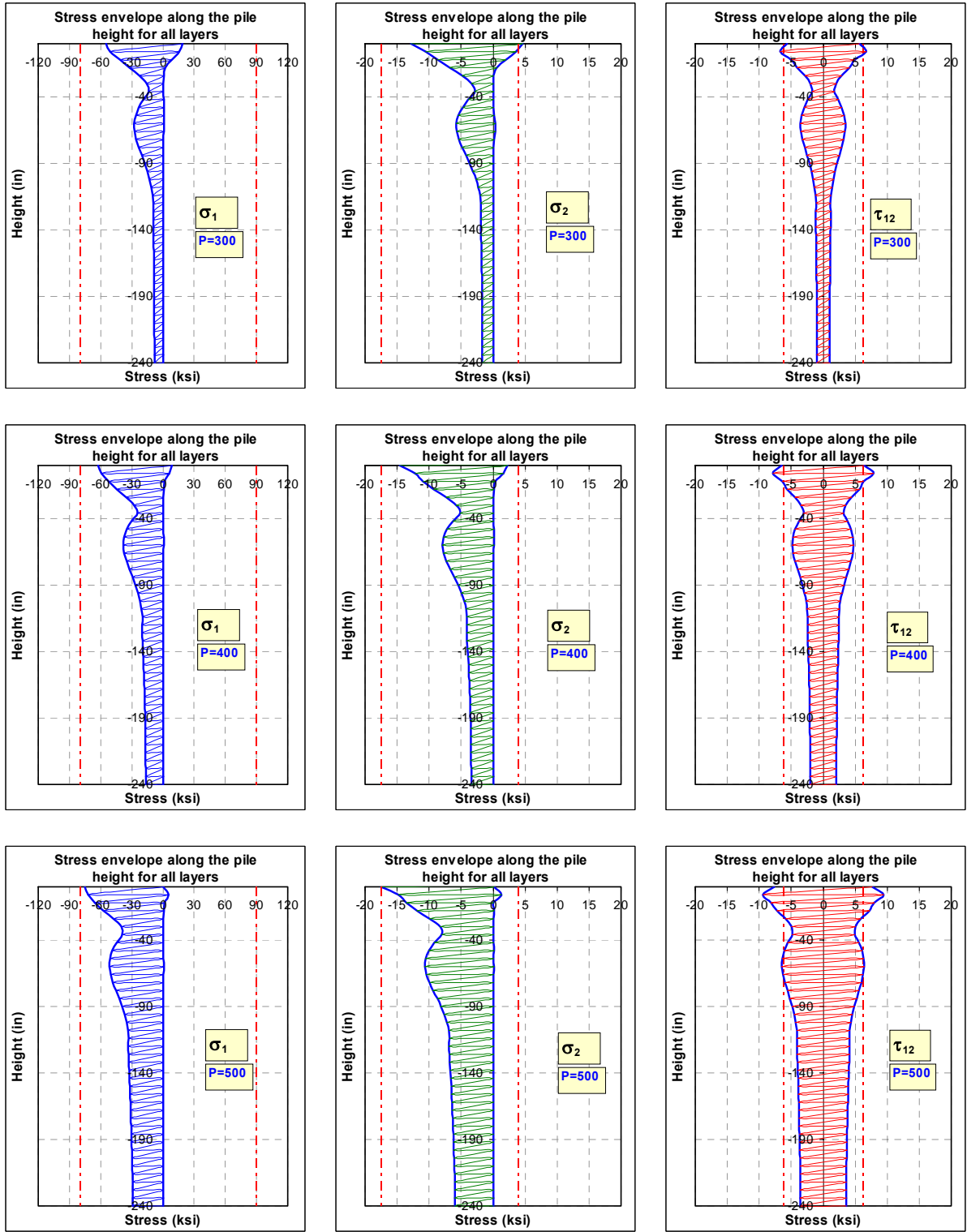


Figure 8-18: Stress envelopes for axial load optimization (cont'd).

SUMMARY, CONCLUSIONS, AND RECOMMENDATIONS

9.1 SUMMARY

Bridges with integral abutments have several advantages over conventional jointed bridges and sometimes are recommended by design engineers for certain types of bridges. Regular bridges are usually designed to have joints at the deck-abutment connection to provide free expansion and contraction for the deck. In integral abutment bridges, the expansion joints are eliminated so that the bridge deck is built integrally with the abutments. Such change will dramatically affect the supporting piles under the abutments. As the temperature changes, the bridge will either expand or contract, which produces pushing or pulling forces on the abutment and piles connected to it. This form of lateral displacements on the pile heads will produce bending moments and bending stresses in addition to the compressive stresses already existing because of the dead loads. The pile group under the abutment will resist the lateral displacements which will produce stresses on both the sub and super structures. This additional stress may reduce the axial capacity of the pile. They have to be designed to provide maximum flexibility but with minimal loss in their axial capacity.

The most common piles used in integral abutment bridges are H-steel piles. They are driven in a single row oriented to allow bending about their weak axis. Steel is a very strong and stiff material but it is not suitable for all environments, especially locations with corrosive soils. Alternative substitutes for steel in such environments are fiber reinforced composite materials.

Three-dimensional finite element models were developed and analyzed using the finite element package ANSYS. Each model consists of three major parts:

1. Composite shell which consists of multi layer unidirectional fibers which have all material properties defined in the three different directions.
2. Concrete filling which is represented by a 3-D element capable of cracking and crushing. The material properties were defined through non-linear stress-strain curves.
3. 3-D spring elements representing the soil resistance in three different locations.

9.2 CONCLUSIONS

An extensive investigation for piles made of FRP composites has been performed in this work. A complex three-dimensional finite element model has been built to simulate the soil-pile interaction process for different types of piles and soils. Based on that investigation, the following conclusions can be drawn:

9.2.1 LITERATURE AND MARKET SURVEY:

- Fiber reinforced composites (FRPs) are the newest construction materials that have been introduced to the construction market recently. The use of

FRPs in rehabilitation and retrofitting of existing structures has achieved a remarkable success in the past decades. Post strengthening of a structure in service becomes essential when its safety and serviceability become suspicious and no longer guaranteed.

- FRP composites have many advantages over conventional materials, especially its high specific strength and resistance to corrosion and chemical attacks.
- Studies on FRP composites as piling materials showed some signs of encouragement that pushed researchers to proceed in that field. Extensive research programs have been performed in several institutes and research centers in the United States (Lampo 1998a and Hardcore 1997). Experimental investigations of FRP composite piles under different types of loading showed that composites are highly competitive to conventional piling materials. Their unique properties such as light weight, specific strength and resistance to corrosion and chemicals make them practical for some applications.
- Composite piles have been installed in multiple locations of demonstration projects in the United States and around the world. Most of its usage was by the navy as marine fenders. They showed better performance over other piles due to their high strength and durability.

9.2.2 PRESENT STUDY

- Stress evaluation in fiber reinforced composites is different from isotropic materials. While stresses are calculated in any direction in structures

made of isotropic material, they have to be calculated in the layer principal material directions in unidirectional laminated structures.

- Structural failure in unidirectional laminated composites can not be decided globally based on the extreme stress locations in the structure; instead it has to be determined locally for each layer based on the failure criteria in layer local coordinates.
- Maximum stresses are concentrated in the upper portions of the pile sections specifically at the points of connection with the abutment.
- Soil properties have a major effect on the behavior of laterally loaded piles. Stiff soils produce higher stresses on the upper portion of the pile. The effect of soil stiffness can be reduced by replacing the upper soil layers with softer soil.
- Fiber glass composites have low stiffness compared to steel and have higher cost compared to concrete. Combining both materials in a form of FRP composite shell filled with concrete will be an economical solution. Concrete confinement with FRP composite materials increases its strength and ductility. Confinement effectiveness depends on the strength and stiffness of the confining material in the hoops direction. Therefore, it is recommended to have some FRP layers with their fibers at 90 degrees with the pile axis.
- Changing concrete compressive strength showed a noticeable effect on the axial stiffness and axial deformations of the pile, but the influence on bending stiffness was minor. Increasing concrete stiffness helped in

reducing the FRP stresses in the compression side of the pile but increased the stresses in the tension side.

- Concrete filling produces more cracks in stiffer soils and stiffer FRP composite shells.
- Composite materials do not have standard mechanical properties like steel and other isotropic materials. The mechanical properties for any composite material depend mainly on the properties of the individual constituents and their fiber volume fraction in the lamina. Polyester and vinyl ester fiber composites are lower in strength and stiffness than epoxy composites. Also carbon fibers composites are stronger and stiffer than glass fiber composites. Based on this, piles made of polyester and vinyl ester glass composite produce lower stresses than piles made of epoxy carbon composites.
- The axial dead load which is applied at the beginning is of a major importance in increasing the capacity of the laterally deformed pile. The dead load stores pre-stressing forces in the installed pile in a compression form so that when the pile is subjected to the bending moments of the lateral deformations, it will release some or all the compression stresses at the tension side of the pile before any tension stresses have started.
- Changing the section geometry of the pile to reduce its moment of inertia while maintaining constant area has a minor effect on the stresses if the pile is fully driven in stiff soils. Reducing the section's inertia in the bending direction will increase the section's width against the soil lateral

resistance. The pile moment of inertia will decrease while the lateral soil resistance increases. However, in piles with predrilled holes the geometry change is more significant on the developed stresses. Sections with smaller moments of inertia produce less stresses even in stiff soils.

- Piles with larger cross-sectional areas produce lower stresses compared to smaller piles with equivalent loading. However, a large pile has much higher stiffness than an equivalent number of small piles.
- The soil-pile stiffness for a single large pile is lower than that of multiple piles with an equivalent capacity when driven without predrilled holes.
- It is recommended to use piles with larger cross-sectional areas when no predrilled holes are provided. When predrilled holes are provided, multiple piles with small cross-sectional areas are recommended.
- Predrilled holes have a dramatic effect on stress reduction in piles in stiff soils. The stress reduction depends on the depth of the predrilled hole. A stress reduction of 70% or more can be achieved by using predrilled holes filled with loose sands. However, predrilled holes are disadvantageous in friction piles because they will decrease the size of the contact area with the pile and result in reducing the pile axial capacity.
- Rectangular piles were found better than circular piles for geometrical optimization purposes. The section dimensions can be proportioned for lowest stress and stiffness.
- Rectangular hollow piles are better than circular when subjected to lateral displacements. A hollow pile with a circular section experienced local

buckling at some locations along its depth. Rectangular sections performed better without local buckling because the two sides parallel to the displacement direction (the webs) provided lateral support to the pile against local buckling.

- The fiber orientations in the layers have a strong effect on the pile behavior. It is strongly recommended to have multiple layers with different fiber orientations. Increasing the number of layers up to a certain limit will improve the pile properties. The fiber orientations should be selected for best performance.
- Due to the nature of concrete and its cracking under tension stresses, the section properties will not be stable under continuous lateral displacements. The loss of section under cracking increases the stresses on the composite shell which requires a change of fiber orientation for best performance as cracks keep growing.
- The directional material properties have a major effect on the optimization results of layer orientations. The optimum fiber directions in each layer in the stack for the desired objective function change with the mechanical properties and their ratios in the composite material.
- Plain concrete improves the pile axial stiffness and increases its load capacity when used as filler with FRP shells.
- FRP improves the strength and the stiffness of confined concrete. The FRP shell strength, stiffness, thickness, and fiber structure are major factors in the percentage of the increase.

- The new pile section has several advantages over traditional pile sections. Its geometrical structure which includes two flanges and two webs gives the cross-section the flexibility to be proportioned for the desired properties. The distance between the two webs is variable and can be changed such that the section can go from a wide flange section when the distance between the webs is zero to a rectangular section when the distance between the webs is the flange width.
- Optimization of the pile section for best fiber orientation is achievable. The best set of layer orientations is not unique, especially when the number of layers is high. It changes based on the load and the resistance magnitudes. It also changes with the mechanical properties of the composite layer.
- Global optimization for a soil-pile system can be achieved by optimizing the following:
 1. The cross-section geometry including the size of concrete filling.
 2. The fiber architecture for all layers.
 3. The dead load magnitude that gives minimum stresses.
- The maximum load capacity of FRP composite pile is dramatically affected by the lateral movement of the pile head. The stress-strain behaviors of fiber reinforced composites are linearly elastic; therefore, pile stresses from different types of loading are added numerically.
- The stress capacity of any FRP pile is constant and can be reached by: axial compression, lateral movement or a combination of both.

9.3 RECOMMENDATIONS FOR FUTURE WORK

- The current study utilized the Winkler method and the modified Ramberg-Osgood model in representing the soil properties. It is recommended that future studies in the same area can use methods other than Winkler's in representing the soil-pile interaction such as the elastic continuum approach.
- The piles in the present study were assumed to be installed in a fully integral abutment with the bridge structure. Future research should have to consider piles in semi integral bridges.
- The soil properties used in this study were of two different profiles from Iowa soils (Amde et al 1982). It is recommended to use more soil profiles from different locations.
- The finite element model in the current study dealt with piles in non-skewed bridges. Studies on composite piles in skewed bridges are recommended in the future.

APPENDIX A

Table A-1: Properties of typical unidirectional composite materials (Daneil 1994)

	E-glass/ epoxy	S-glass/ epoxy	Carbon/ epoxy
Density [lb/in. ³]	0.076	0.072	0.057
Longitudinal modulus E_1 , [Msi]	5.7	6.3	20.5
Transverse modulus, E_2 [Msi]	1.24	1.29	1.5
In-plane shear modulus G_{12} [Msi]	0.54	0.66	1.04
Major Poisson's ratio ν_{12}	0.28	0.27	0.27
Longitudinal tensile strength, F_{1t} [ksi]	157	185	330
Transverse tensile strength, F_{2t} [ksi]	5.7	7.1	8.3
In-plane shear strength, F_6 [ksi]	12.9	10	10.3
Longitudinal compressive strength, F1c [ksi]	90	100	209
Transverse compressive strength, F2c [ksi]	18.6	22.9	33

Table A-2: Properties of typical unidirectional composite materials (Vectorply)

	E-glass/ epoxy	S-glass/ epoxy	Carbon/ polyester
Density [lb/in. ³]	0.064	0.063	0.053
Longitudinal modulus E_1 , [Msi]	4.5	5.3	12.75
Transverse modulus, E_2 [Msi]	1.1	1.1	0.69
In-plane shear modulus G_{12} [Msi]	0.55	0.55	0.32
Major Poisson's ratio ν_{12}	0.26	0.26	0.28
Longitudinal tensile strength, F_{1t} [ksi]	90	141	153
Transverse tensile strength, F_{2t} [ksi]	3.9	4	13
In-plane shear strength, F_6 [ksi]	6.2	6	9
Longitudinal compressive strength, F_{1c} [ksi]	80	119	98
Transverse compressive strength, F_{2c} [ksi]	17.5	18	17

Table A-3: Properties of experimentally tested unidirectional composite materials (Yoon 1993)

	Glass/ vinylester	Glass/ polyester
Longitudinal modulus E_1 , [Msi]	2.579	2.4
Transverse modulus, E_2 [Msi]	1.459	1.2
In-plane shear modulus G_{12} [Msi]	0.528	0.52
Major Poisson's ratio ν_{12}	0.312	0.3
Longitudinal tensile strength, F_{1t} [ksi]	32.3	39.5
Transverse tensile strength, F_{2t} [ksi]	7.6	7
In-plane shear strength, F_6 [ksi]	5.4	5.4
Longitudinal compressive strength, F_{1c} [ksi]	38.7	34.2
Transverse compressive strength, F_{2c} [ksi]	18.9	14.6

APPENDIX B

FORTRAN PROGRAM

This code is part of the model generation which reads its input from the ANSYS main batch file that generates the model. It creates multiple output files to be used by the ANSYS main file. The code generates the load-deformation data points for all springs and all soil types in the model for any pile geometry and mesh size.

```
CHARACTER*51 stype
character*10 st
  REAL KX,yi(1000)
common ii,EH
DIMENSION ND(1000),X(1000),Y1(1000),Z(1000),n1(1000),ND1(1000)
dimension ND2(1000),ND3(1000)
C INP1.DAT HAS THE NO. OF NEW NODES
OPEN(8,FILE='input.dat',STATUS='OLD')
c OPEN(5,FILE='nodes.inp',status='old')
open(6,file='b1.dat',status='unknown')
  open(7,file='b11.dat',status='unknown')
open(10,file='b22.dat',status='unknown')
open(12,file='py.dat',status='unknown')
open(15,file='b33.dat',status='unknown')
open(16,file='b44.dat',status='unknown')
OPEN(18,FILE='b55.dat',STATUS='UNKNOWN')
C-----
c EH: EXPOSED LENGTH OF PILE
C H : TOTAL LENGTH OF PILE
read(8,*)st
read(8,*)XNT,Xnmax,Bpile,Dpile,perpile,H,divl,EH,FAC,AREA
READ(8,*)XNODY,XDEPTH
nt=2*xnt
nmax=xnmax
NODY=XNODY
IFAC=FAC
Bpile=Bpile/12.
Dpile=Dpile/12.
H=H/12.
perpile=perpile/12.
if(st.eq.'densand')stype='densesand'
if(st.eq.'lossand')stype='loosesand'
if(st.eq.'medsand')stype='mediumsand'
if(st.eq.'sftclay')stype='softclay'
if(st.eq.'stfclay')stype='stiffclay'
if(st.eq.'vstclay')stype='vstiffclay'
c stype='mediumsand'
```

```

c      stype='loosesand'
c      EH IN INCHES AND Y1() IN INCHES
c      EH=24

c      ii: real constants
c      ii=4
c      N2=4
c      LOOP=0
c      i1=0
c      mn=0
c      do 5,i=1,2*NT
c5     read(5,*)ND(i)
c      call pudata
c          CALL SORT(ND,NT,1,Y1,NT1,div1)

c      IR=5
c      ii=IR
c      IF (EH.GT.0)THEN
c      WRITE(6,*)'R, ',ii,', ',1,', ',0.
c      WRITE(7,30)ii
c      WRITE(10,30)ii
c      WRITE(15,30)ii
c      WRITE(16,30)ii
c      ii=ii+1
c      IR=IR+1
c      ENDIF
c-----
c SPRING ELEMENTS FOR P-Y  X-DIRECTION
c      NT2=NT1
c      i2=-1
c      do 2 i=1,NT1,2
c      i2=i2+2
c      IF(ABS(Y1(i2)).LT.EH)GOTO 301
c      write(7,30)IR
c      IR=IR+1
30     format('REAL, ',I4)
301    write(7,10)ND(I)-NMAX,ND(I)
c      write(7,10)ND(I+1)-NMAX,ND(I+1)
10     FORMAT('E, ',I7,', ',I7)
2      CONTINUE
c-----
c SPRING ELEMENTS FOR F-Z Y-DIRECTION BOTH SIDES
c      CALL SORT(ND2,NT,3,Y1,NT1,div1)

c      inn=0
c      i2=-1
c      do 6 i=1,NT1,2
c      i 2=i2+2
c      IF(ABS(Y1(i2)).LT.EH)THEN
c      write(10,10)ND(I)-NMAX,ND(I)
c      write(10,10)ND(I+1)-NMAX,ND(I+1)
c      WRITE(16,10)ND2(I)-NMAX,ND2(I)
c      WRITE(16,10)ND2(I+1)-NMAX,ND2(I+1)
c      Else
c      if (inn.eq.1)goto 303

```

```

        write(10,30)IR
        WRITE(16,30)IR
        inn=1
303   write(10,10)ND(I)-NMAX,ND(I)
        write(10,10)ND(I+1)-NMAX,ND(I+1)
        WRITE(16,10)ND2(I)-NMAX,ND2(I)
        WRITE(16,10)ND2(I+1)-NMAX,ND2(I+1)

        endif
6     CONTINUE
C-----
C SPRING ELEMENTS FOR Q-Z BOTTOM
    CALL SORT(ND3,NODY,4,Y1,NT1,0)
    IR=IR+1
    WRITE(18,30)IR
    DO 145 I=1,NODY
    WRITE(18,10)ND3(I)-IFAC*NMAX,ND3(I)
145   CONTINUE
C-----
C SPRING ELEMENTS FOR P-Y Z-DIRECTION
    CALL SORT(ND1,NT,2,Y1,NT1,div1)
    IR=IR+1
    i2=-1
    do 7 i=1,NT1,2
    i2=i2+2
    IF(ABS(Y1(i2)).LT.EH)GOTO 304
    write(15,30)IR
    IR=IR+1
304   write(15,10)ND1(I)-NMAX,ND1(I)
        WRITE(15,10)ND1(I+1)-NMAX,ND1(I+1)
7     CONTINUE
C-----
    XX=XDEPTH
    call py(Bpile,H,nt2,div1,Y1,XX,stype)
    call fz(PERPILE,div1,stype,alfa)
    call qz(AREA,NODY,stype)
    XX=XDEPTH
    call py(Dpile,H,nt2,div1,Y1,XX,stype)
c
c
c   subroutine pudata
c   dimension y(20),p(20)
c   h=50
c   j=4
c   do 101,x=0,h
c   gama=110.
c   c=15
c   eps50=0.005
c   b=12
c   y50=2.5*eps50*b
c   pu1=(3+gama/c*x+j/b*x)*c*b
c   pu2=9*c*b
c   pu=min(pu1,pu2)
c   i=1
c   do 102,y1=0,10
c   p1=pu*.5*(y1/y50)**(1/3.)
c   y(i)=y1

```

```

c      p(i)=p1/1000.
c      i=i+1
c      write(6,*)y,p
c102  continue
c      write(6,110)j,(y(i),p(i),i=1,10)
c      j=j+1
c101  continue
110   format('R','I2',' ',10(f4.1,' ',f7.2,' '))
c
c      call ramberg
      END

```

```

C-----
C      p-y curves
*      x: ft
*      gama: lb/ft^3
*      B: ft
*      Pu: lb/ft
      subroutine py(B,H,nt,divl,Y1,x,stype)
      character*51 stype
      common ii,EH
      real J,ka,kp,ko,kh,Y1(1000)
      write(6,*)'! p-y curve:'
      pi=3.141592654

```

C Soil properties:

```

C-----
c      Soft clay
      if(stype.eq.'softclay')then
        gama=100
        N=3
        J =0.5
        eps50=0.02
        fk=1
        fk2=2.5
        n1=1
        alfa=1.
      elseif(stype.eq.'stiffclay')then
        N=15
        gama=120
        J=0.5
        eps50=0.01
        fk=1
        fk2=2.5
        n1=1
        alfa=.5
      elseif(stype.eq.'vstiffclay')then
        N=50
        gama=130
        J=2.0
        eps50=0.005
        fk=2.
        fk2=2
        n1=2
        alfa=0.25
      elseif(stype.eq.'densesand')then
        phi=40*pi/180.
        alpha=phi/2.

```

```

gama=130.
kp=(TAN(pi/4.+phi/2.))**2.
ka=(TAN(pi/4.-phi/2.))**2.
ko=1-SIN(phi)
beta=(pi/4.)+(phi/2.)
N=30
n1=3
JJ=1500
elseif(stype.eq.'mediumsand')then
phi=35*pi/180.
alpha=phi/2.
gama=120.
kp=(TAN(pi/4.+phi/2.))**2.
ka=(TAN(pi/4.-phi/2.))**2.
ko=1-SIN(phi)
beta=(pi/4.)+(phi/2.)
N=15
n1=3
JJ=600
elseif(stype.eq.'loosesand')then
phi=30*pi/180
alpha=phi/3.
gama=110
kp=(TAN(pi/4.+phi/2.))**2.
ka=(TAN(pi/4.-phi/2.))**2.
ko=1-SIN(phi)
beta=(pi/4.)+(phi/2.)
N=5
n1=3
jj=200
endif
Cu=97.*N+114.
C x=0.
i2=-1
do 31,i=1,nt/2
i2=i2+2
IF(ABS(Y1(i2)).LT.EH)GOTO 31
if(stype.eq.'softclay'.or.stype.eq.'stiffclay'
& .or.stype.eq.'vstiffclay')then
Pu1=(3+(gama/Cu)*x+(J/B)*x)*Cu*B
Pu2=9*Cu*B
Pu=min(Pu1,Pu2)

elseif(stype.eq.'densesand'.or.stype.eq.'loosesand'
& .or.stype.eq.'mediumsand')then
c Units are in lb-ft
Pu1=gama*x*(B*(kp-ka)+x*kp*TAN(alpha)*TAN(beta)
& +x*ko*TAN(beta)*(TAN(phi)-TAN(alpha)))
Pu2=gama*x*(kp**3.+2*kp**2.*ko*TAN(phi)-ka)*B
Pu=min(Pu1,Pu2)
endif

if(stype.eq.'densesand'.or.stype.eq.'loosesand'
& .or.stype.eq.'mediumsand') then
kh=JJ*gama*x/1.35
else
y50=fk2*B*eps50

```

```

        kh=Pu/(fk*y50)
        endif
        WRITE(6,*)'! x=',x
c       write(6,*)'! Pu1,Pu2=',Pu1,Pu2
c       write(6,*)'! kp,ka,ko,gama,B=',kp,ka,ko,gama,B
c       write(6,*)'! tbeta,tphi,talpha=',tan(beta),tan(phi),tan(alpha)
        write(6,*)'! Pu=',Pu*divl/1000.
        write(12,*)'x=',x
        x=x+divl
        if(kh.eq.0.)kh=1
        yu=Pu/kh
c
c           kh for the division divided by 2 for 2 springs
at each level
        kh=kh*divl/2.
        call ramberg(kh,Pu,n1,yu)
31      continue
        end

```

```

C-----
C       f-z curves
        subroutine fz(lg,divl,stype,alfa)
        character*51 stype
        real lg,kv
        common ii,EH
        write(6,*)'! f-z curve:'

c       d=15/12.
c       bf=15/12.
*       fmax:lb/ft
c       fmax=500
*       kv:lb/ft^2
c       kv=150000
c For sand:
        if(stype.eq.'densesand')then
            n=1
            NN=30
            zc=0.033
            fmax=0.04*lg*NN*1000
c       kv=10*fmax/zc
            elseif(stype.eq.'mediumsand')then
                n=1
                NN=15
                zc=0.033
                fmax=0.04*lg*NN*1000.
c       kv=10*fmax/zc
            elseif(stype.eq.'loosesand')then
                n=1
                NN=5
                zc=0.033
c       fmax multiplied by 1000 to covert to lbs.
                fmax=0.04*lg*NN*1000
c       kv=10*fmax/zc
            elseif(stype.eq.'softclay')then
                alfa=1.0
                NN=3
                fcmax1=lg*alfa*(97*NN+114)

```

```

fcmax2=lg*(97*NN+114)
zc=0.021
fmax=min(fcmax1,fcmax2)
elseif(stype.eq.'stiffclay')then
alfa=0.5
NN=15
fcmax1=lg*alfa*(97*NN+114)
fcmax2=lg*(97*NN+114)
zc=0.021
fmax=min(fcmax1,fcmax2)
elseif(stype.eq.'vstiffclay')then
alfa=0.25
NN=50
fcmax1=lg*alfa*(97*NN+114)
fcmax2=lg*(97*NN+114)
zc=0.021
fmax=min(fcmax1,fcmax2)
endif
kv=10*fmax/zc
write(6,*)'! Pu (f-z)kips=',fmax/1000
yu=fmax/kv
c multiply by spring active strip length and divid by number of
springs
kv=kv*divl/4.
n=1
write(12,*)'f-z'
call ramberg(kv,fmax,n,yu)
end

C q-z curves
subroutine qz(AREA,NODY,stype)
character*51 stype
common ii,EH
real kq
write(6,*)'! q-z curve:'
C qmax=40000
C kq=12000000
c qmax=8*NN
if(stype.eq.'densesand')then
NN=30
zc=0.033
if(NN.gt.15)Ncor=15+0.5*(NN-15)
qmax=8*Ncor*1000.
elseif(stype.eq.'mediumsand')then
NN=15
zc=0.33
Ncor=NN
if(NN.gt.15)Ncor=15+0.5*(NN-15)
qmax=8*Ncor*1000.
elseif(stype.eq.'loosesand')then
NN=5
zc=0.033
qmax=8.*NN*1000.
write(6,*)'!Pu (q-z)kips=',qmax/1000.
elseif(stype.eq.'softclay')then
NN=3
qmax=9*(97*NN+114)

```

```

zc=0.021
elseif(stype.eq.'stiffclay')then
NN=15
qmax=9*(97*NN+114)
zc=0.021
elseif(stype.eq.'vstiffclay')then
NN=50
qmax=9*(97*NN+114)
zc=0.021
endif
kq=10*qmax/zc

n=1
yu=qmax/kq
c kq=(kq*AREA/144.)/(NODY-2)
kq=(kq*AREA/144.)/(NODY)

write(12,*)'q-z)'
call ramberg(kq,qmax,n,yu)
end

subroutine ramberg(kh,Pu,n,yu)
COMMON ii,EH
real y1(20),p1(20),kh
if(kh.eq.0.)kh=1.
c yu=Pu/kh
write(6,*)'yu=',yu*12
if(yu.eq.0.)yu=1.
i=1
do 21, y11=0.,18./48,(1/48.)
p1(i)=(kh*y11/(1+abs(y11/yu)**n)**(1./n))/1000.
y1(i)=y11
pp=p1(i)
write(12,*)y1(i)*12,p1(i)
i=i+1
21 continue
write(6,111)ii,(y1(j)*12,p1(j),j=1,3)
111 format('R','I3',' ',3(f7.4,' ',f10.6,' '))
write(6,113)(y1(j)*12,p1(j),j=4,6)
write(6,113)(y1(j)*12,p1(j),j=7,9)
write(6,113)(y1(j)*12,p1(j),j=10,12)
write(6,113)(y1(j)*12,p1(j),j=13,15)
write(6,113)(y1(j)*12,p1(j),j=16,18)
113 format('RMORE',' ',3(F7.4,' ',F10.6,' '))
ii=ii+1
end

C SUBROUTINE SORT (NO1,N,KK,Y1)
SUBROUTINE SORT (NO2,N,KK,Y2,NT1,div1)
C PARAMETER (N=102)
COMMON ii,EH
REAL X(N),Y(1000),Z(N)
REAL X1(N),Y1(N),Z1(N)
REAL Y2(1000)
DIMENSION NO(1000),NO1(1000),NO2(1000)
IF(KK.EQ.1)THEN
NF=9

```



```

open(9,file='NODES.OUT',status='old')
ELSEIF(KK.EQ.2)THEN
NF=14
open(14,file='NODES1.OUT',status='old')
elseif(KK.EQ.3)then
NF=17
OPEN(17,FILE='NODES2.OUT',STATUS='OLD')
ELSEIF(KK.EQ.4)THEN
NF=19
OPEN(19,FILE='NODES3.OUT',STATUS='OLD')
endif
DO 100,I=1,N
READ(NF,*)NO(I),X(I),Y(I),Z(I)
100 CONTINUE
C CLOSE #1
NO1(1)=NO(1)
X1(1)=X(1)
Y1(1)=Y(1)
Z1(1)=Z(1)
DO 201,L=2,N
DO 301, M=L-1,1,-1
IF (Y(L).LE.Y1(M)) GOTO 300
Y1(M+1)=Y1(M)
NO1(M+1)=NO1(M)
X1(M+1)=X1(M)
Z1(M+1)=Z1(M)
301 CONTINUE
300 Y1(M+1)=Y(L)
NO1(M+1)=NO(L)
X1(M+1)=X(L)
Z1(M+1)=Z(L)
201 CONTINUE
C -----

c DIVL=2.
YR=EH
if(kk.eq.4)YR=abs(Y1(1))
K=1
DO 501, J=1,N,2
YI=ABS(Y1(J))
IF(ABS(YI-YR).LT.0.1)THEN
Y2(K)=Y1(J)
Y2(K+1)=Y1(J+1)
NO2(K)=NO1(J)
NO2(K+1)=NO1(J+1)
K=K+2
YR=YR+DIVL*12
ENDIF

C WRITE(12,*)NO1(J),X1(J),Y1(J),Z1(J)
501 CONTINUE
WRITE(12,*)'KK=',KK,'N=',K-1
DO 502, J=1,K-1
502 WRITE(12,*)NO2(J),Y2(J)
NT1=K-1
505 END

```

APPENDIX C

ANSYS INPUT FILE

This file is written using the ANSYS Parametric Design Language (APDL) that's capable of modeling the FRP pile-soil system with different variable parameters.

```
finish
/clear,nostart
/PREP7

!*DIM,THETA,ARRAY,NL,1,0
*CFOPEN,input,dat
!-----
NL=12
NL2=6
H=10*12/1           !pile height
EH=0*12             !inches
DXX=100
XDEPTH=EH/12.      !feet
P=400
U2=2.   !Lateral movement
Pinc=50
PX=10
fc=3.0   !fc'=3.0 ksi
DSS=6
Lcomp=37 !40
Ac=64.8
T=0.3/NL
T2=T
MT1=1
MTN=1
!/input,glass_epoxy1,dat           !Composite type
*vwrite,'vstclay'                  !Soil type
(a7)

!-----
!Afrp=3157.16/H
!T=(Afrp/Lcomp)/NL

THETA1=0
THETA2=0
!-----

THETA3=90
THETA4=0
```

```

THETA5=15
THETA6=0

THETA7=-30
THETA8=30
THETA9=-30
THETA10=0
THETA11=0
THETA12=0

PHI1=0
PHI2=0
PHI3=90

PHI4=90
PHI5=45
PHI6=-45
PHI7=75
PHI8=-75
PHI9=60
PHI10=-60
PHI11=0
PHI12=0
!-----

REAL1=1                !REAL CONSTANT FOR THE FLANGES
REAL2=2                !REAL CONSTANT FOR THE WEBS
topmat=3                !2:3000ksi  3:29e11ksi
iconcrete=2            ! 2:concrete core ,  else: hollow core
itype=0                ! 0:Load bearing  1:friction
ishape=1                ! 0:H or II      1: square or rectangle
!-----
!-----
TP1=NL*T  !PILES THICKNESS=0.5 IN.
TP2=NL*T
DX1=60.
DY1=0.
DZ1=10.
DS=DSS
DS2=Ac/DS
DZ2=((Lcomp-2*(DS+DS2+2*tp1))/4)
!DZ2=0.1
DS2=DS2  !-2*NL*T
DZ3=DZ2
!-----
BPILE=DZ2+2*TP2+DS2+DZ3          !pile-section width
DPILE=DS+2*TP1                    !pile-section depth
PERPILE=2*(BPILE+DPILE)  !+4*DZ2          !PILE PERIMETER
DX2=10.
!H=300.                            !PIECE HEIGHT=20 IN
!L=2*TP1+DS
!DY=WP1-2*(DX2+TP2)
DP=40          !PILE EMBEDMENT IN PIER = 6 INCHS
w1=1
w2=4
w3=1
w4=8/2

```

```

w5=12./2
divl=w5/12.
!AREA=2*DS*TP2+2*BPILE**TP1
AREA=BPILE*DPILE
!-----
!soiltype:
!*vwrite,'lossand'
!(a7)
!*vwrite,'medsand'
!(A7)
!*vwrite,'densand'
!(a7)
!*vwrite,'sftclay'
!(a7)
!*vwrite,'stfclay'
!(A7)
!*vwrite,'vstclay'
!(a7)

/input,glass_epoxyl,dat
*if,REAL2,EQ,1,THEN
/INPUT,anglesrectangleEj,dat
*ELSEIF,REAL2,EQ,2,THEN
/INPUT,anglesrectangleEjvar,dat
*ENDIF

!/OUTPUT,out,out
ET,1,SOLID46,,,,,2,4
keyopt,1,5,2
keyopt,1,8,1
keyopt,1,9,1
ET,2,COMBIN39,,,1
ET,3,COMBIN39,,,2
ET,4,COMBIN39,,,3
ET,5,SOLID65 !65 !CONCRETE
ET,6,SOLID45
!ET,1,SOLID65,,,,,2
!ET,6,solid45
keyopt,5,5,1
keyopt,5,6,3
keyopt,5,7,1
!*do,theta1,0,90,5
R,1,NL
RMORE
RMORE,1,THETA1,T,1,-THETA1,T
RMORE,1,THETA2,T,1,-THETA2,T
RMORE,1,THETA3,T,1,-THETA3,T
RMORE,1,THETA4,T,1,-THETA4,T
RMORE,1,THETA5,T,1,-THETA5,T
RMORE,1,THETA6,T,1,-THETA6,T
R,2,NL2
RMORE
RMORE,1,PHI1,T2,1,-PHI1,T2
RMORE,1,PHI2,T2,1,-PHI2,T2
RMORE,1,PHI5 ,T2,1,PHI6,T2
RMORE,1,PHI7,T2,1,PHI8,T2
RMORE,1,PHI9,T2,1,PHI10,T2
!displ. in the x-direction

```

```

RMORE,1,PHI11,T2,1,PHI12,T2

!MT1=1
!MTN=1
!/input,glass_vinyl2,dat
!/input,glass_epoxy1,dat
!/input,glass_polyester,dat
!/input,carbon_polyester,dat
!/input,glass_vinyl,dat
!/input,glass_polyester1,dat
!/INPUT,STRONGWELL,DAT
!MP,EX,2,7271.3178 !3000
!MP,EY,2,3000
MP,NUXY,2,.18
MP,EX,3,29e11
MP,NUXY,3,.3
MP,EX,4,29000 !STEEL
R,4,1,1,1,1
MTN=4
!/input,carbon_epoxy,dat
!/input,carbon_polyester,dat

R,3
Ec=57*(fc*1000)**0.5
MP,EX,2,Ec
fct=(7.5*(fc*1000)**0.5)/1000.
!Ffrpu=34
t_frp=NL*T
d=DSS
fcop=fc
Epscop=0.002
f1=2*Ffrpu*t_frp/d
fccp=fcop*(-1.254+2.254*sqrt(1+(7.94*f1/fcop)))-2*f1/fcop)
TB,CONCR,2
TBTEMP,0
TBDATA,1,0.2
TBDATA,2,0.5
TBDATA,3,fct
TBDATA,4,-1 !fccp !fc
!/input,MISO1,dat
!/input,mander,dat
!/input,parkpauly,dat
/!input,mirmiranKsi,dat
!-----
C*****
K,1,DX1,DY1,DZ1
K,2,DX1+TP1,DY1,DZ1
K,3,DX1,DY1-H,DZ1
K,4,DX1+TP1,DY1-H,DZ1
KGEN,2,1,4,1,,,DZ2,4
KGEN,2,5,8,1,,,TP2,4
KGEN,2,9,12,1,,,DS2,4
KGEN,2,13,16,1,,,TP2,4
KGEN,2,17,20,1,,,DZ2,4
L,1,2 !LINE 1
LESIZE,1,,1

```

```

L,2,4          !LINE 2
LESIZE,2,w5
L,3,4          !LINE 3
LESIZE,3,,,1
L,3,1          !LINE 4
LESIZE,4,w5
LGEN,2,1,4,1,,,DZ2,4
LGEN,2,5,8,1,,,TP2,4
LGEN,2,9,12,1,,,DS2,4
LGEN,2,13,16,1,,,TP2,4
LGEN,2,17,20,1,,,DZ2,4      !LINES 21-24
L,2,6          !LINE 25
LESIZE,25,,,w1
L,6,10
LESIZE,26,,,1
L,10,14
LESIZE,27,,,w2  !DS2/2
L,14,18
LESIZE,28,,,1
L,18,22
LESIZE,29,,,w3
LGEN,2,25,29,1,-TP1,,, -1      !LINES 30-34
LGEN,2,25,34,1,,, -H,,,2      !LINES 35-44
KGEN,2,1,24,1,TP1+DS,,,24
LGEN,2,1,44,1,TP1+DS,,,24      !LINES 45-88
L,6,29
LESIZE,89,,,w4
L,10,33
LESIZE,90,,,w4
LGEN,2,89,90,1,,,TP2+DS2,8      !LINES 91-92
LGEN,2,89,92,1,,, -H,,,2

TYPE,1
MAT,1
REAL,REAL1
!ESYS,11
      !V,4,8,6,2,3,7,5,1          !volume 1
V,8,6,2,4,7,5,1,3
      !V,8,12,10,6,7,11,9,5      !volume 2
V,12,10,6,8,11,9,5,7
      !V,12,16,14,10,11,15,13,9
V,16,14,10,12,15,13,9,11      !volume 3
      !V,16,20,18,14,15,19,17,13
V,20,18,14,16,19,17,13,15      !volume 4
      !V,20,24,22,18,19,23,21,17      !volume 5
V,24,22,18,20,23,21,17,19      !volume 5
KGEN,2,1,24,1,DS+TP1,,,24
      !V,31,27,25,29,32,28,26,30      !volume 6
V,27,25,29,31,28,26,30,32
      !V,35,31,29,33,36,32,30,34
V,31,29,33,35,32,30,34,36
      !V,39,35,33,37,40,36,34,38
V,35,33,37,39,36,34,38,40
      !V,43,39,37,41,44,40,38,42
V,39,37,41,43,40,38,42,44
      !V,47,43,41,45,48,44,42,46      !volume 10
V,43,41,45,47,44,42,46,48

```

```

!V,35,12,10,33,31,8,6,29
V,12,10,33,35,8,6,29,31
!V,16,39,37,14,20,43,41,18 !volume 12
V,39,37,14,16,43,41,18,20
Real,REAL1
VMESH,1,10 !FLANGES
REAL,REAL2
VMESH,11,12 !WEBS

!-----
*get,nod,node,,num,max
*get,NOE,ELEM,,count

TYPE,5
MAT,2
REAL,3
!V,10,14,16,12,33,37,39,35 !CORE VOLUME
V,12,35,33,10,16,39,37,14
*if,iconcrete,eq,2,then
VMESH,13
*endif
*get,nod1,node,,num,max
*get,NOE1,ELEM,,count
!-----
ksel,s,loc,y,0
kgen,2,all,,1,,2*dp
ksel,all
v,2,6,52,50,1,5,51,49 !volume 14
v,6,10,54,52,5,9,53,51
v,10,14,56,54,9,13,55,53
v,14,18,58,56,13,17,57,55
v,18,22,60,58,17,21,59,57
v,26,30,64,62,25,29,63,61
v,30,34,66,64,29,33,65,63
v,34,38,68,66,33,37,67,65
v,38,42,70,68,37,41,69,67
v,42,46,72,70,41,45,71,69
v,25,29,63,61,2,6,52,50
v,29,33,65,63,6,10,54,52
v,33,37,67,65,10,14,56,54
v,37,41,69,67,14,18,58,56
v,41,45,71,69,18,22,60,58 !volume 28
L,1,49,5 !concrete top
type,6
mat,topmat !top
vmesh,14,28
*get,NOE2,ELEM,,count

NUMCMP,NODE
!-----

C***NSEL,S,LOC,X,DX1+L
!NSEL,S,LOC,Y,-H
C***NSEL,R,LOC,Z,DZ1
C***NSEL,S,LOC,Z,DZ1+DZ2
*GET,MAXNODE,NODE,,NUM,MAX !GET THE HIGHEST NUMBER NODE

```

```

NINC=MAXNODE
NSEL,S,LOC,X,DX1+2*TP1+DS-0.01,DX1+2*TP1+DS+0.01
NSEL,R,LOC,Z,DZ1+DZ2-.01,DZ1+DZ2+.01
NSEL,R,LOC,Y,-H,-EH
*GET,MINNODE,NODE,,NUM,MIN           !find the lowest node number in the
selected set
*GET,MAXND,NODE,,NUM,MAX             !FIND THE HIGHEST NODE NUMBER IN
THE SELECTED SET
!NINC=MAXNODE-MINNODE+5             !DIFFERENCE TO BE ADD TO GENERATE
NEW NODES
!DXX=H/3                             !distance of spring node from
pile edge in the x-dirc.
NGEN,2,NINC,ALL,,DXX                 !GENERATE SPRINGS NODES
NSEL,S,NODE,,MINNODE+NINC,MAXND+NINC
D,ALL,ALL
*GET,NNODES,NODE,,COUNT             !NUMBER OF NODES IN THE SELECTED SET
NLIST,ALL,,,,Y,Z
*VWRITE,NNODES,NINC,BPILE,DPILE,PERPILE,H,divl,EH,1.,AREA   !WRITES
DATA INTO FILE OPENED BY *CFOPEN:INP1.DAT
(2(F5.0,2X),8(F5.1,2X))              !FORMAT FOR
VWRITE
NSEL,ALL
NSEL,S,LOC,X,DX1+2*TP1+DS-0.01,DX1+2*TP1+DS+0.01
NSEL,R,LOC,Z,DZ1+DZ2+2*TP2+DS2-0.01,DZ1+DZ2+2*TP2+DS2+0.01
NSEL,R,LOC,Y,-H,-EH
*GET,MAXND1,NODE,,NUM,MAX
*GET,MINND1,NODE,,NUM,MIN
NGEN,2,NINC,ALL,,DXX                 !GENERATE SPRINGS NODES
nlist,all
NSEL,S,NODE,,MINND1+NINC,MAXND1+NINC
D,ALL,ALL
NSEL,ALL
NSEL,S,LOC,X,DX1+2*TP1+DS+DXX
nlist,all
NSEL,R,NODE,,MINNODE+NINC,MAXND1+NINC
NLIST,ALL,,,,Y,Z
NWRITE,NODES,OUT
NSEL,ALL
!-----
NSEL,S,LOC,X,DX1-.001,DX1+0.001
NSEL,R,LOC,Z,DZ1+DZ2-0.001,DZ1+DZ2+0.001
NSEL,R,LOC,Y,-H,-EH
*GET,MINND4,NODE,,NUM,MIN
*GET,MAXND4,NODE,,NUM,MAX
NGEN,2,NINC,ALL,,-DXX
NSEL,S,NODE,,MINND4+NINC,MAXND4+NINC
D,ALL,ALL
NSEL,ALL
NSEL,S,LOC,X,DX1-.001,DX1+0.001
NSEL,R,LOC,Z,DZ1+DZ2+2*TP2+DS2-.001,DZ1+DZ2+2*TP2+DS2+.001
NSEL,R,LOC,Y,-H,-EH
*GET,MINND5,NODE,,NUM,MIN
*GET,MAXND5,NODE,,NUM,MAX
NGEN,2,NINC,ALL,,-DXX
NSEL,S,NODE,,MINND5+NINC,MAXND5+NINC
D,ALL,ALL
NSEL,ALL

```



```

NSEL,S,LOC,X,DX1-DXX
NSEL,R,NODE,,MINND4+NINC,MAXND5+NINC
NWRITE,NODES2,OUT
NSEL,ALL
!-----
! GENERATING NODES FOR SPRINGS IN THE Z-DIRECTION
NSEL,S,LOC,X,DX1-0.001,DX1+0.001
NSEL,R,LOC,Z,DZ1-0.001,DZ1+0.001
NSEL,R,LOC,Y,-H,-EH
nlist,all
*GET,MINND2,NODE,,NUM,MIN
*GET,MAXND2,NODE,,NUM,MAX
DZZ=-DXX                                !distance of spring nodes
from pile edge z-axis
NGEN,2,NINC,ALL,,,,DZZ
nlist,all
NSEL,S,NODE,,MINND2+NINC,MAXND2+NINC
nlist,all
D,ALL,ALL
NSEL,ALL
NSEL,S,LOC,X,DX1+DS+2*TP1-.001,DX1+DS+2*TP1+.001
NSEL,R,LOC,Z,DZ1-0.001,DZ1+0.001
NSEL,R,LOC,Y,-H,-EH
nlist,all
*GET,MINND3,NODE,,NUM,MIN
*GET,MAXND3,NODE,,NUM,MAX
NGEN,2,NINC,ALL,,,,DZZ
nlist,all
NSEL,S,NODE,,MINND3+NINC,MAXND3+NINC
nlist,all
D,ALL,ALL
NSEL,ALL
NSEL,S,LOC,Z,DZ1+DZZ
nlist,all
NSEL,R,NODE,,MINND2+NINC,MAXND3+NINC
NLIST,ALL,,,,Y,Z
NWRITE,NODES1,OUT
NSEL,ALL
!-----
! q-z curves
!-----
DYY=-DXX
NSEL,S,LOC,X,DX1+TP1-0.001,DX1+TP1+0.001
NSEL,R,LOC,Y,-H
*GET,MINND6,NODE,,NUM,MIN
*GET,MAXND6,NODE,,NUM,MAX
NGEN,2,NINC,ALL,,,,DYY
NSEL,S,NODE,,MINND6+NINC,MAXND6+NINC
nlist,all
!D,ALL,ALL                                !q-z DOF
NSEL,ALL
NSEL,S,LOC,X,DX1+DS+TP1-.001,DX1+DS+TP1+.001
NSEL,R,LOC,Y,-H
*GET,MINND7,NODE,,NUM,MIN
*GET,MAXND7,NODE,,NUM,MAX
NGEN,2,NINC,ALL,,,,DYY
NSEL,S,NODE,,MINND7+NINC,MAXND7+NINC

```

```

!D,ALL,ALL                                !q-z DOF
NSEL,ALL
NSEL,S,LOC,Y,-H+DYY
NSEL,R,NODE,,MINND6+NINC,MAXND7+NINC
NWRITE,NODES3,OUT
*GET,NOFNODES,NODE,,COUNT                !NUMBER OF NODES IN THE SELECTED
SET
*VWRITE,NOFNODES,XDEPTH
(F6.0,1x,F6.1)
NSEL,ALL
!-----

!NSEL,S,LOC,X,DX1+TP1
!NSEL,R,LOC,Z,DZ1+DZ2
!NSEL,R,LOC,Y,-H
!*GET,ND1,NODE,,NUM,MIN
!NGEN,2,NINC,ALL,,DYY
!NSEL,ALL
!NSEL,S,LOC,X,DX1+TP1
!NSEL,R,LOC,Z,DZ1+DZ2+DS2+2*TP2
!NSEL,R,LOC,Y,-H
!*GET,ND2,NODE,,NUM,MIN
!NGEN,2,NINC,ALL,,DYY
!NSEL,ALL
!NSEL,S,LOC,X,DX1+TP1+DS
!NSEL,R,LOC,Z,DZ1+DZ2
!NSEL,R,LOC,Y,-H
!*GET,ND3,NODE,,NUM,MIN
!NGEN,2,NINC,ALL,,DYY
!NSEL,ALL
!NSEL,S,LOC,X,DX1+TP1+DS
!NSEL,R,LOC,Z,DZ1+DZ2+DS2+2*TP2
!NSEL,R,LOC,Y,-H
!*GET,ND4,NODE,,NUM,MIN
!NGEN,2,NINC,ALL,,DYY
!NSEL,ALL
!*VWRITE,ND1,ND2,ND3,ND4
!(4(F6.0,1X))
/sys,del 111.dat
/SYS,soilpile
/input,b1,dat
!TYPE,3
!REAL,11
!E,ND1,ND1+NINC
!E,ND2,ND2+NINC
!E,ND3,ND3+NINC
!E,ND4,ND4+NINC
!D,ND1+NINC,ALL
!D,ND2+NINC,ALL
!D,ND3+NINC,ALL
!D,ND4+NINC,ALL

!-----

!*MWRITE,MAXNODE,NODES,OUT
TYPE,2

```

```

/INPUT,b11,dat           !springs in the x-direction
TYPE,3
/INPUT,b22,dat           !springs in the y-direction, f-z
/input,b44,dat
!/input,b55,dat
TYPE,4
/INPUT,b33,dat           !springs in the z-direction
NSEL,ALL
outpr,all,1
!/PBC,U,,0
finish
!-----
/SOLU
!-----
/NERR,10,50000
OUTRES,ALL,ALL
AUTOTS,ON
SOLCONTROL,ON
!NSUBST,5
EQSLV,FRONT
!NLGEOM,ON
CNVTOL,U,1,.29
neqit,50
NROPT,full

!SOLCONTROL,0
!NEQIT,5                 ! MAXIMUM 5 EQUILIBRIUM ITERATIONS PER STEP
!NCNV,0                  ! DO NOT TERMINATE THE ANALYSIS IF THE
SOLUTION FAILS
!CNVTOL,U                ! CONVERGENCE CRITERION BASED UPON
DISPLACEMENTS AND
!-----
NSEL,S,LOC,Y,2*dp
  NSEL,R,NODE,,1,NINC
  *GET,NND1,NODE,,COUNT
!  F,ALL,FY,-P/NND1
  D,ALL,UZ
  D,all,ux
  !F,ALL,FX,1
  nsel,all
!Asel,s,loc,y,2*dp
!sfa,all,1,pres,P/10/10
!allsel

!-----
!Load bearing pile

*if,itype,eq,0,then
nsel,s,loc,y,-h
d,all,uy
nsel,all
esel,all
*endif
!-----
*DO,i,12,12,3
!nsubst,8
!Asel,s,loc,y,2*dp

```

```

!sfa,all,1,pres,(P/(DPILE-(2*NL*T))/BPILE)*(i/10)
  nsel,s,loc,y,(1/5)*2*dp,2*dp
  NSEL,R,NODE,,1,NINC
  *GET,NND22,NODE,,COUNT
  F,all,fy,-(P/NND22)*i/12

allsel
solve
*enddo
save
!-----
*DO,i,12,12,3
  nsel,s,loc,z,dz1
  nsel,s,loc,y,0/5*2*dp,2*dp
  NSEL,R,NODE,,1,NINC
  D,all,ux,U2*i/12
  !D,all,uz,-2.
allsel,
solve
*enddo
save
!-----
!P=600
*DO,i,4,4
P=P+Pinc
  !nsubst,8
  !Asel,s,loc,y,2*dp
  !sfa,all,1,pres,(P/(DPILE-(2*NL*T))/BPILE)*(i/10)
nsel,s,loc,y,(1/5)*2*dp,2*dp
NSEL,R,NODE,,1,NINC
*GET,NND22,NODE,,COUNT
F,all,fy,-(P/NND22)      !*i/12

allsel
solve
*enddo
save

!-----

!allsel
!SOLVE
!*enddo
!save
FINISH
!-----
/POST1
!NSEL,S,LOC,X,DX1+2*TP1+DS
NSORT,U,Y
*GET,DELTAMXY,SORT,,MAX
*GET,DELTAMNY,SORT,,MIN
NSORT,U,Z
*GET,DELTAMXZ,SORT,,MAX
*GET,DELTAMNZ,SORT,,MIN
NSORT,U,X
*GET,DELTAMXX,SORT,,MAX
*GET,DELTAMNX,SORT,,MIN

```

```

ETABLE, VOLU, VOLU
SSUM
*GET, VOLUME, SSUM, , ITEM, VOLU
ETABLE, FC_ALL, NMISC, 1
ETABLE, VALUE1, NMISC, 2
ETABLE, LAYER_NO, NMISC, 3
etable, fci, nmisc, 4*NL+8+1
etable, valuei, nmisc, 4*NL+8+2
etable, lni, nmisc, 4*NL+8+3
ETABLE, SF_X, NMISC, 4*NL+8+10
ETABLE, SF_Y, NMISC, 4*NL+8+11
ETABLE, SF_Z, NMISC, 4*NL+8+12
ETABLE, SF_XY, NMISC, 4*NL+8+13
ETABLE, SF_YZ, NMISC, 4*NL+8+14
ETABLE, SF_XZ, NMISC, 4*NL+8+15

etable, sff, nmisc, 40
ESORT, ETAB, SF_X, , 1
*GET, SFXMAX, SORT, , MAX
!ESORT, ETAB, LAYER_NO, , 1
!*GET, LAYERS, SORT, , MAX
!SMAX=SMAXI>SMAXJ
!ESEL, S, ELEM, , 1, 5
!PRESOL, S
ETABLE, STRESS, S, Y
!PRETAB, STRESS
ESORT, ETAB, STRESS, , 1
*GET, NN, ETAB, , NCOL, MAX
*GET, SM, SORT, , MAX
*GET, SM, SORT, , MIN
finish
!NSEL, S, LOC, Y, -H
!nset, all
!show, HPGL
/POST1
!/psymb, esys, 1
!epplot
/post1

abbres, new, toolbar

```

BIBLIOGRAPHY

Alampalli, S., O'Connor, J., Yannotti, A. P., and Luu K. T. (1999). "FRPs for bridge construction and rehabilitation in New York." *Materials and construction: Exploring the connection*, ASCE, Reston, VA, 345-350

Amde, A. M.¹, and Greimann, L. F. (1988). "Design Model for Piles in Jointless Bridges." *Journal of Structural Engineering*, ASCE, Vol. 114, No. 6, June, pp. 1354-1371.

Amde, A. M., and Greimann, L. F. (1988). "General Design Details for Integral Abutment Bridges", *Civil Engineering Practice*, *Journal of the Boston Society of Civil Engineers Section/ASCE*, Vol. 3, No. 2, Fall, ISSN: 0886-9685, pp. 7-20.

Amde, A. M., and Klinger, J. E. (1987). "Integral Abutment Bridges Design and Construction." *Department of Civil Engineering, University of Maryland, January, Final Report.*

¹ Also known as Wolde-Tinsae, A. M.

- Amde, A. M., Chini, S. A., and Mafi, M. (1997). "Model Study of H-piles Subjected to Combined Loading." *Geotechnical and Geological Engineering*, August, Technical Notes, pp. 343-355.
- Amde, A. M., Greimann, L. F., and Yang, P. S. (1982). "Nonlinear Pile Behavior in Integral Abutment Bridges." Iowa DOT, February, Final Report.
- Amde, A. M., Greimann, L. F., and Yang, P. S. (1983). "Skewed Bridges with Integral Abutments." *Bridges and Culverts*, TRR No. 903, pp. 64-71.
- Amde, A. M., Greimann, L. F., and Yang, P. S. (1986). "Nonlinear Analysis of Integral Abutment Bridges." *Journal of Structural Engineering*, ASCE, Vol. 112, No. 10, October, pp. 2263-2280.
- Amde, A. M., Greimann, L. F., and Yang, P. S. (1988). "End-Bearing Piles in Jointless Bridges." *Journal of Structural Engineering*, ASCE, Vol. 114, No. 8, August, pp. 1870-1884.
- Amde, A. M., Greimann, L. F., Yang, P. S., and Edmunds, S. K. (1984). "Design of Piles for Integral Abutment Bridges." Final Report, Department of Civil Engineering, Engineering Research Institute, Iowa State University, Ames, August.

- Amde, A. M., Klinger, J. E., and Mullangi, R. (1988). "Bridge Decks Joint Rehabilitation or Retrofitting." Department of Civil Engineering, University of Maryland, December, Final Report.
- Amde, A. M., Klinger, J. E., and White, E. J. (1988). "Performance of Jointless Bridges." *Journal of Performance of Constructed Facilities*, ASCE, Vol. 2, No. 2, May, pp. 111-125.
- Amde, A. M., Klinger, J. E., Mafi, M., Albrecht, P., White, J., and Buresly, N. (1987). "Performance and Design of Jointless Bridges." Department of Civil Engineering, University of Maryland, June, Final Report.
- Amde, A. M., Yang, P. S., and Greimann, L. F. (1982). "Nonlinear Finite Element Study of Piles in Integral Abutment Bridges." Iowa DOT, September, Final Report.
- Arora, J. S. (1997). "Guide to structural optimization." ASCE manuals and reports on engineering practice. America Society of Civil Engineers.
- Ashford, A. S., and Jakrapiyanun, W., (2001). "Driveability of glass FRP composite piling." *Journal of composites for construction*, ASCE, 5(1), 58-60
- ASM International, (1987). "Engineered materials handbook." Vol. 1
- ASM International, (1995). "Engineered materials handbook."

- Barbero, E. J., (1999). "Introduction to composite materials design." West Virginia university, USA..
- Barker, R. M., et al. (1991). "Manuals for the design of bridge foundations." National Cooperative highway research program report, TRB, Washington, D.C.
- Bogdanovic, A., (2002). "Strengthening Circular Concrete Columns using FRP sheets-applications." Composite materials in civil engineering.
- Bowles, J. E. (1996). "Foundation analysis and design." Fifth edition, McGraw-Hill.
- Brunswick Technologies Inc. "Reinforcing through innovation." Brunswick, Maine.
- Bryan, J. W., and Volk, J. M. (1998). "Composite fiberglass pile dolphins." Ports '98 proceedings, ASCE, New York.
- Chellis, R. D. (1961). "Pile foundations." Second edition McGraw-hill, New York.
- Chen, W. F., and Duan, L. (2000). "Bridge engineering handbook." Boca Raton, Fla.
- Chin, J. W. (1996). "Materials aspects of fiber-reinforced polymer composites in infrastructure." National Institute of Standards and Technology, Gaithersburg, MD.
- Coyle, H. M., and Castello, R. R., (1981). " New design correlations for piles in sand, " Journal of the Geotechnical Engineering Division, Proceedings Paper 16379, American Society of Civil Engineers, Vol. 107 (GT7).

- Creative Pultrusions, "Piling products and technical manual." Alum Bank, PA.
- Creese, R. C. (1999). "Overcoming composite cost differentials by life-cycle costing."
A conference on polymer composites: Infrastructure renewal and economic development.
- Creese, R. C., and GangaRao, H., (1999). "A conference on polymer composites: Infrastructure renewal and economic development." Technomic publishing co.
- Daniel, I. M, and Ishai, O., (1994). "Engineering mechanics of composite materials."
Oxford University press, New York, Oxford.
- Engineering and design Composite Materials for Civil Engineering Structures (1997),
- Eric Green Associates (2000). "Marine composites." Second edition, Annapolis, Maryland.
- Fam, A. Z. and Rizkalla, S. H. (2001). "Confinement model for axially loaded concrete confined by circular fiber-reinforced polymer tubes." ACI Struct. J., 98(4), 451-41.
- Fam, A. Z. and Rizkalla, S. H. (2002). "Flexural behavior of concrete-filled fiber-reinforced polymer circular tubes." J. of Struct. Eng. 6(2), 123-132.
- Fleming, W. G., Weltman, A. J., Randolph, M. F., and Elson W. K. (1992). "Piling engineering." Second edition, John Wiley & sons.

Gibson, R. F. (1994).” Principles of composite material mechanics.” McGraw –Hill.

Goldstick, J., and Asaro, R. (1998). “69th street composite pier design in Brooklyn, NY.”

Greimann, L. F., Abendorth, R. E., Johnson, D. E., and Ebner, P. B., (1987). “ Pile design and tests for integral abutment bridges.” Final report, Iowa DOT Project HR-273.

Greinmann, L. F., Yang, P. S., and Amde, A. M., (1984). “Design of piles for integral abutment bridges.” Final Report, Iowa DOT Project HR-252, ISU-ERI-Ames 80026, Iowa State University, Ames, Iowa.

Greimann, L. F., Amde, A. M., (1987). “Design model for piles in jointless bridges.” Journal of structural Engineering, ASCE, Vol. 114, No. 6, pp. 1354-1371.

Gurdal, Z., Haftka, R. T., and Hajela, P. (1999). “Design optimization of laminated composite materials.” John Wiley & sons Inc.

Hardcore Composites (1996). “Composite tubular design guide.” New Castle, Delaware.

Hardcore Composites (1997). “Pile installation and load test report, Hardcore fiberglass tubular piling test program.” New Castle, Delaware.

Hyer, M. W. (1998). “Stress analysis of fiber-reinforced composite materials.” McGraw-Hill.

- Iskandar, M. G., and Hassan, M. (1998). "State of the practice review in FRP composite piling." *J. of composites for construction*, ASCE, 2(3), 116-120.
- Iskander, M. G., Hanna, S., and Stachula, A., (2001). "Drivability of FRP composite piling." *Journal of geotechnical and geoenvironmental engineering*, ASCE, 127(2), 169-176.
- Iyer, S. L., (1991). "Advanced composites materials in civil engineering structures." ASCE, New York.
- Jones, R. M. "Mechanics of composite materials." Second edition, 1999.
- Juvaandes, L., Figueiras, J. A., and Marques, A. T. (1998). "Performance of concrete beams strengthened with CFRP laminates." *Fiber composites in infrastructure*, ICC'98, Tucson, AZ, 126-137.
- Lam, L., and Teng, J. G. (2002). "Strength models for fiber-reinforced plastic-confined concrete." *J. of Struc. Eng.*, 128(5), 612-623.
- Lampo, R., Nosker, T., Barno, D., Busel, J., Maher, A., Dutta, P., and Odello, R. (1998a). "Development and demonstration of FRP composite fender, load bearing, and sheet piling systems." *Construction productivity Advancement research program*, US Army Corps of Engineers.
- Lampo, R., Nosker, T., Dutta, P., and Odello, R. (1998b). "FRP composite piling systems for waterfront applications." *Ports '98 proceedings*, ASCE New York.

- Lancaster Composites. "Engineers and manufacturers of composite piles." PA.
- Langer, J. A., Mosley, E. T., and Thomson, C. D., (1983). "Laterally loaded deep foundations: analysis and performance." Kansas City, MO.
- M'Bazza, I., Missihoun, M., and Labossiere, P. (1996). "Strengthening of reinforced concrete beams with CFRP sheets." Proceedings of the first international conference on composites in infrastructure, ICC'96, Tucson, AZ, 746-759.
- M'Bazza, I., Missihoun, M., and Labossiere, P. (1996). "Strengthening of reinforced concrete beams with CFRP sheets." Fiber composites in infrastructure, ICCI'96,
- Mallick, P. K. (1993). "Fiber-reinforced composites."
- Mander, J. B., Priestley, M. J. N., and Park, R. (1988). "Theoretical stress-strain model for confined concrete." J. Struct. Eng. 114(8), 1804-1826.
- March, F. and Colturi, M. (1998). "Market advancement for composite marine piling and timber." Ports '98 proceedings, ASCE, New York.
- Marques, S. P. C., Marques, D. C., and Silva, J. L. (2004). "Model for analysis of short columns of concrete confined by fiber-reinforced polymer." J. Compos. Contr., 8(4), 332-340.
- Materials and Construction: Exploring the connection, ASCE, Reston, VA, 324-331.
- Matthews, F. L., and Rawlings, R. D. (1994). "Composite Materials: Engineering and science." Chapman & Hall.

- Military Handbook, MIL-HDBK-17-3E (1997).” Material usage, design, and analysis.“ Department of defense, USA.
- Mirmiran A., Kargahi, M., Samman, M., and Shahawy, M. (1996). “Composite FRP-concrete column with bi-directional external reinforcement.” Proceedings of the first international conference on composites in infrastructure, ICCI’96, Tucson, Arizona
- Mirmiran, A., and Shahawy, M. (1997). “Behavior of concrete columns confined by fiber composites.” *J. Struct. Eng.*, 123(5), 583–590.
- Mirmiran, A., and Shahawy, M. (2003). “Composite pile: a successful drive.” *Concrete International*, 80-94.
- Mirmiran, A., and Shahawy, M., and El Echary, H.(1998). “Effect of column parameters on FRP-confined concrete.” *J. Compos. Constr.*, 2(4), 175-185.
- Mosher, R. L. (1984). “Load transfer criteria for numerical analysis of axially loaded piles in sand; Part 1: Load transfer criteria, “Technical Report K-84-1, U.S. Army Engineer Waterways Experiment Station, Vicksburg, MS. (not available yet).\
- Mosher, R. L. and Dawkins, W. P. (2000). “Theoretical manual for pile foundations,” Technical Report TR-00-5, U.S. Army Corps of Engineers.

- Mukherjee, A., Boothby, T. E., Bakis, C. E. (2004). "Mechanical behavior of fiber-reinforced polymer-wrapped concrete columns-complicating effects." *J. Compos. Constr.*, 8(2), 97-103.
- Nshanian, Y. S., and Pappas, M. (1983). "Optimal laminated composite shells for buckling and vibration." *AIAA journal*, 21(3), 430-437.
- Onada Y. (1985). "Optimal laminate configurations of cylindrical shells for axial buckling." *AIAA journal*, 23(7), 1093-1098.
- Picher, F., Rochette, P., and Labossiere, P. (1996). "Confinement of concrete cylinders with CFRP." *Proceedings of the first international conference on composites in infrastructure, ICC'96, Tucson, AZ*, 829-841.
- Plastic Piling Inc. "Plastic marine pilings." Rialto, CA.
- Poulos, H. G., and Davis, E. H. "Pile foundation analysis and design." 1980.
- Prakash, S., and Sharma, H. D., (1990). "Pile foundations in engineering practice." John Wiley & Sons, New York.
- Pritchard, B., (1993). "Continuous and integral bridges: Proceedings of the Henderson colloquium 'towards joint-free bridges'." E & FN Spon.
- Prots '98 proceedings, ASCE New York.
- Rao, S. S., (1996). "Engineering optimization: Theory and practice."

- Razvi, S., and Saatcioglu, M. (1999). "Confinement model for high-strength concrete." *J. of Struc. Eng.*, 125(3), 281-289.
- Reese, L. C. (1983). "Behavior of piles and pile groups under lateral load." U.S. Department of Transportation, FHWA, Washington, D.C
- Reese, L., C., Cox, W. R., and Koop, F. D., (1974)."Analysis of laterally loaded piles in sand." *Proceedings Offshore Technology Conference, Houston, TX, Paper No. OTC 2080, 1974, pp.473-483.*
- Richard, R. M., and Abbott, B. J. (1975)."Versatile elastic-plastic stress-strain formula." *J. Engrg. Mech., ASCE*, 101(4), 511-515.
- Rochette, P., and Labossie`re, P. (2000). "Axial testing of rectangular column models confined with composites." *J. Compos. Constr.*, 4(3),129–136.
- Rosset, J. M., (1999)."Analysis, design, construction, and testing of deep foundations." *Proceedings of the OTRC '99 conference, ASCE, Reston, VA.*
- Samman, M., Mirmiran, A., and Shahawy, M. (1998). "Model of concrete confined by fiber composites." *J of Struc. Eng.*, 124(9), 1025-1031.
- Seaward International Inc."Seapile composite marine piling: Technical manual." Clearbrook, VA.

- Shahawy, M., Beitelman T. E., and Mirmiran, A. (1998). "Analysis and modeling of fiber-wrapped columns and concrete-filled tubes." Florida department of transportation, Tallahassee, Fl.
- Sharif, A., and Baluch, M. H. (1996). "External FRP plates to strengthen reinforced concrete beams." Proceedings of the first international conference on composites in infrastructure, ICCI'96, Tucson, Arizona.
- Smerdov, A. A. (2000). "A computational study in optimum formulations of optimization problems on laminated cylindrical shells for buckling: I. Shells under external pressure." Composite science and technology, 60(11), 2067-2076.
- Smerdov, A. A. (2000). "A computational study in optimum formulations of optimization problems on laminated cylindrical shells for buckling: I. Shells under axial compression." Composite science and technology, 60(11), 2057-2066.
- Sonti, S. S. (1996). "Rehabilitation and strengthening of glulam stringers for bridge superstructures." Proceedings of the first international conference on composites in infrastructure, ICC'96, Tucson, AZ, 800-813.
- Strongwell, "Extren design manual." Bristol, VA.
- Tang, B., and Podolny, W. Jr. (1999). "A good start for FRP composite material bridges."
- Technical letter, Dept. of the Army.

- Tetra Tech. Inc. (1999). "Plastic pier piling evaluation report." Navy environmental leader program, San Diego, California.
- Thippeswamy, H. K., Raju, P. R., and Gangarao, H. V. (1994). "Parametric study of single-span jointless steel bridges." Transportation research record 1460, TRB, National research council, Washington, D.C., 25-36.
- Tsai, S. W., and Hahn, H. T., (1980)."Introduction to composite materials." Technomic publishing co., Westport, CT.
- Vectorply, " Manufacturing and distribution of composite reinforcement fabrics." Phenix City, AL.
- Vijayvergiya, V. N. (1977). "Load-movement characteristics of piles," Proceedings, Ports 77, American Society of Civil Engineers, Vol II, 269-286.
- Wasserman, E. P., Walker, J. H. (1996). "Integral abutments for steel bridges." Highway structures design handbook, Vol. 2, chap. 5, American iron institute.
- Amde, A. M., Greinmann, L. F., and Yang, P. S. (1982). "Nonlinear pile behavior in integral abutment bridges." Final Report, Iowa DOT Project HR-227, ISU-ERI-Ames 82123, Iowa State University, Ames, Iowa.
- Xanthakos, P. P. (1995). "Bridge substructure and foundation design." Prentice Hall, New Jersey.

Yang, P. S., Amde, A. M. and Greinmann, L. F. (1982). "Nonlinear finite element study of piles in integral abutment bridges." "Final Report, Iowa DOT Project HR-227, ISUY-ERI-Ames 82125, Iowa State University, Ames Iowa.

Yang, P. S., Amde, A. M., and Greimann, L. F. (1985). "Effects of Predrilling and Layered Soils on Piles." *Journal of Geotechnical Engineering, ASCE*, Vol. 111, No. 1, January, pp. 18

Yoon, S. J., (1993). "Local buckling of pultruded I-shape columns." Ph.D. dissertation, Georgia Institute of Technology.

Zimmermann R. (1995). "Quick optimal buckling design of axially compressed, fiber composite cylindrical shells." *AIAA Journal* 33(10), 1993-1995.